Table of Contents

CHAPTER 1

THE IMPORTANCE OF pH AND MEMBRANE VESICLES IN METAL-MICROBE INTERACTIONS

CHAPTER 2

CYTOTOXICITY OF ENGINEERED ZINC OXIDE NANOPARTICLES TO
Burkholderia vietnamiensis PR1$_{301}$: COMPARISON TO Zn^{2+} AND THE EFFECTS OF
COUNTER-ION UTILIZATION

CHAPTER 3

MEMBRANE VESICLE PRODUCTION BY *Burkholderia vietnamiensis* PR1$_{301}$ IS
INFLUENCED BY pH AND Zn

CHAPTER 4

INVESTIGATING THE ROLE OF MEMBRANE VESICLES IN METAL-MICROBE
INTERACTIONS

CHAPTER 5

INSIGHTS INTO THE FUNCTION AND FORMATION OF *Burkholderia
vietnamiensis* PR1$_{301}$ MEMBRANE VESICLES PRODUCED NATIVELY AT
DIFFERENT pH

CHAPTER 6

DISCUSSION

List of Tables

List of Figures

Chapter 3

Chapter 4

Appendix B

List of Abbreviations

σ^E	sigma-factor E
2D-LC/MS/MS	two-dimensional liquid chromatography tandem mass spectrometry
4M	modified minimal mineral medium
ABC	ATP binding cassette
AF^4	asymmetric flow- field flow fractionation
AF^4-MALS-ICP-MS	asymmetric flow-field flow fractionation coupled to multi-angle laser light scattering and inductively coupled plasma mass spectrometry
ATR-FTIR	attenuated total reflectance Fourier transform infrared
Bcc	*Burkholderia cepacia* complex
BLM	Biotic Ligand Model
BSD	Biodegradative Strain Database
CAS	chrome azurol S
CDF	cation diffusion facilitator
CERCLIS	Comprehensive Environmental Response, Compensation, and Liability Information System
CF	cystic fibrosis
CFA	cyclopropane fatty acid
CFU	colony forming units
CH34	*Cupriavidus metallodurans* CH34
CI	confidence interval
COGS	Clusters of Orthologous Groups
cps	counts per second
Da	daltons
DEG	diethylene glycol
DLS	dynamic laser light scattering
EC_{50}	concentration required to elicit a 50% inhibition of growth
EDX (or EDS)	energy dispersive X-ray spectroscopy
EM	electron microscopy
EPA	Environmental Protection Agency
EPM	electrophoretic mobility
EPS	extracellular polysaccharides
FA	fatty acid
FAME	fatty acid methyl ester
FFF	field flow fractionation
FI	fiducial interval
FIAM	Free Ion Activity Model
G4	*Burkholderia vietnamiensis* G4
GeLC-MS/MS	gel electrophoresis liquid chromatography tandem mass spectrometry
HAQs	hydroxyalkylquinolines
HEPES	4-(2-hydroxyethyl)-1-piperazineethanesulfonic acid
HMDS	hexamethyldisalizane

^{1}H-NMR	proton nuclear magnetic resonance
HR-TGA	high resolution thermogravimetric analysis
HSL	homoserine lactone
ICP-MS	inductively coupled plasma mass spectroscopy
ICP-OES	inductively coupled plasma optical emission spectroscopy
LB	Luria Bertani
LC_{50}	lethal concentration to render 50% of cells non-viable
LDS-PAGE	lithium dodecyl sulfate-polyacrylamide gel electrophoresis
LPS	lipopolysaccharides
LS	light scattering
MALS	multi-angle laser light scattering
MES	2-(N-morpholino)ethanesulfonic acid
MIC	minimum inhibitory concentration
MNNG	*N*-methyl-*N*'-nitro-*N*-nitrosoguanidine
MS/MS	tandem mass spectrometry
n-MVs	native-membrane vesicles (used in Chapter 5 to discriminate between artificially induced or harvested MVs)
MVs	membrane vesicles
NP	nanoparticle
NTA	nitrilotriacetic acid
OD_{610}	optical density at λ=610 nm
Omp or OMP	outer membrane protein
ORNL	Oak Ridge National Laboratory
PAHs	polyaromatic hydrocarbons
PALS	phase analysis light scattering
PBS	phosphate buffered saline
PCBs	polychlorinated biphenyls
PEG	polyethylene glycol
PLFA	polar lipid fatty acid
ppt	precipitate
PQS	*Pseudomonas* quinolone signal
PR1	*Burkholderia vietnamiensis* PR1$_{301}$
PTMs	post-translational modifications
R_Θ	excess Raleigh ratio
RND	resistance nodulation cell division
RSD	relative standard deviation
SD	standard deviation
SDS	sodium dodecyl sulfate
SE	standard error
SEC-ICP-MS	size exclusion chromatography inductively coupled plasma mass spectroscopy
SEM-EDX	scanning electron microscopy energy dispersive X-ray spectroscopy
sp.	species
spp.	species (*p*)

STEM	scanning transmission electron microscopy
STEM-EDX	scanning transmission electron microscopy energy dispersive X-ray spectroscopy
TCE	trichloroethylene
TEM	transmission electron microscopy
TGA	thermogravimetric analysis
TOM or Tom	toluene orthomonooxygenase
TSP	3-(trimethylsilyl)propionic acid-d_4
ZnO-NP	zinc oxide nanoparticle

BENJAMIN ADAM NEELY

EFFECTS OF pH ON METAL- AND NANOPARTICLE-MICROBE

INTERACTIONS (Under the direction of Drs. Pamela J. Morris

and Paul M. Bertsch)

Understanding metal-microbe interactions is essential in the study of biogeochemical transformations, microbial pathogenicity and bioremediation applications. For this dissertation research we employed *Burkholderia vietnamiensis* PR1$_{301}$ (PR1) as a model microbe to study the effects of pH on metal-microbe interactions. Initially PR1 was used to evaluate ZnO-nanoparticle (NP) toxicity with ZnCl$_2$ as a reference toxicant using different cytotoxicity assays. These results demonstrated that ZnO-NP and ZnCl$_2$ exhibit similar toxicities and both are more toxic at pH 7 than at pH 6. During these investigations we observed that PR1 produces membrane vesicles (MVs), which are 50 to 250 nm structures derived from the outer-membrane ubiquitously produced by Gram-negative bacteria. At pH 7, when Zn^{2+} is 16-fold more toxic to PR1 than at pH 5, MV production was also two-fold greater, while at both pH MV production was inversely related to Zn concentration. Most research to date has focused on the role of MVs in bacterial pathogenicity, and their potential role in metal-microbe interactions has been largely overlooked. Due to their size, prevalence, and multifarious nature, the involvement of MVs in metal-microbe interactions was further investigated. First we demonstrated that MVs at physiological concentrations do not increase or decrease Zn^{2+} toxicity to PR1. Next, we demonstrated that MVs produced at pH 5 and 7 have different surface chemistries and that MVs from pH 7 are able to sorb

greater Zn^{2+} concentrations. Moreover, certain size classes within each MV population appear to sorb relatively more Zn^{2+}. Lastly, the function and formation of MVs from each pH was evaluated using molecular techniques including proteomics. In addition to pH affecting MV production rates, pH also affected the nucleic acid, Fe and Zn concentration and protein composition of MVs. Interestingly, the 203 shared proteins at each pH indicate that in addition to known MV functions, they could also function in extracellular nutrient storage. Also, MVs produced at pH 5 contained greater functional potential including the predicted ability to degrade organic contaminants. Overall, this research highlights not only the importance of pH in metal-microbe interactions, but also the probable involvement of MVs in metal-microbe interactions.

CHAPTER 1

THE IMPORTANCE OF pH AND MEMBRANE VESICLES IN METAL-MICROBE INTERACTIONS

1.1. <u>Introduction</u>

The study of metal-microbe interactions has typically applied to understanding metal toxicity (reviewed by Gadd, 2004), but it is also important in more fundamental microbial processes. In the environment, microorganisms must regulate the import and export of essential required elements such as Co, Cu, Fe, K, Mg, Mn, Mo, and Zn (Perry and Staley, 1997). The ability of a microorganism to regulate intracellular metal accumulation can give a competitive edge and allow for successful colonization. This is true both in environments with high concentrations of metals (due to natural or anthropogenically processes), and in environments with limited metal bioavailability (e.g., the human body). In the latter case, the ability of microorganisms to acquire limited nutrients can affect their overall success, and in the human body their pathogenesis. Interestingly, microorganisms that are able to survive high metal concentrations often have antibiotic resistance (Baker-Austin et al., 2006), implying either a coupling of these phenotypes or a shared mechanism of resistance. Also, pathogenic microorganisms normally have diverse mechanisms to acquire Fe during human pathogenesis ranging from utilizing ferritin bound Fe to secreting compounds called siderophores with high Fe-binding activities (Whitby et al., 2006). In turn, Fe bioavailability and/or uptake is related to the expression of virulence factors (Carpenter et al., 2009). Overall it is evident that metal-microbe interactions are important beyond understanding metal toxicity and are essential in understanding microbial function in the environment as well as in human infection.

One of the more important variables in studying metal-microbe interactions is the effect of pH, which is known to affect metal bioavailability as well as cellular processes.

In anthropogenically disturbed sites, the pH is often low, whereas the human body contains numerous microenvironments ranging from the acidic bladder to the circumneutral lung. Changes in pH can affect metal toxicity in the former and metal bioavailability in the latter. In order to study the effect of pH on metal-microbe interactions, we have developed a model system using the Gram-negative bacterium *Burkholderia vietnamiensis* PR1$_{301}$ (PR1) which we have used in this dissertation research to specifically study Zn-microbe interactions. Previous research with PR1 focused on a specific applied bioremediation scenario, and demonstrated that pH mediates metal toxicity (Van Nostrand et al., 2005), and that pH can thereby affect organic contaminant degradation (Van Nostrand et al., 2007). The effect of pH on metal toxicity/resistance is often counter-intuitive when reconciled against our understanding of metal chemistry and toxicity, and is further complicated by the lack of understanding about the effects of pH on microbial processes. To provide necessary background on these topics we will first discuss why PR1 was chosen as a model system in section 1.2. Then in section 1.3, we will discuss what is known about the effect of pH on metal-microbe interactions. Next in section 1.4, Zn will be discussed in terms of general chemistry and regulation in relation to the effects of pH. Lastly, we will introduce bacterial membrane vesicles as a previously overlooked component of metal-microbe interactions in section 1.5.

1.2. *Burkholderia vietnamiensis* PR1$_{301}$

For our studies, the microorganism *Burkholderia vietnamiensis* PR1$_{301}$ (PR1) was used as a model organism to study metal-microbe interactions. *B. vietnamiensis* is a

Gram-negative bacterium in the phylogenetic taxon β-proteobacteria, determined by its 16S rDNA sequence homology (Gillis et al., 1995). Specifically, PR1 is a *N*-methyl-*N*'-nitro-*N*-nitrosoguanidine (MNNG) induced mutant of *B. vietnamiensis* G4 (G4), generated to constitutively express *o*-toluene monooxygenase (TOM) which confers a constitutive tricholoroethylene (TCE) co-oxidation phenotype (Munakata-Marr et al., 1996). The parent strain of PR1, G4, was isolated from an organochlorine-contaminated holding pond in Florida (Nelson et al., 1986) used to precipitate metals (Malcom Shields, personal communication). G4 is able to co-oxidize TCE when grown on toluene, and is one of the most effective TCE co-oxidizing bacteria (Nelson et al., 1986; Fries et al., 1997; Yeager et al., 2004).

Burkholderia vietnamiensis is one of nine distinct classes of bacteria closely related to *Burkholderia cepacia* (i.e., genomovars) that constitute the *B. cepacia* complex (Bcc; Coenye and Vandamme, 2003). Members of the Bcc are a diverse group and can be found in soil, water (fresh and salt water), and plant rhizospheres as well as in humans and animals as pathogens (Coenye and Vandamme, 2003). Specifically, G4 possesses genes involved in carbon fixation, methane metabolism, photosynthesis, sulfur metabolism, nitrogen metabolism (ORNL, 2007). Because *Burkholderia* species can colonize extremely diverse environments, they have been termed versaphiles (Tiedje et al., 2005). Furthermore, members of the Bcc possess virulence factors such as endotoxins, lipases, siderophores and proteases that not only aid in host invasion and cell damage, but can also elicit an immune response from their eukaryotic host (Mahenthiralingam et al., 2005). In the lungs of patients with cystic fibrosis (CF) and other disabling diseases, the Bcc plays a major role in pathogenicity. *Burkholderia*

infections in CF patients typically lead to decreased life expectancy and increased

morbidity (Tablan et al., 1987). A survey of 606 U.S. CF patients found *B. vietnamiensis*

in 5.1% of patients, the third most frequently isolated member of the Bcc (LiPuma et al.,

2001). Additionally, co-infection of CF patients with *Pseudomonas aeruginosa* and Bcc

members may allow for a more pathogenic, synergistic community structure as Bcc and

P. aeruginosa are able to communicate via quorum sensing, and virulence factors are

under the control of quorum sensing mechanisms (Geisenberger et al., 2000).

In addition to the role *Burkholderia* species have in human disease and carbon

and nutrient cycling in the environment, *Burkholderia* species are significant because of

their capability to degrade organic contaminants. There are 17 species of *Burkholderia*

capable of degrading a total of 40 different compounds including benzoate derivatives,

tetra- and pentachlorophenol, 2-4-D, phenol and toluene (Urbance et al., 2003; O'Sullivan

and Mahenthiralingam, 2005; BSD, 2007). *B. vietnamiensis* G4 has been found to

degrade many organic pollutants (BSD, 2007) and genome annotation has also identified

genes involved in the degradation of organic pollutants (Table 1.1; ORNL, 2007).

Additionally, DNA from PR1 has been analyzed with a functional gene microarray which

contained genes related to organic contaminant degradation and was positive for 51 genes

in this category (Table 1.1; Van Nostrand, 2006). Because of their ability to degrade

organic pollutants, both G4 and PR1 are likely candidates for bioremediation

applications.

PR1 as a model microbe to study metal-microbe interactions. Historically,

metal toxicity to bacteria has been an important field of study due to its direct application

to bioremediation. Presently there are 1,331 superfund sites listed or proposed under the

U.S. Environmental Protection Agency's National Priority List (CERCLIS, 2009). For many of these sites, bioremediation strategies using microorganisms would be the preferred method of mitigation due to the environmental and financial benefits associated with such a strategy. Bioremediation utilizes the ability of microorganisms to degrade diverse organic compounds such as polyaromatic hydrocarbons (PAHs) and polychlorinated biphenyls (PCBs) in addition to reduce metals or radionuclides to less bioavailable oxidation states [e.g., Cr(VI) to Cr(III)] (Lovley and Phillips, 1994; Camargo et al., 2004). Unfortunately, co-contaminant toxicity to microorganisms can limit the degradation or immobilization the target pollutant (Said and Lewis, 1991; Sandrin and Maier, 2003; Van Nostrand et al., 2007). This is significant because superfund sites can contain multiple classes of pollutants including metals, radionuclides, organic solvents, PAHs, PCBs and pesticides. Specifically, both metals and organic pollutants are present at 40% of superfund sites (Sandrin, 2000). Therefore understanding metal-microbe interactions can allow for more efficient and effective bioremediation strategies in a mixed waste scenario.

The potential to use PR1 in a mixed waste scenario application was the initial reason to develop PR1 as a model to study metal-microbe interactions. Due to the ability of PR1 to degrade TCE, studies were conducted to evaluate its use in an application to a contaminated site that contained high levels of U and Ni, as well as TCE. Since the site of interest had a pH 5 to 5.5 (Sowder et al., 2003) and lime treatment is a typically used to decrease metal solubility, laboratory studies were conducted at pH 5, 6 and 7 using a defined media to facilitate metal speciation predictions (Van Nostrand et al., 2005). During the course of these studies a wealth of information was generated about how PR1

Table 1.1. Organic pollutants that G4 can or is predicted to be able to degrade.

Method	Organic Pollutants
Experimental[a]	Benzene, *o*-cresol, *m*-cresol, *p*-cresol, phenol, toluene, trichloroethylene, naphthalene, and chloroform
Genome Annotation[b]	toluene, xylene, carbazole, styrene, tetrachloroethene, ethylbenzene, 1,2-dichloroethane, 3-chloroacrylic acid, γ-hexachlorocyclohexane, biphenyl, atrazine, 1,1,1-trichloro-2,2-bisphenyl-(4'chlorophenyl) ethane (DDT), caprolactam, 2,4-dichlorobenzoate, fluorene, 1,4-dichlorobenzene, benzoate, and nitrobenzene
Gene Array[c]	trihydroxynitrotoluene and phthalate

[a]BSD; Urbance et al., 2003; [b]ORNL, 2007; [c]Van Nostrand, 2006

reacts to pH and different first row transition metals (i.e., Ni, Co, Cd, and Zn). These

data in addition to information from the annotated genome of G4, made PR1 an excellent

model system to further investigate the effect of pH on Zn-microbe interactions.

Additionally, since *B. vietnamiensis* is relevant in human disease, studying how PR1

adapts to changing environmental conditions has potential applications in biomedical

research.

1.3. Importance of pH in metal-microbe interactions

Effect of pH on metal speciation. With increasing pH, transition metal

solubility generally decreases and the free metal ion concentration decreases with a

concomitant shift to hydroxo-metal complexes (Figure 1.1). Metal bioavailability is

influenced by metal speciation; therefore pH can drive metal bioavailability. For

example, Ivanov et al. (1997) predicted that increasing Ni, Cu, and Pb toxicity to

Pseudomonas fluorescens and *Escherichia coli* with pH was due to formation of

monohydroxo-metal species which sorbed to the cell membrane and caused a reversal in

cell wall charge (net negative to positive). Conversely, increased Cd toxicity to a

Burkholderia sp. with pH was not due to $CdOH^+$, since metal speciation modeling

predicted that the concentration of Cd^{2+} was three orders of magnitude greater than the

concentration of $CdOH^+$ (Sandrin and Maier, 2002). Also, the exposed *Burkholderia* sp.

had ~3-fold more Cd associated with the cell at pH 7 versus pH 4, indicating increased

Cd uptake or sorption with increased pH (Sandrin and Maier, 2002). Previous research

on pH-dependent Ni toxicity to PR1 did not identify a species which correlated to toxicity

(Van Nostrand et al., 2005).
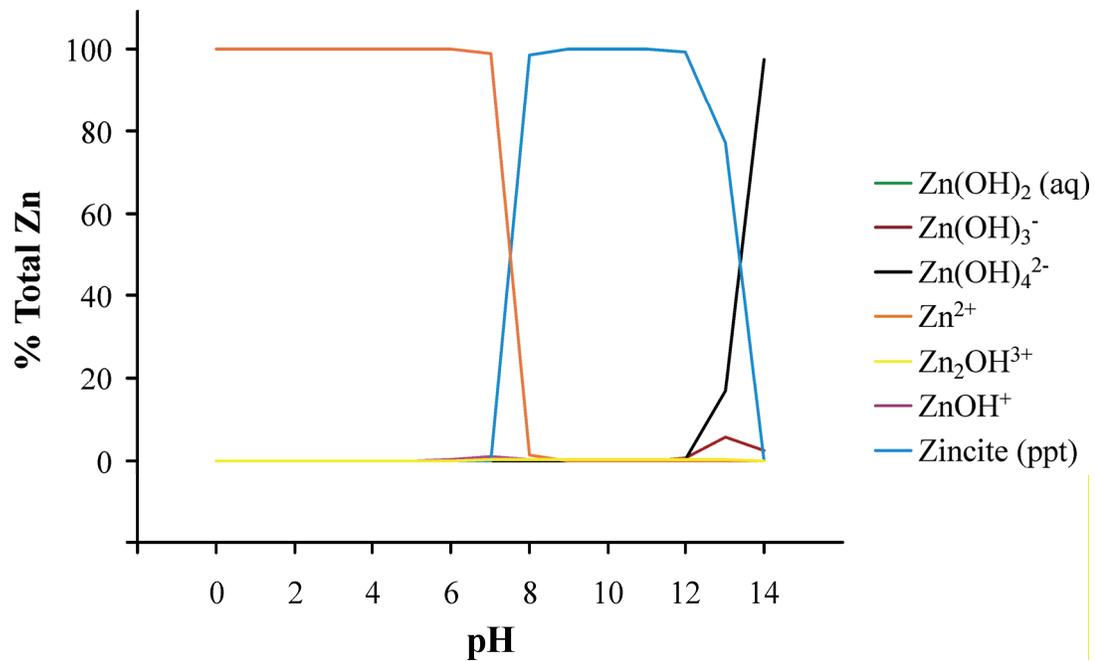
Figure 1.1. Zinc speciation with pH. Data was generated using MINTEQA2 (USEPA, 1999) with 1.53 mM Zn and pH sweep allowing for precipitation (ppt). Zincite is mineral phase of ZnO.

Additionally, metals can be more bioavailable to microorganisms when coordinated with a biologically relevant ligand such as an organic acid normally taken up by the cell. For instance, Ni-citrate was found to be more toxic than Ni^{2+} to *Pseudomonas fluorescens*, presumably because more Ni entered the cell through co-transport with citrate (Joshi-Tope and Francis, 1995). The exchange of metal ions between ligands in the solution outside of the cell as well as formation of hydroxo complexes or other metal species is affected by the pH of the solution. This in turn affects the overall bioavailability and toxicity of the metal to bacteria.

Models to predict aqueous metal toxicity to bacteria. Predicting metal toxicity to microorganisms with changing pH is complex since pH affects potential metal binding sites on the cell membrane as well as metal speciation. Models have been developed to predict how aqueous metal chemistry is related to metal toxicity to organisms (including fish, algae and bacteria). In general, these models use empirical data specific to organisms and chemical species, but can be extrapolated to more complex systems. One such model is the Free Ion Activity Model (FIAM), which relates the acute-toxic response to the free ion concentration (Campbell, 1995). An underlying assumption of the FIAM is that the free ion concentration correlates to the amount of free ion bound to the membrane (Campbell, 1995). Another model is the Biotic Ligand Model (BLM), which is based on the FIAM and relates competitive metal binding to a generic membrane associated biotic ligand to the acute-toxic response (Pagenkopf, 2002). The overall concept of both models is that metal binding to a cell surface will be internalized where it will bind to an intracellular ligand and elicit a toxic response (Figure 1.2).
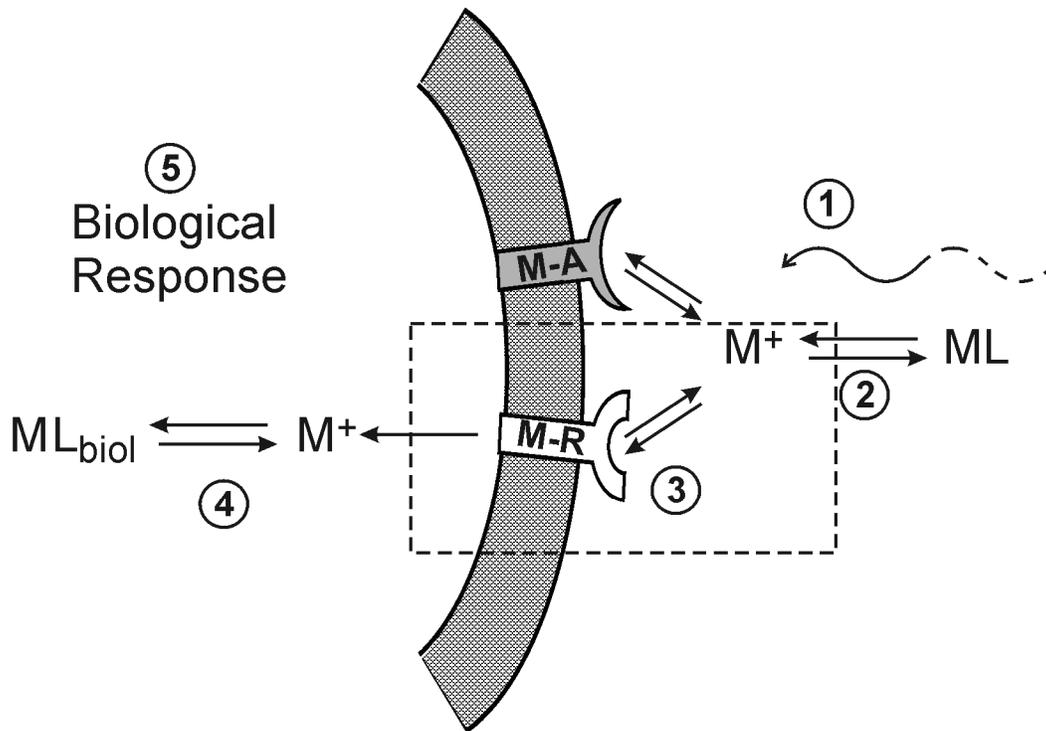
Figure 1.2. Conceptual framework of the FIAM and BLM. This framework includes: (1) mass transport of the free ion in solution as well as formation of hydrophilic complexes with ligands, (2) metal ion speciation between dissociation and complexation with ligands in solution, (3) specific (M-R) or non-specific (M-A) adsorption of the metal ion on the cell membrane surface, and (4) metal transport into the cell after specific binding followed by metal interaction with an intracellular ligand which (5) elicits a biological response. The boxed region represents the part of the model that is empirically derived and is correlated to biological effects (adapted from Hassler et al., 2004).

Both the FIAM and BLM operate under several assumptions (Campbell, 1995; Heijerick et al., 2002; Hassler et al., 2004) which include: (1) biological transport of the metal, (2) the primary site of interaction is the outer membrane, (3) the number of sites on the membrane remain constant, (4) binding at the membrane induces no biological regulation, (5) sites on the surface remain unsaturated, (6) sites on the surface are uniform and do not affect other sites, (7) internalization is a first order reaction, and (8) the acute biological response is directly related to metal internalization or to concentrations of metal bound sites.

In certain cases, the BLM is unable to accurately predict acute metal toxicity because of complexities due to chemistry or biological response which are not accounted for in the simplified assumptions. For example, Zn toxicity to the green algae *Pseudokirchneriella subcapitata* was found to increase with pH and increasing concentrations of Ca, Mg, and Na (Heijerick et al., 2002). Although the BLM accounts for H^+ competition for sites on the cell membrane, the BLM was not able to predict toxicity over a pH range, potentially due to the fact that BLM assumes that the number of binding sites is fixed regardless of cooperative effects (i.e., metal binding is affected by the number of total binding sites and metal bound sites) and that the activity of the metal ion is constant irrespective of pH. By modifying the BLM to incorporate changing dissociation values for Zn with pH, the authors were able to more accurately predict Zn toxicity changes with pH (Heijerick et al., 2002). Although the BLM fails to predict metal toxicity in this scenario, it indicates that a more complex model might be able to predict the observed biological response.

Another scenario where the assumptions of the BLM are violated may be when the acute toxicity of a required element such as Zn is modeled. When Zn toxicity to the algae *Chorella kesslerii* was evaluated, surface bound and solution Zn-chemistry did not predict the observed Zn-uptake and resulting toxicity (Hassler and Wilkinson, 2003). The authors reasoned that because Zn is an essential metal, there is a high degree of regulation, such as the synthesis of Zn-specific transporters, which causes Zn flux to be independent of the Zn^{2+} concentration. Overall, the FIAM and BLM are tools to model and predict the relationship of chemical equilibriums to observed toxicity endpoints, but because of biological and chemical complexities such as biological regulation of metal internalization and export as well as the effect of pH on cell membrane chemistry, these models can fail to accurately predict acute metal toxicity. Despite these drawbacks, the copper BLM is used by the EPA to determine site specific water quality regulations (USEPA, 2003).

Gram-negative bacterial cell membrane structure. Since thermodynamic models to predict metal toxicity rely on assumptions about metal binding and transport, it is important when evaluating the effect of pH on metal-microbe interactions to understand the cell membrane structure of bacteria. One of the most interesting and obvious characteristics of bacteria is that they are in constant interaction with their immediate environment. Specifically, the Gram-negative bacterial cell is enclosed by two bilayer membranes, an inner and outer membrane (Figure 1.3). The inner membrane (IM) is a phospholipid (PL) bilayer containing transmembrane and membrane bound proteins (MP) (White, 2000). The space between the inner and outer membranes, termed the periplasmic space or periplasm (P), contains peptidoglycan (Pg) which is anchored to

13
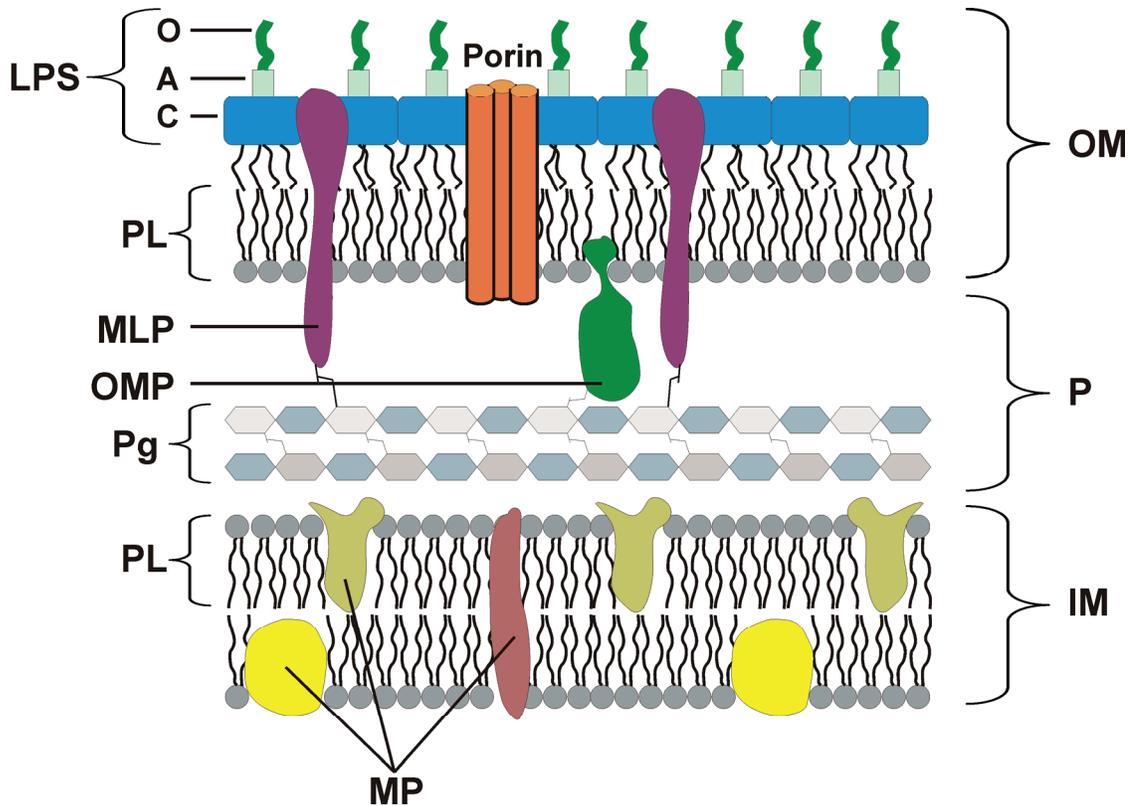
Figure 1.3. Gram-negative cell membrane structure. The Gram-negative cell wall is made of three sections: IM – inner membrane, P – periplasm, and OM – outer membrane. Also, within each section, specific constituents are labeled and discussed within the text.

the outer membrane through murein lipoproteins (MLP) harbored on the inner leaflet. The inner leaflet of the outer membrane is primarily comprised of phospholipids (PL), as well as outer membrane proteins (OMP), while the outer leaflet is mostly comprised of lipopolysaccharides (LPS). LPS is composed of a non-polar lipid A group (A) which anchors the LPS to the outer-membrane, with a core region (C) and polar oligosaccharide group (O) extending into the extracellular matrix (White, 2000). There are also transmembrane proteins in the outer membrane called porins that are thought to allow passive non-specific of solutes <600 daltons (Da) into the periplasm (Blencowe and Morby, 2003).

Effect of pH on cell membrane chemistry. The surface of the outer membrane of Gram-negative bacteria contains proton exchangeable functional groups that are responsible for giving bacterial cells a characteristic negative charge at circumneutral pH (Bayer and Sloyer, 1990). Attenuated total reflectance Fourier transform infrared (ATR-FTIR) spectroscopy has been used to directly analyze that the outer-membrane surface of two *Pseudomonas* spp., and found it possessed carboxyl, amide, phosphate and carbohydrate moieties (Jiang et al., 2004). Additionally, it was demonstrated that overall functional group composition was not altered by media or growth phase (Jiang et al., 2004). Similarly, potentiometric titration measurements have demonstrated that ionizable protonated sites on the Gram-negative cell surface possess distinct pKa values that correspond to carboxylic acids, phosphates, and hydroxyls (Fein et al., 1997). These distinct functional groups undergo protonation or deprotonation depending on pH changes of the extracellular matrix. When the pH is less than the pKa of a functional group, the majority of those groups will be protonated, while the inverse is true at pH

higher than the pKa of the functional group. This means that with varying pH the number of charged sites and the net charge on the outer membrane of a Gram-negative bacterium will change.

pH affects cellular processes. In addition to changes in metal speciation and chemistry of the cell membrane, pH can also alter cellular processes. For instance, DNA microarray analysis found that in *E. coli* stress response and transport genes were induced at lower pH which the author's speculate was responsible for decreased Cd^{2+} toxicity to *E. coli* at lower pH (Worden et al., 2009). Additionally, work by J. D. Van Nostrand utilized a proteomic approach to demonstrate that pH caused changes in protein profiles of PR1 as well as membrane composition (Van Nostrand, 2006). Since one of the major pitfalls in predicting metal toxicity to microorganisms is not being able to account for changes in metal ion sorption and transport, changes to fundamental cellular processes will complicate predictions further as toxicity results can be due to secondary effects of pH induced changes. This highlights the need to go beyond generating empirical evidence and develop a more complete understanding of metal-microbe interactions.

1.4. <u>Zinc – the good, bad and the nano</u>

Metal homeostasis in bacteria. Bacteria maintain levels of essential metal ions by mediating their import, sequestration and/or export (Blencowe and Morby, 2003). Bacterial essential nutrients include K, Mg, and Fe as well as other metals such as Mn, Co, Zn, Cu, and Mo in trace amounts (Perry and Staley, 1997). Metal co-factors are required for different functions ranging from the coordination of a wide-variety of ligands (e.g., Zn^{2+}) and redox capability (e.g., Fe^{3+}). Due to this requirement of metals in

bacterial metabolism, the import, intracellular trafficking and export of metal ions is highly regulated at the level of gene transcription (Nies, 1999). For example, production of Zn-specific pumps that import and export Zn^{2+} is regulated by femtomolar intracellular Zn^{2+} concentrations (Outten and O'Halloran, 2001). These highly regulated processes allow microorganisms to maintain constant intracellular metal concentrations essential to metabolism.

General mechanisms of metal toxicity to microorganisms. Above the required concentrations within the cell, metal ions can become cytotoxic through non-specific binding, displacement of essential metals required in essential enzymes, or by formation of reactive oxygen species (Nies, 1999). Non-specific protein binding can occur because metal cations can bind to sulfur groups on amino acids (Nies, 1999). Upon binding, allosteric protein inhibition can occur as the metal affects the tertiary structure. In many cases, the toxicity of a metal ion can be directly linked to the ability to bind sulfur (Nies, 1999). For example, in *E. coli* the minimum inhibitory concentrations (MIC) for different metals is directly related to the metal-sulfide association constant, i.e., a greater ability to bind sulfur resulted in increased toxicity (Nies, 1999). Additionally, metal ions can displace required metal ions from the active sites of essential enzymes resulting in protein inhibition (e.g., Cd^{2+} and Zn^{2+}; Sandrin and Maier, 2003). Any type of protein inhibition can result in DNA repair inhibition, loss of ATP production, or osmotic disruption as well as loss of other required cellular functions depending on the role of the inhibited protein (Nies, 1999). Lastly, metal ions can cause oxidative stress within the cell by binding glutathione and generating free radicals due to the generation of H_2O_2

(Kachur et al., 1998). Overall, the effects of high intracellular concentrations of metal ions, even essential metals, can be detrimental to cell survival.

Metal resistance in bacteria. Bacteria have developed mechanisms to tolerate high levels of metals and to reduce metal toxicity (Nies, 1999). This is accomplished by either making sensitive targets such as essential proteins less susceptible or by limiting the ability of metal ions to interact with sensitive targets within the cell (Nies, 1999). A potential mechanism to protect sensitive targets, such as an essential enzyme, is to upregulate production of chaperon proteins involved in protein refolding and protein structure protection (Mathew and Morimoto, 1998; Ybarra and Webb, 1998). Additionally, there are six classical mechanisms in bacteria to limit the exposure of metal ions to sensitive targets within the cell: (1) reduced uptake, (2) enhanced efflux, (3) internal sequestration in the periplasm or cytoplasm, (4) surface sequestration, (5) external sequestration, and (6) reduction (Hausinger, 1993). Each of these mechanisms allows bacteria to tolerate higher levels of metal ions. In summary, there are diverse mechanisms of metal resistance present in bacteria which allow them to tolerate high concentrations of metals by maintaining metal homeostasis.

pH-dependent metal toxicity to PR1. The Morris and Bertsch laboratories have previously studied the toxicity of first row divalent transition metals to PR1 and how pH affects metal toxicity (Van Nostrand et al., 2005; Van Nostrand, 2006; Van Nostrand et al., 2007; Van Nostrand et al., 2008). While most metal toxicity data in the literature are generated at circumneutral pH, many natural and anthropogenically-disturbed systems are at low pH. For this reason it is important to evaluate metal toxicity over a range of environmentally relevant pH. Interestingly, PR1 is approximately 20-fold more resistant

to Ni^{2+}, Co^{2+}, Cd^{2+}, and Zn^{2+} at pH 5 compared to pH 7 (Van Nostrand, 2006).

Increasing metal toxicity with increasing pH is counter to the FIAM which predicts that

the concentration of the free-ion concentration of a metal dictates its toxicity (Campbell,

1995). Increasing pH would generally lower the concentration of the free-ion while

increasing the concentration of hydroxo-metal species. However, according to the BLM,

more ionized sites are available on the cell membrane which would allow increased metal

binding sites (Fein et al., 1997) which may account for the observed toxicity according to

the BLM (Di Toro et al., 2001). In order to determine the mechanism of pH-dependent

metal toxicity to PR1, pH-dependent Ni toxicity was focused on specifically.

Initially the genome of PR1 was mined for Ni-resistance gene determinants. This

search showed that PR1 has genes involved in Ni-uptake and utilization such as UreE

which may aid in binding intracellular Ni, thereby lowering the intracellular Ni

concentration, but overall, no genes were present that could be specifically involved in

classic Ni-resistance mechanisms were found (Van Nostrand, 2006). Based on this

result, classical mechanisms of Ni-resistance in PR1 were evaluated with respect to their

ability to function between pH 5, 6, and 7. Potential mechanisms evaluated were: (1)

surface Ni-sequestration, (2) internal Ni-sequestration in the periplasm or cytoplasm, (3)

external Ni-sequestration, (4) reduced Ni-influx, and (5) enhanced Ni-efflux (Hausinger,

1993). The reduction of Ni^{2+} was not evaluated as this is unlikely under physiological

conditions (Nies, 1999).

Internal Ni sequestration was investigated by using ^{63}Ni as well as probing for

production of the cytoplasmic metal binding component polyphosphate which can form

intracellular metal-phosphate complexes (Suzuki and Banfield, 2004). It was found that

there was not a significant difference in ^{63}Ni sequestration or polyphosphate accumulation between pH 5 and 7 (Van Nostrand, 2006). External metal sequestration was also investigated by using size exclusion chromatography inductively coupled plasma mass spectroscopy (SEC-ICP-MS) to evaluate Ni-species in the supernatant of Ni exposed PR1. A Ni peak was identified correlating to ~500 Da, but this peak was also present in the media blanks (Van Nostrand, 2006). This did not eliminate the possibility that a similar sized Ni-binding species was being released by PR1 when exposed to Ni, therefore siderophore (small ferric iron scavenging molecules released by microorganisms; Drechsel and Jung, 1998) production was evaluated but was found to not be significant under experimental conditions (Van Nostrand, 2006). Ni-influx and efflux was also evaluated using ^{63}Ni. It was found that slightly more Ni influx occurred at pH 7 versus 5, though the difference was not statistically significant. Additionally, Ni-efflux occurred only at pH 7, which does not support the observed trend in pH dependent Ni toxicity (Van Nostrand, 2006). In conclusion, PR1 did not possess a classical mechanism of Ni resistance that might be more effective at different pH.

Further research using proteomics demonstrated that the observed pH-dependent metal resistance may be a secondary affect due to changes in cellular processes induced by pH. Since pH and the addition of Ni affects proteins related to cell shape and there were also changes in membrane composition (Van Nostrand, 2006), it appears that at lower pH PR1 may reduce the surface area of the cell exposed to extracellular metal ions while changes in membrane composition may affect the function of Ni-transporters as well as Ni-permeability. These observations may explain why PR1 is more resistant to Ni at pH 5 versus pH 7. Overall, this data about how PR1 responds to pH and high levels

of metals is complementary to the research of this dissertation which focused on how PR1 interacts with the required element Zn.

Zinc in the environment. Zinc (atomic number 30) has five stable isotopes with ^{64}Zn, ^{66}Zn, and ^{68}Zn being the most abundant. Zn is the 23rd most abundant element in the earth's crust at 20 to 200 mg kg^{-1} (Goodwin, 1998), ranging from <10 to 2000 mg kg^{-1} in uncultivated soils (mean 51 mg kg^{-1}; HazDat, 2006). Zinc occurs naturally in soil in varying concentrations as a result of the weathering of Zn-containing parent material. Zinc does not occur as elemental Zn but as 55 minerals, the three most commercially important being ZnS (sphalerite), $ZnCO_3$ (smithsonite) and $Zn_4Si_2O_7(OH_2):H_2O$ (hemimorphite) (HazDat, 2006). Additionally, in nature Zn exists in the Zn(0) and Zn(II) oxidation states, though the Zn(II) oxidation state is the most common (Lindsay, 1979).

Zn requirement and toxicity to humans. Zinc is a required nutrient for vertebrates, invertebrates and plants. In humans, Zn is the second most abundant trace metal found in the body, second to Fe (McCance and Widdowson, 1942). The chemistry of Zn makes it favorable in biochemical reactions. Zn is (1) relatively water-soluble under neutral conditions (2000 g L^{-1} for $ZnCl_2$; Merck Index, 1940), (2) has a full *d*-orbital, (3) does not undergo redox chemistry under physiological conditions, (4) can function as a Lewis acid, (5) does not prefer a specific coordination symmetry, and (6) rapidly exchanges ligands (Williams, 1987). This chemistry allows Zn to be involved in diverse biochemical processes and accordingly is a cofactor in over 300 enzymes (Vallee and Auld, 1990).

In humans, Zn has an average daily requirement of about 10 mg though the average American diet takes in 5 to 16 mg a day (HazDat, 2006). Zinc does not

accumulate in the human body and will normally exit the body in feces or urine (HazDat, 2006). High levels of Zn inhalation can cause metal fume fever and high short-term Zn intake through diet can cause gastrointestinal issues, while long-term exposures can cause anemia, and damage to the pancreas and kidney (HazDat, 2006). In the environment, Zn is present at 395 of 1,302 present and proposed EPA Superfund NPL sites (CERCLIS, 2009) and is ranked 74th on the 2007 CERCLIS Priority List of Hazardous Substances (CERCLIS, 2009). Zn is regulated in drinking water to 5 mg L^{-1} because of taste not health concerns to humans (HazDat, 2006). Overall, Zn is a required nutrient in humans and can cause negative health effects at high concentrations.

Zn toxicity to microorganisms. Due to the biologically useful chemistry and natural abundance of Zn, it is also an essential nutrient for microorganisms. In bacteria, *E. coli* has a Zn-requirement of 2 x 10^5 atoms per colony forming unit, or 0.2 mM intracellular Zn, which is roughly the same as Fe and Ca but less than Mg and K (Outten and O'Halloran, 2001). Unlike in humans, Zn can cause cell death to microorganisms when present at higher concentrations. Degrees of Zn-toxicity and Zn-resistance vary between microorganisms depending on their ability to maintain Zn-homeostasis. For example, *E. coli* has a minimum inhibitory concentration (MIC) of 1 mM Zn (Nies, 1999), while *Cupriavidus metallodurans* CH34 has a MIC of 12 mM Zn (Mergeay et al., 1985. In general, microorganisms must control intracellular metal concentrations because at higher concentrations metal ions can bind with proteins causing toxic effects by disrupting protein function (Nies, 1999). Specifically, Zn is known to inhibit the electron transport chain of *E. coli* by inhibiting NADH oxidase (Beard et al., 1995). Such

protein disruptions, as in the case of Zn uncoupling electron transport, can lead to the formation of reactive oxygen species and prove detrimental to microorganisms.

General Zn-resistance in Gram-negative bacteria. In microorganisms, Zn homeostasis is regulated by limiting influx into the cell, sequestration by metalloproteins and/or increased efflux from the cell (Blencowe and Morby, 2003). Gram-negative bacteria have both an inner and outer bilayer membrane which separates the cell into a periplasm within the envelope and cytoplasm inside of the inner membrane (Figure 1.3). Initially, Zn^{2+} can passively pass through the outer membrane to the periplasm through porins, which form a hydrophilic pore that allows solutes <600 Da passage (Blencowe and Morby, 2003). Once in the periplasm, Zn^{2+} is transported past the inner membrane through both unspecific-Zn and specific-Zn transporters.

Interestingly, many divalent cations have similar ionic diameters (149 ± 11 pm for Mn^{2+}, Fe^{2+}, Co^{2+}, Ni^{2+}, Cu^{2+} and Zn^{2+}) and therefore require highly specific uptake and efflux mechanisms (reviewed by Nies, 1999). Due to high requirement for Zn in cellular processes, internal Zn levels are highly regulated at the transcriptional level by activating or inactivating Zn-specific transporters (Figure 1.4: reviewed by Blencowe and Morby, 2003). This high degree of regulation is necessary since Zn can be toxic at high concentrations while too much Zn efflux would prove wasteful and detrimental to maintaining cellular metabolism. Furthermore, the ability of a bacteria cell to successfully maintain Zn homeostasis dictates their ability to resist higher levels of Zn (Nies, 1999; Choudhury and Srivastava, 2001; Hantke, 2001; Blencowe and Morby, 2003).

High Zn^{2+} concentration

Medium Zn^{2+} concentration
(Non-specific Zn-transport)

Low Zn^{2+} concentration

Zn^{2+} ... Porin ... CzcC ... B ... ZntA ... CzcD ... A ... CorA ... MgtA ... PitA ... ZnHPO$_4$ ... ZnuA ... B ... C

Porin

Outer Membrane

Periplasm

Inner Membrane

Cytoplasm

ATP ADP ... H$^+$ ... ATP ADP ... ZnHPO$_4$ ... ADP ATP

ZntR ... Zn^{2+} ... Zn^{2+} Zur ... zntA ... znuBC

Gene Regulation

ZntR ... Zur ... zntA ... znuBC
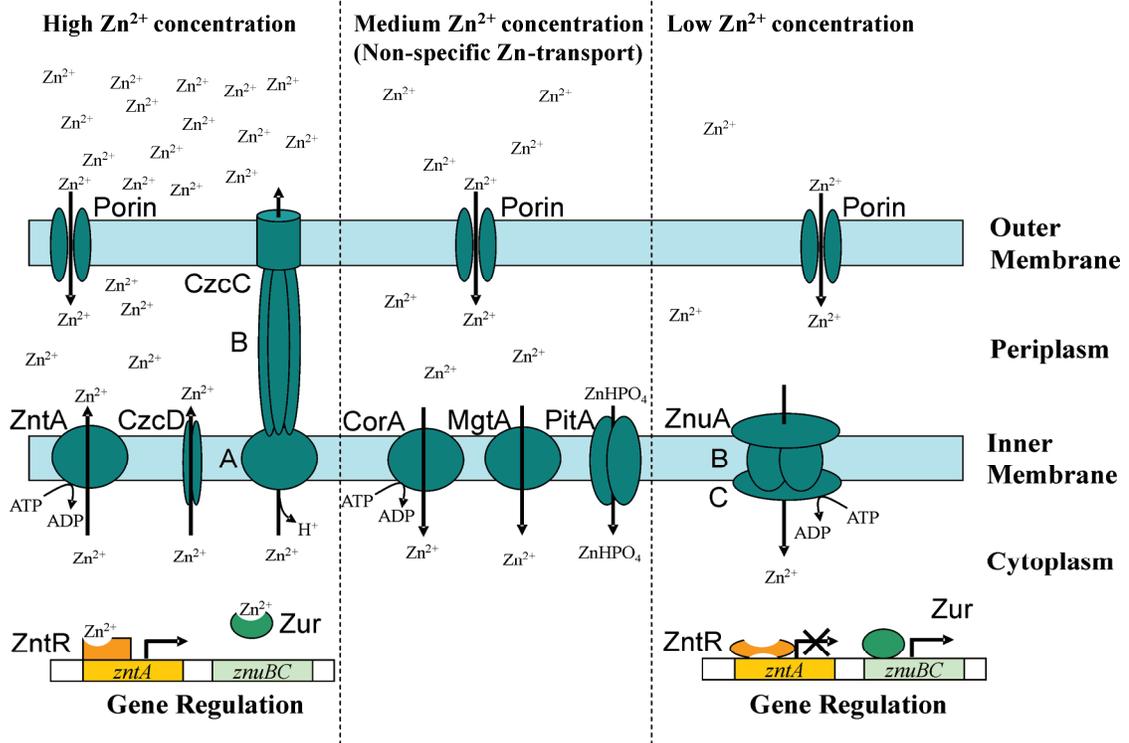
Gene Regulation

Figure 1.4. Pathways and regulation of Zn-transport in Gram-negative bacteria.
Zn is able to enter the periplasm through porins at which point it can enter the cytoplasm through Zn-specific or non-specific influx. Zn-specific influx occurs under low Zn^{2+} concentrations by ZnuABC, a P-type ATPase, which is regulated by the transcription factor Zur. Zn-non-specific influx can occur at all Zn-concentrations but is only shown above during medium Zn^{2+} concentrations. This occurs by transporters responsible for Mg^{2+} or PO$_4^{3-}$ influx. Zn-specific efflux is upregulated during high Zn^{2+} concentrations (e.g., ZntR regulation of ZntA, a P-type ATPase). ZntA and CzcD transport Zn^{2+} into the periplasm while CzcCBA transports Zn^{2+} directly past the outer membrane through chemiosmotic transport. (adapted from Hantke, 2001)

Table 1.2. Zn-resistance determinants in G4. COGS (clusters of orthologous groups) comparison was used to determine each gene designation and BestBLAST vs. SwissProt/TREMBLE Hit was used to determine closet gene homology in other organisms (ORNL, 2007). Gene numbers are prefixed with Bcep1808 in the final annotation.

Gene #	Gene	Description	Organism	% homology
Non-specific Zn influx				
5272	MgtA	Mg^{2+} transport ATPase	*Burkholderia pseudomallei*	82
1954	CorA	Mg^{2+} and Co^{2+} transporters	*Burkholderia pseudomallei*	77
3937	CorA	Cor-A like Mg^{2+} transporters	*Burkholderia pseudomallei*	77
6558	PitA	phosphate/sulfate permease	*Burkholderia pseudomallei*	80
Inducible Zn-specific influx				
7780	Fur	Fe^{2+}/Zn^{2+} uptake regulation	*Burkholderia pseudomallei*	85
3325	Fur	Fe^{2+}/Zn^{2+} uptake regulation	*Burkholderia cepacia*	100
7783	ZnuB	ABC-type Mn^{2+}/Zn^{2+} transport system permease	*Burkholderia pseudomallei*	88
3747	ZnuC	ABC-type Mn/Zn transport system ATPase	*Mycobacterium bovis*	40
7782	ZnuC	ABC-type Mn/Zn transport system ATPase	*Burkholderia mallei*	83
Inducible Zn-specific efflux				
4759	ZntA	cation transport ATPase	*Chromobacterium violaceum*	52
3202	ZntA	cation transport ATPase	*Burkholderia pseudomallei*	72
5568	ZntA	cation transport ATPase	*Cupriavidus metallidurans*	75
6118	ZntA	cation transport ATPase	*Cupriavidus metallidurans*	80
6184	ZntA	cation transport ATPase	*Burkholderia pseudomallei*	69
7468	ZntA	cation transport ATPase	*Burkholderia mallei*	72
5479	CzcD	Co/Zn/Cd efflux system component	*Burkholderia pseudomallei*	74
1275	CzcR	transcriptional activator protein	*Alcaligenes eutrophus*	67
1277	CzcS	transmembrane sensory transduction kinase	*Alcaligenes eutrophus*	41
4761	MMT1	Predicted Co/Zn/Cd cation transporter (CDF)	*Chromobacterium violaceum*	66
7533	MMT1	Predicted Co/Zn/Cd cation transporter (CDF)	*Burkholderia pseudomallei*	75

In addition to possessing determinants for As, Cu, Cr, Co, Ni, Zn, Te and Cd resistance, many genes involved in maintaining Zn homeostasis have been identified within the genome of PR1's parent strain, G4 (Table 1.2). Although the activity of these gene products have not been experimentally confirmed in G4 or PR1, these determinants are predicted to be involved in non-specific Zn-influx, and inducible Zn-specific influx and efflux (Figure 1.4). By using the identity of these genes, the influx and efflux of Zn in PR1 can be predicted.

Non-specific Zn influx in PR1. Extracellular Zn^{2+} could passively enter the periplasm through porins. Once in the periplasm, Zn^{2+} can be non-specifically transported into the cytoplasm by Mg (CorA and MgtA) and inorganic phosphate (P_i) transporters (PitA) present in the genome of G4 (Figure 1.4; Table 1.2). CorA and MgtA can transport Zn^{2+} into the cytoplasm non-specifically because the hydrated Mg^{2+} ion has the largest hydrated radius of all biologically relevant divalent cations (Smith et al., 1995). CorA is found throughout bacteria and in *E. coli*, CorA is constitutively expressed and is responsible for Mg^{2+} as well as Ni^{2+}, Co^{2+} and Zn^{2+} influx (Blencowe and Morby, 2003). MgtA is induced under Mg limiting conditions and is a slower P-type ATPase. In *Salmonella typhimurium*, MgtA has been found to transport Zn better than Mg^{2+} (Snavely et al., 1989). When Zn^{2+} is bound to inorganic phosphate (P_i), it can transport into PR1 via the constitutive non-specific inorganic phosphate transport system, PitA. In *E. coli*, when PitA was disrupted, it was resistant to higher levels of Zn (2.5 mM) than the wild-type (1 mM) due to reduced intracellular Zn^{2+} accumulation (Nies, 1999; Beard et al., 2000). Overall, in PR1, CorA, MgtA, and PitA would allow Zn^{2+} to non-specifically

enter the cytoplasm indicating that PR1 must regulate Zn-homeostasis at the point of Zn-specific influx and efflux.

Inducible Zn-specific influx and efflux. Zinc ions also enter the cytoplasm under Zn-limiting conditions via the inducible, slower, and more specific ATP-dependent transport system ZnuBC (Table 1.2; Blencowe and Morby, 2003; Nies, 2003). ZnuBC expression is regulated by the transcriptional regulator Zur. During normal to high Zn^{2+} levels, Zur binds Zn^{2+} and this complex binds the promoter of *znuBC*, blocking transcription of ZnuBC (Figure 1.4; Patzer and Hantke, 1998; Outten and O'Halloran, 2001). The complete ZnuABC transport system is a high-affinity ABC (ATP binding cassette) Zn-transporter. In this system ZnuA and ZnuB are the periplasmic and membrane components, respectively, and ZnuC is the ATPase subunit (Patzer and Hantke, 1998). G4 possesses genes for Zur, ZnuB and ZnuC though ZnuA has not been identified in the genome of G4 (Table 1.2; ORNL, 2007).

The Zn-influx activity of ZnuABC is counteracted by ZntA dependent Zn-efflux. ZntA is a P-type ATPase which works by coupling ATP hydrolysis to Zn from the cytoplasm to periplasm (Beard et al., 1997; Sharma et al., 2000). Expression of ZntA is regulated by ZntR, which was not identified in the G4 genome (Table 1.2; ORNL, 2007). ZntR is a member of the MerR transcription regulator family and is predicted to stay bound to the *zntA* promoter, down-regulating expression, until Zn^{2+} binds causing a change in confirmation which allows transcription to proceed (Figure 1.4; Brocklehurst et al., 1999). Interestingly, in *E. coli* the overlap of the concentration required for Zur and ZntR activation is 0.5 fM Zn, which is less than one Zn atom per colony forming unit

(Outten and O'Halloran, 2001). This high degree of Zn regulation illustrates the cell's requirement to maintain very specific free Zn^{2+} concentrations within the cell.

Another Zn-transport protein present in the genome is CzcD (Table 1.2). CzcD is a cation diffusion facilitator (CDF) transporter driven by a proton gradient or K^+ from the cytoplasm to periplasm. CzcD was originally discovered in the Zn-resistance bacteria *Cupriavidus metallidurans* CH34 (CH34), and has been found to transport Cd^{2+}, Zn^{2+} and Co^{2+} (Mergeay et al., 1985). The expression of CzcD is regulated by the *czcDRSE* operon. G4 possesses CzcD and CzcRS, but CzcE has not been identified in the annotated genome (Table 1.2). In CH34, the *czcDRSE* operon is under the control of a classic two-component R/S sensor activator system which involves a sensor kinase (S) and response regulator transcription factor (R). The sensor kinase autophosphorlyates upon binding Zn^{2+} and then phosphorylates the response regulator which in turn activates transcription of CzcD (Mergeay et al., 1985; van der Lelie et al., 1997). Neither ZntA or CzcD have been found to confer resistance at high (>1 mM) Zn concentrations when inserted into *E. coli* (Legatzki et al., 2003; Anton et al., 2004), but it is interesting to note that the genome of G4 contains six copies of homologs to ZntA and three copies of CDF transporters (Table 1.2). It is unknown how many copies of each Zn-exporter are expressed in PR1, but this could be a potential Zn-resistance mechanism.

CzcCBA. In addition to Zn^{2+} efflux from the cytoplasm to the periplasm, Zn^{2+} can be directly transported beyond the periplasm by the tri-component chemiosmotic efflux RND (resistance-nodulation-cell division) system, CzcCBA, through proton-motive force. CzcCBA in CH34 was the first member of the RND family identified (Saier et al., 1994) and is capable of exporting Co^{2+}, Zn^{2+} and Cd^{2+} (Mergeay et al.,

1985). CzcA is the RND proton pump, CzcB is the membrane fusion protein and CzcC is the outer membrane component (Nies, 2003). CzcCBA allows CH34 to grow in the presence of 12 mM Zn (Mergeay et al., 1985) though CzcD and ZntA (mentioned above) may be responsible for some of this Zn resistance (Legatzki et al., 2003; Anton et al., 2004). *czcCBA* has not been identified in the genome of G4, but it is interesting that CzcCBA is induced by the afore mentioned *czcDRSE* operon.

Intracellular Zn trafficking. Once inside the cytoplasm, Zn is predicted to not exist in free pools of Zn^{2+} but bound by various metallo-chaperones, including metallothioneins and trafficked within the cell to where Zn^{2+} is required (Outten and O'Halloran, 2001; Blencowe and Morby, 2003). A survey of the G4 genome does not reveal any metallothioneins but does include predicted Zn-metalloenzymes (ORNL, 2007). Zn-trafficking within the bacterial cell in general is not well understood. Outten and O'Halloran (2001) attempted to predict where Zn is bound within the cell by coupling bioinformatic data to a measured Zn quota of an *E. coli* cell. They predicted that 12% of the 0.2 mM intracellular Zn requirement of *E. coli* is bound to 8 proteins, with the majority bound to RNA polymerase and five tRNA synthetases. An unknown amount of Zn was predicted to be tightly bound by 40 different proteins, with any remaining Zn^{2+} associating with 10^{21} predicted low-affinity non-Zn specific binding sites in proteins, amino acids and nucleotide sequences in the genome of *E. coli* (Outten and O'Halloran, 2001). In addition to these Zn-binding sites, Gram-negative bacteria maintain an intracellular concentration of approximately 10 mM glutathione (Fahey, 2001), which is proposed to bind Zn^{2+} when in excess (Nies, 2003). Overall, it is

apparent that there is an overabundance of potential Zn-binding sites within *E. coli* cell and this information can be extrapolated to Zn-trafficking in PR1.

With such high Zn-binding capacity within the bacterial cell, regulation of pools of bound Zn under Zn-excess or limiting conditions must be highly regulated. Under conditions of Zn-excess in *E. coli*, it was found that 9 of 26 upregulated genes were involved in cysteine synthesis which may serve to bind free Zn^{2+} to thiol groups (Yamamoto and Ishihama, 2005). Furthermore, under Zn-limiting conditions in *E. coli*, non-Zn binding ribosomal protein paralogs are expressed that remain functional despite their Zn-deficiency. This may increase intracellular Zn^{2+} levels by allowing Zn-containing ribosomes to be degraded or by decreasing the Zn^{2+} demand from ribosomes (Panina et al., 2003). These mechanisms may allow microorganisms to store Zn^{2+} but may also play a role in Zn-resistance through internal Zn-sequestration.

Zinc oxide nanoparticle. In contrast to wealth of information about Zn regulation and toxicity in bacteria, less is known about how bacteria interact with NPs. With the rapid growth of the nanotechnology industry which produced materials used in $147 billion of goods in 2007 and more than 803 products or product lines in 2008 (Bradley, 2008; Maynard and Michelson, 2008), their inevitable release into the environment becomes inevitable. Zinc oxides comprise one of the most diverse families of nanostructures, with ZnO-NP commonly used in sunscreens, personal care products, and biological and chemical sensors (Wang, 2004b). ZnO-NP has also been found to be toxic to microorganisms (Yamamoto, 2001; Adams et al., 2006; Brayner et al., 2006; Reddy et al., 2007; Zhang et al., 2007; Heinlaan et al., 2008; Jones et al., 2008; Mortimer et al., 2008; Nair et al., 2008).

ZnO-NP chemistry. In its bulk form, ZnO has historically been used as a catalyst in making rubber as well as to slow rubber aging (HazDat, 2006) and in sunscreens and cosmetics as a UV block. Relative to bulk ZnO, ZnO-NP has greater surface reactivity per volume of ZnO increases due to an increased surface area to volume ratio. This allows established manufactured products and processes utilizing ZnO to use ZnO-NP in lower quantities than bulk ZnO. This is one reason for the development and use of ZnO-NP, but ZnO-NP has piezoelectric and pyroelectric properties not found in bulk ZnO that make it valuable as the most diverse family of nanomaterials.

ZnO is a wurtzite structure along with GaN, AIN, ZnS, and CdSe and its structure consists of alternating planes of tetrahedrally coordinated Zn^{2+} and O^{2-} (Figure 1.5). Due to its crystalline asymmetry and resulting polar faces, ZnO has inherent piezoelectric and pyroelectric properties (Wang, 2004a). Along with its intrinsic semi-conducting properties, this makes ZnO unique and valuable for its diversity of applications. Additionally, the polar surfaces of the unit cell structure are stable and allow nanoscale growth into a multitude of structures including nanocombs, -rings, -helixes/-springs, -belts, -wires, and -cages (Wang, 2004b). Many of these structures can be created easily by solid-vapour processes (Wang, 2004a). Taken together, these characteristics make ZnO one of the most useful and versatile families of nanomaterials.

General NP toxicity to microorganisms. Since a wide range of NPs are antibacterial to Gram-negative and Gram-positive bacteria (reviewed by Klaine et al., 2008 and Neal, 2008) and it has been suggested that NPs could alter the ability of microbial populations to function in key ecological processes (Neal, 2008). To address
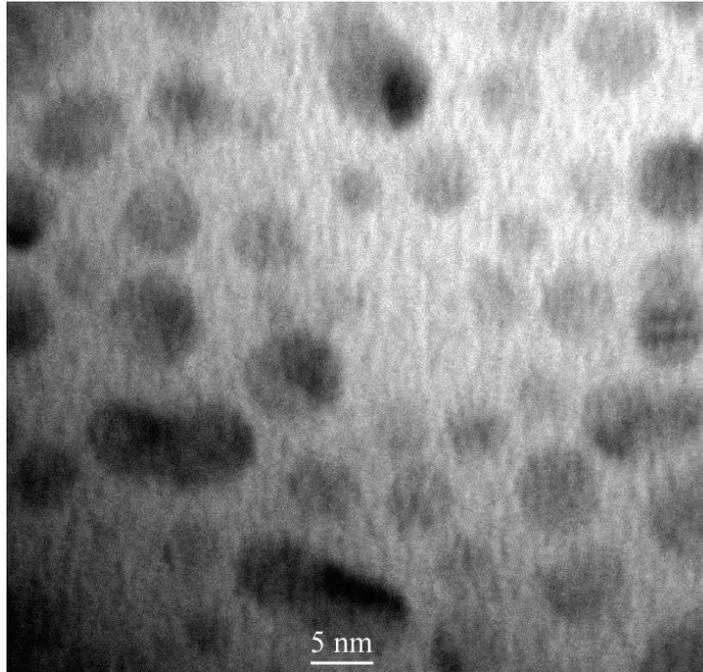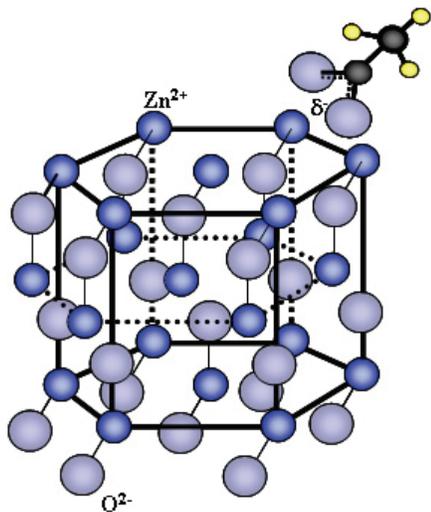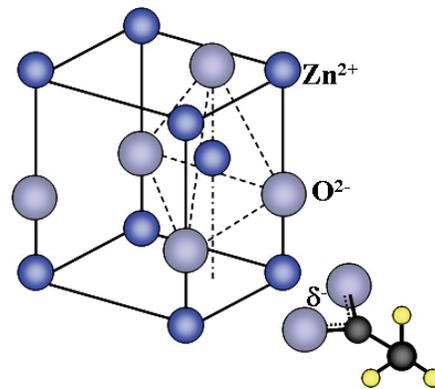
Figure 1.5. Structure of ZnO-NP. (A) TEM of 4 nm ZnO-NP. **(B)** The crystalline unit structure of ZnO demonstrating the lack of symmetry as well as illustrating the polar faces. Acetate is shown coordinating an exterior Zn atom. **(C)** The wurtzite unit cell structure of ZnO demonstrating its piezoelectric properties. Acetate is shown coordinating an exterior Zn atom. (B and C adapted from Wang, 2004a and Wang, 2004b)

these concerns, studies have demonstrated that dosing of soils with C_{60}-fullerene and marine sediments with Ag-NPs do not have a significant effect on the microbial population or their function (Tong et al., 2007; Bradford et al., 2009). A recent study of Au-nanorod partitioning in estuarine mesocosms found that the vast majority of Au-nanorods become associated with biofilms but biological effects were not evaluated (Ferry et al., 2009). In response to the potential toxicity of NPs released into the environment, the EPA began regulating Ag-NPs used as bactericide in 2006 (Weiss, 2006), though to the author's knowledge manufactured NPs have not been detected in the environment.

While the diversity of NP compositions and formulations make it difficult to extrapolate observations between different NPs and microorganisms, there are proposed mechanisms of NP toxicity to microorganisms (reviewed by Klaine et al., 2008). These include: (1) oxidative damage from photocatalytic activation of NPs (Adams et al., 2006), (2) sorption onto cell walls either causing cell aggregation or damage to membrane stability (Stoimenov et al., 2002; Sondi and Salopek-Sondi, 2004), and (3) transport into the cell where NP dissolution can occur resulting in toxicity from primary NP components (Xu et al., 2004; Kloepfer et al., 2005). Additionally, some studies have indicated that the composition, size, shape, and preparation of NPs influence observed biological effects (Cho et al., 2005; Adams et al., 2006; Sayes et al., 2006; Nair et al., 2008). Furthermore, NP uptake and/or toxicity to microorganisms can be influenced by the use of counter-ions (Hirschey et al., 2006), detergents (Cho et al., 2005), surfactants (Nair et al., 2008) or proteins (Kloepfer et al., 2005) used as surface stabilizers.

ZnO-NP toxicity to bacteria. There have been nine studies to date which investigated the toxicity of ZnO-NP to bacteria, and all have demonstrated that ZnO-NP can be toxic to bacteria (Yamamoto, 2001; Adams et al., 2006; Brayner et al., 2006; Reddy et al., 2007; Zhang et al., 2007; Heinlaan et al., 2008; Jones et al., 2008; Mortimer et al., 2008; Nair et al., 2008; Gajjar et al., 2009; Guy et al., 2009; Hu et al., 2009; Jiang et al., 2009). In some cases ZnO-NP has been shown to be more toxic to bacteria than other metal-oxide NPs (Hu et al., 2009; Jiang et al., 2009). It is unclear what the mechanism of ZnO-NP toxicity is to bacteria, but it has been postulated that it involves free radical formation. When Zn^{2+} has been used as a reference toxicant, results have demonstrated that ZnO-NP is not more toxic to bacteria than Zn^{2+} (Gaijjar et al., 2009; Heinlaan et al., 2008; Jiang et al., 2009; Mortimer et al., 2008). This suggests that ZnO-NP toxicity may be due to indirect toxicity from Zn^{2+} which would result from ZnO-NP dissolution, yet only a few studies have measured ZnO-NP dissolution (Franklin et al., 2007; Heinlaan et al., 2008; Huang et al., 2008; Jiang et al., 2009). Overall, ZnO-NP is an emerging potential contaminant and a solid understanding of Zn-microbe interactions is required to interpret these toxicological results.

1.5. <u>Membrane vesicles</u>

Bacteria have evolved to tolerate high concentrations of metal ions by utilizing resistance mechanisms which broadly limit the exposure of sensitive targets such as proteins to metals (Nies, 1999). The most common mechanism of resistance involves efflux, and Zn-efflux is predicted to occur in PR1 based on determinants in its genome (Table 1.2). Additional mechanisms of metal resistance rely on sequestering metals

internally, on the membrane surface and externally (Hausinger, 1993). Internal

sequestration can occur by binding excess metal ions in the cytoplasm to compounds

such as polyphosphate, which in the case of *Arthrobacter ilicis* resulted in uranyl

phosphate granules (Suzuki and Banfield, 2004). Intracellular metal deposits in bacteria

can also include non toxic metal species such as Co and Se (Langley, 2006).

Extracellular sequestration of metals through the release of a chelating compound such as

proteins (Kurek et al., 1991) or extracellular polysaccharides (EPS; Kamashwaran and

Crawford, 2003), can decrease metal toxicity by decreasing the extracellular metal ion

concentration (reviewed by Gadd, 2004). In a similar manner, bacterial biofilms are

more resistant to metals (Teitzel and Parsek, 2003). These sequestration mechanisms

represent key processes by which bacteria interact with their environment beyond

molecular changes within the cell (e.g., efflux) and for the majority of this dissertation we

will be investigating whether membrane vesicles (MVs) play a role in metal-microbe

interactions.

In Gram-negative bacteria, are constitutively produced extracellular structures

derived from the outer membrane, and range in size from 50 to 250 nm in diameter

(Figure 1.5; Beveridge, 1999). Every Gram-negative bacterium that has been evaluated

for MV production has been found to produce them, implying it is a conserved

phenotype, and some Gram-positives and Archea have also been shown to produce MVs

(Table 1.3). Membrane vesicles were first described more than 40 years ago in *E. coli*

and *Vibrio cholerae* (Knox et al., 1966; Chatterjee and Das, 1967). The composition of

MVs generally reflects the outer membrane and periplasm of the vesiculating cell and

consists of phospholipids, LPS, outer membrane proteins, DNA, RNA, as well as a
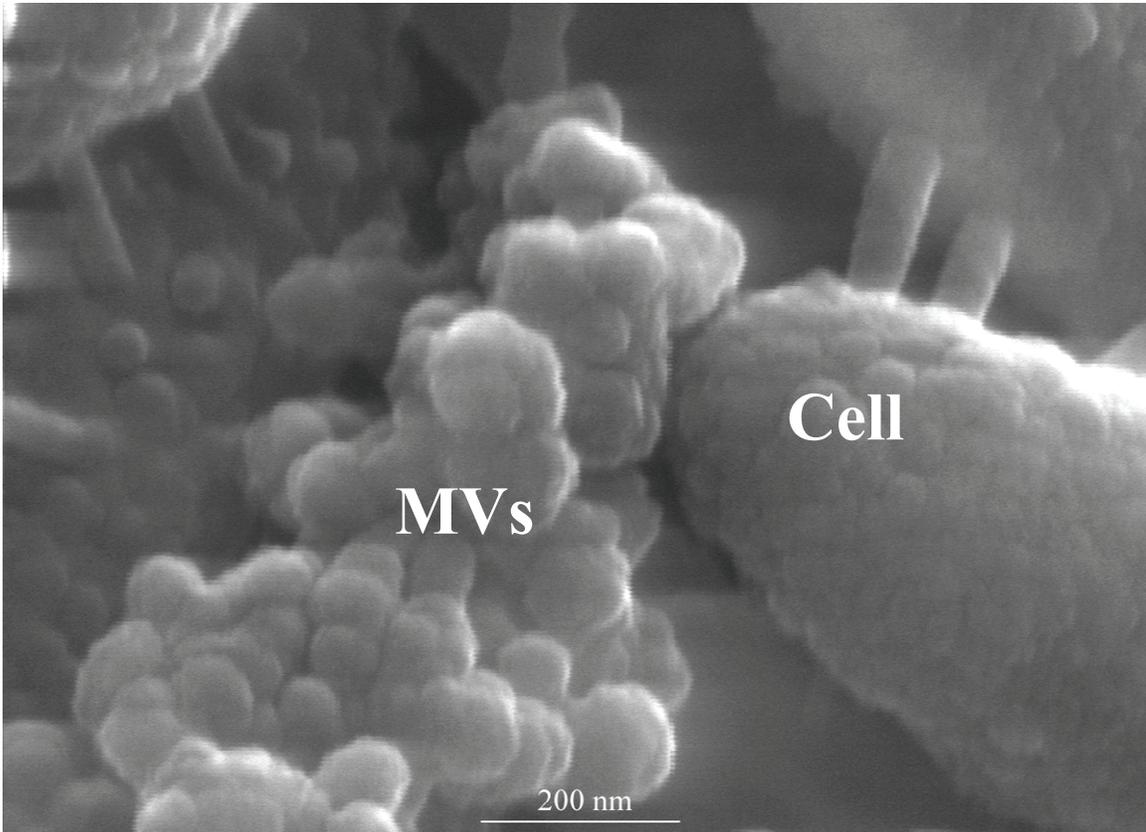
Figure 1.6. Scanning electron micrograph of PR1 cells and associated MVs. The size of PR1 cells is typically 2 μm by 0.5 μm while associated MVs typically range from 25 nm to 150 nm in diameter. The structures linking the cells together are pili.

Table 1.3. Microorganisms known to produce MVs. Microorganisms are grouped by genus with their respective references.

Microorganism	Reference (s)
Gram-negative	
Aeromonas sp.	(Kadurugamuwa and Beveridge, 1997)
Aggregatibacter (*Actinobacillus*) *actinomycetem-comitans*, *A. pleuropnemoniae*	(Karched et al., 2008), (Negrete-Abascal et al., 2000)
Agrobacterium tumefaciens	(Dorward and Garon, 1990)
Aquaspirillum spp.	(Kadurugamuwa and Beveridge, 1997)
Azolla microphylla associated cyanobacteria	(Zheng et al., 2009)
Bacteroides buccae, *B. fragilis*, *B. succinogenes*, *Bacteroides* spp.	(Williams and Holt, 1985) (Patrick et al., 1996) (Forsberg et al., 1981)
Bordetella pertussis	(Dorward and Garon, 1990)
Borrelia burgdorferi	(Whitmire and Garon, 1993)
Brucella melitensis	(Gamazo and Moriyon, 1987)
Burkholderia cepacia, *B. cenocapacia*, *B. vietnamiensis*	(Allan et al., 2003), (Smirnova et al., 2008)
Campylobacter jejuni	(Logan and Trust, 1982)
Citrobacter freundii	(Li et al., 1998)
Escherichia coli (incl. enterohemorrhagic, enterotoxigenetic, extraintestinal pathogenic, and uropathogenic)	(Lee et al., 2007) (Wai et al., 2003) (Yokoyama et al., 2000) (Berlanda Scorza et al., 2008) (Kouokam et al., 2006)
Enterobact agglomerans	(Li et al., 1998)
Haemophilus influenzae, *H. parainfluenzae*	(Kahn et al., 1983; Dorward and Garon, 1990)
Helicobacter pylori	(Keenan and Allardyce, 2000)
Klebsiella pneumoniae	(Li et al., 1998)
Legionella pneumophila	(Fernandez-Moreira et al., 2006)
Magnetospirillum sp.	(Kadurugamuwa and Beveridge, 1997)
Mogranella morganii	(Li et al., 1998)
Moraxella osloensis	(Dorward and Garon, 1990)
Myxococcus xanthus	(Palsdottir et al., 2009)
Neisseria gonorrhoeae, *N. meningitidis*	(Dorward et al., 1989; Post et al., 2005)
Porphyromonas (*Bacteroides*) *gingivalis*, *Bacteroides asaccharolyticus*, *B. endodontalis*	(Mayrand and Holt, 1988)
Proteus vulgaris	(Li et al., 1998)
Psuedoalteromonas antarctica NF3	(Nevot et al., 2006)
Psuedomonas aeruginosa strains: PAO1, soil isolate, and CF isolates	(Bauman and Kuehn, 2006)
Psuedomonas putida, *P. trifoli*	(Li et al., 1998; Kobayashi et al., 2000)
Salmonella arizonae, *S. cholera-suis*, *S. pullorum*, *S. typhimurium*	(Dorward and Garon, 1990; Li et al., 1998)
Serratia marcescens	(Li et al., 1998)
Shewenella oneidensis MR-1, *S. putrefaciens* CN32	(Gorby et al., 2008)
Shigella dysenteriae, *S. flexneri*	(Dorward and Garon, 1990)
Treponema denticola	(Rosen et al., 1995)
Vibrio anguillarum, *V. cholerae*, *V. parahaemolyticus*	(Chatterjee and Das, 1967; Kondo et al., 1993; Hong et al., 2009)
Xanthomonas campestris pv. *campestris*	(Sidhu et al., 2008)
Xenorhabdus nematophilus	(Khandelwal and Banerjee-Bhatnagar, 2003)
Yersinia pestis	(Dorward and Garon, 1990)

Table 1.3. – continued

Microorganism	Reference (s)
Gram-positive	
Bacillus cereus, *B. subtilis*	(Dorward and Garon, 1990)
Thermoanaerobacterium thermosulfurogenes EM1	(Mayer and Gottschalk, 2003)
Archaea	
Ignicoccus sp. strain KIN4I	(Nather and Rachel, 2004)
Sulfolobus acidocaldarius, *S. solfataricus*, *S. tokodaii*	(Ellen et al., 2009)
Sulfolobus spp.	(Prangishvili et al., 2000)
Thermococcus spp.	(Soler et al., 2008)

diverse proteome (reviewed by Lee et al., 2008). This diverse composition allows MVs

to function in virulence factor transport (Kadurugamuwa and Beveridge), protein (Ciofu

et al., 2000) and DNA exchange (Yaron et al., 2000), cell-cell communication (Mashburn

and Whiteley, 2005), biofilm formation (Schooling and Beveridge, 2006), and

modulating host-pathogen interactions (Ismail et al., 2003). In contrast to typical

secretion mechanisms, MVs allow bacteria to disseminate components into the

extracellular matrix and cause interactions independent of the cell (Bomberger et al.,

2009).

     Observed and predicted MV functions. The last 15 years have seen an

increasing focus on the function of MVs, mostly with respect to their role in bacterial

pathogenesis and bacteria-bacteria transport. Pathogenic bacteria can transport virulence

factors in MVs, which can include proteases, toxins, and autolysins (reviewed by Kuehn

and Kesty, 2005). Releasing virulence factors in MVs appears more efficient than typical

secretion mechanisms since it eliminates the need for direct pathogen-host interaction and

provides a vector that shields the components from degradation. Additionally, packaging

of certain toxins into MVs increases the toxin activity to host cells, such as a ClyA and

VacA in *E. coli* and *Helicobacter pylori*, respectively (Wai et al., 2003; Chitcholtan et al.,

2008). Furthermore, a recent study demonstrated that MVs from *P. aeruginosa* contain

multiple virulence factors (β-lactamase, hemolytic phospholipase C, alkaline

phosphatases and Cif) that are released into host cells in a coordinated 'attack' and

theoretically would promote host-colonization (Bomberger et al., 2009). These results

and work by others (Bauman and Kuehn, 2006) suggest that bacteria are able to sort

specific proteins into MVs, though the mechanism by which this occurs is unknown.

In addition to transporting toxins between pathogen and host, MVs are also capable of delivering components between bacteria, either in a beneficial or predatory role. Membrane vesicles can benefit bacterial populations by facilitating the transfer of proteins and DNA. The benefit of transporting these components inside MVs is that they can be protected from the extracellular matrix which can contain proteases and nucleases. One of the more interesting cases of beneficial protein exchange via MVs is the transfer of β-lactamase between *P. aeruginosa* cells (Ciofu et al., 2000) which theoretically could confer protection to cells that are sensitive to β-lactam antibiotics. Likewise, MVs from many bacteria have been found to contain DNA (Table 1.4), for example MVs produced by *E. coli* O157:57 contained virulence genes (Kolling and Matthews, 1999), but it is unclear whether this DNA can successfully be exchanged between cells. The potential of MVs as transformative vectors has only been confirmed in *E. coli* (Yaron et al., 2000), *Haemophilus influenzae* (Kahn et al., 1983) and *N. gonorrhoeae* (Dorward et al., 1989). Lastly, MVs can function in predatory roles to other bacteria via delivery of toxins and proteases, and would be advantageous in the environment during niche competition (Li et al., 1998). Overall, the importance of transporting cargo in a concentrated and protected manner makes MVs an efficient mechanism of bacteria to disseminate material into the extracellular environment.

Influences on MV function and production. One of the more interesting and confounding characteristics of MVs is their diversity of functions. Even between strains of the same bacterium, MVs can have different functions. For example, a study of MVs produced by five clinical *Burkholderia* spp. found that MVs from each species had differences in protein and enzymatic activity (Allan et al., 2003). Similarly, a proteomic

Table 1.4. Microorganisms known to produce DNA-containing MVs. References are given for each microorganism.

Microorganism	Reference
Agrobacterium tumefaciens	(Dorward and Garon, 1990)
Azolla microphylla associated cyanobacteria	(Zheng et al., 2009)
Bordetella pertussis	(Dorward and Garon, 1990)
Escherichia coli O157:H7	(Kolling and Matthews, 1999)
Escherichia coli O157:H7	(Yaron et al., 2000)
Escherichia coli 11775	(Dorward and Garon, 1990)
Haemophilus influenzae	(Kahn et al., 1983)
Haemophilus influenzae	(Dorward and Garon, 1990)
Haemophilus parainfluenzae	(Dorward and Garon, 1990)
Moraxella osloensis	(Dorward and Garon, 1990)
Neisseria gonorrhoeae	(Dorward et al., 1989)
Neisseria gonorrhoeae	(Dorward and Garon, 1990)
Pseudomonas aeruginosa 10145	(Dorward and Garon, 1990)
Psuedomonas aeruginosa H103 and ATCC 19660	(Kadurugamuwa and Beveridge, 1995)
Psuedomonas aeruginosa PAO1	(Renelli et al., 2004)
Psuedomonas aeruginosa PAO1	(Schooling et al., 2009)
Salmonella typhimurium	(Dorward and Garon, 1990)
Serratia marcescens	(Dorward and Garon, 1990)
Shigella dysenteriae	(Dorward and Garon, 1990)
Shigella flexneri	(Dorward and Garon, 1990)
Yersinia pestis	(Dorward and Garon, 1990)

investigation of MVs produced by clinical and environmental strains of *P. aeruginosa* demonstrated that MVs produced by each strain had different proteomic compositions (Bauman and Kuehn, 2006). Additionally, different bacteria seem to produce different quantities of MVs, but due to differences in MV quantification, this evidence is largely anecdotal.

MV formation. Although many functions of MVs have been reported, surprisingly little is know about the mechanism of MV formation. Presently there are three proposed mechanisms of formation (Figure 1.7; reviewed by Mashburn-Warren and Whiteley, 2006). **(Mechanism 1)** MV formation occurs due to detachment of the outer membrane from the peptidoglycan anchor in the periplasm. This occurs in specific regions of the membrane and causes a localized detachment of the outer membrane which eventually gets blebbed off. Support for this theory was recently established by Deatherage et al. (2009) when they demonstrated that altering proteins involved in connecting the outer membrane to the peptidoglycan (i.e., lipoproteins) or inner membrane (i.e., Tol-PAL complexes) resulted in increased vesiculation in a *Salmonella* sp. Moreover the authors postulated that MV production via this detachment can occur during cell membrane remodeling and during cell division, with the latter possibly allowing for the cell to sort specific proteins into the forming MV. **(Mechanism 2)** MV formation occurs due to outward pressure from the periplasm. This theory is supported by experiments which have shown that lower peptidoglycan turn over in *Porphyromonas gingivalis* results in increased MV formation (Hayashi et al., 2002), as well as the work by McBroom et al. (2007) which demonstrated that over-expressed nonsense proteins (i.e., misfolded) where exported from the cell by MVs, and that MV production

42
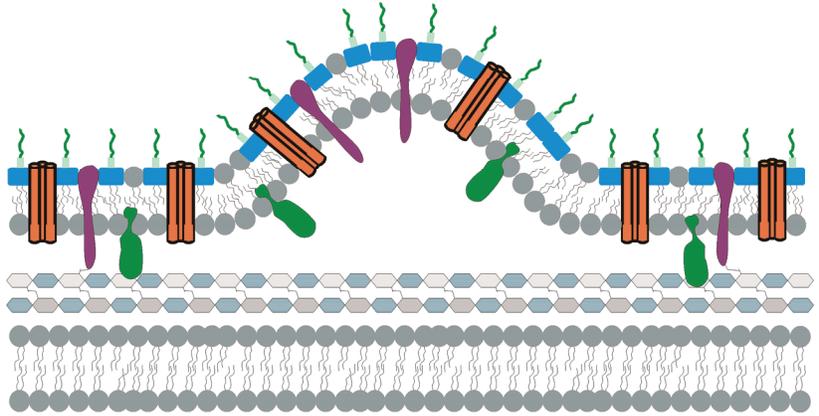
Mechanism 1

Mechanism 2
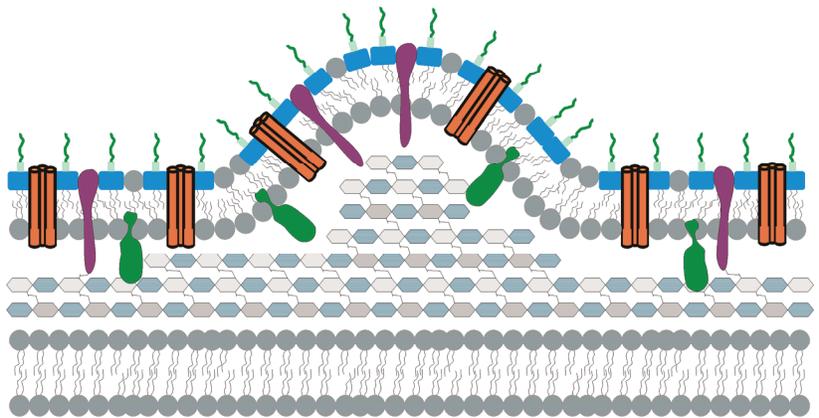
Mechanism 3

Symbol key

- LPS
- lipoproteins
- phospholipid
- peptidoglycan
- porin
- negative charge
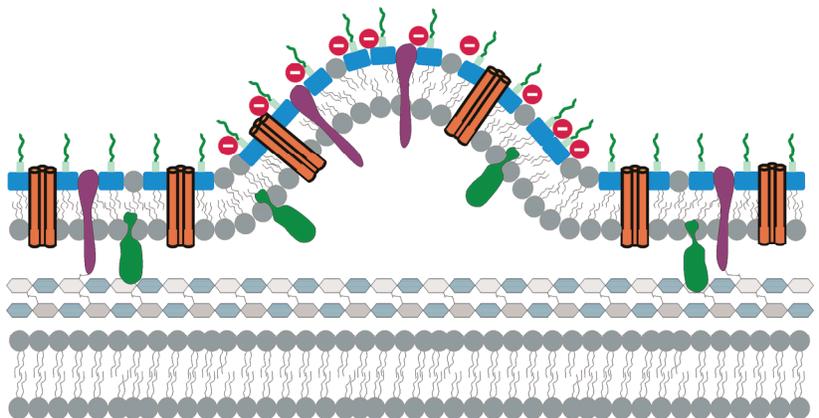
Figure 1.7. Proposed mechanisms of MV formation. Each mechanism is described in the text (adapted from Mashburn-Warren and Whiteley, 2006).

correlated to protein levels in the periplasm. This suggests that the build up of these proteins may have forced the outer membrane to bleb off. **(Mechanism 3)** Membrane instability and MV blebbing occurs due charge repulsion between LPS groups on the cell surface. Research on MVs produced by *P. aeruginosa* has demonstrated that MVs are enriched in more negative LPS (B-band) than parent cells which contain both A-band (neutral) and B-band LPS (Kadurugamuwa and Beveridge, 1995; Sabra et a., 2003; Schooling et al., 2006). Regions of the cell wall that are enriched in B-band are thought to be less stable and allow for MV formation. Overall, it is still unclear what causes certain regions of the membrane to form MVS and also how bacteria are able to sort specific proteins into MVs.

Membrane vesicle chemistry. The surface chemistry of MVs is predicted to be similar to the cell membrane. Since the outer membrane of bacteria is capable of sorbing and immobilizing metal ions (Beveridge and Schultze-Liam, 1995), we would predict the same would be true of MVs. For example, MVs from two *Shewanella* spp. were capable of reducing heavy metals, radionuclides and Fe which resulted in accumulation of precipitated material on the MV surface (Gorby et al., 2008). Similarly, MVs produced by E. coli were found to sorb Ag-NPs (Li et al., 2009), though this result was not investigated further. These results indicate that MVs may play a role in metal-microbe interactions, though to date, this has not been addressed thoroughly.

1.7. <u>Significance of research</u>

Studying the effects of pH on metal bioavailability/toxicity and microbial processes is necessary to develop a better understanding of how bacteria interact with

their environment. Metal speciation and bioavailability is influenced by pH which affects the distribution of metal species between free ion, hydroxo-complexes and organic and inorganic complexes. In environments of high total concentrations of metal (natural or anthropogenically disturbed), changes in pH can alter metal toxicity to bacteria. In a mixed-waste (i.e., inorganic and organic contaminants) bioremediation scenario, raising the pH to reduce metal solubility can increase metal toxicity and limit the ability of bacterial degradation of organic pollutants (Van Nostrand et al., 2007; Sandrin and Maier, 2002). But pH is also important in environments such as the human body where metal bioavailability is low and successful colonization by pathogens is dependent on their ability to sequester required metals (e.g., Ni sequestration by *H. pylori* in the acidic gastric environment is required for pathogenesis; Belzer et al., 2007). Despite the importance of pH in affecting metal speciation, it is rarely accounted for in laboratory experiments.

In addition to the importance of pH in affecting metal bioavailability/toxicity, pH can also alter microbial processes which can affect metal toxicity. For example, decreased pH elicited a stress response in *E. coli* which resulted in increased Cd resistance (Worden et al., 2009). Additionally, pH can affect membrane chemistry which can change the metal binding capacity of the cell (Chubar et al., 2008). For example, *Bacillus jeotgali* sorbed 3-fold more Zn at pH 7 versus pH 5 (Green-Ruiz et al., 2008). Since pH can affect microbial processes as well as metal-speciation, evaluating metal-microbe interactions requires an interdisciplinary approach to understanding not only changes in chemistry that is occurring at or near the bacterial membrane, but also the biological response of the bacterium.

For this dissertation, we investigated the effect of pH on metal- and nanoparticle-microbe interactions using PR1 as a model system. Initially we were interested in whether ZnO-NP was more toxic than Zn^{2+} to PR1. In Chapter 2 we describe that ZnO-NP toxicity is similar to Zn^{2+} and that both are more toxic at pH 6 than 7. During these investigations we observed that PR1 produces MVs. Since the role of MVs in metal-microbe interactions has not been evaluated (Mashburn-Warren and Whiteley, 2006), we hypothesized that due to their ubiquitous and multifaceted nature, MVs also play a role in modulating pH-dependent Zn toxicity to PR1. We predicted that MVs could modulate Zn toxicity by three general mechanisms. First, MVs may facilitate Zn-export from the cell and this mechanism may be more effective at pH 5 than 7. In Chapter 3 we found that MV production was higher at pH 7 than 5, and that MV production decreased with increasing Zn concentrations, suggesting that MVs were not involved in Zn export. Second, MVs may bind Zn extracellularly thereby decreasing the extracellular concentration though this might potentially increase Zn-bioavailability to PR1. In Chapter 4 we demonstrate that although MVs are capable of binding Zn, they do not increase or decrease pH-dependent Zn toxicity to PR1. Lastly, MVs produced at pH 5 and 7 may have different functions which correlate to Zn toxicity. In Chapter 5 we found that MVs produced at different pH contain different protein compositions and nutrients (e.g., DNA, RNA, Fe and Zn), but these differences do not appear related to Zn-toxicity. Overall, our investigations indicate that pH causes changes in cellular processes in PR1 which allow it to grow in the presence of higher concentrations of Zn. Furthermore, these studies are the first to investigate the effects of an environmental variable pH on MV production and function. These results demonstrate that by evaluating the microbial

response to pH in parallel to pH-dependent changes in metal speciation, we can develop a

better understanding of how bacteria interact with their environment

CHAPTER 2

CYTOTOXICITY OF ENGINEERED ZINC OXIDE NANOPARTICLES TO *Burkholderia vietnamiensis* PR1$_{301}$: COMPARISON TO Zn^{2+} AND THE EFFECTS OF COUNTER-ION UTILIZATION

2.1. Introduction

The emerging nanotechnology industry, which produced materials used in $147 billion of goods in 2007 and more than 803 products or product lines in 2008, is projected to be a $3.1 trillion market by 2015 (Bradley, 2008; Woodrow Wilson Center, 2008). Nanoparticles (NPs) in particular are used in sunscreens, cosmetics, and clothing in addition to having broad biomedical and industrial applications (Mazzola, 2003). With increased NP use and production, their release to the environment becomes inevitable. Although the transport, fate, bioavailability, and toxicity of engineered NPs released in the environment is largely unknown, a recent study of Au-nanorod partitioning in estuarine mesocosms found that the vast majority of Au-nanorods become associated with biofilms (Ferry et al., 2009). Since a wide range of NPs are antibacterial to Gram-negative and Gram-positive bacteria (reviewed by Klaine et al., 2008; Neal, 2008), it has been suggested that NPs could alter the ability of microbial populations to function in key ecological processes (Neal, 2008). For example, fullerene-NPs (C_{60}) have been shown to be toxic to *Escherichia coli* and *Bacillus subtilis* in liquid media (Lyon et al., 2005), but dosing of a soil with fullerene-NPs resulted in minimal changes in the microbial community composition and general metabolic activity (Tong et al., 2007). Some initial studies have also indicated that the composition, size, shape, and preparation of NPs influence observed biological effects (Cho et al., 2005; Adams et al., 2006; Sayes et al., 2006; Nair et al., 2008). Thus, determining the mechanisms of toxicity to microorganisms for NPs is essential for evaluating risks to the environment, as well as regulating the manufacturing and release of NPs.

While the diversity of NP compositions and formulations make it difficult to extrapolate observations between NPs and specific microorganisms, there are proposed mechanisms of NP toxicity to microorganisms (reviewed by Klaine et al., 2008). These include (1) oxidative damage from photocatalytic activation of NPs (Adams et al., 2006), (2) sorption onto cell walls either causing cell aggregation or damage to membrane stability (Stoimenov et al., 2002; Sondi and Salopek-Sondi, 2004), and (3) transport into the cell where NP dissolution can occur resulting in toxicity from primary NP components (Xu et al., 2004; Kloepfer et al., 2005). Furthermore, NP uptake and/or toxicity to microorganisms can be influenced by the use of counter-ions (Hirschey et al., 2006), detergents (Cho et al., 2005), surfactants (Nair et al., 2008) or proteins (Kloepfer et al., 2005) used as surface stabilizers. Therefore, when microorganisms are exposed to NPs over incubation times, bacterial utilization of surface stabilizers as a carbon source may occur. For example, some commonly employed NP stabilizers [e.g., tri-*n*-octylphosphine oxide and diethylene glycol (DEG)] can increase growth of *E. coli* (Brayner et al., 2006; Reddy et al., 2007). Utilization of NP counter-ions or surface stabilizers may alter NP structure and chemistry, which could in turn cause changes in NP bioavailability and toxicity.

To address these concerns, we have developed a model system to examine NP-microorganism interactions, specifically focusing on the effects of microbial growth on NP structure and toxicity. Acetate stabilized, engineered ZnO-NPs with an average size of 1.5 nm was used in these studies. Zinc oxides comprise one of the most diverse families of nanostructures, with ZnO-NP commonly used in sunscreens, personal care products, and biological and chemical sensors (Wang, 2004). ZnO-NP has also been

found to be toxic to microorganisms (Yamamoto, 2001; Adams et al., 2006; Brayner et al., 2006; Reddy et al., 2007; Zhang et al., 2007; Heinlaan et al., 2008; Jones et al., 2008; Mortimer et al., 2008; Nair et al., 2008; Gajjar et al., 2009; Guy et al., 2009; Hu et al., 2009; Jiang et al., 2009) and has been found to be more toxic to bacteria than other metal-oxide NPs (Hu et al., 2009; Jiang et al., 2009). *Burkholderia vietnamiensis* $PR1_{301}$ (PR1), a Gram-negative constitutive trichloroethylene degrader (Van Nostrand et al., 2007) previously characterized by our laboratory for its resistance to divalent metals, including Zn^{2+} (Van Nostrand et al., 2005) was selected as our model microorganism. PR1 is more resistant to Zn^{2+} at lower pH, e.g., 20-fold more resistance to Zn^{2+} at pH 5 versus pH 7. We have investigated classical mechanisms of metal resistance in PR1 and have yet to identify the specific mechanism(s) of this effect (Van Nostrand, 2006; Van Nostrand et al., 2007; Van Nostrand et al., 2008). Furthermore, the experimental media we have utilized has been developed specifically to minimize interactions with metal ions, i.e., chelation and precipitation (Van Nostrand et al., 2005). This model system has allowed us to examine the cytotoxic effects of engineered ZnO-NP on PR1 as referenced to Zn^{2+} (as $ZnCl_2$) and how counter-ion (acetate) utilization by PR1 affects changes in ZnO-NP cytotoxicity.

2.2. **Materials and Methods**

Bacterial cultures. Unless otherwise noted, all experiments employed a medium (modified minimal mineral medium; 4M) designed to minimize phosphate chelation/precipitation of metals by using 2-(N-morpholino)ethanesulfonic acid (MES) as a zwitterionic buffer and β-glycerophosphate as the source of inorganic phosphorous (Van Nostrand et al., 2005), along with 20 mM lactate as the carbon source. *B.*

vietnamiensis PR1$_{301}$ (PR1) was provided by Malcolm Shields (Idaho State University).

Before each experiment, 20 μL of thawed culture was plated onto Luria Bertani (LB)

agar plates and incubated at 30°C in the dark for 48 h to verify purity. Colonies were

then transferred to 4M at pH 6 and incubated at 24°C with shaking (200 rpm) for 24 h. A

4% (v/v) transfer was then inoculated into 4M at pH 6 and incubated in the dark at 30°C

with shaking (200 rpm). After 14 h to 16 h, the culture was pelleted by centrifugation

and resuspended in 4M at pH 6 to an optical density at λ=610 nm (OD$_{610}$) of 2.4 ± 0.05

for use as the inoculum in each experiment (0.25 mL into 25 mL media).

ZnO-NP formulation. Pinnacle^{AF} ZnO nanoparticle suspensions with a reported

primary particle size of 2 nm to 6 nm and pH of 4.5 were purchased from Applied

Nanoworks (http://www.appliednanoworks.com). Metals analysis of the stock was

accomplished by inductively coupled plasma optical emission spectroscopy (ICP-OES;

Perkin Elmer 4300 DV) and ion chromatography (IC; Dionex, Sunnyvale, CA USA) was

used to quantify acetate in the stock. The removal of acetate by calcination was

confirmed by high resolution thermogravimetric analysis (HR-TGA) by using a TA

instruments, Inc. (New Castle, DE USA) model 2950 HR-TGA. TGA curves were

obtained as following: 10 to 15 mg of sample was placed in the TGA pan in a nitrogen

atmosphere. Weight-loss curves were measured over a temperature range of 20 to 800°C.

Between thermal events, the heating rate was set at 50°C min^{-1}. The resolution and

sensitivity were set at 5 and 8 respectively. Size was determined by transmission electron

microscopy (TEM; FEI Tecnai 20). Diluted aliquots of the ZnO-NP stock were placed

on a copper grid for TEM analysis. To evaluate the effect of calcination on ZnO-NP

structure, a nanoparticle subsample was dried in an oven at 60°C overnight and then

transferred to a furnace where it was calcined at 450°C. This allowed the acetate in the sample to volatilize. The resulting solids were resuspended in 1.5 mL of DDI water. After good dispersion, a drop was deposited on a copper grid for TEM analysis. Also, the average hydrated diameter of the ZnO-NP in the stock solution was determined by light scattering using a DynaPro Titan TC (Wyatt Technologies, Santa Barbara, CA USA).

Acetate influence on PR1 growth, carbon utilization and NP cellular localization. Media was amended with acetic acid before inoculation using a 3.08 M acetic acid stock made using glacial acetic acid (Fisher Scientific, Pittsburgh, PA USA), adjusted to pH 5, 6, or 7 with 10 M NaOH and filter sterilized using sterile 0.2 μm nylon syringe filters (Acrodisc, Pall Corporation, Ann Arbor, MI USA). PR1 was grown in the dark at 30°C with shaking (200 rpm) and 0.6 mL aliquots were removed every 2 to 4 h, centrifuged at 16,100 g for 10 min at 4°C and 0.5 mL of the supernatant was removed and stored at -40°C in sealed amber glass GC vials until analysis. Prior to ^{1}H-NMR analysis, samples were thawed and amended to a final concentration of 10% (v/v) D_2O, 0.1% (w/v) sodium azide, and 0.2 mM 3-(trimethylsilyl)propionic acid-d_4 sodium salt (TSP). ^{1}H-NMR spectra were obtained at 305 K using a Bruker DMX spectrometer operating at 500.13 MHz equipped with a 5 mm triple-resonance, inverse, z-gradient probe. One-dimensional spectra were acquired using a standard three-pulse, presaturation pulse sequence for water suppression in which the water resonance was selectively irradiated during the 2.5 s relaxation delay. Lactate and acetate were quantified using TSP response. Additionally, 1 mL aliquots were taken during growth at 4 and 8 h for scanning transmission electron microscopy with energy dispersive X-ray

(STEM-EDX) and TEM analysis. Electron microscopy (EM) samples were centrifuged 16,100 g for 2 min and fixed for 1 h in 1 mL cold 2% (v/v) glutaraldehyde (EM Grade, Electron Microscopy Sciences, Hatfield, PA USA) buffered in 4M pH 7 without lactate to minimize Zn^{2+} or ZnO-NP chelation as well as maintain pH and ionic strength during fixation. The sample was then centrifuged 16,100 g for 2 min, resuspended in 1 mL cold 18.2 MΩ water and kept on ice for 10 min before centrifuging again and resuspended in 1 mL water at which point 10 µL was dropped onto carbon/formvar coated 200-mesh copper grids (Electron Microscopy Sciences, Hatfield, PA USA) for 10 sec before blotting off.

Growth-response assays. Concentrated zinc stocks, 62.5 mg Zn L^{-1}, were prepared from ZnCl$_2$ (Fisher Scientific, Pittsburgh, PA USA) in 25 mL, 18.2 MΩ water, acidified with 5 drops Optima HNO$_3$ (Fisher Scientific, Pittsburgh, PA USA), and filter sterilized using a sterile 0.2 µm nylon syringe filter. Before each experiment, a small aliquot of the ZnO-NP stock was filter sterilized using a sterile 0.2 µm nylon syringe filter, otherwise the stock was stored in the dark at room temperature. Acetate concentrations in all samples were normalized to 10.7 mM using filter sterilized and buffered 3.08 M acetate (described above). Media amended with ZnO-NP or ZnCl$_2$ to a concentration of 0, 25, 50, 75, 100, 150, 200, or 250 mg Zn L^{-1} and acetate concentrations normalized to 10.7 mM were inoculated with PR1 inoculum and incubated in the dark at 30°C with shaking (200 rpm). Aliquots were removed from cultures at 0, 4, 8, 12, 16 and 24 h and growth was determined by OD$_{610}$, which was previously demonstrated to correlate with total protein in PR1 (Van Nostrand, 2006; Van Nostrand et al., 2007). To evaluate gross changes in cell morphology as well as evaluate ZnO-NP localization,

aliquots were removed from 24 h from cultures grown at pH 6 amended with 75 mg Zn

L^{-1} and 250 mg Zn L^{-1} as $ZnCl_2$ or ZnO-NP. Aliquots were fixed for scanning electron

microscopy by pressing them onto 0.2 μm polycarbonate filters using a Swinnex filter

holder. Fixation was accomplished by a 1 h incubation with 2% glutaraldehyde in 4M

pH 7 (as described above). Next, samples were dehydrated by an ethanol series of 25, 50,

75, 85, 90, 95, 100, 100% ethanol and were brought to critical point dryness using 1 ml of

hexamethyldisalizane (Electron Microscopy Sciences). Filters were then removed and

affixed to stubs and stored in a desiccator until SEM analysis. To evaluate changes in

growth response, the total Zn concentration required to elicit a 50% inhibition of growth

(EC_{50}) was determined using OD_{610} at 24 h. For each condition, % inhibition was

calculated as [OD_{610} condition] ÷ [OD_{610} of the unamended culture] x 100. To determine

the EC_{50}, the data were fit to a nonlinear model using a 3 parameter logistic plot with

SigmaPlot 8.0 (SYSTAT Software Inc., San Jose, CA USA). Comparing EC_{50} between

ZnO-NP and $ZnCl_2$ was accomplished with an F-test (Motulsky and Christopoulos,

2003).

Resting cell assays. PR1 inoculum was prepared and 1 mL used to inoculate 100

mL of 4M pH 6. These cultures were grown for 8 h at 30°C with shaking (200 rpm),

centrifuged at 6,400 g for 5 min and resuspended in 100 mL sterile 100 mM $NaNO_3$.

This wash was repeated 5 times to remove surface bound contaminant cations (Yee and

Fein, 2003) and after the last centrifugation the cells were resuspended in 100 mL sterile

pH 6, 100 mM MES. Aliquots (1.5 mL) of this suspension were placed in acid-washed

sterile 1.5 mL microcentrifuge tubes (polypropylene, VWR, West Chester, PA USA)

containing ZnO-NP, $ZnCl_2$, and acetate to yield predicted Zn concentrations of 0, 25, 50,

75, 100, 150, 200, or 250 mg Zn L^{-1} and 10.7 mM acetate. All tubes were placed in the

dark at 30°C and inverted at 6 rpm for 4 h. Serial dilutions from 100 μL aliquots were

plated on LB agar plates for colony forming units (CFU) mL^{-1} determination. The

remaining sample was centrifuged at 16,100 g for 10 min at 4°C except for EM samples

which were centrifuged for only 2 min and were fixed as described above using a 1.5 mL

total volume. Colony forming units were used to calculate percent viability for each

condition based on the assumption that if a cell was yielded unculturable it was no longer

viable. A lethal Zn concentration to render 50% of cells non-viable (LC$_{50}$) was

determined by first calculating percent viable cells based on CFU mL^{-1} of condition

versus CFU mL^{-1} of unamended culture and then analyzing the data by probit analysis

assuming a logistic distribution using Minitab 14 (Minitab Inc., State College, PA USA).

Metal analysis. Aliquots (1 mL) of supernatant from resting cell assays were

weighed into acid-washed 25 mL scintillation vials and diluted either 10- or 100-fold

(sequentially) with 1% (v/v) Optima HNO$_3$ in 18.2 MΩ water. Non-inoculated controls

containing 100 mM MES with ZnCl$_2$ or ZnO-NP and acetate were sampled in parallel to

serve as abiotic controls. Metals analysis was accomplished using a Perkin Elmer 4300

DV ICP-OES at a wavelength of 213.9 nm for Zn. Drift during the run was corrected for

using multiplicative drift correction (Salit and Turk, 1998). These data demonstrated that

measured Zn concentrations for abiotic ZnO-NP conditions were greater than predicted,

therefore we used these measured Zn concentrations in LC$_{50}$ and sorption calculations

(reflected in x-axis of Figure 2.10). We also investigated this discrepancy to determine if

MES or acetate were affecting ZnO-NP structure and therefore measured Zn

concentration. It was found that the effect of MES or acetate on measured Zn

concentrations of ZnO-NP solutions was within the experimental error of the experiment (<15%) and therefore not responsible for measured ZnO-NP concentrations being higher than predicted (data not shown).

Electron microscopy. SEM was used to evaluate cells during growth-response assays with a LEO 982 field emission scanning electron microscope (FE-SEM, LEO Electron Microsopy, Inc., Thornwood, NY USA) was operated at 15 keV unless back scatter and EDX were used which required 20 keV. EDX was accomplished with an Oxford EDX analyzer. TEM and STEM-EDX were used to investigate samples described above from acetate growth-response assays and resting-cell assays. A Hitachi HD2000 STEM operating under variable pressure in back scatter dark-field Z-contrast mode at 200 keV with an INCA Energy 200 EDS detector was used for STEM and EDX mapping. A Hitachi TEM 9500 at 300 keV was also used to analyze samples by bright field TEM.

2.3. <u>Results</u>

ZnO-NP stock characterization. The manufactured ZnO-NP stock solution was initially characterized to determine the Zn concentration and acetate concentration. ICP-OES confirmed the presence of zinc (72,000 mg Zn L^{-1}) and IC detected a significant amount of acetate (3.08 M) in the stock solution. Using TEM, we found that particles in the ZnO-NP stock were 1 nm to 3 nm with an average diameter of 1.5 nm (Figure 2.1A). Additionally, the average hydrated diameter was determined to be 1.2 nm by light scattering (data not shown). Since we were interested in the affect of acetate removal on
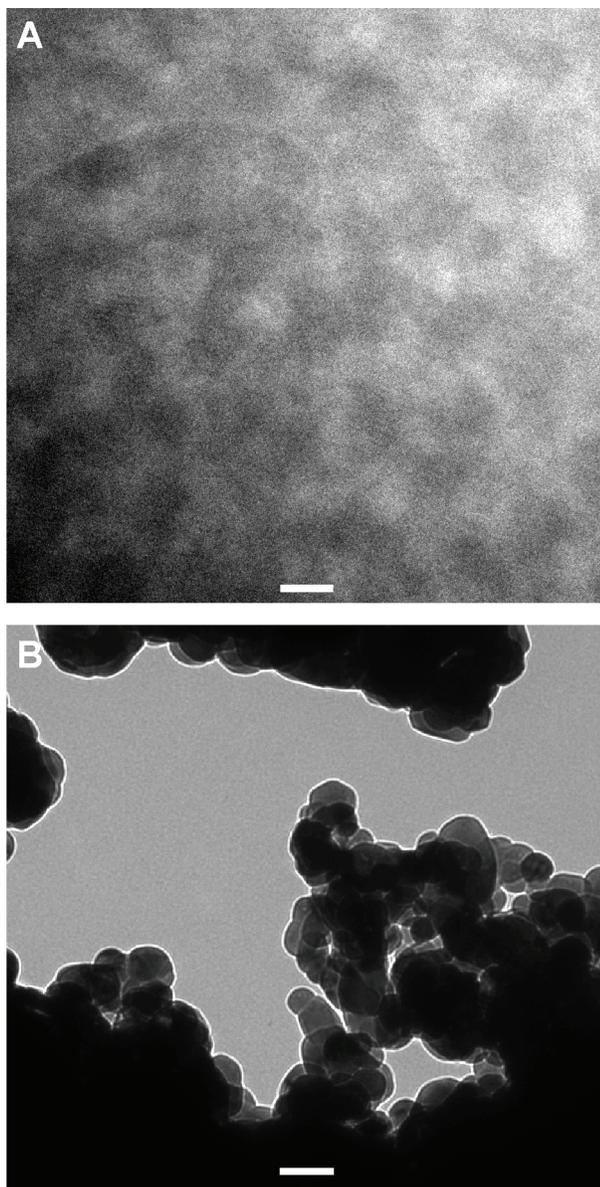
Figure 2.1. Transmission electron micrographs of ZnO-NP. (A) ZnO-NP stock, scale bar is 2 nm. **(B)** Calcined ZnO-NP, scale bar is 100 nm.
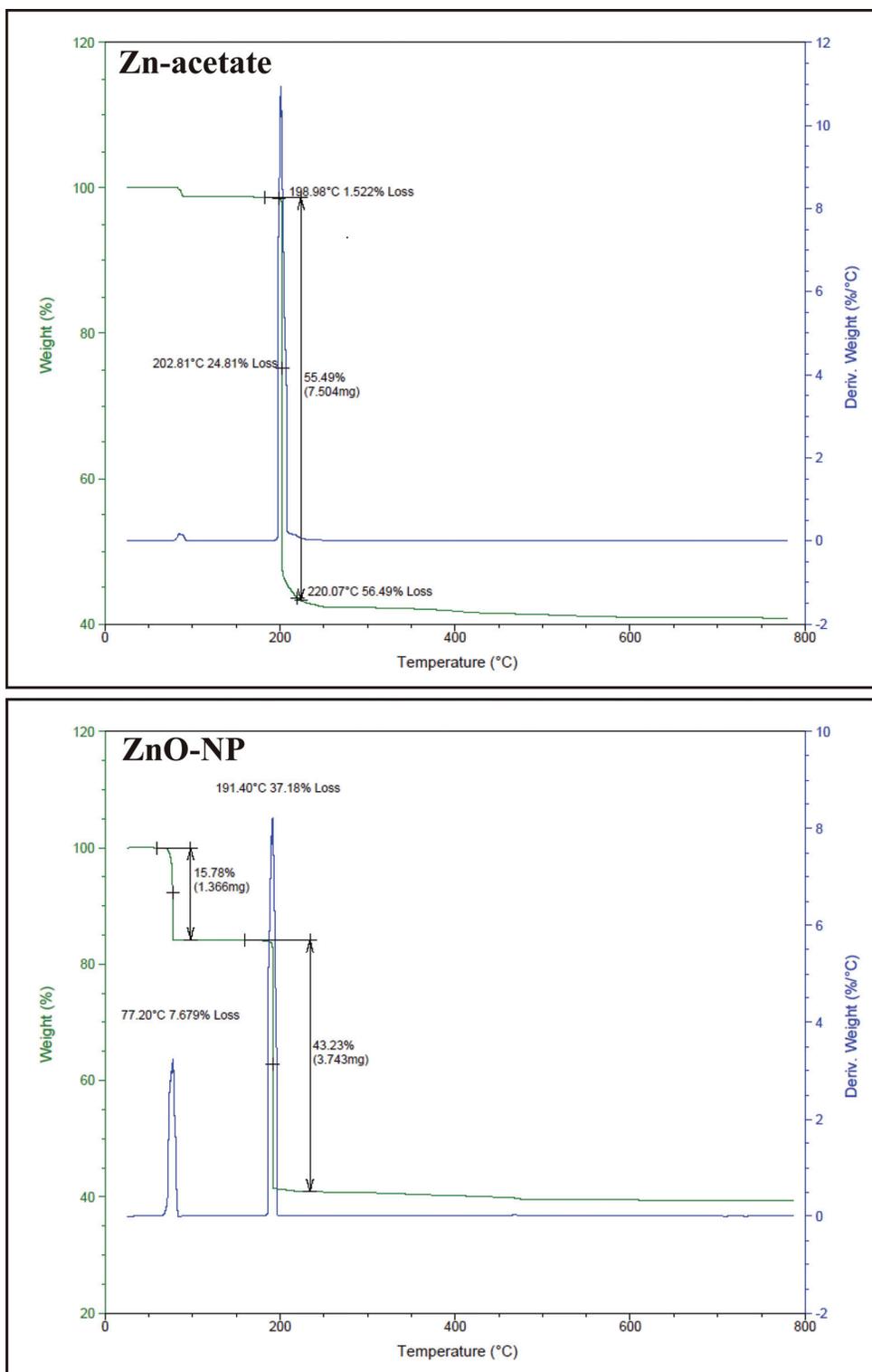
Figure 2.2. High resolution thermogravimetric analysis of Zn-acetate and ZnO-NP.
Weight-loss curves were measured over a temperature range of 20 to 800°C.

NP structure, we first demonstrated that calcination would remove acetate from the ZnO-NP stock using HR-TGA. The ZnO-NP stock had two significant loss peaks at 77°C and 191°C (Figure 2.2). We also evaluated Zn-acetate by HR-TGA and found it had a major loss peak at 203°C which we believe represents the loss of acetate (Figure 2.2). This allowed us to confirm that in the ZnO-NP stock, water is removed at 77°C and acetate is removed at 191°C. Next, we used TEM to evaluate the effect of calcination on ZnO-NP structure and found that calcination results in approximately 100-fold larger particles (Figure 2.1B).

Effect of acetate on PR1 growth. Since the engineered ZnO-NP stock contained 3.08 M acetate, we first evaluated the influence of acetate on the growth of PR1. In the presence of 10.7 mM acetate, PR1 did not grow at pH 5 while at pH 6 and 7 growth was enhanced by approximately 10% (Figure 2.3). This concentration corresponds to the acetate associated with 250 mg Zn L^{-1} as ZnO-NP. Therefore, pH 5 was not further evaluated. PR1 utilization of acetate and lactate, measured by ^{1}H-NMR, demonstrated that at pH 6 and 7, 95% of both 10.7 mM acetate and 20 mM lactate were depleted after 12 h growth (Figure 2.4). In addition, both acetate and lactate exhibited similar biphasic utilization patterns. The average utilization rates (± SD) over the initial 4 h period at pH 6 and 7 were 0.3 ± 0.1 and 0.7 ± 0.1 mM h^{-1} for acetate and lactate respectively, while from 4 to 12 h, the average utilization rates were 1.2 ± 0.1 and 2.2 ± 0.3 mM h^{-1} respectively.

Bioavailability of ZnO-NP associated acetate. To determine whether PR1 was able to utilize ZnO-NP associated acetate, utilization of acetate in the absence of lactate was evaluated. The sub-lethal concentration of 100 mg Zn L^{-1} as ZnO-NP was used,
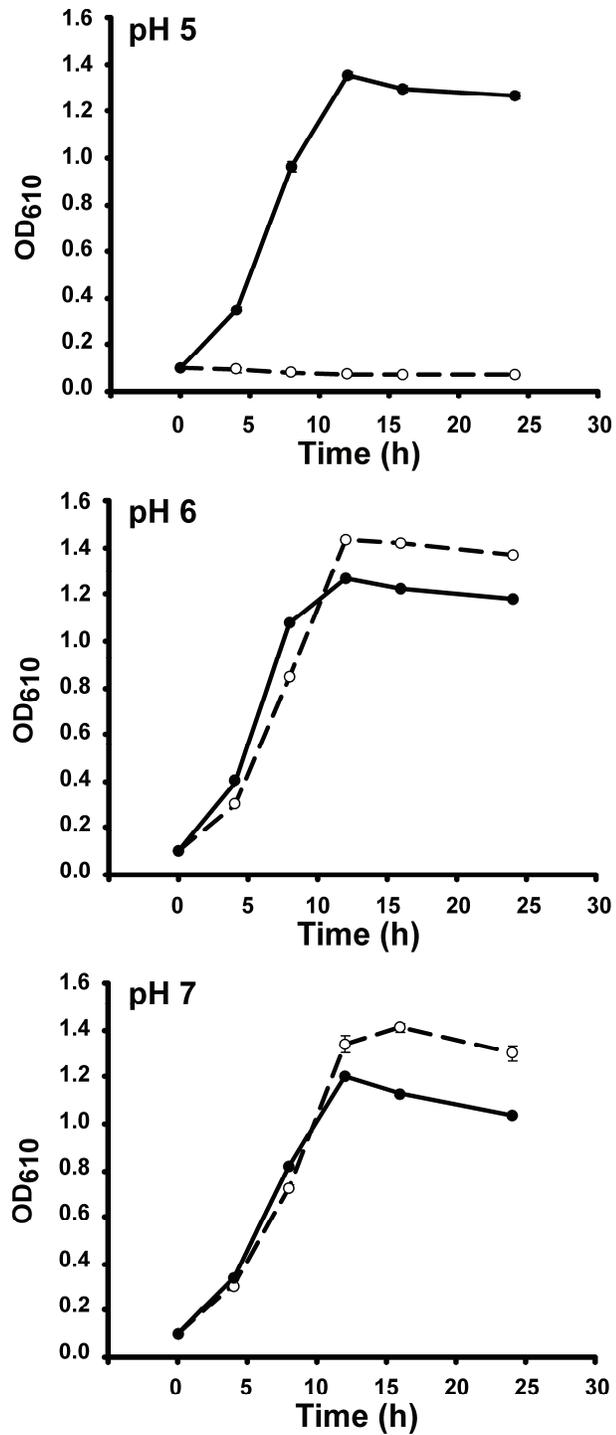
Figure 2.3. Growth of PR1 at pH 5, 6, and 7 with and without 10.7 mM acetate amendment. Growth without acetate (●) and with 10.7 mM acetate (○) was measured by OD_{610}. Error bars represent ± 1.0 standard deviation based on triplicate measurements.
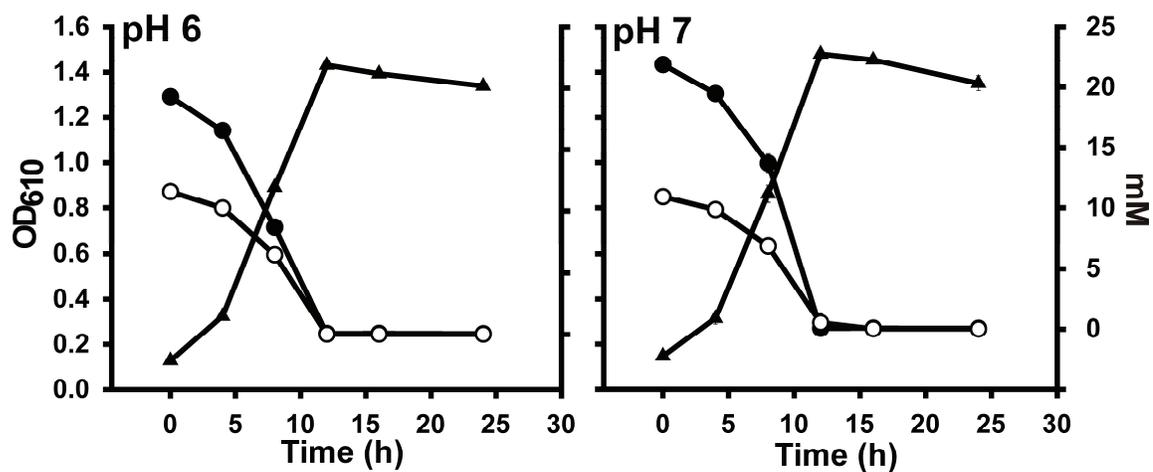
Figure 2.4. Lactate and acetate utilization by PR1 at pH 6 and 7. Growth measured by OD_{610} (▲), lactate concentration (●) and acetate concentration (○) as mM. Error bars represent ± 1.0 standard deviation based on triplicate measurements.
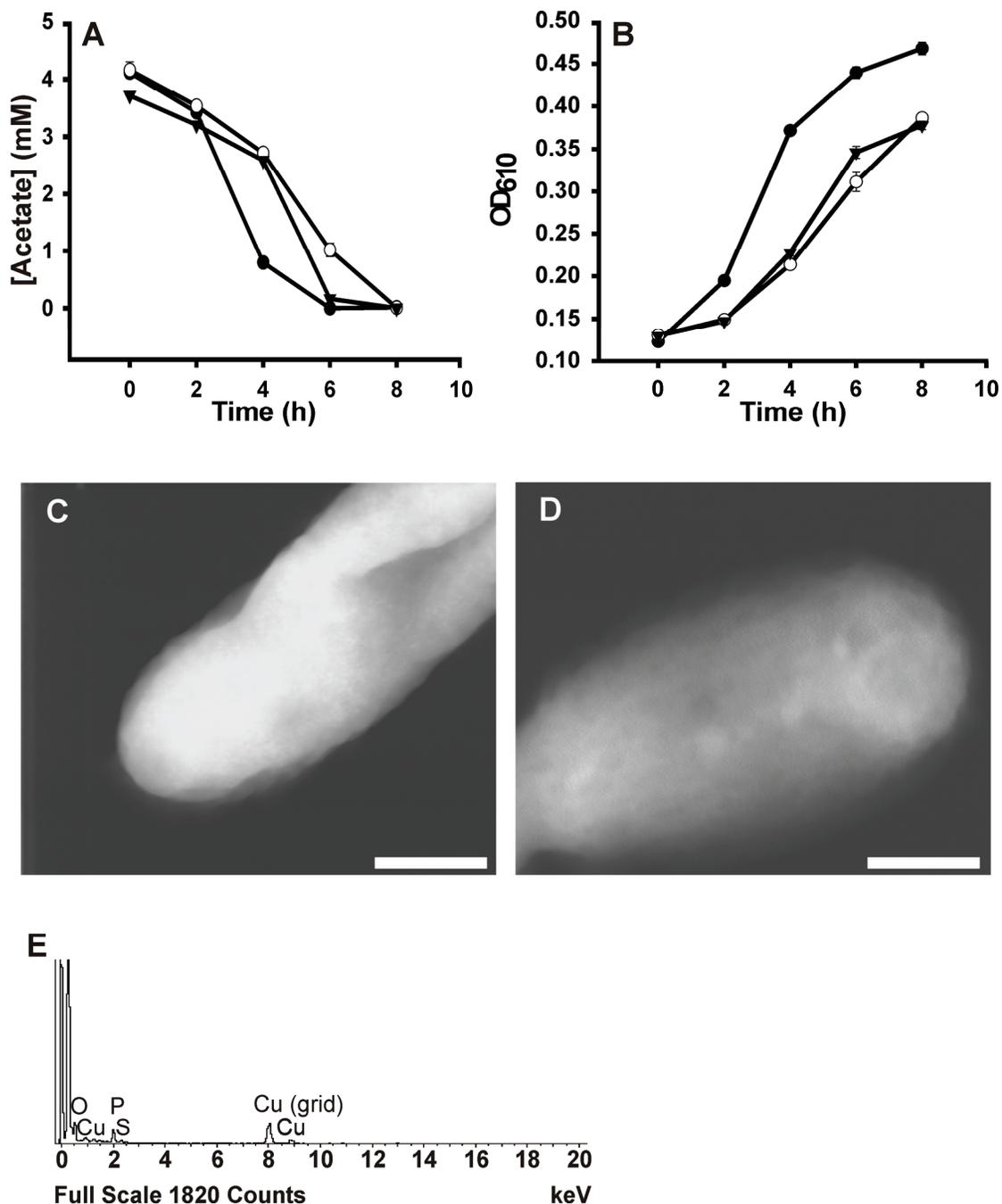
Figure 2.5. PR1 utilization of ZnO-NP associated acetate. **(A)** Acetate utilization with growth. **(B)** Growth measured by OD_{610}. 4.3 mM free acetate (●), 100 mg Zn L^{-1} as ZnO-NP (▼), and 4.3 mM acetate with 100 mg Zn L^{-1} as $ZnCl_2$ (○). Error bars represent ± 1.0 standard deviation based on triplicate measurements. **(C-E)** Dark-field scanning transmission electron micrographs of PR1 cells during NP-acetate only growth at 4 h **(C)** and 8 h **(D)** with corresponding energy dispersive x-ray spectrum for image at 4 h **(E)**. Scale bar is 300 nm. Electron dense regions in (C) contain phosphorous but no detectable Zn.

corresponding to an acetate concentration of 4.3 mM. Acetate was added to a final

concentration of 4.3 mM either as acetate only, 100 mg Zn L^{-1} as ZnO-NP (which

contained 4.3 mM acetate) or acetate with 100 mg Zn L^{-1} as $ZnCl_2$. Under each of these

three conditions, acetate was utilized with an average initial slow utilization phase (± SD)

of 0.3 ± 0.0 mM h^{-1} followed by a fast utilization phase of 0.9 ± 0.3 mM h^{-1}, with

complete acetate utilization in all three conditions by 8 h (Figure 2.5A). The length of

the initial slow phase was different between conditions, with ZnO-NP associated acetate

and acetate with $ZnCl_2$ taking longer to be utilized. Acetate utilization under all

conditions tracked growth of PR1 (Figure 2.5).

Since we found that calcination of ZnO-NP, which results in the loss of acetate,

caused ZnO-NP size to change (Figure 2.1), we were interested in how biotic removal of

acetate might affect particle structure. To investigate whether acetate utilization by PR1

could affect ZnO-NP structure and cellular localization, whole cell mount samples of

PR1 with 100 mg Zn L^{-1} as ZnO-NP without lactate were removed at 4 and 8 h

corresponding to 30% and 100% acetate utilization respectively (Figure 2.5). Intact ZnO-

NPs were not evident by STEM at either time point (Figure 2.5) and EDX did not detect

ZnO-NPs. There were electron dense regions <10 nm in diameter observed with cells at

4 h that were determined to be phosphorous containing bodies, and Zn was not detected

(Figure 2.5E). Due to the size and low contrast nature of ZnO-NP (Figure 2.1A) this

result was not surprising.

Growth inhibition and cytotoxicity of ZnO-NP relative to $ZnCl_2$ at pH 6 and

7. Growth inhibition based on OD_{610} at 24 h (Figure 2.6) was used to calculate $EC_{50} \pm$

SE values for Zn as ZnO-NP or $ZnCl_2$ at pH 6 and 7 (Figure 2.7). The EC_{50} of Zn as
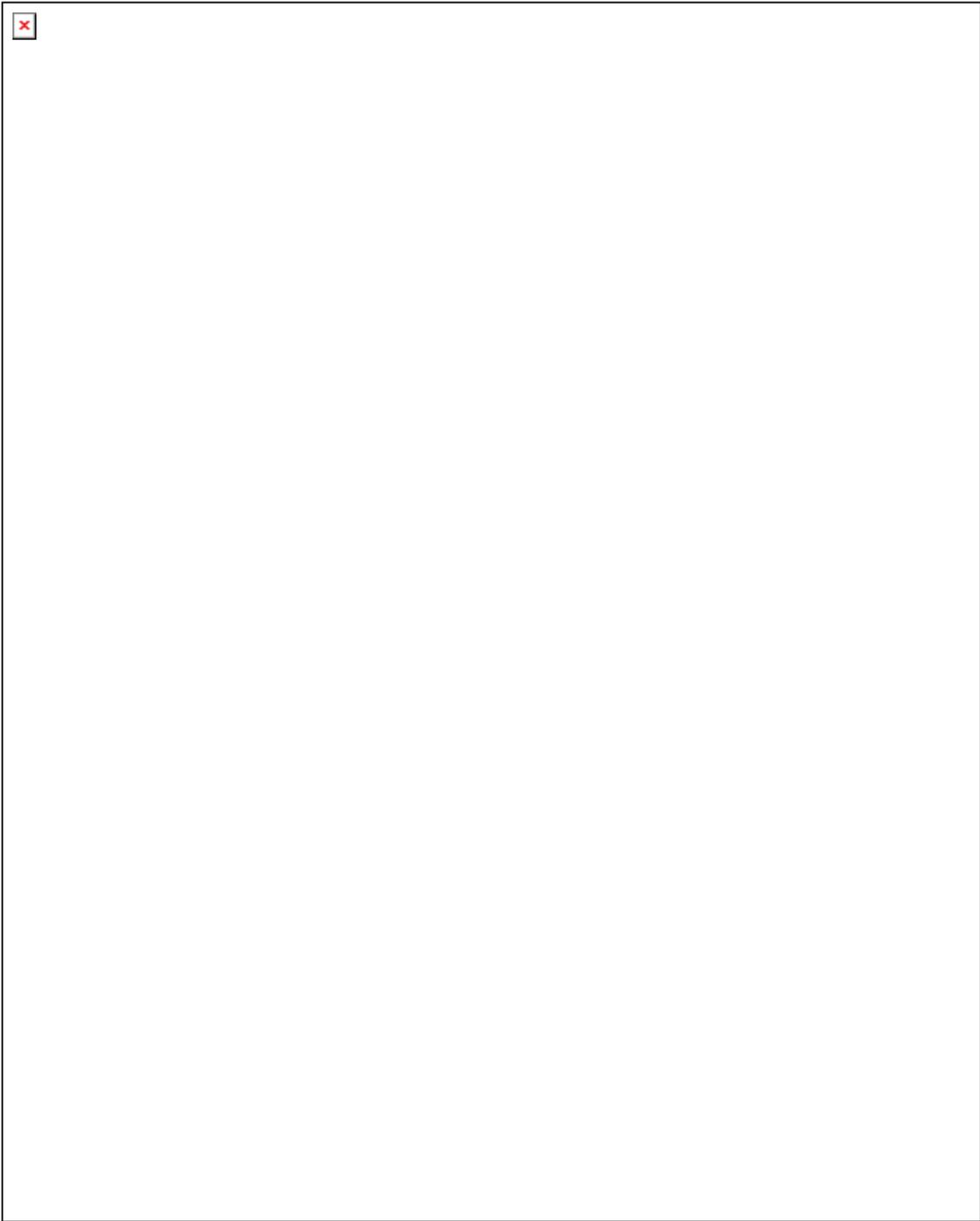
Figure 2.6. Growth of PR1 in the presence of Zn as ZnO-NP or ZnCl₂ at pH 6 and 7. Error bars represent ± 1.0 standard deviation based on triplicate measurements.
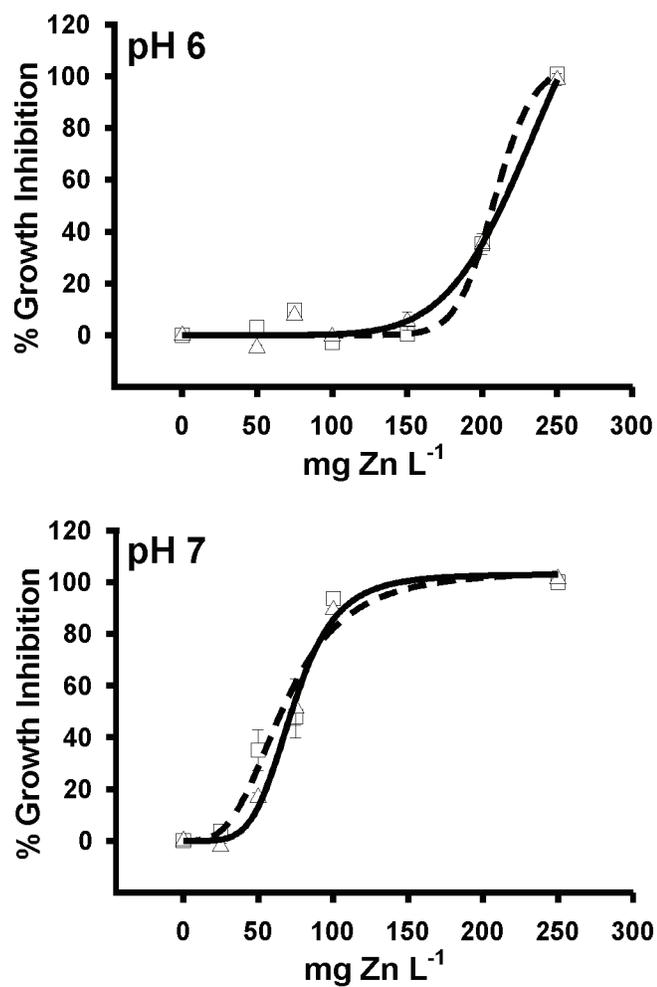
Figure 2.7. Comparison of 24 h percent growth inhibition by ZnO-NP and ZnCl₂ at pH 6 and pH 7. Logistic regression lines plotted, ZnO-NP is dotted line and $ZnCl_2$ is solid with data points, ZnO-NP (△) and $ZnCl_2$ (□). Error bars represent ± 1.0 standard deviation based on triplicate measurements.

66

ZnO-NP or $ZnCl_2$ was 244 ± 36 and 209 ± 15 mg Zn L^{-1} respectively at pH 6, while at

pH 7, the EC_{50} of Zn as ZnO-NP or $ZnCl_2$ was 73.1 ± 1.8 and 67.5 ± 4.1 mg Zn L^{-1}

respectively (Figure 2.7). At each pH, EC_{50} values were not significantly different

between ZnO-NP and $ZnCl_2$ (F-test; $p<0.05$), although EC_{50} values were 70% lower at

pH 7 versus pH 6. In addition, growth determined by OD_{610} was almost identical at each

pH (Figure 2.6).

Despite the toxicity of ZnO-NP and $ZnCl_2$ to PR1 being nearly identical, we were

interested in whether we could observe NPs by SEM as well as any accompanying

changes in cell morphology that would indicate a different mechanism of toxicity

between ZnO-NP and $ZnCl_2$. We found that after 24 h growth in 4M pH 6 amended with

75 mg Zn L^{-1} or 250 mg Zn L^{-1}, PR1 cells did not appear different but we did observe 50-

100 nm extracellular formations at both conditions (Figures 2.8 and 2.9). We were not

able to detect any significant Zn signal from these formations by EDX in cultures grown

with 75 mg Zn L^{-1} (Figure 2.8), though at 250 mg Zn L^{-1} we detected Zn, Fe and P

(Figure 2.9). Furthermore, we observed the same formations and composition in cultures

grown with ZnO-NP or $ZnCl_2$.

Although ZnO-NP and $ZnCl_2$ similarly inhibited growth of PR1, it was unclear

whether acetate utilization was affecting ZnO-NP toxicity. Thus, the cytotoxicity of ZnO-

NP to metabolically inactive PR1 in a resting cell assay was evaluated. Percent viable

cells determined by CFU mL^{-1} after 4 h of exposure was used to determine LC_{50} with

95% Fiducial Intervals (FI) values (Figure 2.10). The LC_{50} of Zn as ZnO-NP or $ZnCl_2$

was 90.4 (86.5-94.5) and 84.4 (81.1-87.9) mg Zn L^{-1} respectively. These values were not
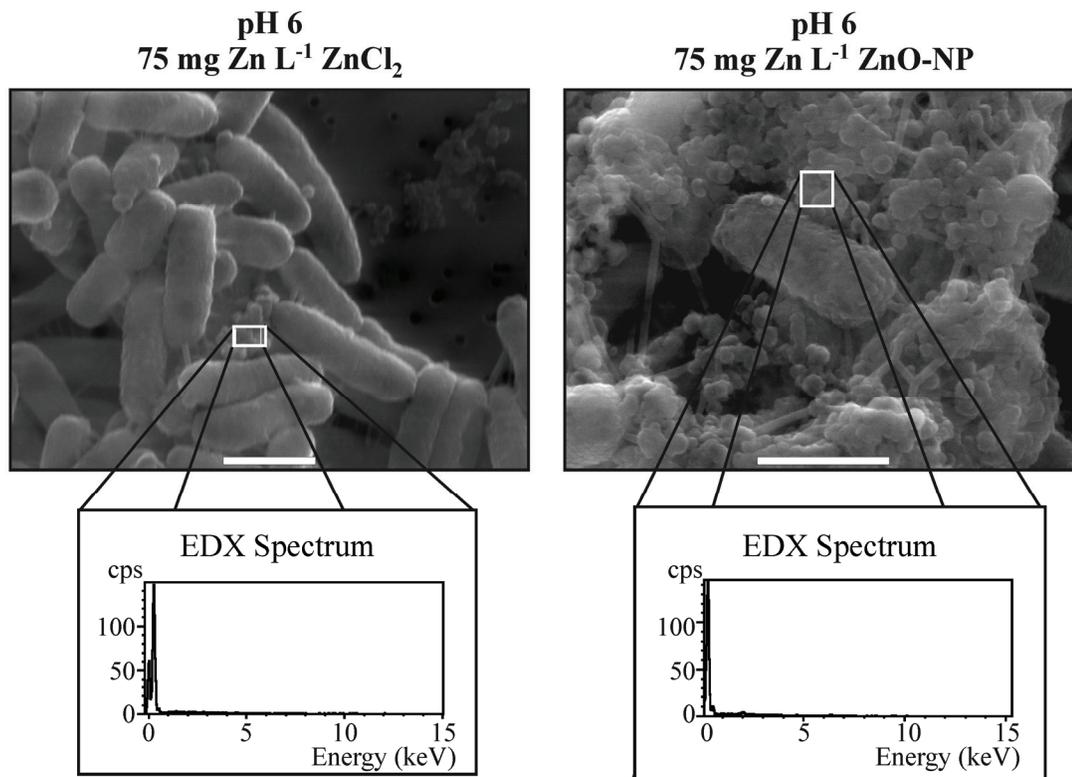
Figure 2.8. Scanning electron micrographs of PR1 cultures amended with ZnO-NP or ZnCl₂ at 24 h growth. EDX spectra are from regions indicated in micrographs by a white square. Scale bar is 1 μm.
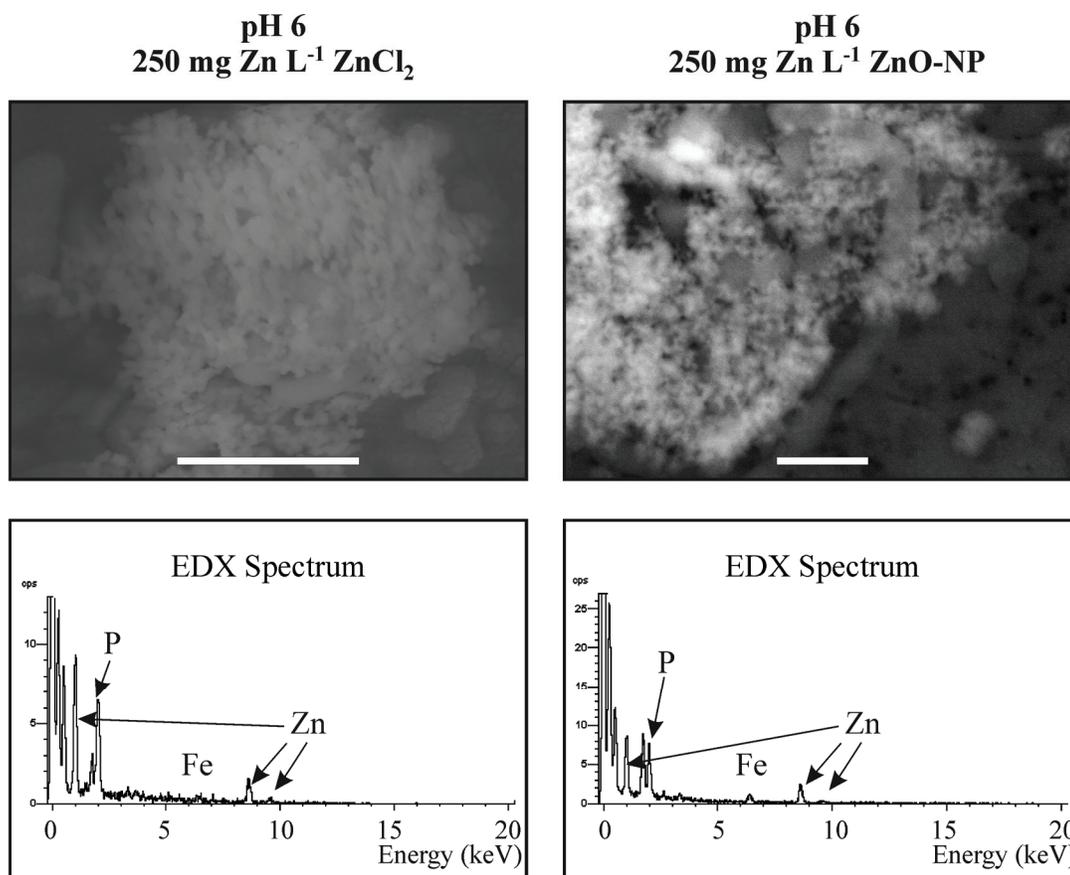
Figure 2.9. Scanning electron micrographs of PR1 cultures amended with ZnO-NP or ZnCl₂ at 24 h growth. Back scatter was used in conjunction with SEM of cultures grown with ZnO-NP, therefore brighter regions indicate electron dense areas. EDX spectra are from regions in the center of the micrographs. Scale bar is 2 μm.

significantly different based on the overlap of the 95% FI ($p=0.05$). Furthermore, LC_{50}

values were approximately 60% lower than respective pH 6 EC_{50} values.

During the resting cell assay, we expected that we might detect ZnO-NP

associated with cells if acetate utilization had been responsible for NP dissolution in the

growth response assay. Electron micrographs of cells exposed to 0, 25, 100 and 280 mg

Zn L^{-1} as ZnO-NP and 0, 25, 100 and 250 mg Zn L^{-1} as $ZnCl_2$ demonstrated that above

100 mg Zn L^{-1} ZnO-NP and $ZnCl_2$ the cell membrane appeared slightly diffuse indicating

possible membrane damage, though extensive cell damage was not evident under any

conditions (Figure 2.11). Furthermore, electron dense regions were observed but these

were similar between ZnO-NP and $ZnCl_2$ exposed cells (Figure 2.11). Although analysis

by EDX demonstrated Zn was associated with cells, Zn levels were homogenous across

the cells in all conditions, indicating that the electron dense regions observed by TEM

likely did not contain Zn (Figure 2.12).

ZnO-NP and $ZnCl_2$ sorption to resting cells. Due to the detection limits of

EDX and the low contrast nature of ZnO-NP, elemental analysis with ICP-OES was used

to quantify Zn sorption to PR1 resting cells (Figure 2.10). Zn sorption was minimal at Zn

concentrations less than 100 mg Zn L^{-1} as ZnO-NP or $ZnCl_2$, while at concentrations

greater than 100 mg Zn L^{-1} negative and positive sorption values were measured for both

ZnO-NP and $ZnCl_2$.
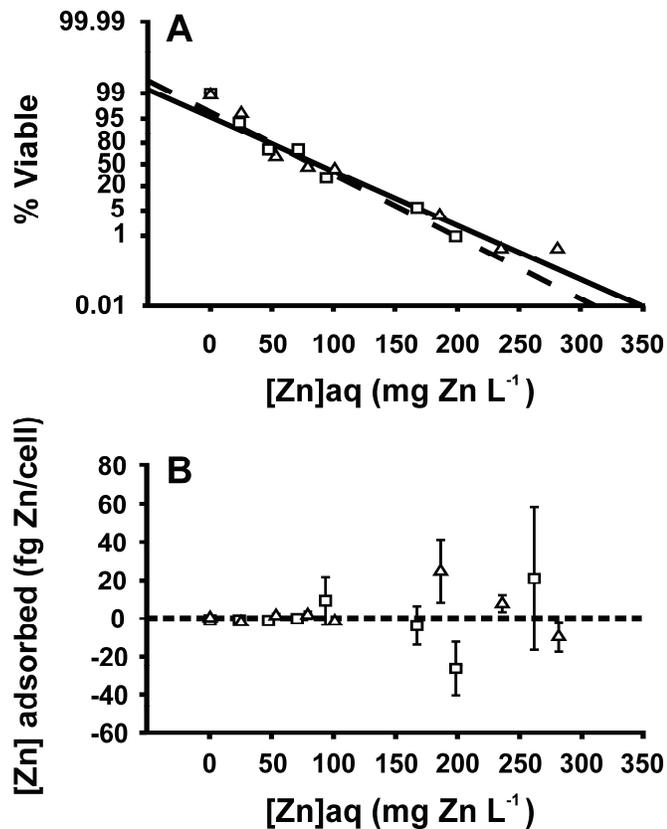
Figure 2.10. Toxicity and sorption of Zn as ZnO-NP or ZnCl₂ to resting cells. (A) Probit analysis of ZnO-NP (△) and ZnCl₂ (□) 4 h viability, and **(B)** Zn-sorption to PR1 when exposed to ZnO-NP (△) or ZnCl₂ (□). Probit analysis with logistic regressions displayed as a solid line for ZnO-NP and dotted line for ZnCl₂. Fiducial intervals for each regression are not displayed. For Zn-adsorption, [Zn]aqueous was determined by abiotic controls for each condition. Error bars in (B) represent ± 1.0 standard deviation based on triplicate measurements.
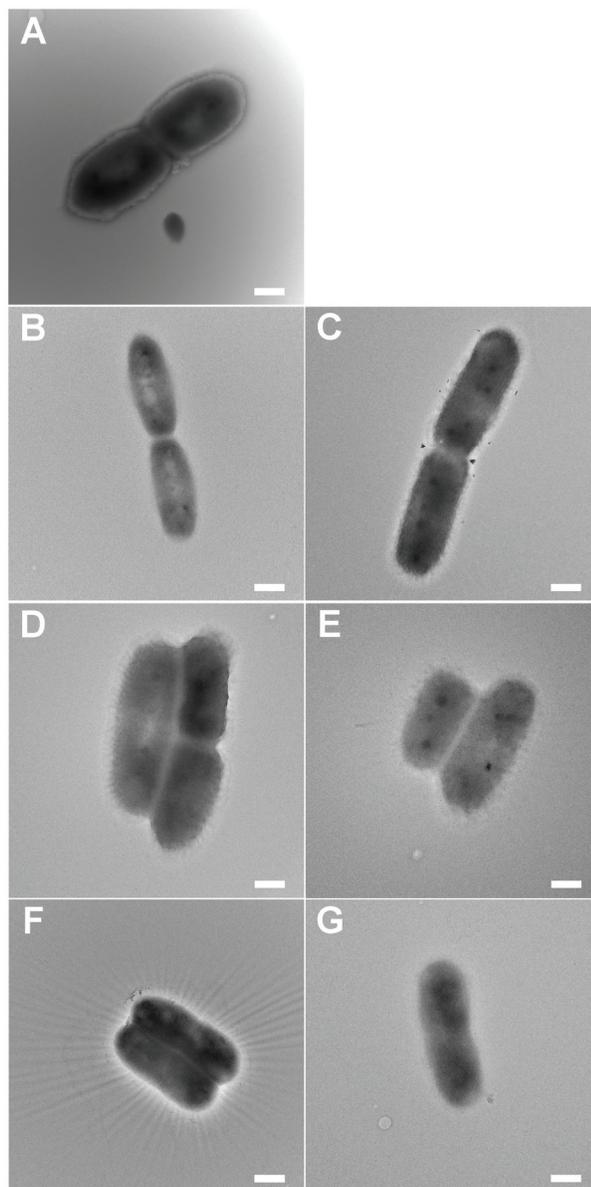
Figure 2.11. Transmission electron micrographs of PR1 exposed to ZnO-NP or ZnCl₂ for 4 h. **(A)** 0 mg Zn L^{-1}, **(B, D, F)** ZnO-NP exposed cells at 25, 100, 280 mg Zn L^{-1}, and **(C, E, G)** ZnCl₂ exposed cells at 25, 100, 250 mg Zn L^{-1}, respectively. Scale bar is 500 nm. Corresponding EDX spectra can be found in Figure 2.12. These conditions correlated to 100%, 100%, 70 to 50% and 0% viable cells respectively.
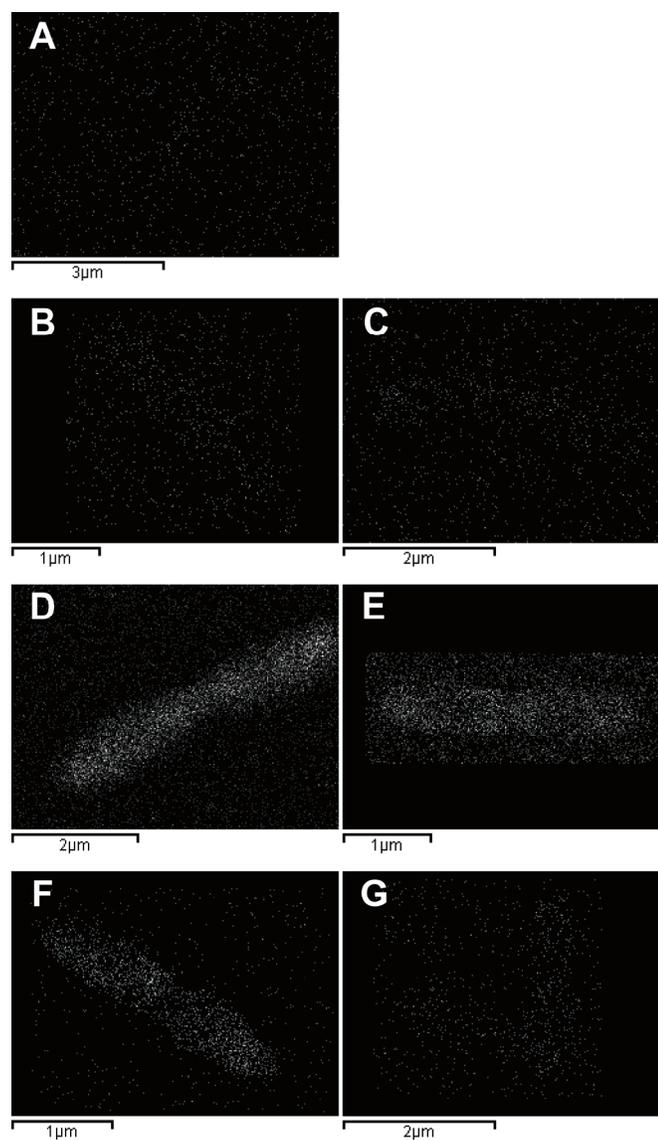
Figure 2.12. Energy dispersive X-ray maps of PR1 exposed to ZnO-NP or ZnCl₂ for 4 h. **(A)** 0 mg Zn L^{-1}, **(B, D, F)** ZnO-NP exposed cells at 25, 100, 280 mg Zn L^{-1} and **(C, E, G)** ZnCl₂ exposed cells at 25, 100, 250 mg Zn L^{-1}. Scale bars are below figures and maps correlate to conditions in Figures 5 and 6. EDX maps have not been manipulated, and in the case of (B), (E), and (G), the regions without data are the result of mapping an area smaller than full field.

2.4 Discussion

Counter-ion cytotoxicity and utilization. Since counter-ions and surface stabilizing agents are frequently used in manufactured NP formulations, evaluating the microbial response to these compounds is essential to understanding NP-microbe interactions. In our system, the counter-ion acetate was cytotoxic to PR1 at pH 5 (Figure 2.3). Acetate can be cytotoxic to microorganisms at low pH due to the ability of the undissociated acid to cross the bacterial membrane and dissociate in the cytoplasm, causing osmotic disruption and/or increasing internal acetate anion concentrations (Diez-Gonzalez and Russell, 1997). Some surface stabilizing agents, such as sodium dodecyl sulfate, have been found to be toxic to *E. coli*, while other compounds like TOPO and polyoxyethylene stearyl ether have been shown to increase *E. coli* growth (Brayner et al., 2006). Similarly, we also found that at pH 6 and 7, PR1 could utilize acetate as a carbon source, which has been observed in the parent strain of PR1, *B. vietnamiensis* G4 (G4) (Nelson et al., 1986) as well as *B. kururiensis* (Zhang et al., 2000). The sequenced genome of G4 contains the gene for acetate kinase, an entry point for acetate into pyruvate metabolism (ORNL, 2007), which would explain why 10.7 mM acetate increases the growth of PR1 at pH 6 and 7 and why PR1 utilizes both lactate and acetate. These results allowed us to further investigate how acetate utilization might be influencing ZnO-NP cytotoxicity by comparing toxicity to growing and resting cells.

ZnO-NP effects on growing cells. Some studies to date investigating engineered ZnO-NP toxicity to microorganisms have used a Zn^{2+} component (Heinlaan et al., 2008; Mortimer et al., 2008; Gajjar et al., 2009; Guy et al., 2009; Jiang et al., 2009), although most do not include a reference toxicant (Adams et al., 2006; Brayner et al., 2006; Reddy

et al., 2007; Zhang et al., 2007; Jones et al., 2008; Nair et al., 2008; Hu et al., 2009). Our

results show that both ZnO-NP and $ZnCl_2$ were 3-fold more toxic at pH 7 than pH 6

(Figures 2.6 and 2.7). To our knowledge, this is the first study demonstrating a trend of

pH-dependent toxicity for an engineered NP, although pH-dependent Zn^{2+} toxicity has

previously been observed in PR1 (Van Nostrand et al., 2005; Van Nostrand et al., 2007).

While the mechanism of Zn-resistance in PR1 is unknown, the parent strain G4 possesses

multiple copies of genes for the Zn^{2+} exporters ZntA and CzcD (ORNL, 2007), which are

involved in maintaining Zn-homeostasis by exporting Zn^{2+} from the cytoplasm. When

internal Zn^{2+} levels reach high concentrations, cell death is predicted to be caused by

disruption of the electron transport chain by Zn^{2+} binding to NADH oxidase (Beard et al.,

1995). Although we did not detect internalized intact ZnO-NP, it is possible that ZntA or

CzcD could transport ZnO-NP similar to how a multi-drug efflux transporter was able to

decrease 80 nm Ag-NPs cytoplasmic accumulation in *Pseudomonas aeruginosa* (Xu et

al., 2004). Additionally, based on the hydrodynamic diameter of the ZnO-NP in the stock

solution (1.2 nm), it would be possible for it to pass into the cell (Xu et al., 2004;

Kloepfer et al., 2005) but it is unknown whether the ZnO-NP maintains this size in our

experiments and moreover whether ZnO-NP would be able to inhibit NADH oxidase in

the same manner as Zn^{2+}. The observation that ZnO-NP follows a similar pH-dependent

toxicity trend implies either that the mechanism of Zn^{2+} resistance in PR1 is effective for

ZnO-NP exposure, that the mechanism of toxicity is very similar, or that ZnO-NPs

undergo extracellular or intracellular dissolution.

We also used SEM to evaluate changes in cell morphology with Zn exposure, as

well as determine whether NPs were detectable by SEM. Since previous studies have

demonstrated ZnO-NP aggregation can occur (Gajjar et al., 2009), there was the possibility that the 1.5 nm ZnO-NPs could form aggregates also. Our electron micrographs demonstrated that there were extracellular formations associated with cells at pH 6 amended with 75 and 250 mg Zn L^{-1} ZnO-NP and $ZnCl_2$ (Figures 2.8 and 2.9). Furthermore, EDX confirmed that these formations contained Zn, Fe, and P at 250 mg Zn L^{-1} ZnO-NP and $ZnCl_2$. Similar to other studies that fail to use a reference toxicant or confirm microscopy by EDX or similar techniques (Brayner et al., 2006; Applerot et al., 2009; Jiang et al., 2009), we could have identified these formations as ZnO-NP. Since the formations are present at lower Zn concentrations (75 mg Zn L^{-1}) with no detectable Zn, and at higher Zn concentrations are present with ZnO-NP and $ZnCl_2$, we confirmed they are not NPs. We have sense identified the formations at 75 mg Zn L^{-1} (Figure 2.8) as membrane vesicles which will be elaborated on later in Chapters 3 and 4.

In addition to quantifying growth-response effects of ZnO-NP, we also investigated the bioavailability of ZnO-NP associated acetate. Previous studies have demonstrated that surface modifiers can affect the growth and survival of NP exposed microorganisms. For example, *E. coli* grown with 1 mM ZnO-NP stabilized with DEG appears to enhance growth by 50% versus non-NP exposed cultures (based on figures; Reddy et al., 2007), whereas ZnO-NP stabilized with polyethylene glycol (PEG) was more toxic to *E. coli* than starch capped ZnO-NP (Nair et al., 2008). We found that at pH 6, PR1 is able to utilize ZnO-NP associated acetate at a rate similar to acetate amended $ZnCl_2$ (Figure 2.5). Since acetate removal by calcination results in changes to ZnO-NP structure (Figure 2.1), it would also be predicted that removal of acetate by PR1 could affect ZnO-NP structure, although we did not observe this (Figure 2.5). Ongoing

research investigating the nature of ZnO-NP associated acetate will greatly improve our understanding of counter-ion bioavailability and utilization.

ZnO-NP cytotoxicity to resting cells. It has been demonstrated that NPs exhibit different toxicity to growing cells versus resting cells. Thill et al. (2006) found that CeO-NPs were toxic to metabolically inactive cells, but noted they were not toxic to growing cells. Our resting cell assay attempted to limit cell growth by not including a carbon source, although there was an available carbon source for PR1 to utilize since acetate concentrations were constant between conditions. Due to this, slight growth was evident by the number of viable cells over the 4 h incubation period increased by $12 \pm 13\%$ (Figure 2.10) and the presence of cells undergoing division (Figure 2.11). Since the presence of acetate was unavoidable and growth was minimal, we predict that acetate metabolism was minimal. Using this resting cell assay we demonstrated that ZnO-NP was more toxic to resting cells than growing cells at pH 6 with 4 h LC_{50} values approximately 60% lower than 24 h EC_{50} values (Figures 2.7 and 2.10). Similarly, ZnO-NP and $ZnCl_2$ LC_{50} values were not significantly different at 95% FI. With increasing ZnO-NP and $ZnCl_2$ concentration, we did not observe extensive membrane damage (Figure 2.11). Conversely, Applerot et al.(2009), Zhang et al. (2007) and Nair et al. (2008) observed membrane damage 4 h, 5 h and 24 h, respectively, after *E. coli* were exposed to ZnO-NP in LB broth (predicted pH 7.0) and Brayner et al. (2006) observed membrane disorganization as well as unconfirmed ZnO-NP internalization in *E. coli* treated overnight in LB broth (predicted pH 7.0). Similar to studies of other NPs demonstrating NP attachment to the cell wall, Jiang et al. (2009) found ZnO-NPs attached to *Pseudomonas fluorescens* cells, but it was unclear whether this contributed to

77

ZnO-NP toxicity. Interestingly, Huang et al. (2008) found 60 nm polyvinyl alcohol coated ZnO-NP were internalized by *Staphylococcus aureus* grown overnight in pH 7.2 beef extract broth. Internalization was confirmed by selected-area electron diffraction analysis, which demonstrated internalized ZnO was less crystalline than ZnO-NP outside the cells that maintained its wurtzite structure. In our studies we detected electron dense regions associated with ZnO-NP and $ZnCl_2$ exposed cells (Figure 2.11), but EDX mapping did not identify similar regions of Zn, and instead demonstrated that Zn was evenly distributed across the cell (Figure 2.12). These findings highlight the necessity of elemental confirmation along with electron microscopy as well as the importance of using an appropriate toxicant control to evaluate NP-microorganism interactions.

Nanoparticle sorption onto cells has been well documented in the case of Ag-NPs (Sondi and Salopek-Sondi, 2004), MgO-NPs (Stoimenov et al., 2002), and CeO-NPs (Thill et al., 2006), to name a few. In addition to using EDX to evaluate cellular localization of Zn, we measured Zn adsorbed to cells exposed to ZnO-NP or $ZnCl_2$ by ICP-OES. We found that ZnO-NP and $ZnCl_2$ sorption did not correlate to increasing Zn concentrations and that both had uncharacteristic sorption curves (Figure 2.10). Since the irregular sorption values occurred when cells were exposed to ZnO-NP or $ZnCl_2$ concentrations greater than 100 mg Zn L^{-1} and less than 7% the of cells were viable, we predict that non-viable cells introduced confounding variables into the experimental analysis. For this reason we cannot say with certainty whether ZnO-NP and $ZnCl_2$ associate with PR1 cells differently, although they do exhibit similar cytotoxicity. Overall, our growth-inhibition and cytotoxicity values of ZnO-NP to PR1 seem to be in agreement with other ZnO-NP studies (Reddy et al., 2007; Zhang et al., 2007; Jones et

al., 2008; Nair et al., 2008). It is impossible, however, to accurately compare our results to others because Zn^{2+} is typically not used as a reference toxicant. Similar to our results, studies which used a Zn^{2+} control demonstrated that ZnO-NP was not more toxic to microorganisms than Zn^{2+} (Heinlaan et al., 2008; Mortimer et al., 2008; Jiang et al., 2009). Due to the broad differences in test microorganisms, media, growth conditions, and NP formulations, a reference toxicant is invaluable in comparing data sets.

  ZnO-NP stability and the influence of microbial growth. It is unclear how counter-ion utilization may change the physicochemical characteristics of a given NP. Since counter-ions and surface modifiers are often used to keep engineered NPs in a stable suspension, their removal should affect NP stability. Also, removing surface modifiers may allow NPs to react more directly with cells (Neal, 2008). Since microorganisms release compounds into the extracellular milieu, NPs may also react with these constituents thereby changing the physicochemical properties of the NP. For example, CdSe-QDs were more stable with *P. aeruginosa* than in abiotic samples (Priester et al., 2009). Interactions with compounds like proteins may improve NP stability, but may also allow for increased NP-uptake by microorganisms (Kloepfer et al., 2005). Our data indicates that counter-ion utilization does in fact occur, emphasizing the need to understand the physicochemical changes NPs undergo due to microbial growth in order to accurately interpret toxicological results.

  In addition to microbial metabolism affecting NP structure, there may also be abiotic processes that can affect NP stability. Media components, such as large organic molecules found in undefined media like LB, could potentially affect NP aggregation or agglomeration similar to humic acid (Baalousha et al., 2008; Klaine et al., 2008). How a

NP is stabilized will also change how pH and ionic strength affects NP stability (Yang and Xie, 2006; Baalousha et al., 2008; Christian et al., 2008; Klaine et al., 2008; Limbach et al., 2008). Furthermore, concentration dependent effects have been observed for some NPs, emphasizing the importance to characterize NP structure at experimental concentrations (reviewed by Christian et al., 2008). These variables may affect ZnO-NP dissolution, which has been measured and can confound results. In a study of bulk ZnO and ZnO-NP toxicity to freshwater microalga, toxicity was attributed to Zn^{2+} based on similar toxicity and measured dissolution of both bulk and nano-ZnO (Franklin et al., 2007). Additionally, Zn^{2+} has been detected with ZnO-NP exposure to microorganisms. Using an electrode system, Zn^{2+} was measured in an 0.8% ZnO nanofluid (Zhang et al., 2007) and by using a biosensor to measure bioavailable Zn^{2+}, both 1 mg Zn L^{-1} bulk ZnO and ZnO-NP contained 84% bioavailable Zn^{2+} (Heinlaan et al., 2008). Due to the low-contrast nature of ZnO-NP, small size, and lack of UV-Vis response in our system, we were not able to confirm ZnO-NP structure changes.

The dissolution of NPs to their individual constituents can confound toxicity results yet few studies have characterized ZnO-NPs under experimental conditions (Franklin et al., 2007; Heinlaan et al., 2008; Huang et al., 2008). As the field of nanotoxicology has progressed, more research groups are addressing NP dissolution as mechanism of toxicity, albeit indirect toxicity (Mahendra et al., 2008; Navarro et al., 2008; Priester et al., 2009). Determining how environmental factors, both biotic and abiotic, affect the physicochemical properties of NPs is essential to understanding their fate and environmental impact. Future studies evaluating ZnO-NP, or other soluble NPs, will need to not only address the effect of surface stabilizers on microorganisms, but also

how microbial metabolism and experimental matrix may affect NP physicochemistry and

stability in order to provide accurate toxicity conclusions.

CHAPTER 3

MEMBRANE VESICLE PRODUCTION BY *Burkholderia vietnamiensis* PR1$_{301}$ IS INFLUENCED BY pH AND Zn

3.1. Introduction

Evaluating metal-microbe interactions requires an interdisciplinary approach to understanding not only chemistry that is occurring at or near the bacterial membrane, but also the biological response of the bacterium. Metal toxicity to bacteria can be expressed in terms of the effects of the total metal concentration, but strong evidence exists that metal toxicity is often determined by metal speciation (Deheyn et al., 2004). Models have been developed to serve as a framework to examine how changes in metal-speciation cause a biological response. Most notable are the Free Ion Activity Model (FIAM) and Biotic Ligand Model (BLM), which predict toxicity based on the free ion concentration of a metal, as well as what factors affect its binding to a biotic ligand which is assumed to elicit a biological response (Campbell, 1995; Pagenkopf, 2002).

The underlying assumption of the FIAM and BLM is that the free metal ion concentration is proportional to metal toxicity, such that the free metal ion concentration is an index of reactivity (Deheyn et al., 2004). It has been suggested that metal species other than the free metal ion can be responsible for metal toxicity in bacteria. For example, hydroxo-metal complexes have been implicated in metal toxicity owing to the ability to effectively bind to and penetrate the membrane of bacteria (Ivanov et al., 1997). Depending on medium composition as well as pH, the distribution of metal species between the free ion, hydroxo-complexes and organic and inorganic complexes can vary greatly. Additionally, pH can affect cell membrane chemistry with increasing pH resulting in increasing negative charge on the membrane surface facilitating increased metal sorption (Chubar et al., 2008). For example, *Bacillus jeotgali* sorbed 3-fold more Zn at pH 7 versus pH 5 (Green-Ruiz et al., 2008). In addition to changes in

physicochemistry of the cell membrane and extracellular matrix, pH and metal

concentration can also affect the biological response. For example, increasing Zn

concentrations elicited increased efflux rates in the Gram-positive bacteria *Rhodococcus*

opacus (Mirimanoff and Wilkinson, 2000), while decreased pH elicited a biological

response in *Escherichia coli* which resulted in increased Cd resistance (Worden et al.,

2009).

Bacteria are able to respond to metal ions by reducing uptake, enhancing efflux,

internal sequestration in the periplasm or cytoplasm, surface sequestration, external

sequestration, and/or metal reduction (Hausinger, 1993). These mechanisms broadly

result in decreasing the availability of biological targets (e.g., essential proteins) to metal

ion binding (Nies, 1999). Membrane vesicles (MVs) produced by bacteria can also

export compounds and have been shown to accumulate metal ions on their surface

(Gorby et al., 2008; Bomberger et al., 2009). To date, the role of MVs in metal-microbe

interactions has not been evaluated despite their diverse functional capacities (Mashburn-

Warren and Whiteley, 2006). Membrane vesicles are 50 to 250 nm extracellular

structures produced by a wide range of bacteria derived from the outer membrane

(Beveridge, 1999). Membrane vesicles are known to function in virulence factor

transport (Kadurugamuwa and Beveridge, 1995), protein (Ciofu et al., 2000) and DNA

exchange (Yaron et al., 2000), cell-cell communication (Mashburn and Whiteley, 2005),

and biofilm formation (Schooling and Beveridge, 2006). Due to their ubiquitous and

multifaceted nature, it seems likely that MVs also play a role in metal-microbe

interactions.

Previous research in our laboratory has focused on pH-dependent metal resistance in *Burkholderia vietnamiensis* PR1$_{301}$ (PR1) (Van Nostrand et al., 2005; Van Nostrand, 2006; Van Nostrand et al., 2008). We have previously observed that PR1 produces MVs (Figure 2.8). Since pH not only affects metal speciation but may also affect biological responses, such as MV production, the first step in addressing the involvement of MVs in metal-microbe interactions was to evaluate MV production. The goal of this chapter was to investigate how MV production is related to pH and Zn concentration, while in Chapter 4 the role of MVs in metal-microbe interactions will be investigated.

3.2. <u>Materials and Methods</u>

Bacterial cultures. The growth medium used was 4M (refer to Chapter 2), which was modified at pH 5 to have the same Na concentrations as pH 7. This was accomplished by the addition of 37.6 mL of 2.5 M NaCl per liter of pH 5 medium before the pH was adjusted. The PR1 inoculum prepared before each experiment was grown as previously described (refer to Chapter 2).

Evaluating Zn toxicity at pH 5 and 7. To evaluate the toxicity of Zn to PR1 at different pH values, a growth-response assay was conducted as described earlier (Chapter 2), except that acetate was not added. Briefly, media at pH 5 and 7 was amended with Zn to yield final concentrations of 0, 1.53, 3.82, 7.65, 15.3, 22.9, 30.6, and 45.9 mM Zn and 0, 0.38, 0.76, 1.53, 2.29, 3.06, and 3.82 mM Zn, respectively. Triplicates of each condition were inoculated with PR1, were incubated at 30°C with shaking (200 rpm) and growth was monitored at 0, 4, 8, 12, 16, and 24 h by removing a 0.6 mL aliquot and measuring the optical density at $\lambda = 610$ nm (OD$_{610}$). Toxicity was quantified by

determining the total Zn concentration required to elicit a 50% inhibition of growth (EC_{50}) at 24 h. For each condition, % inhibition at 24 h was calculated as 1- [OD_{610} condition ÷ OD_{610} of the unamended culture] x 100. To determine the $EC_{50} \pm SE$ (standard error) at each pH, the data were fit to a nonlinear model using a 3 parameter logistic plot using SigmaPlot 8.0 (SYSTAT Software Inc., San Jose, CA USA).

Quantifying MV production. To evaluate MV production during growth of PR1, aliquots (0.25 mL) of inoculum were added to five triplicate sets of sterile 125 mL screw-top flask containing 24.75 mL of 4M media at pH 6. At 0, 4, 8, 12, and 24 h, 0.1 mL aliquots were removed to determine whole cell lysate protein concentration. Purity was confirmed during experiments by streaking growth cultures on Luria Bertani (LB) plates. Aliquots of whole cell lysate were stored at -20°C until analysis and purity plates were incubated at 30°C for 48 h. The remaining 24.3 mL was centrifuged 6,000 g for 5 min at 5°C. The supernatant was passed through sterile 32 mm Acrodisc® syringe filters with a 0.45 μm Supor® membrane (Pall Corporation, Ann Arbor, MI). Plating of 0.25 mL of this filtrate onto LB plates showed no growth after 48 h at 30°C indicating the absence of viable cells. To pellet the MVs, the filtrate was centrifuged at 75,600 g for 3 h at 10°C. The supernatant was removed and the remaining pellet was resuspended in 1 mL of 50 mM HEPES (pH 6.8) and transferred to 1.5 mL Eppendorf tubes. These samples were centrifuged 16,100 g for 30 min at 4°C, the supernatant removed, and the HEPES wash and centrifugation was repeated. These MV pellets were resuspended in 1 mL of 50 mM HEPES (pH 6.8) and stored at -20°C until analysis. Protein concentration of whole cell lysate aliquots and MV aliquots was determined using the Bradford method (Bradford, 1976). To evaluate MV production in response to Zn at pH 5 and 7, PR1 was

grown in 4M amended with 0, 0.76, 3.82, and 7.65 mM Zn at pH 5 and 0, 0.15, 0.38, and

0.76 mM Zn at pH 7. Growth at 12 h was measured by OD_{610} to confirm that the chosen

Zn concentrations were not inhibiting growth of PR1. Three experiments were

performed on consecutive days to generate triplicate samples for each condition. Each of

the three experiments yielded 8 MV fractions which were processed as described above

and protein concentration was quantified using the Bradford method (Bradford, 1976).

Electron microscopy. Scanning electron microscopy (SEM) was used to

evaluate the structure of MVs produced by PR1 during growth in 4M at pH 6. To prepare

MVs for analysis by SEM, a glass microscope slide was broken into a piece that was less

than 13 mM wide, dipped into a solution of poly-L-lysine, and allowed to dry. An

aliquot of purified MVs from 12 h growth was dropped onto the slide which was then

incubated with Os vapor in a glass petri dish overnight. Due to evident formation of

crystals on the slide, the slide was rinsed with 0.45 μm filtered 18.2 MΩ water. Once

dried, the slide was fixed to the specimen mount using conductive carbon adhesive tabs

(Electron Microscopy Sciences, Hatfield, PA). SEM images were attained using a LEO

982 field emission SEM (Zeiss SMT, Peabody, MA).

Thermodynamic modeling. Visual MINTEQA2 (v. 2.51; Gustafsson, 2009),

which is a Windows version of the DOS-based MINTEQA2 v. 4.03 (USEPA, 1999), was

used to model chemical speciation in 4M at different pH and with different Zn

concentrations. Although previous modeling studies of Ni-speciation in 4M modified the

database to include MES, nitrilotriacetic acid (NTA), and lactate (Van Nostrand et al.,

2005), the present version of MINTEQA2 contains thermodynamic data for these Zn-

species, except Zn-MES$^+$. The absence of this species is supported by studies which have

demonstrated that Zn-binding to MES is negligible (Poulson and Drever, 1996; Soares et al., 1999). All components in the media were used in the modeling experiments (Table A.1). Briefly, a Davies b parameter of 0.3 was used, oversaturated solids were allowed to precipitate, pH was fixed, and ionic strength was allowed to vary during the reaction. Additional details can be found in Appendix A and B which contain the complete input and output data for the results presented in this chapter.

3.3. <u>Results</u>

Zn toxicity to PR1 is influenced by pH. All of the research contained in Chapters 3, 4 and 5 utilize a media with normalized Na concentrations at pH 5 and 7. Previous research quantifying metal toxicity to PR1 (Van Nostrand et al., 2005; Van Nostrand et al., 2007; Van Nostrand et al., 2008), as well as data in Chapter 2, did not adjust Na concentrations between different pH media. Using empirical data (i.e., how much NaOH is used to bring 4M to pH 5 or pH 7), the Na concentration of 4M at pH 5 and pH 7 was predicted to be 5.7 mM and 99.72 mM, respectively. To account for this large discrepancy in Na concentrations, additional NaCl was added to 4M at pH 5 so that both pH would contain 99.72 mM Na, though this did result in 100.63 mM Cl at pH 5 (compared to 0.91 mM at pH 7). Due to these media modifications as well as a need for complete Zn-toxicity data set, initially we confirmed previous results by Van Nostrand et al. (2005) which demonstrated that divalent first row transition metals are more toxic to PR1 at pH 7 versus pH 5. Using the Na normalized media, calculated EC_{50} concentrations (±SE) for Zn were 23.5 ± 0.3 and 1.47 ± 0.1 mM at pH 5 and 7 respectively.
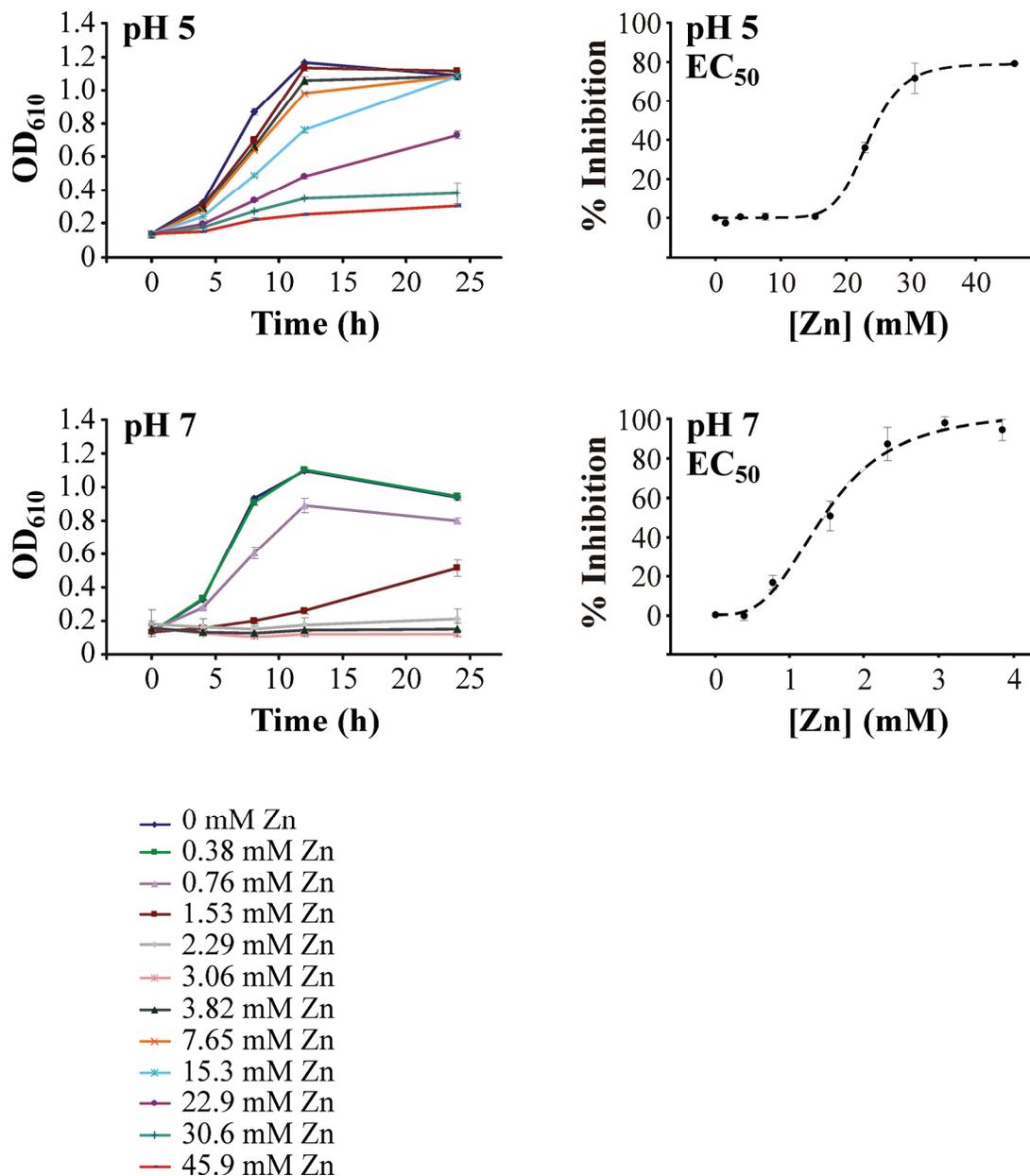
Figure 3.1. Growth of PR1 with Zn at pH 5 and 7. Growth curves were generated using OD_{610}. Zn EC_{50} values for each pH were determined by fitting 24 h growth inhibition at each Zn concentration to a 3 parameter logistic curve (dotted line). Error bars represent ± 1.0 standard deviation based on triplicate measurements.

Thermodynamic modeling to predict changes in Zn-speciation between pH.

Since previous research has indicated that pH-dependent Ni toxicity to PR1 does not appear related to Ni^{2+} concentration (Van Nostrand et al., 2005), we evaluated changes in Zn-speciation between pH as it related to toxicity. To identify Zn-species which correlated to Zn-toxicity at each pH, concentrations of Zn-species were plotted against logistic regression plots of total Zn concentration and 24 h growth inhibition (Figure A.1). At pH 5, the majority of species had a linear relationship versus total Zn concentration (Figures 3.2 and A.1). Conversely, at pH 7, most Zn-species exhibited a sigmoidal relationship to total Zn concentration (Figures 3.2 and A.2). For both pHs, Zn^{2+} concentration is shown as a point of reference since metal toxicity models (e.g., FIAM and BLM) assume the free ion concentration is the key indicator of metal toxicity.

To further explore the involvement of each Zn-species in the observed pH-dependent toxicity, Zn-species concentrations were plotted against pH in modified 4M with 1.53 mM Zn (Figure A.7). Zn-species that would be driving Zn-toxicity to PR1 would be expected to increase from pH 5 to 7. This analysis indicated that Zn^{2+} concentration did not correlate to changes in Zn-toxicity across pH (Figure 3.3). The concentrations of $ZnOH^+$ and $ZnNH_3^{2+}$ did increase with pH, indicating their possible involvement in pH-dependent Zn-toxicity (Figure 3.3). If the concentration of these Zn-species was related to pH-dependent metal toxicity, then we would expect similar concentrations to correspond to Zn-toxicity at each pH. Also, we would expect them to correlate to Zn toxicity at different media conditions used in this dissertation which varied Na concentration and included acetate. Therefore, growth inhibition data
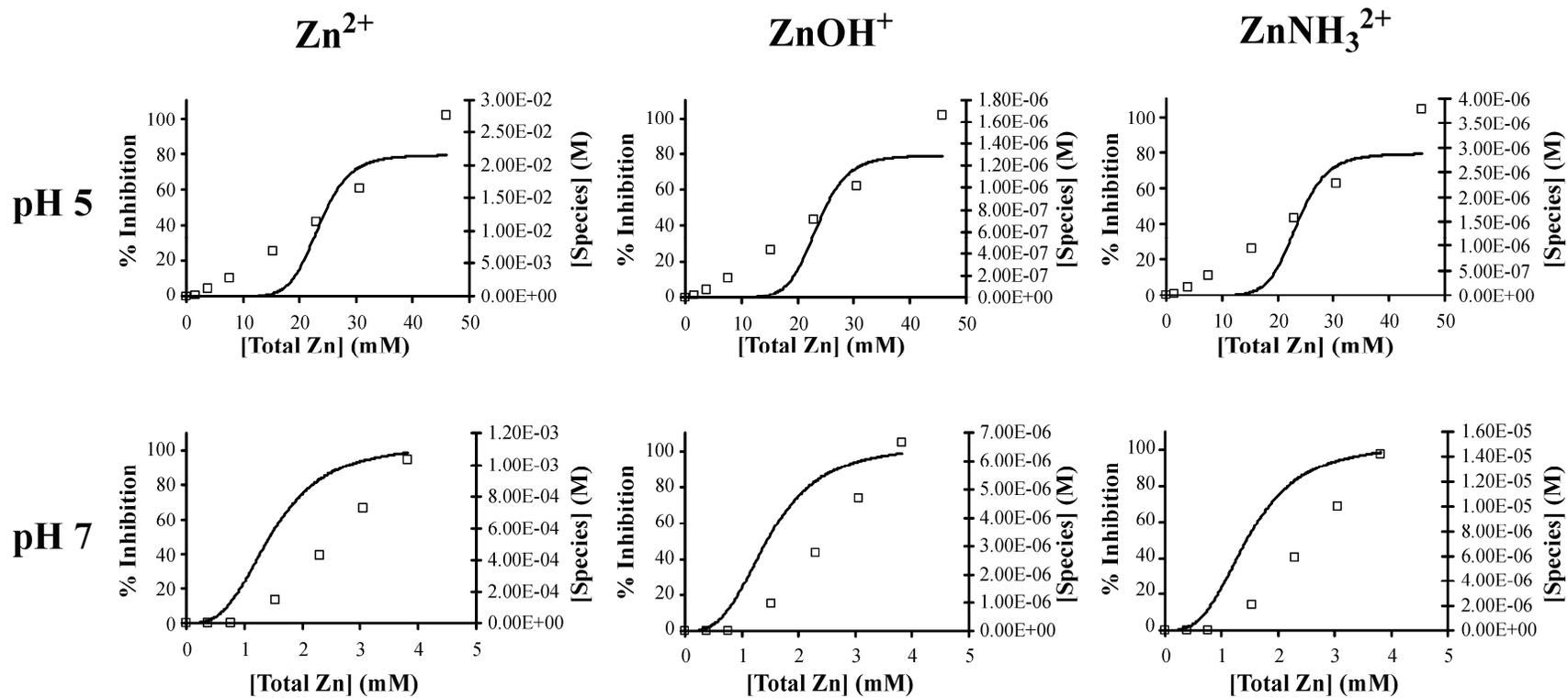
Figure 3.2. Changes in Zn-speciation at pH 5 and 7 correlated to Zn toxicity. Output from MINTEQA2 for select Zn-species at total Zn concentrations used in determining Zn-toxicity to PR1 was plotted against curves fit to 24 h growth inhibition data.
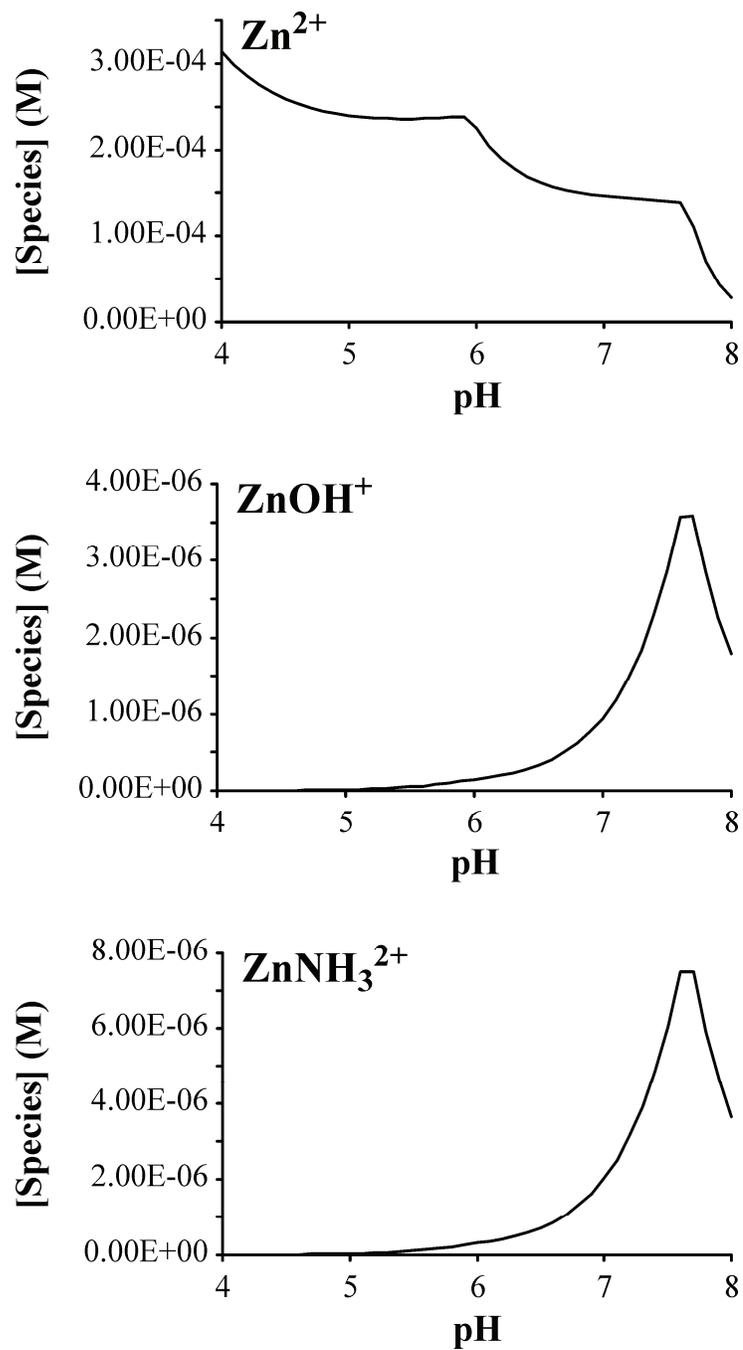
Figure 3.3. Changes in Zn-species concentration in relation to pH. Graphs were plotted using data generated by modeling a pH sweep in modified 4M with 1.53 mM Zn. Results for other Zn-species can be found in Figure A.7.

Table 3.1. Comparison of the concentration of select Zn-species at calculated EC$_{50}$ values under different conditions. All concentrations are molar. Data from experiments listed below the dotted line can be found in Chapter 2 and Appendix A.

Experiment	[Total Zn]	[Zn^{2+}]	[ZnOH$^+$]	ZnNH$_3$$^{2+}$]
pH 5	2.35 E-2	1.16 E-2	7.25 E-7	1.61 E-6
pH 7	1.50 E-3	1.26 E-4	8.13 E-7	1.74 E-6
pH 5 (5.7 mM Na)	4.36 E-2	2.64 E-2	1.85 E-6	3.79 E-6
pH 6 (41.7 mM Na)	9.49 E-3	3.37 E-3	2.39 E-6	4.80 E-6
pH 6 (+ 10.7 mM Acetate)	3.20 E-3	7.01 E-4	4.90 E-7	9.94 E-7
pH 7 (+ 10.7 mM Acetate)	1.03 E-3	3.50 E-5	2.23 E-7	4.81 E-7

presented in this chapter, as well as EC_{50} data collected at pH 5 with 5.7 mM Na, at pH 6 with and without 10.7 mM acetate, and at pH 7 with 10.7 mM acetate (Chapter 2) was used to evaluate this hypothesis. We found that $ZnOH^+$ and $ZnNH_3^{2+}$ concentrations were similar at EC_{50} values from different experiments (Table 3.1), at 1.08 ± 0.85 μM $ZnOH^+$ and 2.23 ± 1.7 μM $ZnNH_3^{2+}$ (average RSD of 77%). If EC_{50} values from experiments where 10.7 mM was used are omitted, the average concentrations were 1.44 ± 0.8 μM $ZnOH^+$ and 2.98 ± 1.6 μM $ZnNH_3^{2+}$ (average RSD of 54%). In contrast, Zn^{2+} concentrations at these same EC_{50} values were not similar at $7,040 \pm 10,500$ μM and $10,400 \pm 11,700$ μM. This demonstrates that $ZnOH^+$ and $ZnNH_3^{2+}$ concentrations correlate to Zn-toxicity under different media conditions better than Zn^{2+}, though the presence of acetate decreased this correlation.

Developing a method to quantify MV production. In Chapter 2, we observed that PR1 produces MVs (Figure 2.8) and images of cells after 24 h growth with $ZnCl_2$ or ZnO-NP at pH 6 indicated that MVs had associated Zn (Figure 2.9). To investigate this further, we developed a method to quantify MV production by PR1. Growth of PR1 in modified 4M at pH 6 and MV production was measured over 24 h (Figure 3.4). To confirm that measured MV protein concentrations were above experimental background, we also analyzed samples from uninoculated medium. In addition, to determine that cells were not present in this purified MV fraction, aliquots were plated on LB agar and no colony growth occurred over 48 h. During growth at pH 6, MV production lagged behind growth such that maximum MV production occurred from mid-log to early stationary phase (Figure 3.4). Additionally, maximum MV yield at 12 h was 3 μg mL^{-1}, which is approximately 1% of total culture protein which is typically 300 μg mL^{-1}.

A
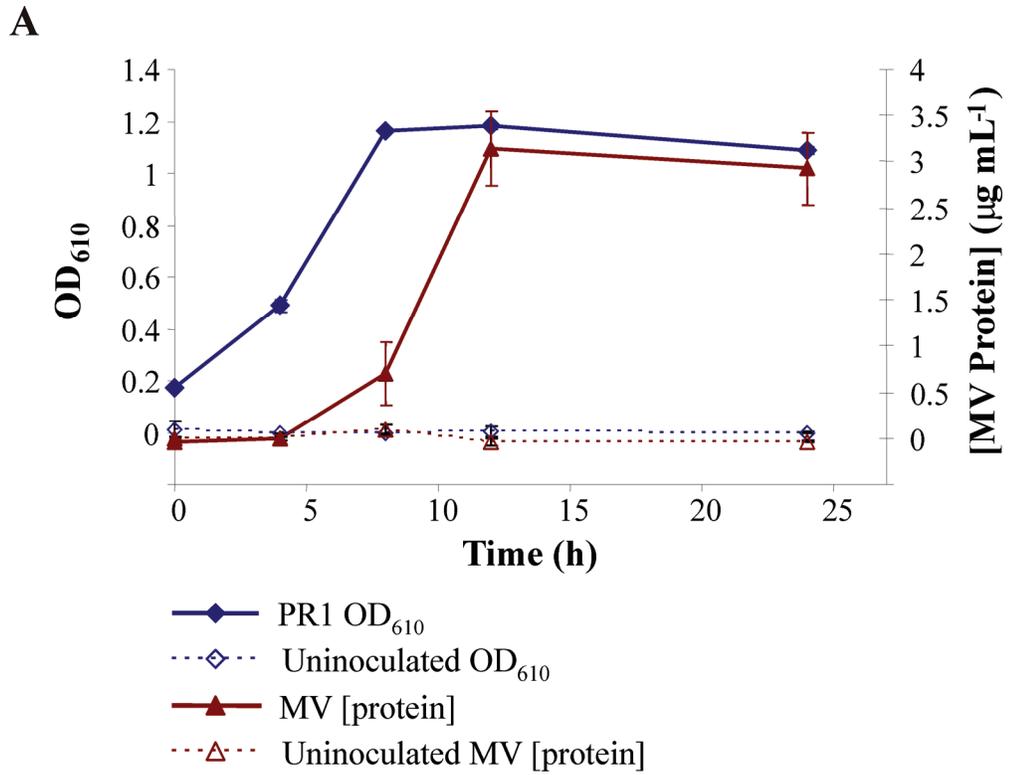
B
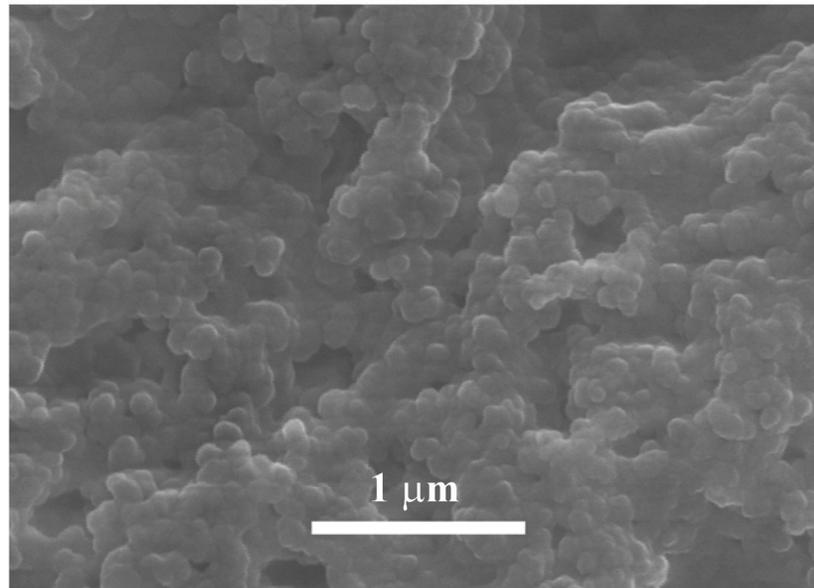
Figure 3.4. MV production by PR1. (A) MV production during growth of PR1 at pH 6, with a control, uninoculated, measured in parallel to detect any MV protein background. Error bars represent ± 1.0 standard deviation based on triplicate measurements. **(B)** Scanning electron micrograph of MVs produced at 12 h growth at pH 6.

Samples of harvested MVs from 12 h were also evaluated by SEM and demonstrated that the MVs were spherical with an approximate average diameter of 100 nm, ranging 50 to 125 nm (Figure 3.4). For subsequent experiments, 12 h was used to harvest MVs since this represents maximum MV production in PR1. Also, this time point is used in subsequent experiments (Chapters 4 and 5) requiring ultrapurification of MVs since there is less cell debris caused by cell death relative to points during stationary growth phase.

Quantifying MV production at different pHs. Since Zn toxicity is 16-fold different between pH 5 and 7, we addressed the question of whether MV production is also influenced by pH. PR1 was grown without Zn amendment for 12 h and MVs were harvested in the same manner described above. MV production was observed to increase from pH 5 to 7, going from 1.5 ± 0.3 μg mL^{-1} to 4.7 ± 0.5 μg mL^{-1} (Figure 3.5).

Quantifying MV production in response to Zn at different pHs. In order to compare MV production in response to Zn at 12 h growth, sub-lethal Zn concentrations were chosen to minimize changes in MV production due to growth phase (Figure 3.4), since at higher Zn concentrations, the length of exponential phase growth as well as changes in overall cell density were observed (Figure 3.1). Concentrations used at pH 5 and 7 were 0, 0.76, 3.82 and 7.65 mM Zn and 0, 0.15, 0.38, and 0.76 mM Zn, respectively. The results demonstrate that increasing Zn concentration at both pHs caused a decrease in MV concentration (Figure 3.6). Across the Zn concentrations tested, MV concentrations decreased dramatically at pH 5 from 0.76 to 3.82 mM Zn and from 0 to 0.76 mM Zn at pH 7. Additionally, when purifying MVs from cultures grown with 7.65 mM Zn at pH 5, there was a white precipitate visible that did not contain detectable
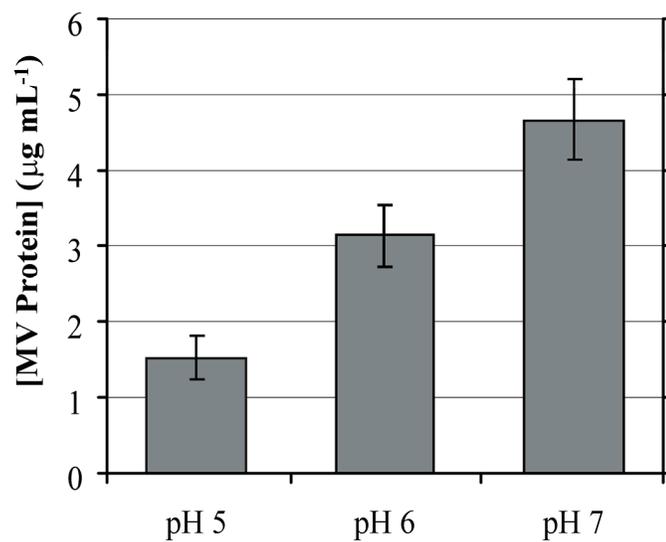
Figure 3.5. MV production increases with increasing pH. MV production by PR1 at three pHs after 12 h growth. Error bars represent ± 1.0 standard deviation based on triplicate measurements.
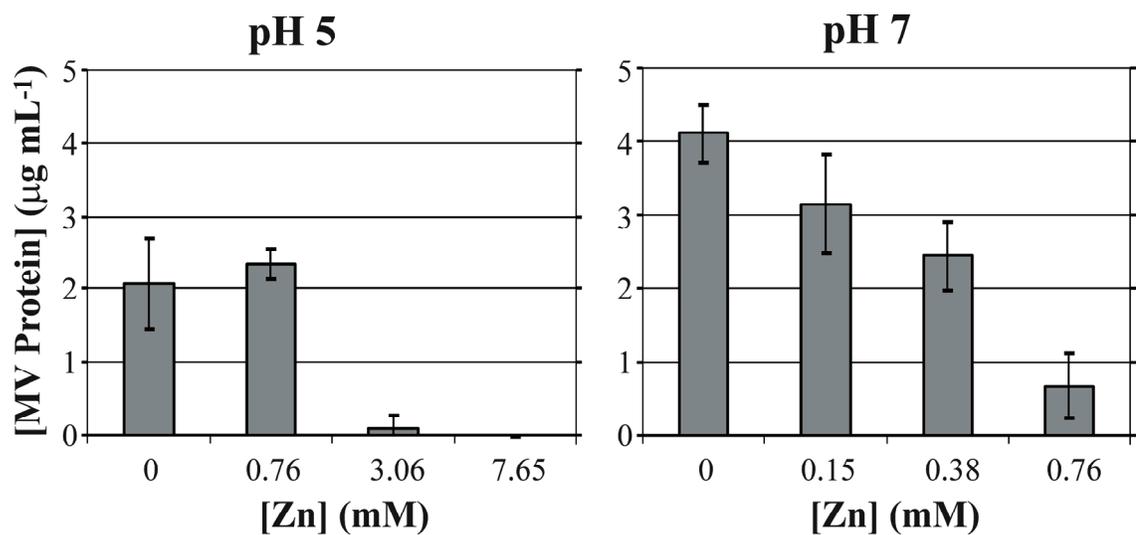
Figure 3.6. MV production at sub-lethal Zn concentrations. MV concentration measured by protein concentration at 12 h growth in media at pH 5 or 7 amended with Zn. Error bars represent ± 1.0 standard deviation based on triplicate measurements.

amounts of protein. This result will be discussed in more detail in Chapter 4, where it is

demonstrated that Zn precipitates to an unknown Zn-species.

Evaluating changes in Zn-speciation in relation to changes in MV

production. Similar to the analysis of Zn-speciation in relation to Zn-dependent toxicity,

we evaluated whether predicted changes in Zn-speciation corresponded to observed

changes in MV production. At pH 5, most Zn-species tracked with the change in MV

production and it was unclear that a specific species may be driving this change (Figure

B.1). At pH 7, there was relatively little change in Zn-speciation from 0 to 0.38 mM Zn,

while the majority of species then increased between 0.38 and 0.76 mM Zn (Figure B.2).

Closer inspection reveals that species were changing by orders of magnitude between 0

and 0.38 mM Zn, but this change was minimal compared to the change between 0.38 and

0.76 mM Zn. Since $ZnOH^+$ and $ZnNH_3^{2+}$ appeared to be significant indicators of pH-

dependent Zn-toxicity, these concentrations were plotted against % inhibition of MV

production, with Zn^{2+} as a point of reference, using a log scale instead of a linear scale

(Figure 3.7). At both pHs, the relationship between the decrease in MV production is

directly proportional to the log-concentration of Zn-species. Although only three species

of interest are shown here, most Zn-species follow identical trends at both pHs (Figures

B.1 and B.2). For this reason, it is difficult to determine any single species that is

affecting MV production, since all species vary collinearly at these Zn concentrations.
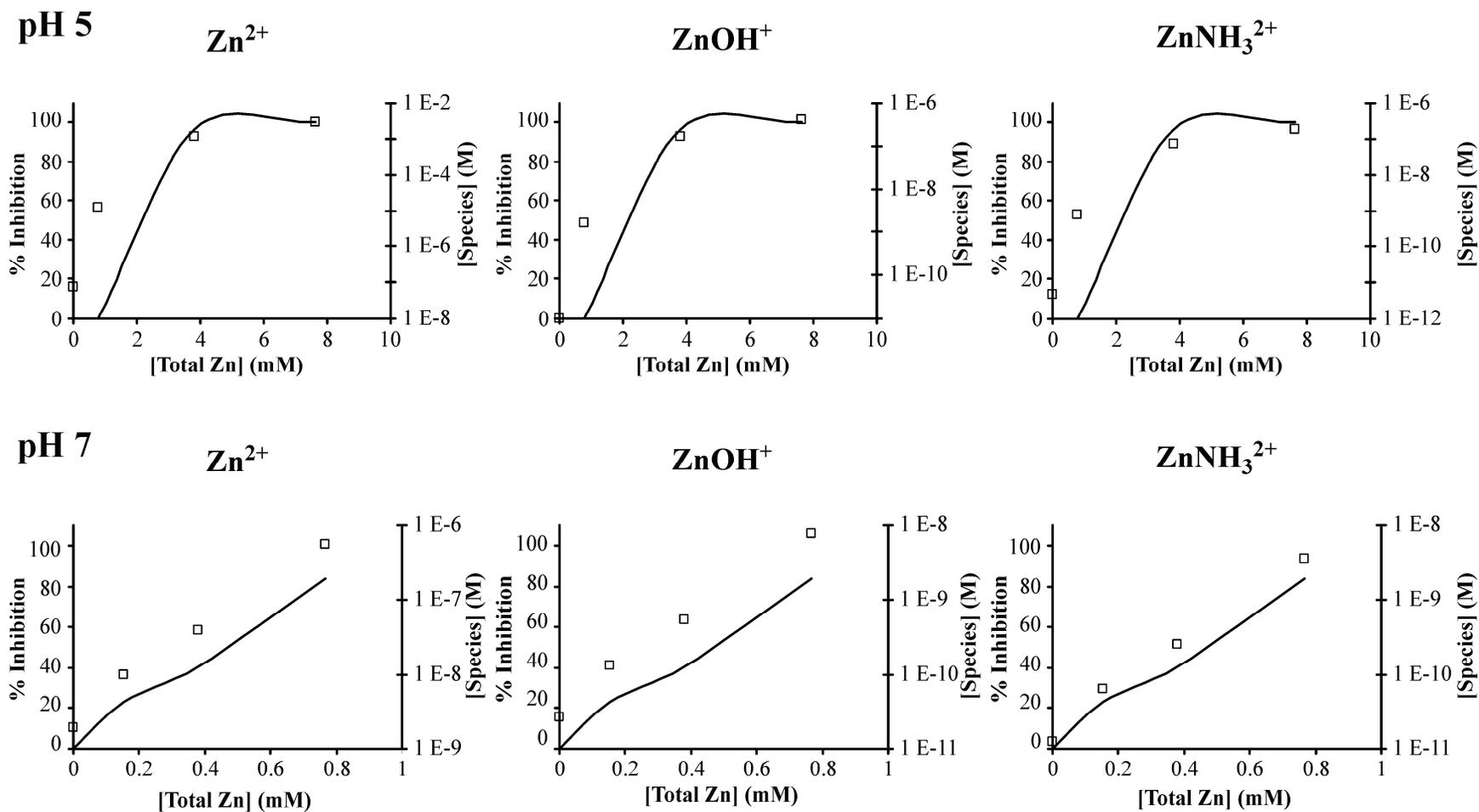
Figure 3.7. Changes in Zn-speciation at pH 5 and 7 correlated to MV production. Output from MINTEQA2 for select Zn-species at total Zn concentrations used in determining the effect of Zn on MV production by PR1 was plotted against % MV production inhibition curves. These curves are only four points connected with a smoothed line.

3.4. __Discussion__

Correlating toxicity endpoints to changes in Zn-speciation. Coupling

thermodynamic modeling results to toxicity endpoints is a useful tool to determine metal

species that correlate to the observed toxicity. Previous research on PR1 and Ni-toxicity

demonstrated that the free ion metal concentration did not correlate to increased toxicity

at pH 7 versus pH 5 (Van Nostrand et al., 2005). In this chapter, the toxicity of Zn to

PR1 was evaluated, and a similar trend that Zn was 16-fold more toxic at pH 7 than pH 5

was observed (Figure 3.1). Similarly, studies of Cd^{2+} toxicity to *E. coli* and a

Burkholderia sp. demonstrated that the free ion concentration decreased as metal toxicity

increased (Sandrin and Maier, 2002; Worden et al., 2009). In the case of Cd-toxicity to

E. coli, formation of $CdOH^+$ species, although much less abundant than Cd^{2+}, correlated

more strongly to changes in toxicity with pH (Worden et al., 2009). These studies of Ni

and Cd toxicity across pH evaluated the influence of different metal species by

comparing changes in predicted speciation at discrete inhibitory metal concentrations as

well as broad changes in speciation across pH. In contrast, we employed a more robust

method to evaluate changes in Zn-speciation to observed changes in toxicity.

In order to evaluate and establish which Zn-species correlate to changes in Zn-

toxicity between pH, three criteria had to be satisfied. First, a Zn-species had to correlate

to changes in toxicity to PR1 at each pH, using 24 h growth inhibition as an endpoint.

Second, a Zn-species had to increase in concentration with pH since Zn toxicity increases

with pH. Lastly, concentrations of Zn-species that correlate to toxicity had to be

relatively similar at EC_{50} Zn concentrations between experiments. In previous studies

correlating metal speciation and metal toxicity to bacteria, often only the second criteria

is satisfied, whereas coupling this data to toxicity data in the first criteria can lead to successful identification of metal species which correlate to observed changes in toxicity. For example, Zeng et al. (2009) used this technique to determine that intracellular Zn-concentration was the best predictor of Zn-toxicity to *Microcystis aeruginosa*. Using our three criteria, we demonstrate that $ZnOH^+$ and $ZnNH_3^{2+}$ concentrations are predicted to increase with increasing pH and correlate to observed Zn-toxicity (Figures 3.2 and 3.3). Moreover, the concentration of these species at Zn EC_{50} concentrations was similar between the conditions evaluated in this chapter, as well as Zn toxicity in the presence of acetate (Chapter 2) and with varying Na concentrations at pH 5 (Table 3.1). Conversely, the free ion Zn^{2+} concentration does not fulfill these criteria since it was predicted to decrease in concentration as pH increased and its corresponding concentration at EC_{50} Zn concentrations decreased by one-order-of-magnitude per pH unit increase. Thus, these data suggests that $ZnOH^+$ and $ZnNH_3^{2+}$ concentrations are a better indicator of Zn toxicity to PR1 as a function of pH than Zn^{2+} concentrations.

The effect of pH on metal speciation tends to cause a shift from the free ion to inorganic complexes with increasing pH. In eukaryotic systems, this shift is predicted to render metals less toxic by decreasing the free ion concentration of the metal; for example, the formation of Zn hydroxide complexes correlates to reduced toxicity to flathead minnow (Santore et al., 2002). In bacteria hydroxylated metal complexes have been implicated in increased toxicity to *Pseudomonas fluorescens*, *E. coli*, and *Mycobacterium phlie* due to the ability of this complex to more readily penetrate cell membranes (Ivanov et al., 1997). Conversely, a study of Cd-toxicity to a *Burkholderia* sp., trivialized the role of $CdOH^+$ in Cd-toxicity since its concentration was three-orders-

of-magnitude lower than Cd^{2+} (Sandrin and Maier, 2002). In a recent study of Cd-toxicity to *E. coli*, a similar trend was observed where $CdOH^+$ concentration was three-orders-of-magnitude less than the free ion Cd^{2+} concentration, but since it tracked with increased toxicity, the authors suggest that this species is much more toxic than Cd^{2+} (Worden et al., 2009). Similar to these studies, we found that, although $ZnOH^+$ and $ZnNH_3^{2+}$ concentrations correlated well to changes in Zn-toxicity to PR1, at Zn EC_{50} concentrations they were five-orders-of-magnitude less than Zn^{2+} at pH 5, and two-orders-of-magnitude less at pH 7 (Table 3.1). This does not prove that these species are more toxic than the free ion Zn^{2+}, but that these species may be a more accurate index of Zn-toxicity within our system. Taken together, these results and other studies demonstrate that the free ion concentration does not always correspond to metal toxicity to bacteria, and other metal species or measurements may be better at predicting toxicity.

MV production is affected by pH and Zn. Gram-negative bacteria are known to produce MVs and research has focused on characterizing their functional properties (reviewed by Lee et al., 2008). Although much has been learned in the last 15 years about functions of MVs, much less is known about factors which affect MV production. We found that MV production was greatest when cells were rapidly dividing during log-phase growth (Figure 3.4). Similarly, during growth of *Pseudomonas aeruginosa*, maximum MV production correlated to exponential growth (Bauman and Kuehn, 2006). These observations support the recent hypothesis that MV formation is related to cell division (Deatherage et al., 2009), and will be discussed in greater detail in Chapter 5. Consistent with the results of Bauman and Kuehn (2006), we found that MV production

levels off during stationary phase growth, but since the details of MV cycling in bacteria are unknown, the mechanism responsible for this observation is unclear.

Environmental factors such as pH, nutrient composition, and external stressors can affect numerous biological processes in bacteria. For example, cells grown in nutrient rich medium (e.g., Luria Bertani) versus nutrient deplete medium (e.g., minimal media) are almost twice as large in size (Outten and O'Halloran, 2001). Additionally, previous research on PR1 has demonstrated that pH affects protein expression patterns, many related to cell shape and morphology such as putative rod-shape determining protein MreB and actin-like ATPase, (Van Nostrand et al., 2008). External stressors such as metal ions can elicit a plethora of biological responses, which can include stress responses as described by Worden et al. (2009) when investigating Cd-toxicity to *E. coli*. We found that MV production was influenced by pH and Zn concentration which suggests that MV production is also influenced by environmental factors. To date, only a single study has evaluated the effects of environmental factors (i.e., different media) on MV composition, though MV production was not quantified (Sidhu et al., 2008).

Membrane vesicles related to stress response. Production of MVs by *E. coli* is thought to be linked to extra-cytoplasmic stress response, although it is unclear whether MV production is directly controlled by this pathway or simply a secondary effect (McBroom et al., 2006; Button et al., 2007; McBroom and Kuehn, 2007). The extra-cytoplasmic stress response via sigma-factor E (σ^E) in Gram-negative bacteria is modulated by sigma factor RpoE and mutations affecting the RpoE regulon can both increase and decrease MV production (McBroom et al., 2006; Button et al., 2007). Although RpoE does not appear necessary for bacterial viability, it is essential in

104

responding to many stressors including pH and Zn (Egler et al., 2005; Maurer et al., 2005; Button et al., 2007). In *E. coli*, the anti-sigma regulator *rseAB* was upregulated at lower pH which triggers a depression of RpoE activity (Maurer et al., 2005). Likewise, an *rseA* knockout in *E. coli* caused increased MV production versus wild type (McBroom et al., 2006). That PR1 was found to produce two-fold greater MVs at pH 7 versus pH 5 is in agreement with these studies since *rseAB* upregulation at lower pH would predictably result in decreased MV production.

In addition to the effect of pH on extra-cytoplasmic stress response, Zn is also able to affect this response in bacteria. For instance, Zn elicits a stress response in *E. coli* which includes upregulation of genes in the RpoE regulon (Egler et al., 2005; Yamamoto and Ishihama, 2005). Furthermore, RpoE seems to be required for Zn resistance in *E. coli* (Yamamoto and Ishihama, 2005). If MV production was controlled by RpoE, MV production would likely increase with Zn concentrations, although our results show the opposite (Figure 3.6). We also found that 0.76 mM Zn does not decrease MV production at pH 5, though it does decrease MV production at pH 7. Furthermore, all Zn-species correlated to MV production at these pHs (Figures 3.7, B.1, and B.2). This implies that MV production is affected by Zn-speciation, and given that $ZnOH^+$ and $ZnNH_3^{2+}$ correlate to Zn-toxicity between pH, it is plausible that these species are modulating MV formation independent of RpoE activation. Additional experiments measuring the extra-cytoplasmic stress response of PR1 to Zn at pH 5 and 7 would help reconcile these results.

Overall, the molecular mechanisms controlling the effect of Zn on MV production are unknown. One of the predicted roles of MVs is their involvement in the export of

mis-folded proteins, which become abundant during bacterial stress (Button et al., 2007; McBroom and Kuehn, 2007). When *E. coli* is exposed to Cd, gene expression patterns of proteins involved in mediating stress due to mis-folded proteins are upregulated (Worden et al., 2009). If MVs were serving a similar role in exporting mis-folded proteins, MV production would increase with increasing Zn concentrations. Given that MV production decreases at sub-lethal Zn concentrations, it may indicate that a process other than stress response is influencing MV production. It is unclear what the mechanism or benefit of decreasing MV production in response to Zn is, but the observation that sub-lethal Zn concentrations elicit a cellular response suggests that MVs may be involved in metal-microbe interactions.

CHAPTER 4

INVESTIGATING THE ROLE OF MEMBRANE VESICLES IN METAL-MICROBE INTERACTIONS

4.1. <u>Introduction</u>

Bacteria have evolved to tolerate high concentrations of metal ions by utilizing resistance mechanisms which limit the exposure of sensitive targets such as proteins to metals (Nies, 1999). Many of these mechanisms rely on sequestering metals internally, on the membrane surface, and/or externally (Hausinger, 1993). Internal sequestration can occur by binding excess metal ions in the cytoplasm to compounds such as polyphosphate, which in the case of *Arthrobacter ilicis* resulted in uranyl phosphate granules (Suzuki and Banfield, 2004). Intracellular metal deposits in bacteria can also include non toxic metal species such as Co and Se (Langley, 2006). Extracellular sequestration of metals through the release of chelating compounds such as proteins (Kurek et al., 1991) or extracellular polysaccharides (Kamashwaran and Crawford, 2003), can decrease metal toxicity by decreasing the extracellular metal ion concentration. In a similar manner, bacterial biofilms are more resistant to metals (Teitzel and Parsek, 2003). Overall, these sequestration mechanisms represent key processes by which bacteria interact with their environment beyond molecular changes within the cell.

Studying metal-microbe interactions relies on techniques to quantify metal binding to the cell and extracellular components. Since metal binding to a bacterial cell is influenced by the charge of the membrane, measurements of surface charge under varying conditions are commonly achieved via acid-base titration or determination of electrophoretic mobility (EPM). Due to surface moieties on the bacterial membrane (e.g., carboxyl, amide, phosphate and carbohydrate), this charge is typically negative at circumneutral pH (Bayer and Sloyer, 1990; Jiang et al., 2004). The distribution of moieties can be predicted using potentiometric investigations across pH and ionic

strength (Fein et al., 2005; Neal et al., 2007). In turn, this data can be used in conjunction with sorption isotherms, which measure metal sorption with increasing metal concentrations, to determine binding capacity and determine the metal affinity of the different moieties (Yee and Fein, 2003). Together, this type of analysis provides a detailed understanding of the metal binding capacity of the cell membrane, as well as the effects of environmental factors such as pH on this capacity.

In contrast to these approaches, extracellular metal binding components require separation of the component from the cell and matrix before its metal content can be quantified. To accomplish this, a separation technique can coupled either off-line (e.g., centrifugation and filtration) or in-line (e.g. liquid chromatography) to elemental analysis. Field flow fractionation (FFF) is useful to separate complex mixtures due to its dynamic separation range and high resolving power (Giddings, 1995). There are four types of flows used in conjunction with FFF, but for these studies we employed asymmetric flow-FFF (AF^4). In this type of analysis, once the sample has been focused in the flow chamber, different size species are eluted, which in normal separation mode is smaller particles first, although in the case of particles >1 μm, steric (or hyper-layer) separation mode occurs which causes larger particles to elute before smaller particles (Giddings, 1995). We measured eluting fractions by multi angle laser light scattering (MALS) and inductively coupled plasma mass spectrometry (ICP-MS). This set-up allowed us to measure how metal was distributed across size classes of bacterial membrane vesicles (MVs), which is a novel application of these technologies.

Correlative observations have indicated that MVs might be involved in pH-dependent Zn toxicity to *Burkholderia vietnamiensis* PR1$_{301}$ (PR1; refer to Chapter 3).

Production of MVs by PR1 is greater when Zn is more toxic to PR1, at pH 7 versus pH 5, yet MV production at both pHs decreases with increasing Zn concentration. This implies that MVs are not decreasing Zn toxicity through Zn-export, but may be increasing Zn-bioavailability through extracellular binding. To address this hypothesis, we characterized Zn-binding properties of MVs and developed experiments which allowed us confirm the effect of MVs on pH-dependent metal toxicity to PR1.

4.2. <u>Materials and methods</u>

Bacterial growth conditions. *B. vietnamiensis* PR1$_{301}$ (PR1) inoculum was prepared and grown in 4M at 30°C with shaking (200 rpm), as previously in Chapter 3. Growth was measured by OD$_{610}$.

MV and cell purification. MVs were purified from cultures grown in 4M at pH 5 or 7 for 12 h. Separation of MVs from cells, pili and cellular debris was accomplished using the method described in Chapter 5. Cells were purified from 25 mL cultures grown in 4M at pH 5 or pH 7 for 12 h, and pelleted by centrifuging at 6,000 g for 5 min. To remove residual MVs, the cells were washed five times with equal volumes of 100 mM MES at either pH 5 or 7 depending on the pH the cells were grown in, by centrifuging at 6000 g for 5 min. Next, to mimic the final wash steps in purifying MVs, cells were washed two times in 10 mM HEPES 0.85% (w/v) NaCl, pH 7.4 (OmniPur, EMD Biosciences, Inc., San Diego, CA). On the last wash step, cell pellets were resuspended in 5 mL 10 mM HEPES 0.85% (w/v) NaCl, pH 7.4 and kept at -20°C until further analysis. The protein concentration of purified cells and purified MVs was determined using the Bradford method (Bradford, 1976).

Electrophoretic mobility analysis. The electrophoretic mobility (EPM) and size of purified MVs and cells were measured using a Zetasizer Nano ZS particle analyzer (Malvern Instruments, Westborough, MA). Aliquots of purified MVs and cells from each pH were suspended in 1.2 mL 10 mM HEPES at pH 5 or pH 7 before 0.6 mL was transferred to a disposable 1 cm cuvette for size determination or a disposable folded capillary cell used for EPM measurements. Size was determined by dynamic laser light scattering (DLS) with a negative non-linear least squares model to convert correlogram to size distribution. Internal data quality was assessed with the manufactures software which was based on distribution and cumulants residuals. Phase analysis light scattering (PALS) was used to determine EPM, with units of μm cm V^{-1} s^{-1}. Statistics were performed using Minitab 14 (two-sample *T*-test; $\alpha=0.05$).

Zn sorption to MVs and cells. Thermodynamic modeling using MINTEQA2 of the growth media predicts the formation of $Zn_3(PO_4)_2$ and Vivianite [i.e., $Fe_3(PO_4)_2$], refer to Chapter 3 and Appendix A. Therefore Zn sorption experiments were conducted with 10 mM HEPES, and qualitative experiments found Zn did not precipitate at concentrations used at either pH 5 or 7. Zinc stocks were prepared by diluting a 955.8 mM Zn stock in 10 mM HEPES pH 5 or pH 7 to a final Zn concentration of 65 mM. Purified MV and cell stocks were also diluted to a concentration of ~1 mg mL^{-1} protein. Next, 10 mM HEPES pH 5 or pH 7 was added to sterile 0.5 mL microcentrifuge tubes followed by aliquots of Zn stock to yield the desired Zn concentration. Aliquots of MVs or cells were then added to the tubes and incubated at 30°C for 1, 2, 3, 4, or 6 h while being rotated end over end at 6 rpm. Next, the incubated samples were centrifuged at 16,100 *g* for 30 min at 4°C, at which point the samples were aspirated. The resulting

pellet was transferred to a digestion vessel with the addition of 0.3 mL of HNO_3 (Optima; Fisher Scientific), followed by 5 min sonication. This was followed by the addition of 0.2 mL of HNO_3 to the digestion vessel and 1 mL of 18.2 MΩ water. Digestion was accomplished with a focus microwave (CEM Discover; CEM, Matthews, NC) with a 2 min ramp to 150°C at 230 psi and held at 2 min without stirring. The digestion solution was transferred with three rinses of 18.2 MΩ water into 15 mL polypropylene tubes (Corning, Corning, NY) to a final volume of 10 mL. Final sample dilutions were determined gravimetrically. Analysis was performed using an inductively coupled plasma mass spectrometer (ICP-MS; Thermo X Series[II], Bremen, Germany) running collision cell mode utilizing an 8% H_2 in He collision gas to reduce isobaric interferences. Zn was calibrated using an external calibration curve gravimetrically prepared from a 3168a Zinc Standard Solution with [101]Ru as an internal standard. Reported values are from [66]Zn which were normalized to protein concentrations of MVs. Statistical analysis was performed using Minitab 14 (one-way ANOVA followed by a pairwise comparison using Tukey's method; two-sample T-test, α=0.05).

Measurement of Zn partitioning across MV size. Asymmetric flow field flow fractionation coupled to multi-angle-light scattering and inductively coupled plasma mass spectrometry (AF^4-MALS-ICP-MS) was used to evaluate MV size distributions and correlate Zn-sorption to MV size. Purified MVs were resuspended in 10 mM HEPES at pH 5 or 7 with 2.29 mM Zn as described in the Zn-sorption experiments with the modification that except final volumes were 100 μL in a GC vial insert and incubations were 2 h. For characterization of MVs in the absence of Zn, this incubation step was omitted. FFF was accomplished using a Wyatt Eclipse 3 (Wyatt Technologies) using

112

0.05% (w/v) SDS (brought to pH 7.0 with acetic acid) with 200 mg L^{-1} sodium azide which passed through a 10 kDa mwco regenerated cellulose membrane before entering the flow channel. A 25 μL injection volume was used followed by a 2 min equilibration, 2 min injection, 6 min focusing, 40 min elution and 10 min flushing. A 30 cm flow channel with a 250 μm spacer was used and elution flow rates were 1 mL min^{-1} detector flow, 1 mL min^{-1} focus flow and a 0.3 mL min^{-1} constant cross-flow. In-line MALS (Wyatt DAWN Heleos 2; Wyatt Technologies) was used to gather LS data during elution, which was followed by in-line ICP-MS analysis using an Agilent 7500cx ICP-MS in normal mode, with a quartz concentric nebulizer and Peltier cooled quartz Scott-type spray chamber. To evaluate size and number density of eluting MVs, MALS data was fit to a model assuming spherical particles using the manufactures program (ASTRA) and the excess Raleigh ratio (R_θ), which is the ratio of scattered light to incident light of the sample, is shown as an indicator of the light scattering (LS) data across the fractogram. To generate size distribution graphs, the size density output from ASTRA was fit to a Weibull distribution using MINTAB 14. The detection of Zn in parallel was accomplished by measuring ^{66}Zn cps. To combine the MALS and ICP-MS fractograms, a 1.5 min delay was measured between the MALS and ICP-MS and was used to correct the ICP-MS data. The resulting ^{66}Zn cps was also baseline corrected by subtracting the minimum cps value of each run.

Exposing growing cells to MVs and Zn. Since previous research (refer to Chapter 3) has demonstrated that maximum MV production by PR1 occurs during late log-phase and early stationary phase growth, we exposed mid-log phase cells to MVs and Zn. First, PR1 was grown in 250 mL of 4M at pH 5 and 7 for 4 h, after which cultures

were centrifuged at 6,000 g for 5 min at 5°C. The supernatant was removed and the pellet was resuspended in 250 mL of 0.1 M MES at either pH 5 or pH 7. This wash process was repeated five times and following the last centrifugation-washing step, pellets were resuspended in 250 mL fresh 4M at pH 5 or 7. An aliquot was removed to measure OD_{610} before 10 mL was dispensed into sterile 50 mL flasks. Filter-sterilized (0.2 μm) unbuffered 955.8 mM Zn stock was used to amend these flasks to a concentration of 0, 7.65 or 30.6 mM Zn for pH 5 flasks and 0, 0.76 or 1.15 mM Zn for pH 7 flasks. Next, aliquots of purified MVs were added, the flasks incubated for 4 h at 30°C with shaking (200 rpm), and 0.3 mL aliquots removed after 2, 3 and 4 h to monitor growth.

Electron microscopy. Electron microscopy was used to evaluate the effect of Zn on purified MVs and cultures of PR1, as well as for control samples of media amended with Zn. Preparation of MVs incubated with Zn for analyses by scanning electron microscopy (SEM) included removal of aliquots following 4 h incubation at 30°C with shaking (200 rpm). Preparation of samples from PR1 cultures in the presence of Zn involved removal of aliquots following 12 h growth. Samples were pushed onto a 13 mM 0.2 μm polycarbonate filter (Whatman, Piscataway, NJ) using Swinnex® filter housings (Millipore, Billerica, MA). They were then incubated with 2% glutaraldehyde (Electron Microscopy Sciences) at room temperature for 1 h, dehydrated, and brought to critical point dryness with hexamethyldisalizane (refer to Chapter 2). Imaging of PR1 grown in the presence of Zn by scanning transmission electron microscopy (STEM) involved removal of 5 μL after 12 h growth which were transferred to carbon/formvar coated 200-mesh copper grids (Electron Microscopy Sciences) and fixed with Os vapors

overnight. Analysis of SEM samples was performed using a JEOL 5600LV (Tokyo, Japan) SEM running at 15 keV and TEM samples were analyzed with a Tecnai20 TEM (FEI, Inc., Hillsboro, OR) with LaB6 emitter running at 200 keV and images were taken on a Teitz camera. Imaging samples by STEM was performed using a Hitachi HD2000 operating under variable pressure in back scatter dark-field Z-contrast mode at 200 keV with an INCA Energy 200 EDS detector was used for energy dispersive X-ray (EDX) mapping.

4.3 <u>Results</u>

Measurement of size distribution and EPM of MVs and cells. In order to confirm the purity of the purified MVs and cells, we used DLS to measure their size distributions in 10 mM HEPES at pH 5 and 7 (Table 4.1). Cells from both pHs were composed mostly (>95%) of particles with a radius greater than 690 nm. The majority (~75%) of the measured peak volume of MVs produced at pH 5 had a radius of 400 to 475 nm, while 25% corresponded to 100 to 125 nm. MVs produced at pH 7 were between 115 and 175 nm in radius although the samples were too polydisperse to meet distribution analysis quality criteria. Given that independent TEM analyses of the purified MV samples indicated a size distribution ranging from 25 to 75 nm (Figure 5.4), the size estimates derived from DLS likely do not reflect cellular contamination but rather indicate that the MVs were aggregated.

The EPM of cells and purified MVs produced at pH 5 and 7 was measured in 10 mM HEPES at pH 5 and pH 7. MVs had significantly different EPM than cells (two-sample *T*-test; $p<0.05$), with an average ($\pm$SD) of -0.99 $\pm$ 0.2 μm cm V^{-1} s^{-1} compared to

the EPM of cells, which were found to be -1.85 ± 0.2 µm cm V^{-1} s^{-1}. The low negative surface charge of MVs supports the hypothesis that MVs would aggregate under the experimental conditions utilized. Additionally, MVs and cells had greater EPMs at pH 7 than at pH 5; however, only a single measurement was made for each condition (Figure 4.1). These results suggest that MVs might have different Zn-binding capacities at pH 5 and 7.

Evaluating Zn sorption by MVs produced at pH 5 and 7. In Chapter 3, it was demonstrated that PR1 produces less than 10 µg mL^{-1} MVs (as measured by protein concentration) when grown at pH 5 or pH 7 (Figure 3.5). To insure detectable Zn sorption by purified MVs, we used a higher MV concentration of 40 µg mL^{-1} to evaluate whether Zn sorption to MVs increased when incubated with increasing Zn concentrations. First, Zn-sorption to MVs over 6 h was examined and detectable Zn sorption was observed after 2 h incubation (data not shown). Next, MVs were equilibrated with Zn in 10 mM HEPES at the pH that MVs were produced. MVs produced at pH 5 and 7 bind less than 0.1% of total Zn over all conditions. Additionally, Zn-binding to MVs increased with increasing Zn (Figure 4.2). Zn-sorption to MVs produced at pH 7 increased significantly at concentrations greater than 2.3 mM Zn, while Zn-sorption to MVs produced at pH 5 was significantly higher only at 3.06 mM Zn (Figure 4.2). Additionally, MVs produced at pH 7 appeared to bind more Zn than MVs produced at pH 5, which was statistically significant at 0.38 mM Zn and 2.29 mM (two-sample T-test; $p<0.05$). Based on these results, we used 2.29 mM Zn to evaluate Zn sorption for the remaining experiments.

Table 4.1. Analysis of size distribution of MVs and cells by DLS. Samples were placed in 10 mM HEPES pH 5 or 7 and immediately analyzed. Peak numbers refer to different size populations determined by DLS which are given as relative volume of total and are the result of a single measurement.

Sample	Buffer	Radius (nm) by Volume (%)		
		Peak 1	**Peak 2**	**Peak 3**
MVs from pH 5	pH 5	108.9 (16.6%)	411.1 (78.7%)	2692.5 (4.6%)
	pH 7	126.1 (23.7%)	472.8 (73.4%)	2707.5 (2.9%)
MVs from pH 7	pH 5	*118.8 (100%)	-	-
	pH 7	*175.3 (100%)	-	-
Cells from pH 5	pH 5	693.5 (94.8%)	75.5 (5.2%)	-
	pH 7	963.5 (94.6%)	107.2 (5.4%)	-
Cells from pH 7	pH 5	841.5 (97.3%)	91.0 (2.7%)	-
	pH 7	699 (95.1%)	70.3 (4.9%)	-

* data for these measurements did not pass instrument quality control criteria; they are
  shown here for reference
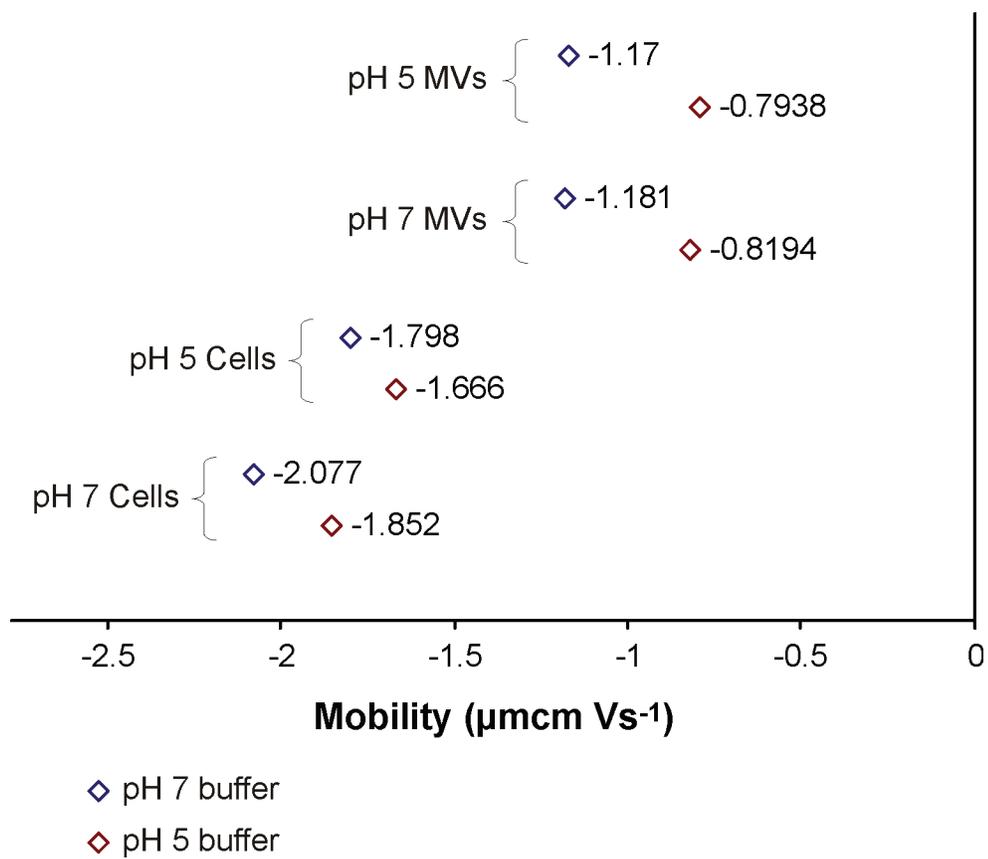
Figure 4.1. Electrophoretic mobility of purified MVs and cells at pH 5 and 7.
Plotted data are the result of a single measurement.

Comparison of Zn sorption by MVs and cells. Since EPM measurements of MVs and cells demonstrated that pH affected EPM, we next examined whether pH also affected Zn-sorption. Cells and MVs produced at different pH were incubated with 2.29 mM Zn in 10 mM HEPES at pH 5 and 7. Cells bound more Zn than MVs per µg of protein, with an average (±SD) of 0.42 ± 0.1 and 0.27 ± 0.1 nmoles Zn µg^{-1} protein respectively (Figure 4.3). Zn-sorption to MVs and cells produced at pH 5 remained relatively the same at both pHs, while MVs and cells from pH 7 sorbed more Zn at pH 7 than pH 5 (two-sample *T*-test; p=0.029 and 0.120, respectively).

Measuring Zn partitioning across MV size. Since MVs were most likely aggregated when sized by DLS, the size distribution was measured using AF^4-MALS. Additionally, the question of whether Zn-sorption influences MV size distribution or if Zn preferentially sorbed to a size range of MVs could be examined by AF^4-MALS-ICP-MS. MVs were successfully separated using a constant cross-flow and light scattering (LS) data over approximately 20 min was collected. The overall size distribution of MVs was approximately 80 nm to 140 nm in geometric radius (Figure 4.4). The size distribution of MVs produced at pH 5 and 7 was different, with mean radius of 96.5 and 112.8 nm respectively. Additionally, equilibration with Zn resulted in larger MVs at both pH. MVs produced at pH 5 were approximately 30 nm larger at both pH, while MVs produced at pH 7 were 7.6 and 2.5 nm larger at pH 5 and 7 respectively. LS data also allowed for determination of absolute number of MVs, and demonstrated that MVs from both pHs had the same average number, though there was considerable variation between samples (35 to 40% RSD; Figure 4.4).

pH 5
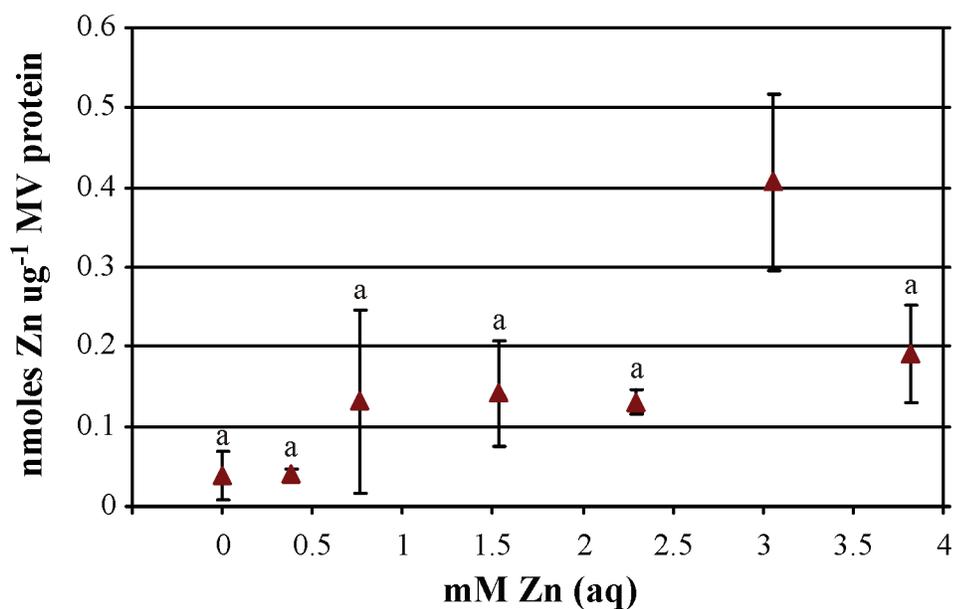
pH 7
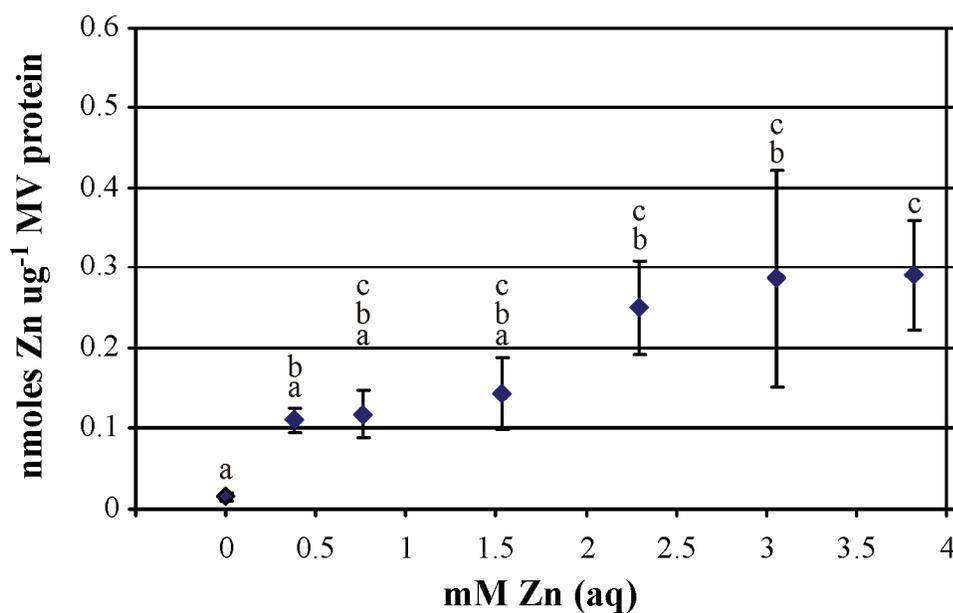
Figure 4.2. Zn sorption to MVs produced at pH 5 and 7. Zn sorption after 2 h incubation with MVs was measured for **(pH 5)** MVs produced at pH 5 in pH 5 buffer and **(pH 7)** MVs produced at pH 7 in pH 7 buffer. The same letter(s) within each pH indicates conditions are not significantly different (one-way analysis of variance followed by Tukey's; $p<0.05$). Error bars represent ± 1.0 standard deviation based on triplicate measurements.
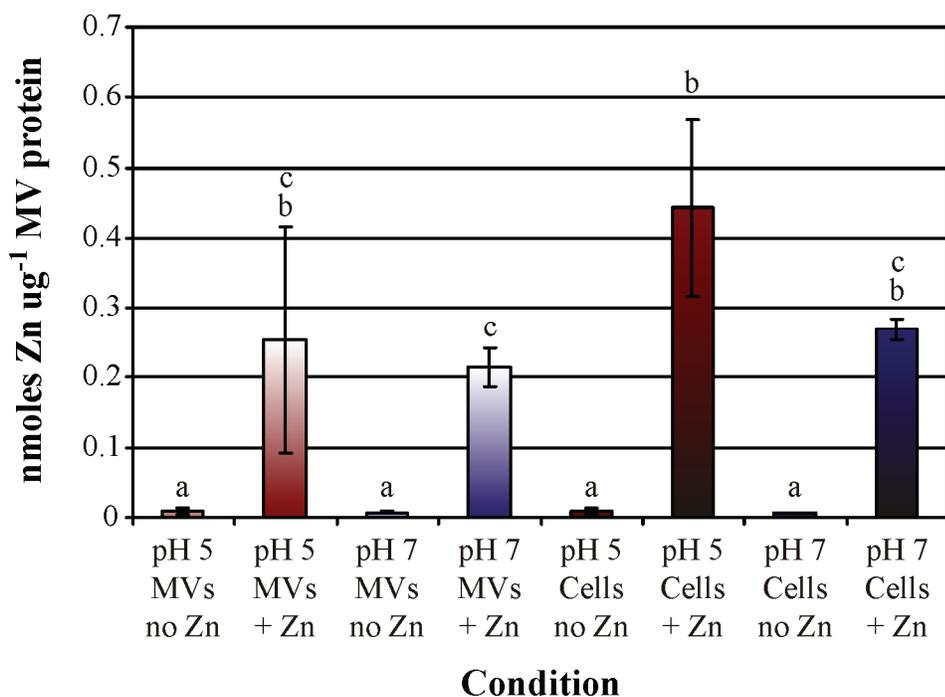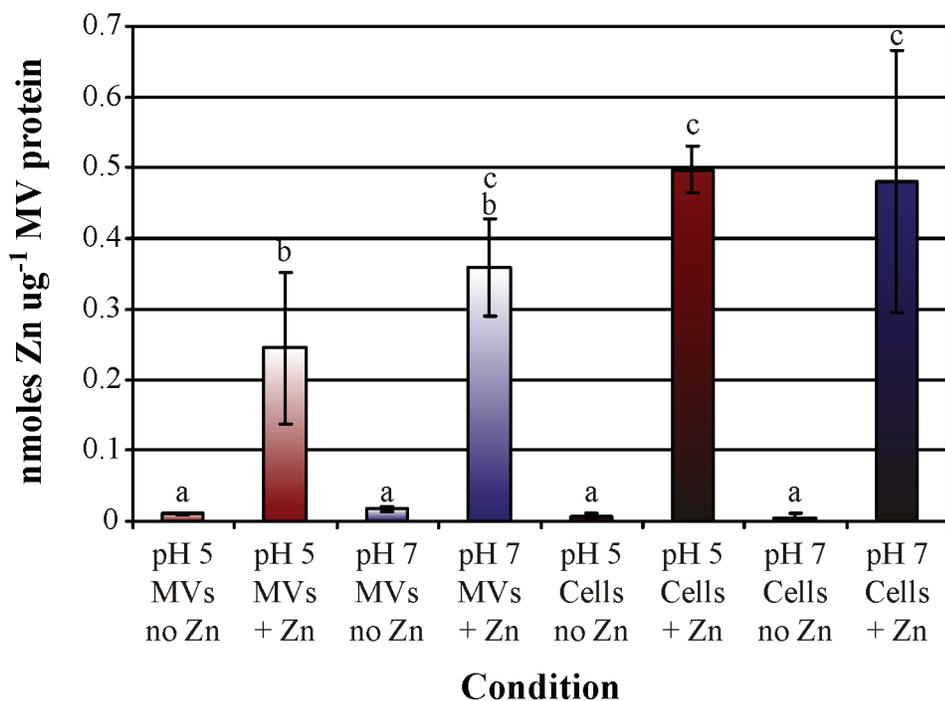
Figure 4.3. Zn sorption to MVs and cells when incubated with 2.29 mM Zn. Graphs show Zn sorption after 2 h incubation in pH 5 and pH 7 buffer. Labels on the x-axis refer to the pH MVs or cells were produced. The same letter(s) within each figure indicates they are not significantly different (one-way analysis of variance followed by Tukey's; $p<0.05$). Error bars represent $\pm$ 1.0 standard deviation based on triplicate measurements.

When MVs equilibrated with Zn were analyzed AF^4-MALS-ICP-MS, a Zn peak was detected which consistently eluted prior to the main peak associated as indicated by excess Rayleigh ratio (R_θ) versus Zn counts per second (cps; Figures 4.5 and 4.6). The LS data which corresponded to the Zn peak could not be fit to a size model and only the retention times shown in Figures 4.5 and 4.6 yielded LS data. Since Zn was retained in the flow channel, it indicates that Zn was associated with a component in the purified MV mixture, but it was not possible to evaluate size class. Overall, AF^4-MALS-ICP-MS analysis demonstrated that MVs produced at different pH have different size distributions, and after equilibration with Zn, MVs from both pH increase in size.

Effect of MVs on Zn toxicity to PR1. To evaluate whether MVs modulate Zn toxicity to growing cells through extracellular binding, the effect of MVs on growing PR1 cells were evaluated. Mid-log-phase cells were washed to remove any MVs and resuspended in fresh media with a relatively low (3 µg mL^{-1}) and high (6 µg mL^{-1}) concentration of purified MVs chosen based on MV production by PR1 at different pHs (refer to Chapter 3). MVs from both pHs did not affect the growth of PR1 at either concentration at pH 5 or pH 7 (Figure 4.7). Next, MVs were added to growing cells along with a minimum inhibitory Zn concentration (between 10 and 25% growth inhibition; 7.65 and 0.76 mM Zn at pH 5 and 7 respectively) and a Zn concentration which caused near complete growth inhibition (between 50 and 90% growth inhibiton; 30.6 and 1.15 mM Zn at pH 5 and 7 respectively). Increased Zn toxicity to PR1 in the presence of MVs would be expected at the lower Zn concentration if MVs increase Zn toxicity. Whereas decreased Zn toxicity at the higher Zn concentration would indicate MVs decrease Zn toxicity. Instead, MVs did not affect Zn toxicity to PR1 under all conditions examined (Figure 4.8).

A
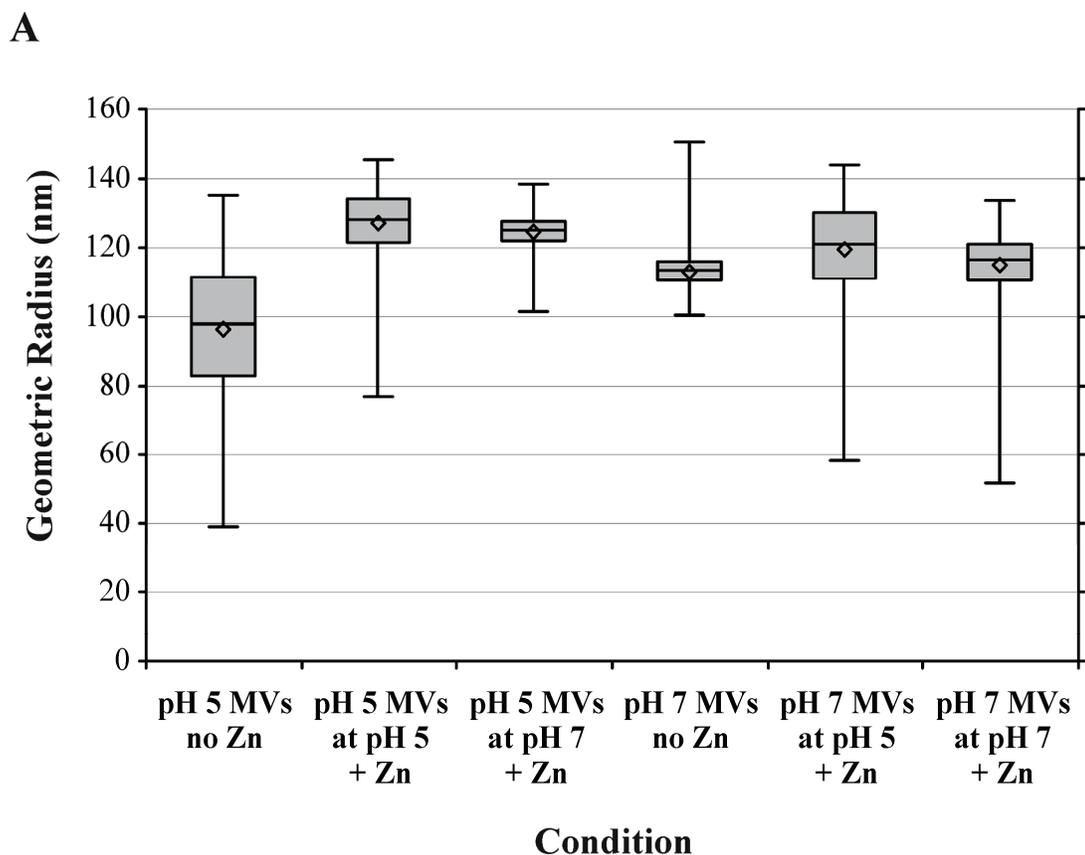
B

	pH 5 MVs no Zn	pH 5 MVs at pH 5 + Zn	pH 5 MVs at pH 7 + Zn	pH 7 MVs no Zn	pH 7 MVs at pH 5 + Zn	pH 7 MVs at pH 7 + Zn
abs. num. (25 μL)	6.78E+05	2.91E+05	4.78E+05	4.60E+05	2.96E+05	6.31E+05
num. μg^{-1} MV	6.78E+08	2.91E+08	4.78E+08	4.60E+08	2.96E+08	6.31E+08

Figure 4.4. Size and absolute number of MVs after equilibration with Zn. (A) Box-plots representing MV size distribution data. The size distribution output data was fit to a Weibull distribution which generated the median, second and third quartile data shown. The whiskers of the plot represent the minimum and maximum radii measured for each sample, and the hollow diamond is the mean of the measured size distribution. **(B)** Absolute number (abs. num.) of MVs in 25 μL injection and as number μg^{-1} MV protein.
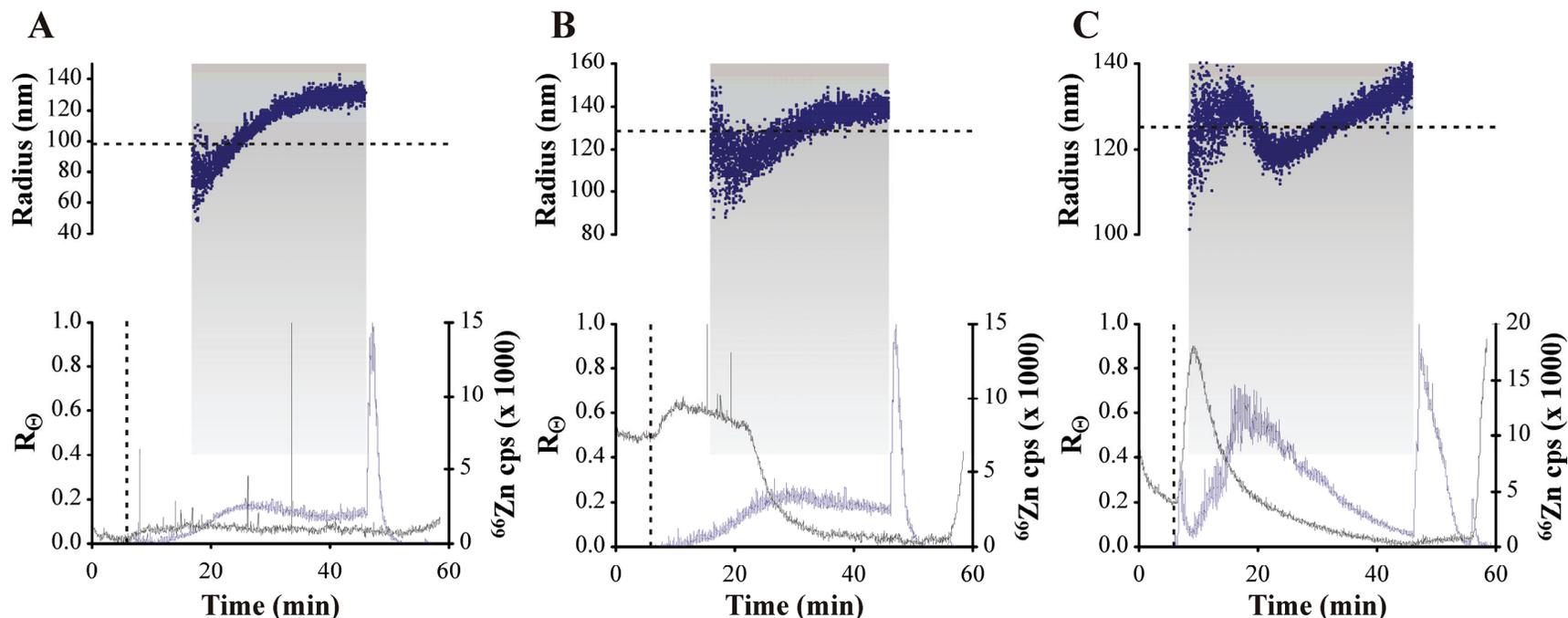
Figure 4.5. Analysis of MVs produced at pH 5 by AF⁴-MALS-ICP-MS. (A) MVs not incubated with Zn, **(B)** MVs incubated at pH 5 with Zn. **(C)** MVs incubated at pH 7 with Zn. The lower frame of each graph is an overlay of the excess Rayleigh ratio (R_θ; blue line) and the Zn response measured in cps (black line). The dotted line indicates when elution began out of the flow chamber. The top frame of each graph is a plot of the geometric radius of particles over elution time, and the dotted line indicates the median of the size distribution. The shaded box that goes between the two frames is shown to indicate the retention time of the light scattering data was used.

Figure 4.6. Analysis of MVs produced at pH 7 by AF^4-MALS-ICP-MS. (A) MVs not incubated with Zn, **(B)** MVs incubated at pH 5 with Zn. **(C)** MVs incubated at pH 7 with Zn. The lower frame of each graph is an overlay of the excess Rayleigh ratio (R$_\theta$; blue line) and the Zn response measured in cps (black line). The dotted line indicates when elution began out of the flow chamber. The top frame of each graph is a plot of the geometric radius of particles over elution time, and the dotted line indicates the median of the size distribution. The shaded box that goes between the two frames is shown to indicate the retention time of the light scattering data was used.
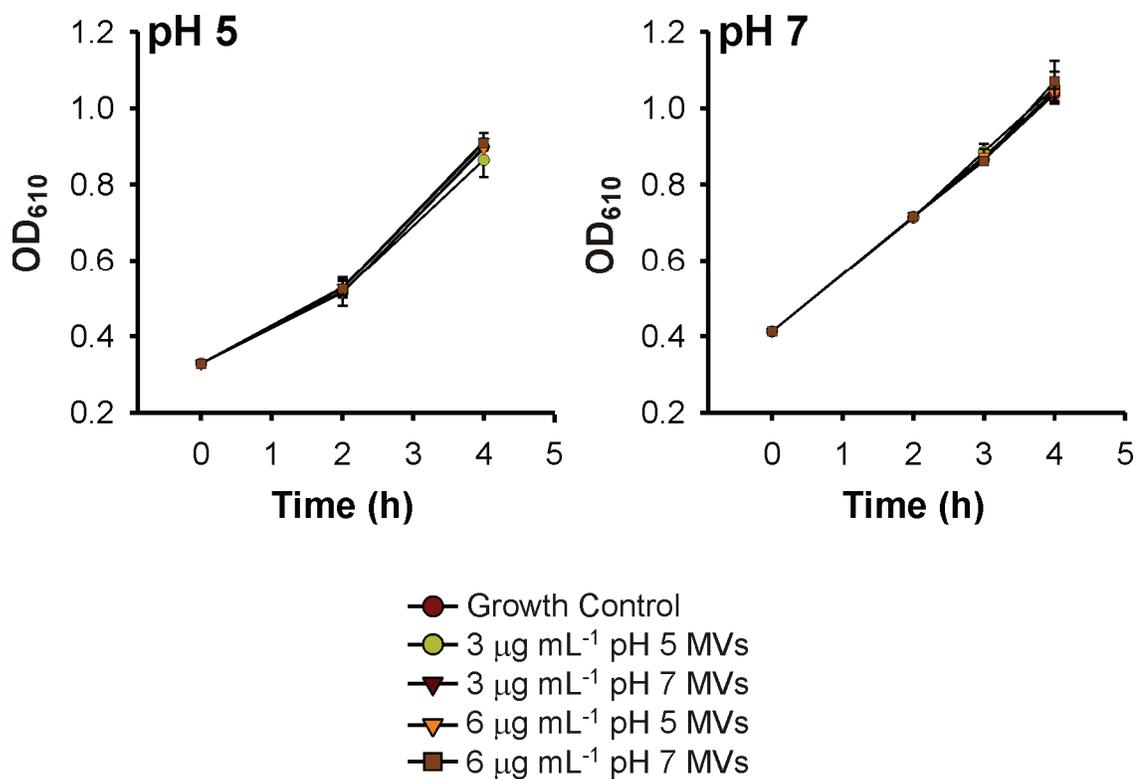
Figure 4.7. The effect of MVs on growing cells. PR1 was grown at pH 5 and pH 7, and after 4 hours, cells were washed, resuspended in fresh media and amended with MVs produced at pH 5 or 7 at two concentrations. Error bars represent ± 1.0 standard deviation based on triplicate measurements.
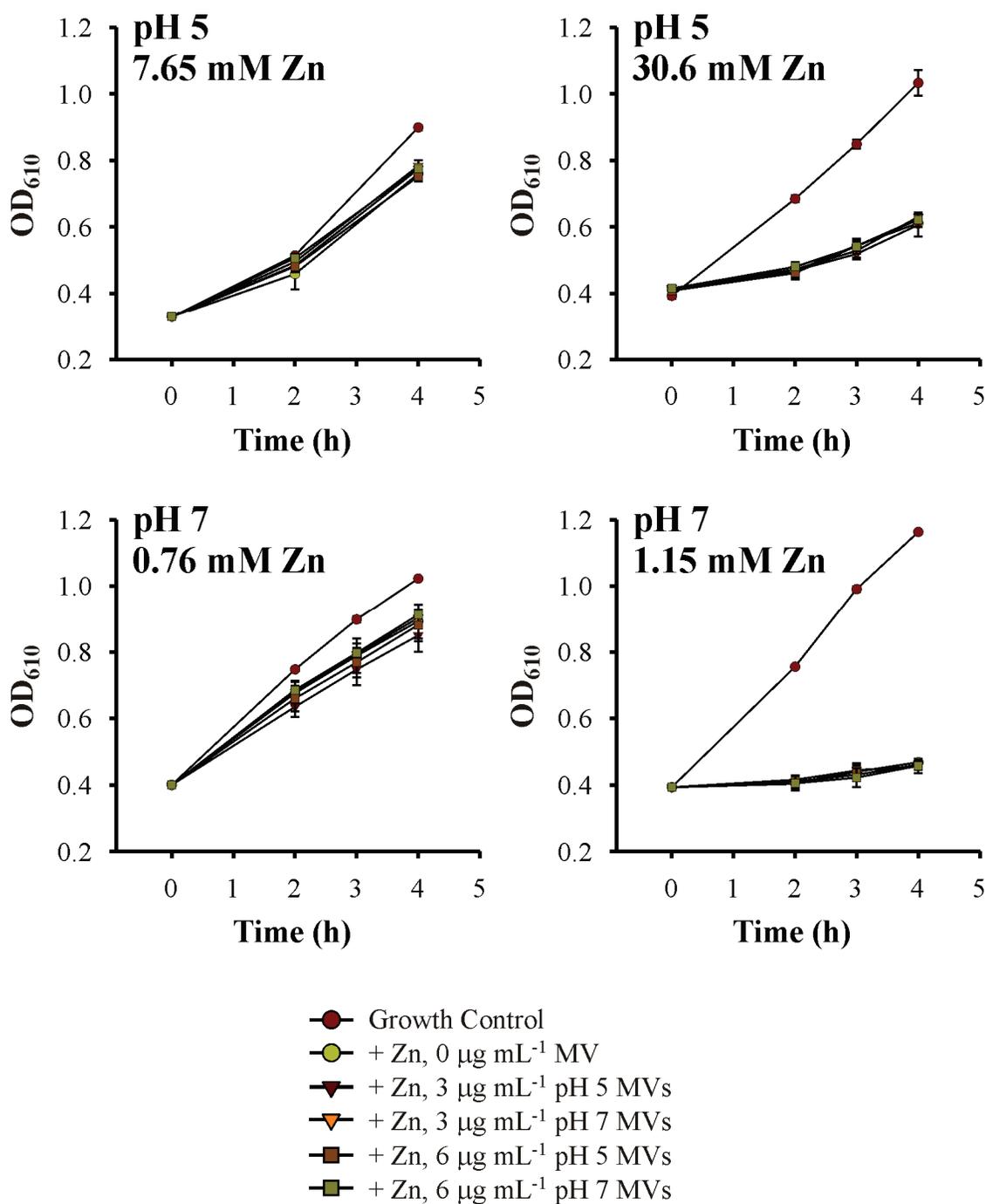
Figure 4.8. Effect of MVs on Zn toxicity to PR1. PR1 was grown at pH 5 and pH 7, and after 4 h, cells were washed, resuspended in fresh media and amended with MVs produced at pH 5 or 7 at two concentrations as well as different Zn concentrations. Error bars represent ± 1.0 standard deviation based on triplicate measurements.

Zinc forms a nano-phase precipitate under PR1 growth conditions.

Previously we observed extracellular Zn flocs associated with PR1 cells and concluded

that they were MVs associated with Zn (refer to Chapter 2). Therefore SEM was used to

confirm whether these flocs formed after purified MVs were incubated at high Zn

concentrations (relative to toxicity; 30.6 and 1.15 mM Zn at pH 5 and 7, relative to

toxicity). Similar to previous observations (Figure 2.9), spherical electron dense flocs

that were approximately 100 nm in diameter were evident (Figure 4.9). However, when

Zn was incubated in the absence of MVs under the same conditions, similar formations

were also observed (Figure 4.9). Therefore previous observations were re-evaluated by

examining PR1 grown in the presence of high Zn concentrations (relative to toxicity; 30.6

and 1.53 mM Zn at pH 5 and 7) following 12 h of growth. Similarly sized spherical

electron dense flocs associated with cells at both pHs were visible and these same

formations were present when uninoculated controls (Figure 4.10). Based on these

observations, it seems likely that previous conclusions that these features were Zn-

associated MVs actually are nano-phase Zn precipitates. One of the more spectacular

imaging data sets of was from PR1 grown at pH 7 with 1.53 mM Zn, which includes

STEM electron micrographs and corresponding EDX maps (Figure 4.11). Additionally,

the ratios of detected elements were measured across the mapped region (Figure 4.12),

which further confirms that these precipitates are a combination of Zn- and Fe-

phosphates and sulfates. If the stoichiometry of detected Zn and Fe was assumed to be

$ZnPO_4$ and $FePO_4$, then 25% of the total P signal by EDX can be accounted for. Still, the

inherent limitations of EDX make it impossible to determine the exact identity of the

observed formations.

pH 5
30.6 mM Zn
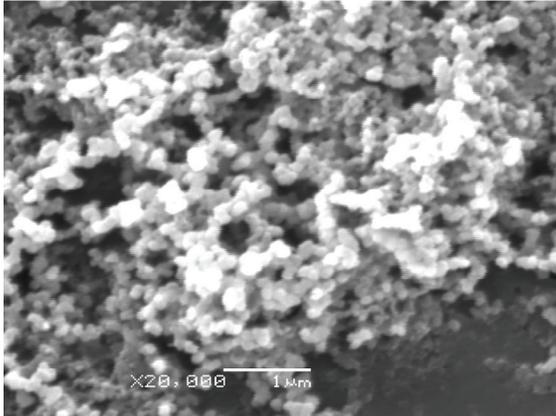
MVs	Abiotic
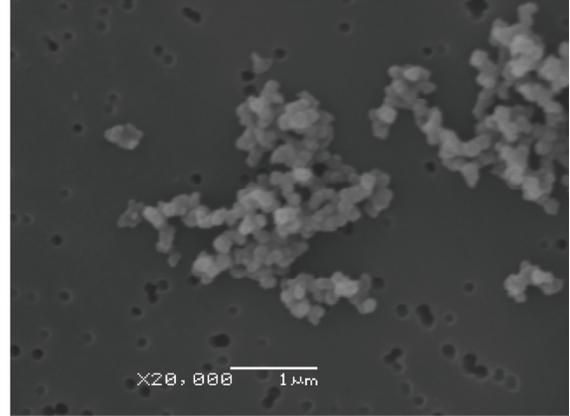
pH 7
1.53 mM Zn
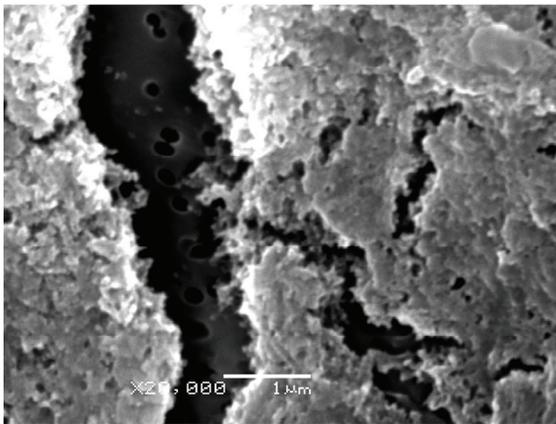
MVs	Abiotic
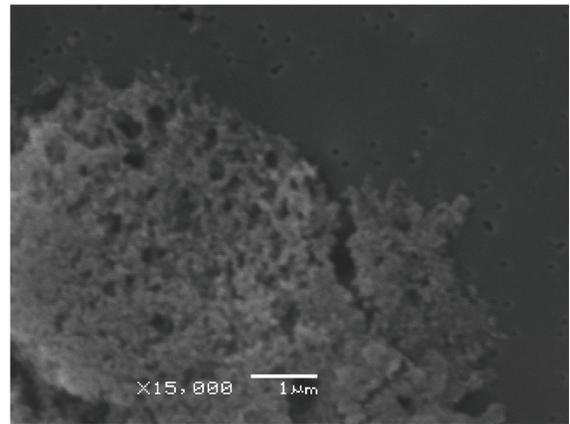
Figure 4.9. Electron micrographs of MVs equilibrated with Zn. Purified MVs were equilibrated with Zn under conditions identical to the 4 h MV exposures to cells. In parallel, Zn was added to media that did not contain MVs. Under both conditions at both pH, similar electron dense flocs were observed by SEM. Scale bars are labeled within each electron micrograph.

pH 5
30.6 mM Zn
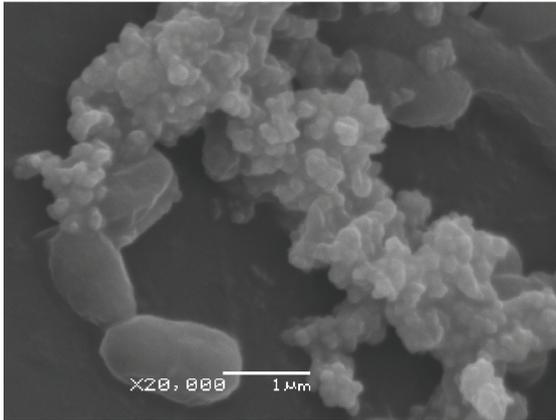
<u>Cells</u>   <u>Abiotic</u>
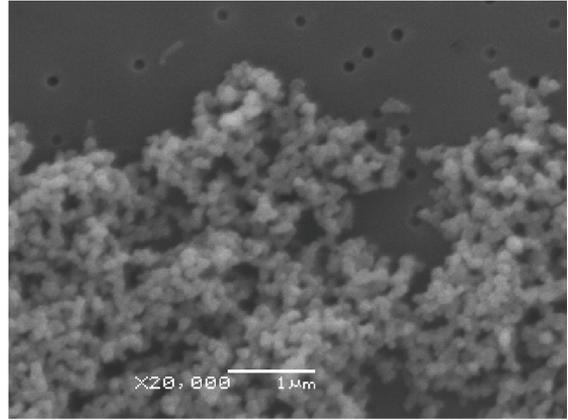
pH 7
1.53 mM Zn
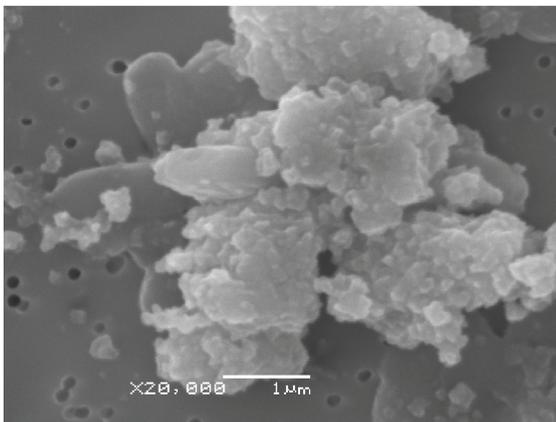
<u>Cells</u>   <u>Abiotic</u>
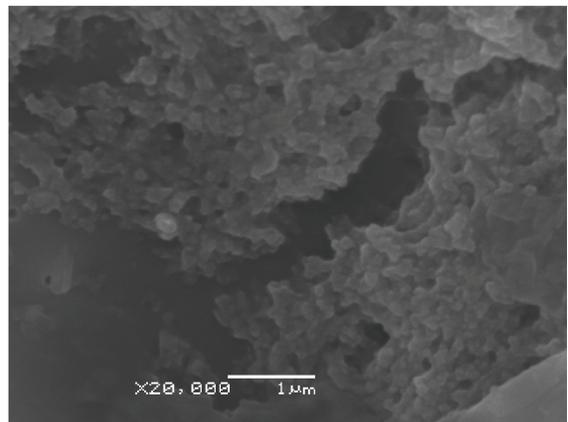
Figure 4.10. Electron micrographs of PR1 grown with Zn. PR1 was grown under conditions when electron dense flocs had been observed associated with cells. Similar electron dense flocs were evident by SEM with and without cells. Scale bars are shown within each electron micrograph.
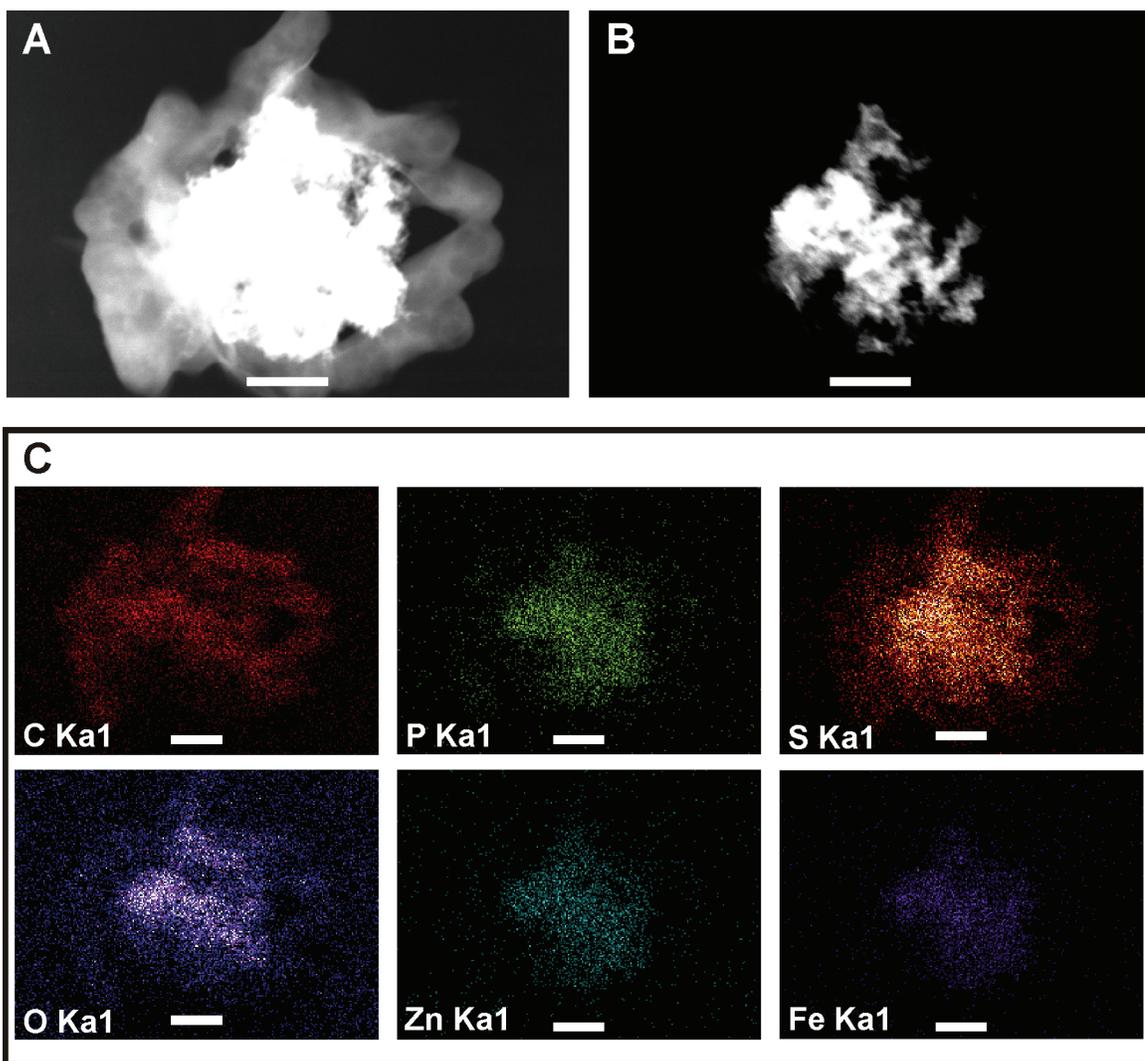
Figure 4.11. Electron micrographs and EDX maps of PR1 grown with Zn. (A and B) Electron micrographs generated in dark-field mode STEM. **(C)** EDX maps of the same region demonstrating the co-localization of Zn, Fe, P, S, and O. Scale bars are 1 μm.
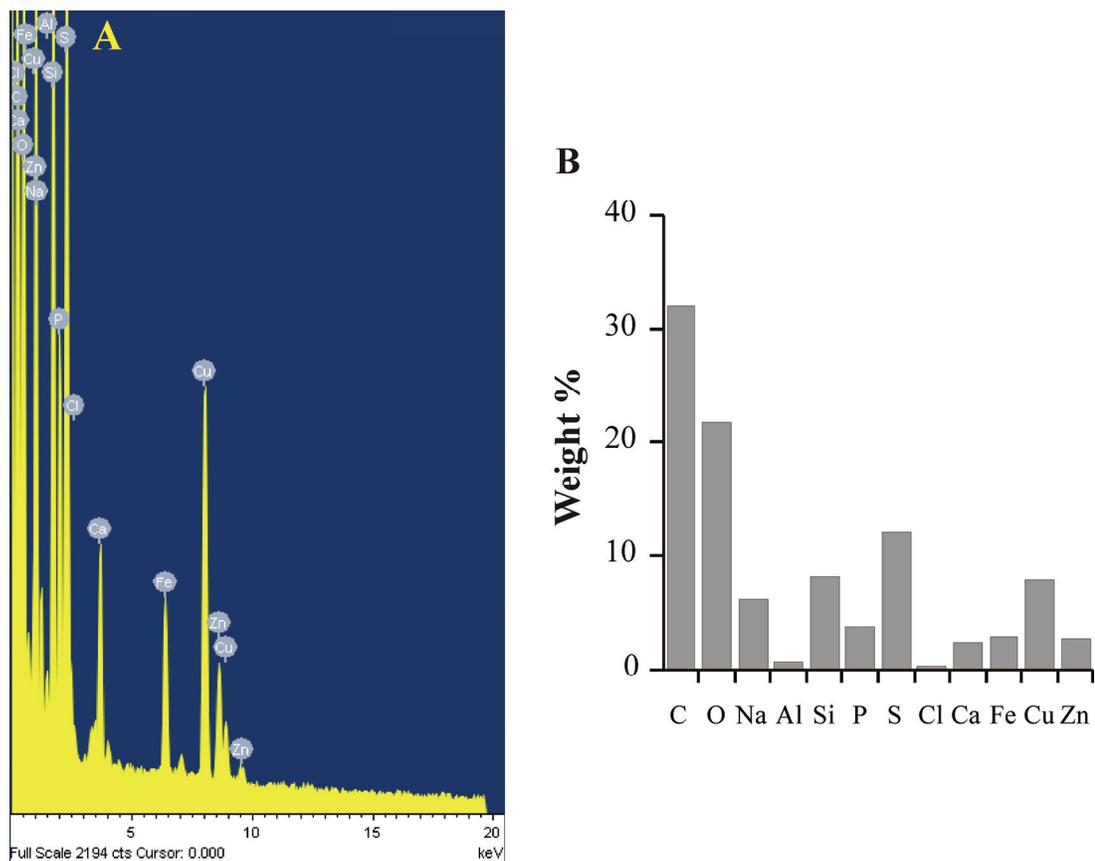
Figure 4.12. EDX data of mapped region. EDX results are shown both as **(A)** a raw spectrum with labeled peaks and **(B)** quantitative results which are based on the elemental response over the mapping time period. This data is based on the complete mapped area shown in Figure 4.11.

4.4. <u>Discussion</u>

Membrane vesicles are a versatile tool which Gram-negative bacteria utilize to interact with their environment and understanding the functional potential of MVs has led to a clearer understanding of bacterial pathogenesis (Bomberger et al., 2009), biofilm formation (Schooling and Beveridge, 2006), and bacteria-bacteria exchange (Renelli et al., 2004). As MVs are released into the environment around the cell, understanding their chemistry is important to predicting their interactions with compounds (organic and inorganic) independent of the cell. It has been shown that the surface of MVs can sorb heavy metals, radionuclides, and Fe (in the case of *Shewanella putrefaciens*; Gorby et al., 2008) and sorb Ag-nanoparticles (in the case of *Escherichia coli*; Li et al., 2009). MVs can also bind organic constituents such as DNA (Schooling et al., 2009) and toluene (Kobayashi et al., 2000). Based on these observations, properties of MVs were examined to determine if MVs modulate pH-dependent Zn toxicity to PR1.

Characterization of MVs has historically relied on molecular techniques (e.g., antibodies, proteomics, etc.) and electron microscopy (Beveridge, 1999; Lee et al., 2008), which elucidates the molecular components of MVs, but does not provide accurate physical data (e.g., size, number). Typical fixation protocols utilize cross-linking compounds to preserve ultra-structural features during dehydration, but it is understood that the size of biological structures after fixation is different than *in situ*. We found that direct DLS measurement of MVs was also not accurate due to MV aggregation. Utilizing AF^4-MALS we were able to accurately measure the *in situ* geometric radius of MVs, which we found to be 100 to 130 nm (Figure 4.4). Analysis of these samples by SEM and TEM suggested that MVs were much smaller, between 12 and 75 nm in radius

(Figures 3.4 and 5.4). Furthermore, most studies rely on a normalization factor (such as protein concentration in this chapter), though an absolute number of MVs with *in situ* size data would allow for accurate conclusions about molecular composition and sorting since surface area and volume could be used. We demonstrated that AF^4-MALS is well suited to provide these data, and with additional method development the absolute number precision could be improved from the high (>30%) RSD we observed (Figure 4.4). Future studies correlating MV *in situ* size and number data to other molecular analyses will greatly improve our understanding about fundamental MV processes.

To date, only one study has investigated the surface chemistry of MVs, and this focused specifically on their ability to sorb DNA (Schooling et al., 2009). Using EPM measurements of MVs derived from *Pseudomonas aeruginosa* PAO1 biofilms, Schooling et al. (2009) found that MV surface charge became more negative from pH 8 to pH 5.5. Since MVs have similar surface chemistry as the outer membrane, we would expect surface charge to become less negative with decreasing pH, which has been demonstrated in Gram-negative (Guine et al., 2006) and Gram-positive bacteria (Fein et al., 2005). This suggests that these results were probably due to increased MV aggregation with decreasing pH. We used a similar technique to measure EPM but only measured changes at pH 5 and 7. Our results indicate that MVs have different chemistries than cells as evidenced by a less negative surface charge. Previous studies of MVs produced by *Burkholderia cepacia* and *P. aeruginosa* have found that MVs have a different LPS content than cells (Kadurugamuwa and Beveridge, 1995) (Sabra et al., 2003) (Allan et al., 2003). Specifically, *P. aeruginosa* MVs are enriched in longer electronegative B-band LPS, though the affect this has on metal sorption to MVs has not been evaluated. The

difference in surface charge between MVs and cells indicates that a sorting mechanism during MV formation occurs, but additional analysis is needed to identify the cause of decreased MV surface charge.

The different surface charge of MVs and cells was further reflected by our results which found that cells sorb more Zn than MVs when normalized to total protein (Figure 4.3). Additionally, MVs and cells from cultures grown at pH 7 sorbed significantly more Zn at pH 7 than 5, whereas MVs and cells from pH 5 sorbed similar amounts of Zn at both pHs. This result was not predicted by our EPM measurements, and indicates that although MVs have different chemistries than cells, there are shared properties between MVs and cells. Since there was no energy source (e.g., carbon source) in the buffer used in sorption experiments, it suggest either that a passive transporter (e.g., porin or cation diffusion transporter) is present in PR1 at pH 5 or 7, or that the cell membrane structure of PR1 at pH 5 and 7 undergoes different conformational changes exposing different ligands to interact with Zn. These hypotheses are discussed in detail in Chapter 6.

To further evaluate Zn-binding to MVs, we measured the distribution of Zn among MV size classes using AF^4-MALS-ICP-MS. The majority of the Zn was retained in the flow channel and eluted before MVs, but reliable size data could not be generated for this peak. Using a similar approach to analyze U binding to cell suspensions of *Shewanella oneidensis* MR-1, Jackson et al. (2005) predicted that an extracellular polymer was responsible for the elution of U before cells. Similar to these conclusions we propose that Zn is being retained in the column due to MV-bound Zn and the shortened elution time indicates either that Zn is bound to large MV aggregates which are eluting in steric separation mode or smaller MVs which are eluting under normal

135

separation mode. Future studies will address this result by optimizing MV separation such that absolute MV number can be used to monitor recoveries (between conditions) and calculate absolute shifts in MV size distribution.

Based on previous research (refer to Chapter 3) that demonstrated MV production by PR1 is affected by pH and Zn, and results in this chapter that MVs are capable of binding Zn, the question of whether MVs modulate pH-dependent metal toxicity to PR1 was examined. A method was developed to expose mid-log phase cells to different MV and Zn concentrations, using MV concentrations based on the level of MV production PR1 produces at pH 5 and 7 (3 and 6 μg mL^{-1}). Under these conditions, MVs from either pH at either concentration did not decrease or increase Zn toxicity to PR1. Furthermore, we determined that what we had initially identified as MV-associated Zn (Figure 2.9) is most likely a Zn-phosphate precipitate. Although these results suggest that extracellular (or exogenous) MVs do not modulate Zn-toxicity, this mechanism may still occur in other microorganisms. Using absolute number and size of MVs, as well as average CFU mL culture protein (~ 1 e^9 CFU mL^{-1} at 12 h growth; Chapter 2 and other data) and the size of a PR1 cell based on SEM (0.5 μm x 2 μm), we can extrapolate that in 1 mL of early stationary phase growth PR1 cultures containing 6 μg mL^{-1}, MVs would account for 500 mm^2 of surface area compared to 3,500 mm^2 for cells. Since these concentrations and values are reasonable to apply to *P. aeruginosa* (MV concentrations based on Bauman and Kuehn, 2006), we would predict that the negatively charged B-band LPS containing MVs produced by *P. aeruginosa* could affect extracellular metal concentrations with 15% of total surface area. Overall, these results highlight the

complexity of studying MV chemistry as well as the potential for great progress using tools such as AF^4-MALS.

CHAPTER 5

INSIGHTS INTO THE FUNCTION AND FORMATION OF
Burkholderia vietnamiensis PR1$_{301}$ MEMBRANE VESICLES
PRODUCED NATIVELY AT DIFFERENT pH

5.1. <u>Introduction</u>

Membrane vesicles (MVs) are constitutively produced extracellular structures derived from the outer membrane of Gram-negative bacteria that range in size from 50 to 250 nm in diameter (Beveridge, 1999). Membrane vesicles were first described more than 40 years ago (Knox et al., 1966; Chatterjee and Das, 1967) and have been proposed as a new mechanism of protein secretion in Gram-negative bacteria (Kuehn and Kesty, 2005; Bomberger et al., 2009). Although the general mechanism of MV formation is uncertain, there are many proposed mechanisms of formation (Mashburn-Warren and Whiteley, 2006; Deatherage et al., 2009) and an emerging body of research on MV characterization (Beveridge, 1999; Kuehn and Kesty, 2005; Mashburn-Warren and Whiteley, 2006; Lee et al., 2008). The composition of natively produced n-MVs, as opposed to detergent extracted or artificially induced MVs (Kadurugamuwa and Beveridge, 1995; Claassen et al., 1996), generally reflects the outer membrane and periplasm of the vesiculating cell and consists of phospholipids, LPS, outer membrane proteins, DNA, RNA, as well as a diverse proteome (reviewed by Lee et al., 2008). This diverse composition allows n-MVs to function in virulence factor transport (Kadurugamuwa and Beveridge, 1995), protein (Ciofu et al., 2000) and DNA exchange (Yaron et al., 2000), cell-cell communication (Mashburn and Whiteley, 2005), biofilm formation (Schooling and Beveridge, 2006), and modulating host-pathogen interactions (Ismail et al., 2003). In contrast to typical secretion mechanisms, MVs allow bacteria to disseminate components into the extracellular matrix and cause interactions independent of the cell (Bomberger et al., 2009).

Membrane vesicles have been observed in numerous clinical and environmental strains of Gram-negative bacteria (Table 1.3; Dorward and Garon, 1990; Kuehn and Kesty, 2005), yet MV function and composition in *Burkholderia* spp. is poorly understood. *Burkholderia* spp. are relevant both in the environment and in human disease due to their antibiotic-resistance, ability to colonize diverse environments, and ability to utilize numerous energy sources (Coenye and Vandamme, 2003; Mahenthiralingam et al., 2005; O'Sullivan and Mahenthiralingam, 2005). With respect to human disease, *Burkholderia vietnamiensis* is one of nine distinct classes of bacteria (genomovars) related to *Burkholderia cepacia* that constitute the *B. cepacia* complex (Bcc), and is the third most frequently isolated member of the Bcc from cystic fibrosis (CF) patients (LiPuma et al., 2001). *Burkholderia* infections in CF patients typically leads to decreased life expectancy and increased morbidity (Tablan et al., 1987) and the composition of n-MVs is thought to be important determinant of *Burkholderia* pathogenicity (Allan et al., 2003). In contrast to the role of *Burkholderia* spp. in disease, they are valuable from a bioremediation perspective due to their ability to degrade numerous organic contaminants (O'Sullivan and Mahenthiralingam, 2005). For example, *B. vietnamiensis* G4 (G4), is one of the most effective trichloroethylene (TCE) co-oxidizing bacteria (Yeager et al., 2004). In the environment, MVs are structural components of biofilms (Schooling and Beveridge, 2006) and are involved in transport of DNA (Renelli et al., 2004) and signaling molecules (Mashburn and Whiteley, 2005). Although n-MVs from environmental strains of *Burkholderia* have not been evaluated, it would be predicted that they would possess many functions, albeit different than their clinical counterparts. For example, n-MVs produced by environmental and clinical

Pseudomonas aeruginosa strains were able to illicit an immune response from epithelial cells, despite having different protein compositions and therefore potentially different functions (Bauman and Kuehn, 2006).

In the environment as well as human disease, environmental factors such as nutrient composition and pH affect bacterial phenotypes. For instance, in many pathogens Fe concentration regulates expression of virulence factors (Carpenter et al., 2009). Changes in pH can also lead to a cellular response. For example, our laboratory has demonstrated that *B. vietnamiensis* $PR1_{301}$ (PR1), a constitutive TCE degrading mutant of G4, is more resistant to divalent transition metals at pH 5 versus pH due to an undefined mechanism of pH-dependent metal resistance (Van Nostrand et al., 2005). In conjunction with cellular changes, MV composition can also change with environmental factors. For instance, Fe concentration affected the VacA and protease composition of n-MVs produced by *Helicobacter pylori* (Keenan and Allardyce, 2000). Furthermore, in chapter 4 of this dissertation we demonstrated that MVs produced by PR1 grown at different pH have different capacities to sorb Zn. Additionally in chapter 3 we have demonstrated that MV production in PR1 is influenced by pH and Zn. Clearly the environment affects MV production by PR1 as well as MV surface properties.

Based on these data, we hypothesized that n-MVs produced by PR1 under different pH would also have different compositions and that any shared properties would be related n-MV formation and reflect core n-MV function. To address this hypothesis, we used proteomics and chemical characterization to compare the molecular and physicochemical differences between n-MVs produced by PR1 at pH 5 and 7. The shared properties we observed provide insights into the mechanism of n-MV formation in

PR1. Furthermore, our data demonstrates that the environmental variable pH influences

n-MV production and function. In contrast to chapters 3 and 4 that focused on the

potential role of MVs in metal-microbe interactions, the data herein will provide an

expanded understanding of the roles of MVs which has broad clinical and environmental

implications.

5.2. <u>Materials and Methods</u>

Bacterial Growth. Similar to chapters 3 and 4, PR1 was grown in modified 4M

(modified minimal mineral medium; refer to chapter 3) at pH 5 and 7. The PR1

inoculum prepared before each experiment was grown as previously described (refer to

chapter 2). To evaluate MV production during growth of PR1, aliquots of the inoculum

(0.25 mL) were added to five triplicate sets of sterile 125 mL screw-top flask containing

24.75 mL 4M media at pH 5 and 7. At 0, 4, 8, 12, and 24 h, aliquots were removed to

determine whole cell lysate protein concentration and were stored at -20°C until analysis.

Purity was confirmed during experiments by streaking growth cultures on Luria Bertani

(LB) plates. The remaining culture was subjected to the method described below in order

to purify MVs for quantification.

Biofilm production. A colorimetric method, modified from Stepanovic et al.

(2000) and Burton et al. (2007), was used to quantify biofilm production of PR1 grown in

96-well plastic titre plates. Aliquots (5 μL) of overnight cultures of PR1 grown in 4M pH

6 were added to wells containing 200 μL of 4M at pH 5 or pH 7. Plates were grown

stationary or with 120 rpm shaking at 30°C for 48 h. Cultures were aspirated from the

plates, followed by two washes with 1x Dubelco phosphate buffered saline (PBS;

Electron Microscopy Sciences, Hatfield, PA) with 15 min between each wash. Crystal violet, 0.4% (w/v), was added and let incubate for 15 min. Plates were then rinsed with water to remove unbound crystal violet and let dry 15 min. To solubilize the bound crystal violet, 200 μL of 33% (v/v) acetic acid was added to each well, and absorbance at 570 nm as well as 630 nm was measured using a SpectraMaz Plus[384] absorbance microplate reader (Molecular Devices, Sunnyvale CA).

MV quantification during growth. The method used to quantify n-MVs during growth was the same as previously described (refer to chapter 3). Briefly, the culture was centrifuged 6,000 g for 5 min at 5°C. Next, the supernatant was passed through sterile 0.45 μm Supor® membrane syringe filters (Pall Corporation, Port Washington, NY). Plating of 0.25 mL of this filtrate onto LB plates showed no growth after 48 h at 30°C indicating the absence of viable cells. Next, the filtrate was centrifuged at 75,600 g for 3 h at 10°C and the supernatant was removed and the remaining pellet was resuspended in 1 mL 50 mM HEPES pH 6.8 (OmniPur, EMD Biosciences, Inc., San Diego, CA) and transferred to 1.5 mL Eppendorf tubes. Samples were next centrifuged 16,100 g for 30 min at 4°C, the supernatant was removed and the HEPES wash and centrifugation was repeated. Protein concentration of whole cell lysate aliquots and MV aliquots was determined using the Bradford method (Bradford, 1976).

MV purification. An ultrapure n-MV fraction was generated for the remaining characterization approaches using a purification scheme developed based on Bauman et al. (2006). PR1 was grown as described previously in two sets of three 1 L sterile flasks containing 200 mL 4M pH 5 or 7 each, across three consecutive days. At 12 h, aliquots were removed to measure OD_{610} to confirm consistent growth across replicates, as well as

6 mL from each flask for whole cell lysate. The sample for whole cell lysate was centrifuged at 16,100 g for 30 min at 4°C, washed with 1 mL 50 mM HEPES (pH 6.8), centrifuged again, aspirated and stored at -80°C until processing for polar lipid fatty acid (PLFA) analysis. The remaining culture was centrifuged at 6,000 g for 10 min at 5°C. The supernatant was vacuum filtered through 47 mm 0.45 μm Supor®-450 membrane filters (Pall Corporation, Port Washington, NY) held by autoclaved glass frets. The filtrate was precipitated with 60% ammonium sulfate overnight at 4°C in the dark. The precipitate was collected by centrifuging at 10,000 g for 40 min at 4°C without deceleration. The supernatant was immediately poured off and the resulting pellet was resuspended in 50 mM HEPES (pH 6.8). Next pellets were combined within conditions, brought to 40 mL 50 mM HEPES (pH 6.8) and centrifuged 3 h at 75,600 g at 10°C. The resulting pellet was washed in 50 mM HEPES (pH 6.8) as described above and stored at -20°C. MV pellets were further purified from cell debris and pili using an OptiPrep Density Gradient (Axis-Shield, Oslo, Norway). The gradient used was selected based on its ability to float the MVs to approximately 2 mL below the top of the gradient (Bauman and Kuehn, 2006). All the following OptiPrep concentrations were made from a 60% (v/v) OptiPrep stock and 10 mM HEPES 0.85% (w/v) NaCl, pH 7.4. Each concentrated crude MV aliquot was centrifuged 16,100 g for 30 min at 4°C, and resuspended in 45% OptiPrep and placed in the bottom of a12 mL polyethylene terephthalate tube (Sorvall, Asheville, NC). The gradient was poured on top of the sample and consisted of (from bottom to top) 2 mL 40%, 2 mL 35%, 2 mL 30%, 2 mL 25%, 1 mL 20%, and 1 mL 15% OptiPrep. Gradients were centrifuged at 24,200 rpm (100,000 g; Sorvall TH-641 rotor) at 4°C for 16 h at which point 1 mL aliquots were removed from the top into sterile

Eppendorf tubes. A band was visible in all gradients at 3 to 4 mL from the top of the

gradient as well as debris on the bottom of the tube. Next, we used lithium dodecyl

sulfate-polyacrylamide gel electrophoresis (LDS-PAGE) to visualize the proteins present

in each 1 mL fraction. Aliquots, 9.75 μL, were removed and solubilized using LDS

sample buffer and reducing agent (Invitrogen, Carlsbad, CA) and heated at 70°C for 10

min, before loading onto a 1.0 mm x 15-well Bis-Tris 4-12% NuPAGE gel (Invitrogen).

The gel was run at room temperature at 200 V for 40 min followed by stepwise staining

(Westermeier, 2006) with colloidal coomassie (Brilliant Blue G-250, Fisher Scientific,

Fair Lawn, NJ). It was confirmed that fractions 3 and 4 mL from the top of the gradient

contained MVs, and these fractions were combined and brought to 40 mL 10 mM HEPES

0.85 % (w/v) NaCl, pH 7.4 and centrifuged 75,600 g for 3 h at 10°C. The remaining

pellet was washed in 10 mM HEPES 0.85 % (w/v) NaCl, pH 7.4 as described above to

concentrate to 1 mL. From this ultrapure MV aliquot, 100 μL was removed and stored at

-20°C for further analysis, while the rest was centrifuged and decanted and stored at -

80°C for PLFA analysis.

    Electron microscopy. Electron microscopy was used to evaluate growing

cultures of PR1 and confirm purity of the ultrapure n-MVs as well as evaluate their

physical characteristics. For analysis of cultures by scanning electron microscopy

(SEM), aliquots were removed at 12h growth a pushed onto a 13 mM 0.2 μm

polycarbonate filter (Whatman, Piscataway, NJ) using Swinnex® filter housings

(Millipore, Billerica, MA). Samples were incubated with 2% glutaraldehyde (Electron

Microscopy Sciences) at room temperature for one hour, then dehydrated and brought to

critical point dryness with hexamethyldisalizane (refer to chapter 2). To prepare samples

for analysis by transmission electron microscopy (TEM), 5 µL aliquots from each of the ultrapure MV fractions was dropped onto carbon/formvar coated 200-mesh copper grids (Electron Microscopy Sciences) and fixed with Os vapors overnight. Analysis of SEM samples was performed using a JEOL 5600LV (Tokyo, Japan) SEM running at 15 keV and TEM samples were analyzed with a Tecnai20 TEM (FEI, Inc., Hillsboro, OR) with LaB6 emitter running at 200 keV and images were taken on a Teitz camera.

DNA and RNA quantification. Nucleic acid quantification was accomplished using selective fluorescence probes for DNA and RNA. Aliquots of 20 µg of ultrapure n-MVs from each condition were centrifuged 16,100 g for 30 min at 4°C, aspirated and resuspended in 100 µL 50 mM HEPES (pH 6.8), then re-centrifuged and gently aspirated. The resulting pellets were subjected to endonuclease treatment at 37°C for 1 h with either DNase (New England BioLabs, Ipswich, MA) or RNaseA (Pharmacia Biotech, Piscataway, NJ) in 100 µL of appropriate buffer. Nucleic acids were extracted from endonuclease treated n-MV pellets with 20 µL TES [10 mM Tris-HCl, 100 mM EDTA, 0.5% (v/v) Sarkosyl] pH 8.0 for DNA and pH 5.1 for RNA. Samples were vortexed and incubated at room temperature for 10 min. Nucleic acid quantification was performed using a Qubit Fluorometer (Invitrogen) according to the manufactures guidelines. Statistics were performed using Minitab 14 (two-sample t-test, $\alpha=0.05$).

PLFA Analysis. Whole cell lysate and ultrapure MV aliquots were directly transferred into extraction tubes, using phosphate buffer as a transfer solution. Samples were extracted in a mixture of phosphate buffer, chloroform, and methanol; using 1, 2-dinonadecanoyl-sn-glycero-3-phosphocholine (Avanti Lipids, Alabaster, AL) as internal standard. Clean glass rods were used to manually disrupt the cellular pellets, maximizing

146

lipid exposure to extraction solvents. The extractant was dried under nitrogen and eluted through activated silicic acid (Silica Gel 60, 70-230 mesh; Electron Microscopy Sciences), thereby fractionating neutral lipids, glycolipids, and polar lipids. The PLFA fractions were dried under nitrogen and were transesterified into methyl esters with 0.2 M methanolic potassium hydroxide. Resulting polar lipid methyl esters were concentrated to 1 mL in hexane and analyzed on a gas chromatograph equipped with a flame ionization detector and a DB-5 capillary column (30 m× 0.025 mm I.D., 0.25 um film thickness; J&W Scientific, Folsom, CA). Samples were introduced via auto-injection at 250°C, splitless mode with constant pressure at 13 psi and a variable temperature program. All components were identified based on retention time and elution order relative to BAME and FAME-37 standards (Sigma-Aldrich, St. Louis, MO). Statistics were performed using Minitab 14 (one-way analysis of variance followed by Tukey's test; a=0.05).

Metals analysis. Aliquots (60 μL), of the concentrated ultrapure n-MV stocks were added to 1.5 mL Eppendorf tubes and centrifuged 16,100 g for 30 min at 4°C. The resulting pellet was transferred to a digestion vessel with the addition of 0.3 mL of HNO_3 (Optima; Fisher Scientific), followed by 5 min sonication before transferring. This was followed by 0.2 mL of HNO_3 added to the digestion vessel and 1 mL of 18.2 MΩ water was then added. Digestion was accomplished with a focus microwave (CEM Discover; CEM, Matthews, NC) with a 2 min ramp to 150°C at 230 psi and held at 2 min without stirring. The digestion solution was transferred with three rinses of 18.2 MΩ water into 15 mL polypropylene tubes (Corning, Corning, NY) to a final volume of 10 mL. Final sample dilutions were determined gravimetrically. Analysis was performed using an

inductively coupled plasma mass spectrometer (ICP-MS; Thermo X Series[II], Bremen, Germany) running collision cell mode utilizing a 8% H_2 in He collision gas to reduce isobaric interferences. Zn and Fe were calibrated using an external calibration curve gravimetrically prepared from NIST SRM 3126a Iron Standard Solution and 3168a Zinc Standard Solution. Reported values are from [54]Fe and [66]Zn which were normalized to protein concentrations of n-MVs. Statistics were performed using Minitab 14 (two-sample t-test, $\alpha=0.05$).

Chrome azurol S assay. Siderophoric activity was assayed using the chrome azurol S (CAS) assay (Schwyn and Neilands, 1987). Aliquots (10 μL) of purified n-MVs from each pH and 40 μL of 0.1 M 2-(N-morpholino)ethanesulfonic acid (MES) buffered to either pH 5 or 7 were placed in plastic 0.6 mL cuvettes. CAS reagent (50 mL) was added to each cuvette, and the color was allowed to evolve for 24 h. Blanks were prepared in parallel which were 10 μL of 10 mM HEPES 0.85 % (w/v) NaCl, pH 7.4. Deferoxamine B was used as a positive control to confirm the performance of the CAS reagent.

Proteomic analysis. Protein concentrations of ultrapure n-MV stocks were determined using the Bradford assay (Bradford, 1976). For LDS-PAGE, volumes to yield 15 μg protein were removed from whole cell lysate and n-MV aliquots to fresh Eppendorf tubes, and centrifuged 30 min. Each sample was resuspended in LDS buffer, reducing reagent and 18.2 MΩ water according to manufacturer's instructions, sonicated 5 min, and boiled for 10 min. The gel was stained with colloidal coomassie for two days (Westermeier, 2006) and imaged using a G:BOX imager (Syngene, Frederick, MD). For proteomics profiling of n-MVs from pH 5 and 7, gel electrophoresis liquid

chromatography tandem mass spectrometry (GeLC-MS/MS) was used. For the first

dimension, LDS-PAGE, volumes to yield 15 μg of n-MV protein were removed to fresh

tubes, centrifuged 30 min and gently aspirated. Each sample was then mixed with LDS

buffer, reducing reagent and 18.2 MΩ water according to manufacturer's instructions

(Invitrogen) and heated at 70°C for 10 min. Samples were added to a 1.0 mm x 12-well

Bis-Tris 4-12% NuPAGE gel (Invitrogen) in a manner such that empty lanes separated

each condition to minimize cross-contamination. Anti-oxidant was added to the inner

chamber and the gel was run at room temperature for 40 min at 200 V. The gel was

stained with colloidal coomassie for two days, transferred to 20% (w/v) ammonium

sulfate, then excised into six pieces, with 5 being approximately equal and one containing

only the prominent band at 42.5 kDa. These gel plugs were transferred to Eppendorf

tubes and 250 mM ammonium bicarbonate was added. The plugs were reduced with 10

μL of 45 mM DTT (Fluka, Milwaukee, WI) for 30 min at 50°C. Once the plugs were

cooled to room temperature, they were alkylated with the addition of 10 μL of 100 mM

iodoacetamide (Sigma-Aldrich) and reacted for 30 min. Tubes were spun down and the

supernatant was removed. Plugs were then washed with 100 mM ammonium bicarbonate

for 10 min. The plugs were then de-stained with 25mM ammonium bicarbonate in 50%

acetonitrile for 10 minutes, and repeated until stain was not visible. The plugs were then

dehydrated with 100% acetonitrile for 10 min and dried in a speedvac. Each gel plug was

covered with proteomics grade trypsin (Promega, Madison, WI) and incubated at 37°C

overnight with shaking (200 rpm). The plugs were centrifuged and the supernatant was

collected to a clean Eppendorf tube. Peptides were further extracted with one wash of

25mM ammonium bicarbonate with sonication for 20 min and three washes of 5% formic

149

acid, 50% acetonitrile in water with sonication for 20 min each. The supernatant from each wash was pooled and dried down in a speedvac to ~2µl. Prior to nano-LC-MS/MS analysis the samples were reconstituted with 10µl of 2% acetonitrile and 0.2% formic acid.

Peptide analysis was performed using a linear ion trap mass spectrometer (LTQ; Thermo Finnigan, San Jose, CA) coupled to a nano-LC system (LC Packings, Amsterdam, Netherlands). A 75 micron C-18 reversed phase LC column (Micro-Tech Scientific, Vista, CA) was utilized with a 60 min gradient from 2% acetonitrile, 0.2% formic acid to 70% acetonitrile, 0.2% formic acid. Data dependant analysis was utilized on the LTQ to perform MS/MS on all ions above an ion count of 500. Dynamic exclusion was set to exclude ions from MS/MS selection for 3 min after being selected 2 times in a 30 sec window.

The MS/MS data was searched against a CDS translation library generated from the genome of *Burkholderia vietnamiensis* G4 (ORNL, 2007) using Bioworks 3.3 software (Thermo Scientific, Waltman, MA). Variable modifications of methionine oxidation and cysteine alkylation and 3 post-translational modifications (PTMs) per peptide with a peptide tolerance of 2 amu and fragment tolerance of 1 amu were considered. Protein identifications met the minimum criteria of a Protein Probability of 1.0 e^{-3} or better and had an X_{corr} vs charge state $> 1.5, 2.0, 2.5$ for +1, +2, and +3 ions, with at least 2 unique peptides matching the protein, and a good match for at least 4 consecutive y or b ion series from the MS/MS spectra. Since we generated a peptide library from the genome of the microorganism in question, there was no need to evaluate false positives, which is normally performed when evaluating results based on non-

redundant protein libraries. Venn diagrams were generated using the Venn Diagram

Plotter from the Pacific Northwest National Laboratories Biological MS Data and

Software Distribution Center (http://omics.pnl.gov/). Further analysis of identified

proteins was accomplished with PSORTb v. 2.0.4 (http://www.psort.org/psortb/) as well

as secondary analysis with PA-SUB v. 2.5 (http://www.cs.ualberta.ca/~bioinfo/PA/Sub/).

5.3. Results

MV production during growth of PR1 at pH 5 and 7. To determine maximum

n-MV production in PR1, we measured n-MV production at different points during

growth at pH 5 and 7 by quantifying the protein concentration of n-MV preparations.

Membrane vesicle production correlated to growth measured by total culture protein,

with maximum production (1% and 3% of whole cell lysate protein) occurring during

exponential phase growth and early stationary phase growth (Figure 5.1). Since pH

affects metal toxicity, we also determined whether pH also affects n-MV production.

After 12 h of growth, there were 2.6 μg/ml and 5.7 μg/ml n-MV protein at pH 5 and 7,

respectively, corresponding to 1.3% and 2.6% of whole cell lysate protein (Figure 5.1).

The measured increase in n-MV production at pH 7 was also confirmed by SEM and the

two-fold difference in n-MV production was reflected by fewer MVs present at pH 5 than

pH 7 (Figure 5.2). SEM also confirmed that cells had the same general morphology at

each pH. Furthermore, the size of n-MVs produced at each appeared the same size (25 to

150 nm in diameter; Figure 5.5).
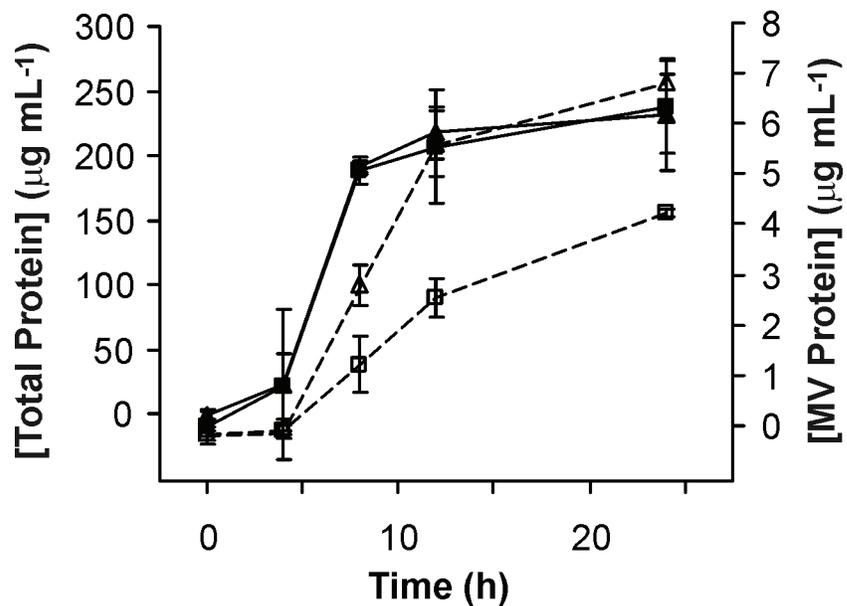
Figure 5.1. Membrane vesicle production during growth of PR1 at pH 5 and 7.
Total culture protein concentration at pH 5(■) and pH 7(▲) with n-MV protein
concentration at pH 5 (□) and pH 7(△) plotted with time. Error bars represent ± 1.0
standard deviation based on triplicate measurements.
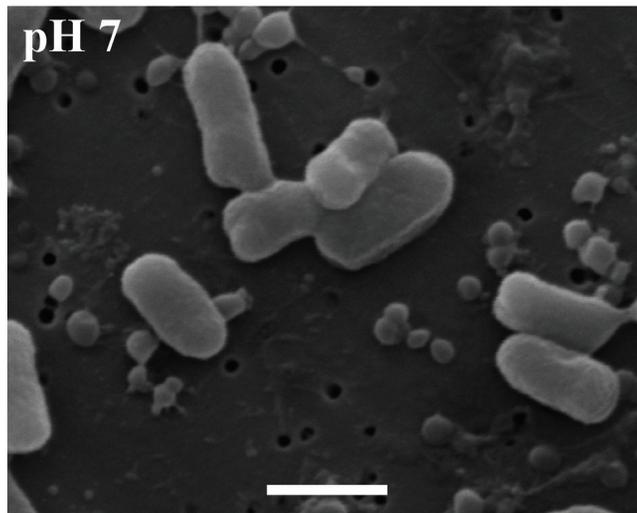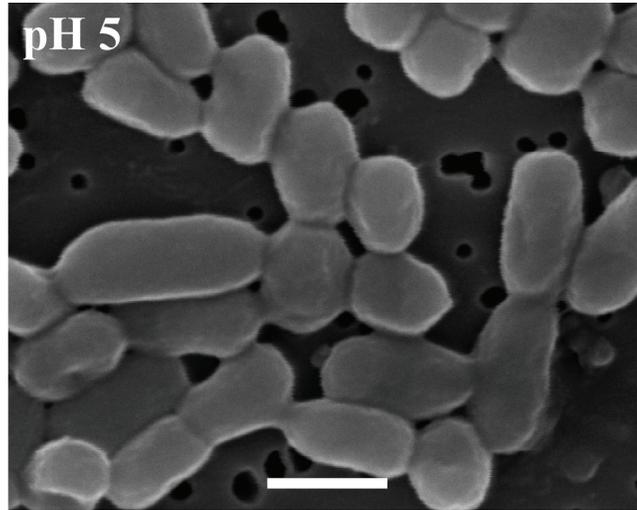
Figure 5.2. Scanning electron micrographs of 12 h cultures. Micrographs reflect the difference in n-MV production between pH. Scale bar is 1 μm.
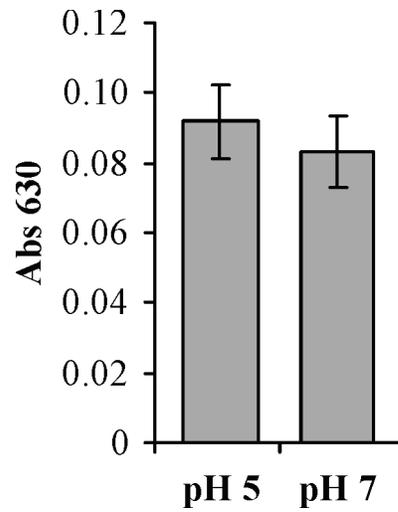
Figure 5.3. Biofilm production by PR1 at different pH. Biofilm production was quantified by a crystal violet assay. Error bars represent ± 1.0 standard deviation based on triplicate measurements.

Effect of pH on biofilm formation by PR1. Previous research has demonstrated that MVs are components of bacterial biofilms (Schooling and Beveridge, 2006; Palsdottir et al., 2009) and that *B. cepacia* biofilms have associated MVs (Smirnova et al., 2008). We were interested in whether biofilm formation by PR1 at pH 5 and 7 corresponded to differences observed in n-MV production. Analysis of biofilm formation demonstrated that pH did not affect biofilm formation (Figure 5.3).

Confirming ultrapure n-MVs. In order to accurately characterize n-MVs, a stringent purification protocol was used to eliminate contamination by cells, cell debris, or pili. After removing cells by centrifugation and filtration, pili could still be present (Bauman and Kuehn, 2006), therefore density gradient centrifugation was used to further purify n-MVs. Ultrapure n-MVs floated to the section of the gradient with a density of 1.137 g/ml, which corresponds to previously reported n-MV densities (Bauman and Kuehn, 2006). To confirm n-MV purity, aliquots of each 1 mL fraction were evaluated by LDS-PAGE (Figure 5.4). The most diverse protein profile occurred at 3 to 4 mL from the top of the gradient in both pH 5 and pH 7 samples. Similar to previous studies, there was evidence of pili and debris in the more dense fractions as indicated by the different protein banding pattern (Horstman and Kuehn, 2000; Kesty and Kuehn, 2004; Bauman and Kuehn, 2006). Based on our results, fractions 3 to 4 mL from the top were pooled and evaluated by TEM to confirm purity. TEM demonstrated that these fractions in all replicates were free of cells, pili and other cell debris (Figure 5.4). The MVs appear to contain a single membrane and range in size from approximately 25 to 150 nm in diameter, and these characteristics are conserved between pH 5 and 7. Based on these observations, these fractions were used as ultrapure n-MVs for further analysis.
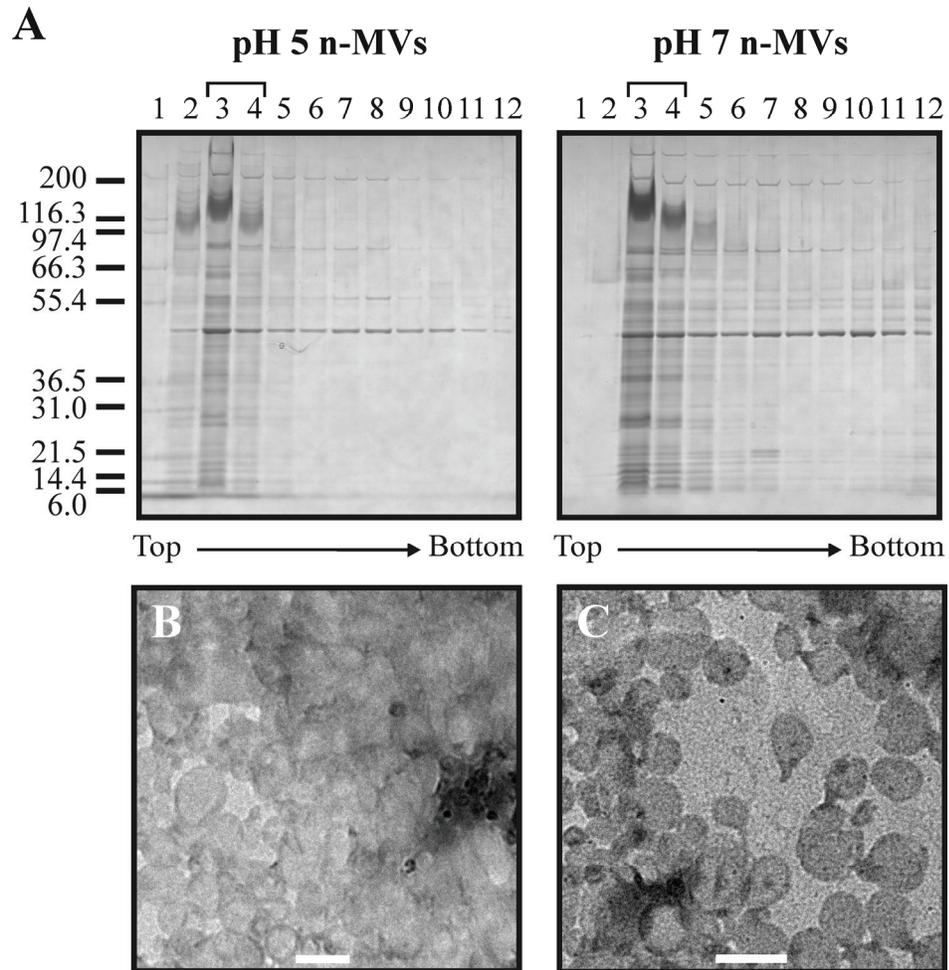
Figure 5.4. Differential centrifugation was used to generate ultrapure n-MVs from both pH. (A) Representative LDS-PAGE of 1 mL fractions recovered from density gradient centrifugation of n-MVs from each pH. Molecular weights from protein standards are given on left as kDa. Fractions indicated by brackets were combined and evaluated by TEM. (B,C) Transmission electron micrographs of ultrapure n-MVs from (B) pH 5 and (C) pH 7. Ultrapure n-MVs at each pH were similar in size and were free of pili and cellular debris. Scale bar is 200 nm.

PLFA analysis of n-MVs produced by PR1 at pH 5 and 7. Since the lipid composition of n-MVs is related to formation and function, we investigated whether n-MVs had a PLFA composition different than cells and whether pH affected PLFA composition. We used whole cell lysate samples to represent the cellular PLFA profile, despite the fact that these consisted of cells and n-MVs, since previously it was determined that n-MVs content is less than 3% of the total outer membrane protein content of *E. coli* (Kuehn and Kesty, 2005). When PLFA profiles of both cells and n-MVs were compared between pH 5 and 7, relative percents of C16:0, C18:1ω9t/ C18:1ω7c decreased at pH 5 while C18:0 was increased at pH 7 (Figure 5.5). Additionally, relative to cells at each pH, n-MVs were enriched in 16:0, 16:1ω7c, and C18:1ω9t/C18:1ω7c. The only PLFA that maintained a similar relative percent in cells and n-MVs was C18:0. Lastly, PLFA which were not significantly different in cells between pH (i.e., C16:1ω7c, 17:0 cyc and C19:0 cyc) were also not significantly different between n-MVs ($p<0.05$).

Quantification of nucleic acids in n-MVs. Nucleic acids contained within MVs were functionally defined as nucleic acids which resisted nuclease treatment of intact MVs. Using fluorometric dyes, we measured the DNA and RNA content of n-MVs to evaluate whether pH affected n-MV nucleic acid composition. Overall, the average DNA and RNA content was 2.5 ± 1.7 and 0.58 ± 0.07 ng μg^{-1} MV protein, respectively (Figure 5.6). Although n-MVs from pH 5 contained on average more DNA than n-MVs from pH 7, differences between pH were not statistically different ($p<0.05$). Overall, the effect of pH on DNA and RNA content was minimal.
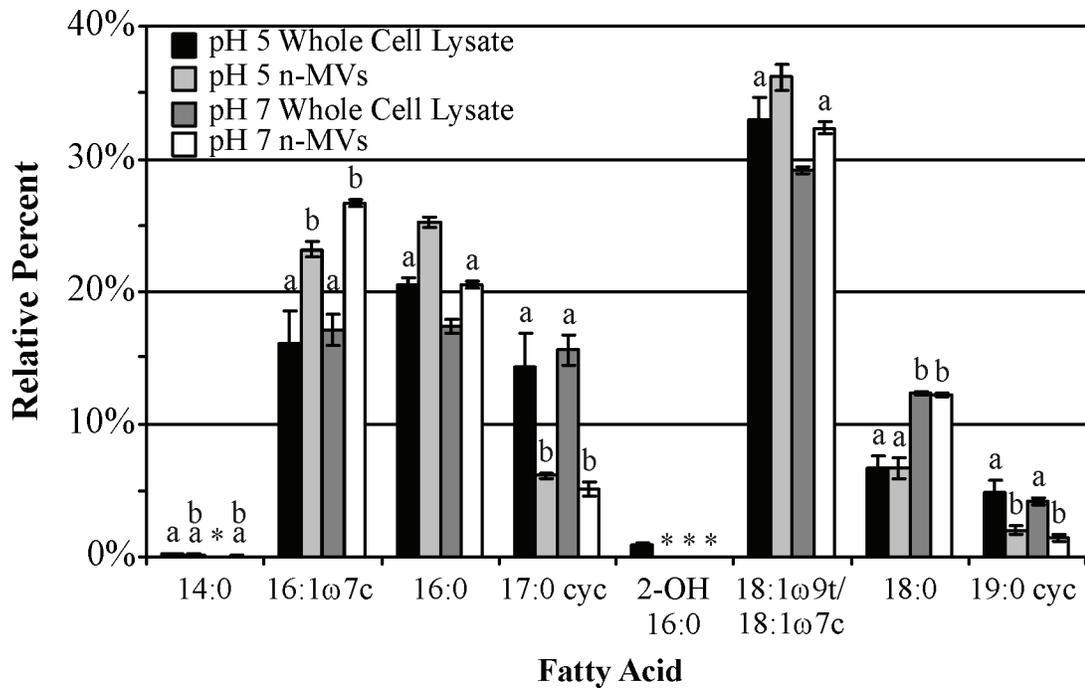
Figure 5.5. Polar lipid fatty acid (PLFA) composition of whole cell lysate and n-MVs at pH 5 and pH 7. Significant differences within each PLFA species were determined by one-way ANOVA followed by Tukey's test. Similar letters within each PLFA indicate they are not significantly different ($p<0.05$) and samples that fatty acids that were not detected in are indicated by an *. Error bars represent ± 1.0 standard deviation based on triplicate measurements.
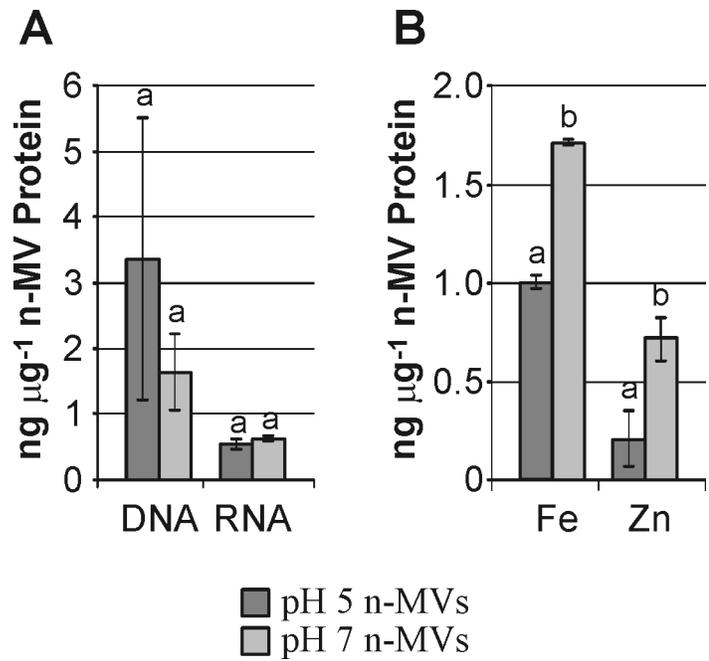
Figure 5.6. n-MVs produced at pH 5 and 7 contain beneficial components. (A) Nucleic acid concentrations of nuclease treated n-MVs were determined and (B) Fe and Zn concentrations were compared between n-MVs produced at pH 5 and 7. Similar letters indicate values were not significantly different between pH ($p<0.05$). Error bars represent $\pm$ 1.0 standard deviation based on triplicate measurements.

Zn and Fe composition of n-MVs. Since the metal content of MVs has never been reported, and due to our interest in their involvement in metal-microbe interactions, we quantified the Zn and Fe concentration of n-MVs produced at pH 5 and 7. The Zn and Fe concentration associated with n-MVs produced at pH 7 was approximately two-fold greater than at pH 5 (Figure 5.6). To evaluate whether n-MVs may be capable of binding Fe similar to siderophores (Drechsel and Jung, 1998), a CAS assay was employed to assay their siderophoric activity. The results (not shown) were negative for n-MVs produced at both pH, which simply indicates that n-MVs are not capable of stripping Fe(III) from chrome azurol S and does not negate their ability to sorb metal ions as was demonstrated previously (refer to chapter 4).

n-MV proteomics. Initially, LDS-PAGE was used to separate and visualize the protein composition of ultrapure n-MVs from both pH along with whole cell lysates. Relative to whole cell lysate, n-MVs from both conditions contained fewer distinct bands while certain bands appear enriched in n-MVs versus whole cell lysates, while many distinct bands present in whole cell lysates are absent in n-MVs (Figure 5.7). For example, the double banding pattern present between 66.3 and 55.4 kDa in the whole cell lysate is absent in respective n-MV lanes where only a single band is evident.

For global proteomic analysis of n-MVs produced at pH5 and 7 was accomplished using GeLC-MS/MS. Using this technique we were able to identify 538 and 394 unique gene products at pH 5 and 7, respectively, and we had strong overlap within conditions, with 68% and 73% of gene products being identified in at least two of the three triplicates (Figure 5.8). Next, redundant gene products were removed from this pool of 408 unique gene products identified in at least two of the three triplicates. Additionally, hypothetical
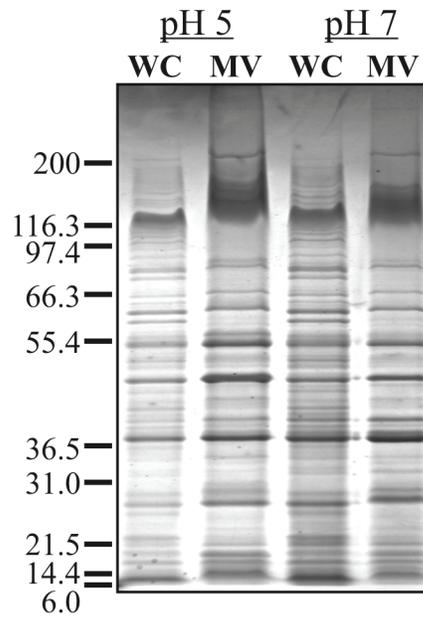
Figure 5.7. Representative LDS-PAGE of whole cell (WC) and ultrapure n-MV (MV) lysates from different pH. Each lane was loaded with 15 μg of protein and n-MV fractions contained fewer bands than whole cell lysates and have a different banding pattern between pH. Molecular weights are given to the left as kDa.
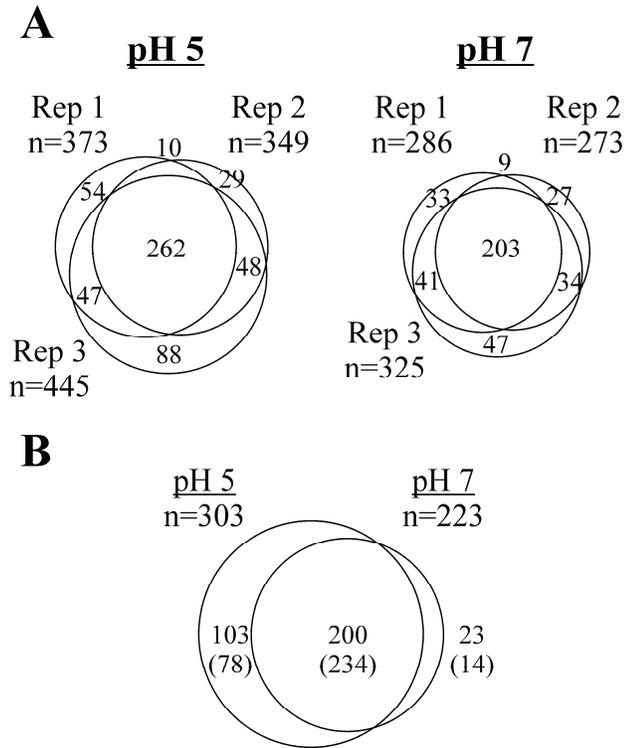
Figure 5.8. Comparison of proteins (A) within triplicates and (B) between conditions. Values in parenthesis in (B) represent values after comparing positive hits to all triplicates and thus indicate truly unique proteins.

and putative proteins were evaluated for homology using the basic local alignment search tool for proteins (BLASTp) algorithm from NCBI. The remaining 326 unique proteins were used to compare between the conditions (Figure 5.8 and Table C.1). On average 61%, or 200, of these unique proteins were shared, though pH 7 only had 23 unique proteins versus 103 at pH 5 (Figure 5.8). Furthermore, comparing these unique proteins to all three triplicates, we found that actually only 78 and 14 were unique to pH 5 and 7 respectively (Figure 5.8). These proteins have a high degree of certainty of being truly unique based on the experimental setup and stringent analysis.

Predicted protein subcellular localization. A useful approach to analyzing proteomic results from n-MVs is to employ protein prediction algorithms, such as PSORTb, to evaluate the proteome of n-MVs. Using the sequences of the identified unique proteins at both pH, this analysis was performed. Although 46% of the unique proteins we identified did not have predicted subcellular localizations using PSORTb, the remaining 54% were predicted to have localizations in every cellular compartment (Figure 5.9). Under both conditions, an average of 18% of the proteins with predictions were predicted to be extracellular, outer membrane, or periplasmic. Additionally, at both conditions an average of 73% of the proteins are predicted to be associated with the inner membrane or cytoplasm, with 41% and 21% localized to the cytoplasm at pH 5 and 7 respectively. Based on the sorting assignments of PSORTb, the most notable change between n-MVs produced at both pH conditions was that n-MVs produced at pH 5 have twice as many proteins predicted to localize to the cytoplasm.
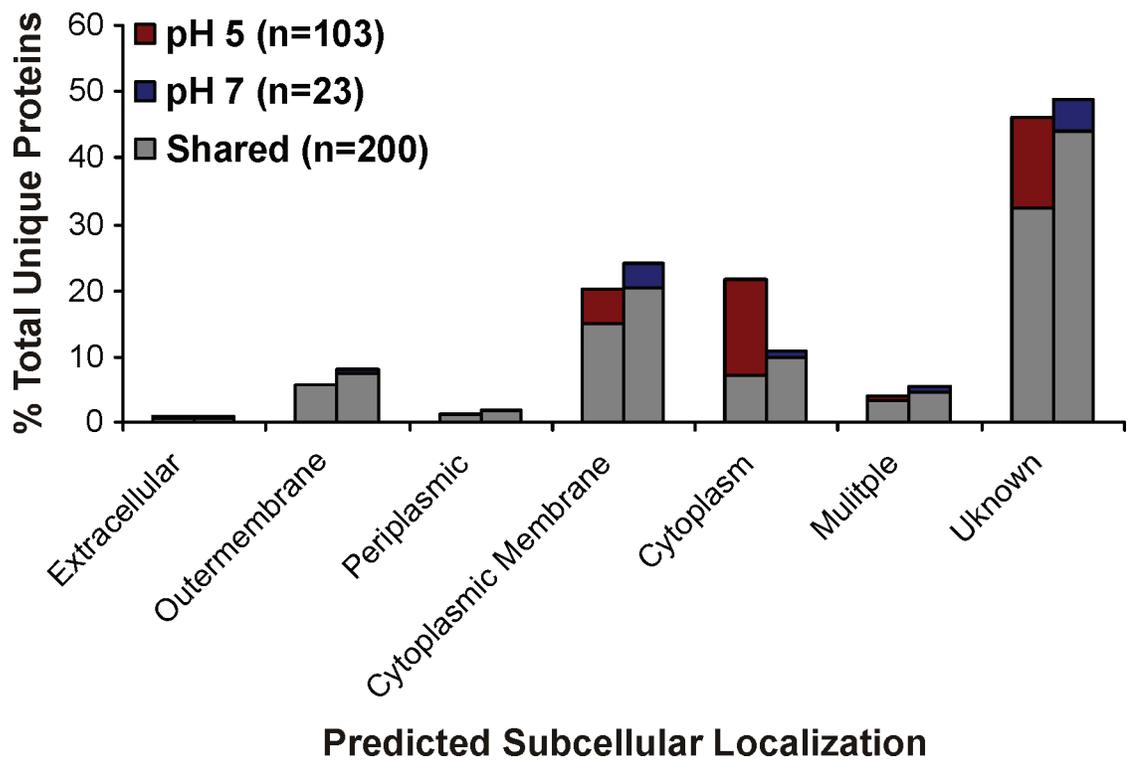
Figure 5.9. Subcellular sorting predictions of unique proteins as determined by PSORTb. Subcellular localizations are based on POSRTb output for unique proteins identified at pH 5 and 7 (i.e., present in two of three replicates at each pH). Percent total unique proteins was calculated within each pH such that total proteins at pH 5 was 303 and at pH 7 was 223. This illustrates the distribution of pH specific proteins and shared protein for each localization prediction.

5.4 <u>Discussion</u>

Maximum n-MV production occurs at stationary phase. The growth phase during which maximum n-MV production occurs is related to the underlying mechanism of MV formation. It has been proposed that MVs are formed during cell division (Deatherage et al., 2009), and therefore maximum n-MV production should occur during exponential growth phase. Membrane vesicle production by PR1 correlated to growth measured by total culture protein, with maximum production (1% and 3% of whole cell lysate protein) occurring during exponential phase growth and early stationary phase growth (Figure 5.1). This trend was also demonstrated in n-MV production during growth of *P. aeruginosa* PA01. Furthermore, outer membrane protein concentrations in n-MVs from four *P. aeruginosa* strains were between 0.75% and 2.5% of the total outer membrane protein concentration, similar to our results. (Bauman and Kuehn, 2006). Since *Pseudomonads* and *Burkholderias* are closely related, this might indicate a conserved mechanism of MV formation.

Since maximum n-MV production rates in PR1 occurred during exponential phase and into early stationary phase, n-MV production may be related to cell division as has been proposed (Deatherage et al., 2009). Additionally, maximum n-MV concentrations occur at high cell densities, which may also indicate that n-MV production is influenced by quorum signaling. Recent evidence has suggested that in *P. aeruginosa*, Pseudomonas quinolone signal (PQS) stimulates MV formation through interactions with LPS on the cell surface (Mashburn-Warren et al., 2008; Mashburn-Warren et al., 2009). Although *Burkholderia* spp. produce 4-hydroxy-2-alkylquinolines (HAQs), which are structurally related to PQS (Vial et al., 2008), the parent strain of PR1, *B. vietnamiensis*

G4, utilizes C_{10}-homoserine lactone (C_{10}-HSL) as its quorum sensing molecule and does not produce HAQs (Conway and Greenberg, 2002). Despite the lack of a homologous PQS compound, the alkyl chain of C_{10}-HSL may interact with LPS on the cell wall similar to PQS in *P. aeruginosa*. Another explanation of maximum n-MV production occurring during late exponential phase growth is that n-MV production is a costly endeavor to cells that are rapidly dividing. For instance, mutations in *E. coli* DH5a that result in an over-vesiculating phenotype cause reduced bacterial growth rates (McBroom et al., 2006) indicating that MV production can be costly to growing cells. Overall, to the author's knowledge this is the first study to quantify n-MV production during growth under different conditions and demonstrates that although pH influences n-MV production, and at both pH n-MV production occurs during the same growth phase.

pH affects n-MV production. In bacterial pathogenesis as well as in the environment, pH can be an important variable. For instance, pathogenic bacteria in the lungs of CF patients must be able to adapt as the lung becomes acidic (Tate et al., 2002). Additionally, we have demonstrated that PR1 is more resistant to divalent metal cations at pH 5 versus pH 7, which is important since a typical first step in treatment of a metal contaminated site is to raise the pH (Van Nostrand et al., 2005). Due to the multifarious functions of bacterial MVs, we hypothesized that n-MVs may act as a key intermediary in metal-microbe interactions. Similar to previous work with a summer student, Venetia Lyles, which demonstrated that n-MV production increases with pH (refer to chapter 3), we also found a two-fold increase in n-MV production at pH 7 versus pH 5 (Figure 5.1). Furthermore, analysis of these cultures at 12 h by SEM reflected this two-fold difference in n-MV production (Figure 5.2). Contrary to previous research by Van Nostrand et al.

(2008) which found PR1 exhibited different cell morphology at 8 h of growth at pH 5 and 7, we found that cells had the same general morphology at each pH. Furthermore, similar to data in chapter 4 of this dissertation, we found that the size of n-MVs produced at each appeared the same size (25 to 150 nm in diameter; Figure 5.2). Similarly, n-MVs produced by a clinical *B. vietnamiensis* strain were found to be 65.7 ± 40.4 nm in diameter (Allan et al., 2003). Overall, it is interesting that pH has significant effect on n-MV production. If this trend is also true for other *Burkholderia* spp., it would indicate that a decrease in the lung pH of CF patients could have a deleterious effect on bacterial function.

pH does not affect biofilm formation. Previous research has indicated that MVs are components of bacterial biofilms (Schooling and Beveridge, 2006; Palsdottir et al., 2009), including *B. cepacia* biofilms (Smirnova et al., 2008). Furthermore, it has been demonstrated that DNA contained in MVs is required for biofilm formation in *P. aeruginosa* (Whitchurch et al., 2002). Based on these observations, we were interested in whether a concurrent increase in biofilm formation occurred with increased n-MV production by PR1 at pH 7. Analysis of biofilm formation demonstrated that pH did not affect biofilm formation (Figure 5.3). This indicates that levels of n-MVs in planktonic cell cultures do not determine the level of biofilm formation, further supporting the idea that biofilm and planktonic derived n-MVs are functionally different (Schooling and Beveridge, 2006; Schooling et al., 2009).

Confirming ultrapure n-MVs. Purifying MVs is the most critical aspect of any MV characterization study since cell debris of pili can lead to misinterpretation of results. For this reason, we employed differential centrifugation and filtration followed by density

gradient purification, similar to Bauman et al. (2006). Interestingly, all resulting fractions from density gradient centrifugation contained a prominent band at 42.5 kDa, though the intensity of this band decreased in denser fractions (figure 5.4). Allan et al. (2003) also observed an intense protein at approximately 41.7 kDa in n-MVs collected from *Burkholderia cenocepacia*, though it was not identified (Allan et al., 2003). Overall, our analysis of fractions by LDS-PAGE demonstrated that MVs 3 to 4 mL from the top of the gradient were pure, as was reflected by TEM images from these fractions (Figure 5.4). This was deemed ultrapure and free of cellular debris and pili and was used for the remaining characterization studies.

MV polar lipid content. To date, little is known about the lipid composition of n-MVs. Broad lipid compositions of n-MVs have have been evaluated (Horstman and Kuehn, 2000; Post et al., 2005; Nevot et al., 2006), though modern lipidomic approaches that determine the fatty acid composition of lipid classes have been applied to n-MVs in only a few cases (Kobayashi et al., 2000; Post et al., 2005). Since the lipid composition of n-MVs would provide insights into n-MV formation, we compared the PLFA profile of n-MVs at different pH with respective cellular profiles. For this analysis, whole cell lysate samples were used to represent the cellular PLFA profile, despite the fact that these consisted of cells and n-MVs, since previously it was determined that n-MVs content is less than 3% of the total outer membrane protein content of *E. coli* (Kuehn and Kesty, 2005).

(i) Insights into MV formation. In the simplest sense, n-MV formation is hypothesized to be the result of a random pinching off of the outer membrane, and therefore the n-MV PLFA profile should reflect that of the cell (Mashburn-Warren and

Whiteley, 2006). When we compared PLFA profiles of n-MVs between pH, we observed

that they reflected similar changes as the cellular PLFA (i.e., decreased levels of C16:0,

C18:1ω9t/ C18:1ω7c at pH 5 and increased levels of C18:0 at pH 7; Figure 5.5).

Intriguingly, when we compared the PLFA profile of n-MVs to cells, we found that n-

MVs were enriched in 16:0, 16:1ω7c, and C18:1ω9t/C18:1ω7c relative to cellular PLFA

profiles. Furthermore, the increased monosaturated C16 and C18 PLFAs we observed

correlate to respective decreases in their related cyclopropane fatty acids, C17:0 cyc and

C19:0 cyc. Similarly, n-MVs from *N. meningitis* where enriched in shorter PLFAs and

contained less longer PLFAs relative to cells, though cyclopropane fatty acids were not

detected (Post et al., 2005). The PLFA profile of n-MVs produced by PR1 is similar to

that observed in n-MVs from *P. putida* (grown at pH 7) where the major species were

C16:0 and C16:1, though we detected higher amounts of C18:1 and cyclopropane fatty

acids (Kobayashi et al., 2000). Cyclopropane fatty acids (CFAs) are known to be formed

by stationary phase cells, and are thought to increase membrane rigidity (Munoz-Rojas et

al., 2006). By having relatively less cyclopropane PLFA and more unsaturated C16

PLFA, regions of the membrane that formed n-MVs would predictably be less rigid than

the surrounding cellular membrane.

　　　Taken together, this data implies that regions of less rigid PLFA in the membrane

may be a driver for n-MV formation in PR1, though it is unclear why specific regions of

the membrane would interact differently with CFA synthase which forms CFA from *cis*-

monounsaturated FAs (Grogan and Cronan, 1997). Recently a mechanistic theory has

been proposed that explains how dimpling on the cell surface can slow coalescence of

phospholipids, thereby preserving lipid domains in the cell membrane over time (Ursell

et al., 2009). Using SEM we have observed that PR1 has a dimpled cell membrane, which may be indicative of lipid domains prone to form MVs (Figure 1.6). Interestingly, given that these regions of less rigid PLFA may be more likely to bulge outward, they may recruit proteins from the periplasm into forming MVs using cell membrane curvature, a phenomenon recently described in *Bacillus subtilis* during spore formation (Ramamurthi et al., 2009). Overall, these results and previous studies (Kobayashi et al., 2000; Post et al., 2005) demonstrate the role of membrane composition in n-MV formation, but further studies will be needed to more accurately compare lipid shifts in n-MVs versus the outer membrane and how this influences not only n-MV formation but also protein recruitment.

MVs contain nucleic acids. The presence of DNA has been confirmed in n-MVs from numerous Gram-negative and Gram-positive bacteria as well as Archaea (Table 1.4), while RNA has only been described in n-MVs from *N. gonorrhoeae* (Dorward et al., 1989). The presence of DNA and RNA in n-MVs of PR1 would signify that they could function in transfer of genetic material or actively transcribing proteins. We found that n-MVs from PR1 contained DNA and RNA, though the pH did not affect this composition (Figure 5.6). The measured DNA concentration was similar to values reported for *P. aeruginosa* PAO1 biofilm derived MVs (Schooling et al., 2009), but is more than 150-fold greater than the DNA content of n-MVs isolated from planktonic *P. aeruginosa* PAO1 (Kadurugamuwa and Beveridge, 1995; Renelli et al., 2004). Similar to the trace amounts of RNA in n-MVs produced by *N. gonorrhoeae* (Dorward et al., 1989), we also found that RNA concentrations were much less than DNA concentrations.

170

Because n-MVs produced by PR1 harbor nucleic acids, they may be involved in transport of specific genes, or mRNA coding specific proteins. For instance, n-MVs produced by *E. coli* O157:57 contained virulence genes (Kolling and Matthews, 1999) and MVs produced by *N. gonorrhoeae* and *E. coli* are able to act as transformative vectors (Dorward et al., 1989; Yaron et al., 2000). Since it has demonstrated that MVs can transfer their contents to other bacteria (Kadurugamuwa and Beveridge, 1999), n-MVs should be capable of not only transferring DNA to other bacteria, but also mRNA coding for specific proteins. Similar to how bacteria can secrete beneficial proteins in n-MVs (i.e., *P. aeruginosa* clinical isolates package β-lactamases in n-MVs; Ciofu et al., 2000), as well as virulence factors (Kuehn and Kesty, 2005), transferring mRNA in n-MVs could be an efficient mechanism of disseminating proteins to other cells. Furthermore, transporting nucleic acids in MVs allows them to be shielded from nuclease activity, thereby being a more effective vector than simply secreting nucleic acid into the extracellular milieu. Although the precise role of nucleic acids in n-MVs from PR1 is unclear, ongoing research is investigating the sequence and nature of DNA and RNA contained in n-MVs released at pH 5 and 7.

MVs contain Fe and Zn. Previous research on n-MVs produced by bacteria has mostly focused on their involvement in bacterial virulence, including the transport of proteins and metabolites. However, little is known about the nutrient composition of n-MVs. Previous research comparing MVs derived from planktonic and biofilm cultures of *P. aeruginosa* PAO1 found that biofilm derived MVs had a red color (Schooling and Beveridge, 2006). Similarly, we observed that n-MVs produced by PR1 were red, indicating the presence of Fe. Since in *E. coli*, the Zn requirement of a cell is similar to

Fe (Outten and O'Halloran, 2001), and Zn serves numerous functions as a cofactor in multiple classes of proteins, we were interested in the Fe and Zn content of n-MVs. We found that the Fe and Zn concentration in n-MVs produced at pH 7 was almost two-fold greater than in n-MVs produced at pH 5 (Figure 5.6). Additionally, since experiments in chapter 4 demonstrated that MVs are capable of sorbing Zn, we evaluated the siderophoric activity of n-MVs using a CAS assay (Schwyn and Neilands, 1987) and demonstrated that they were not siderophoric. This result does not necessarily conflict with results in chapter 4, since this assay relies on removal of Fe from chrome azurol S, and if Fe binding by n-MVs is due only to surface complexation then we would not expect it to show positive in this assay. Since a common host defense against bacteria is Fe limitation (Radtke and O'Riordan, 2006), factors which allow bacteria to sequester or store Fe are often associated with virulence. Therefore, packaging Fe extracellularly into MVs could be a host invasion strategy. Additionally, packaging Fe and Zn into MVs would make them beneficial to any cell that accessed the contents and could thereby enhance the virulence of a population of bacteria.

MV proteomics. To evaluate global changes in the protein composition of n-MVs produced at pH 5 and 7, GeLC-MS/MS was used. This technique is widely accepted and implemented in large scale proteomic analyses (Hu et al., 2007) since pre-fractionation of whole proteins prior to digestion and MS/MS analysis increases identification of up to 5-fold more proteins than conventional 2D-LC/MS/MS (Nesatyy and Suter, 2008) and allows for better detection of less abundant proteins as well as analysis of membrane proteins (Bell et al., 2001). Before we evaluated protein differences between n-MVs at different pH, we first evaluated whether LDS-PAGE

effectively separated MV proteins, and whether this banding pattern was different than respective cellular protein banding patterns. We found that LDS-PAGE effectively separates n-MV proteins and that n-MVs from both pH contain fewer distinct protein bands (Figure 5.7). Although we did not compare the outer membrane, periplasm and inner membrane individually, other studies have demonstrated that n-MVs have specific protein profiles relative to cells (Renelli et al., 2004; Bauman and Kuehn, 2006; Sidhu et al., 2008). Since there were subtle differences in the banding pattern between n-MVs from each pH, we further evaluating the proteome of n-MVs from pH 5 and 7.

Detailed proteomic analysis of n-MVs has only been reported for *E. coli* (Lee et al., 2007; Scorza et al., 2008), *Legionella pneumophila* (Galka et al., 2008), *Neisseria meningitidis* (Post et al., 2005; Ferrari et al., 2006), *Pseudoalteromonas antarctica* (Nevot et al., 2006), *P. aeruginosa* (Bauman and Kuehn, 2006), and *Xanthomonas campestris pv. campestris* (Sidhu et al., 2008). Except for Lee et al. (2007), these studies relied on single proteomic experiments for protein identification. In contrast, we used n-MVs produced at pH 5 and 7 from three independent cultures. We had good overlap within each condition of approximately 70% (Figure 5.8) and using strict criteria, identified 326 unique proteins at both pH. This number of unique proteins is high relative to reported numbers compiled by a review by Lee et. al (2008) of unique proteins identified in n-MVs. Even compared to the only study that employed a similar proteomics approach to evaluate n-MVs from *E. coli* DH5α (Lee et al., 2007), this value is almost two-fold greater. One reason for the difference in identified proteins may be that the genome of *E. coli* is roughly half the size of PR1's at 8.5 Mb, which may allow for greater protein diversity in general. Overall, the experimental design employed and

criteria for defining unique proteins allows a high degree of certainty that identified

proteins are in fact present in n-MVs and that certain proteins are unique to each pH.

Furthermore, we predict that the shared proteins which were identified at both pH in at

least 2 of 3 triplicates represent the core n-MV functionality in PR1.

(i) Predicted protein subcellular localization. A useful approach to analyzing

proteomic results from n-MVs is to employ protein prediction algorithms, such as

PSORTb, to evaluate the proteome of n-MVs. Although 46% of the unique proteins we

identified did not have predicted subcellular localizations using PSORTb, the remaining

54% were predicted to have localizations in every cellular compartment (Figure 5.9).

Under both conditions, an average of 18% of the proteins with predictions were predicted

to be extracellular, outer membrane, or periplasmic. Previous studies have found

approximately 50% to 70% of the identified proteins in n-MVs localize to these

compartments (Ferrari et al., 2006; Lee et al., 2007; Scorza et al., 2008; Sidhu et al.,

2008). One explanation for this difference is that these studies identified fewer total

proteins (36 to 141 proteins), which would skew relative numbers. It may also be that the

outer membrane and periplasm in n-MVs produced by PR1 do not contain as many

different kinds of proteins. Additionally, at both conditions an average of 73% of the

proteins are predicted to be associated with the inner membrane or cytoplasm, with 41%

and 21% localized to the cytoplasm at pH 5 and 7 respectively. Lee et al. (2007)

employing a similar method of protein analysis found 40% of identified unique proteins

were cytoplasmic. Based on the sorting assignments of PSORTb, the most notable

change between n-MVs produced at both pH conditions was that n-MVs produced at pH

5 have twice as many proteins predicted to localize to the cytoplasm. Whether this is an

artifact of the analysis as discussed above, or is a result of a different mechanism of formation or sorting, is unclear yet the data does demonstrate fundamental difference in the protein composition at each pH.

Although the abundance of inner membrane and cytoplasmic proteins we observed could indicate contamination by cell lysis, previous studies have demonstrated that PSORTb predictions do not agree with experimental results (Ferrari et al., 2006; Williams et al., 2007). For example, Ferrari et al. (Ferrari et al., 2006) determined that 13 assignments of n-MV proteins to the cytoplasm were probably incorrect based on previous studies and experimental evidence. Additionally, within our results, comparing proteins which were predicted as cytoplasmic to another sorting algorithm, PaSub, demonstrated that only 58% were still predicted to be cytoplasmic (data not shown). Sorting algorithms provide useful information, and although they can accurately predict where a protein is abundant, it doesn't rule out the protein being present in a different compartment.

(ii) Shared proteins between pH. Of the 326 unique proteins identified in MVs produced at pH 5 and 7, there were 200 proteins shared at both conditions. Many of these identified proteins are similar to those found in other studies of n-MVs from different bacteria (Post et al., 2005; Ferrari et al., 2006; Nevot et al., 2006; Lee et al., 2007; Galka et al., 2008; Scorza et al., 2008; Sidhu et al., 2008). Similar to these reviewed studies, we found ABC transporters (NodT, ChrA, and ZntA), proteins involved with nutrient uptake (TonB), chaperonin proteins (GroEL), OstA, murein transglycosylase protein domain similar to soluble lytic transglycosylase (SLT), translation machinery (30S and 50S proteins, and EF-Tu), porins, OMP (OmpA, OmpW),

VacJ, peptidases, and proteins involved in metabolism (Table C.1). Other proteins detected in n-MVs from PR1 can be attributed to species differences, for example, OmpA and OmpW were the only OMP's we detected since those are the only OMP's PR1 produces (ORNL, 2007). Also, because PR1 n-MVs contained cobalamin synthesis protein, it was not surprising that we didn't detect any cobalamin transporters similar to studies of n-MVs produced by *E. coli* (Lee et al., 2007; Scorza et al., 2008), which lacks the ability to synthesize cobalamin. Furthermore, taken along with our results that n-MVs contain Fe, it is interesting to note that most n-MV studies to date have found TonB receptors for uptake of siderophores (Post et al., 2005; Nevot et al., 2006; Lee et al., 2007; Scorza et al., 2008; Sidhu et al., 2008), as well as cobalamin transporters (Lee et al., 2007; Galka et al., 2008), which is also able to bind Fe. This strongly indicates that n-MVs may have a conserved function across species as in extracellular storage of Fe.

Interestingly, one protein that is consistently observed in other n-MVs studies, flagellin (Post et al., 2005; Bauman and Kuehn, 2006; Lee et al., 2007; Galka et al., 2008), was not present in our study though it is present in the genome of PR1 (ORNL, 2007). Also, other n-MV proteomic studies found multidrug efflux pumps (Post et al., 2005; Ferrari et al., 2006; Nevot et al., 2006), and while these were absent in our study, it may be due to the annotation of the genome we used for protein identification (ORNL, 2007). For example, hydrophobe/amphiphile efflux-1 HAE1 and RND transporters were identified that may function as multidrug efflux transporters (Poole, 2001). Moreover, although PR1 is not a clinical isolate of *B. vietnamiensis*, we did observe proteins involved in virulence such as OmpA (Weiser and Gotschlich, 1991), OmpW (Nandi et al., 2005), GroEL (Garduno et al., 1998), and TPR repeat protein (DebRoy et al., 2006).

Furthermore, we detected three types of antigens (Rickettsia 17 kDa, D15, and O-antigen), which, along with LPS, can modulate the host immune response. In addition to n-MVs containing virulence related proteins, studies have also identified metal transporters in n-MVs, (e.g., ZnuA Zn^{2+} importer in *E. coli*; Lee et al., 2007). We also identified two metal exporters in n-MVs at both pH, ChrA (chromate efflux) and ZntA (Zn^{2+} efflux). Overall, the proteins present in n-MVs at both pH reflect the core functionality of n-MVs produced by PR1, indicating they could serve in transport of beneficial factors between cells (including nucleic acids) as well as function in host-cell interactions.

      (iii) Different proteins between pH. To date, only one other study has evaluated changes in the proteomic composition of n-MVs produced by a bacterium under different conditions. Sidhu et al. (2008) found 70% of proteins in n-MVs produced by *Xanthomonas campestris* were different when grown in two different media. Our data shows greater overlap of protein composition between n-MVs from different pH (Figure 5.8), which is probably due to only altering pH versus carbon source or nutrient composition. Since the majority of proteins we detected are present at both pH, and pH 7 contains few unique proteins, n-MVs at pH 7 seem to represent the core functionality of n-MVs. The additional functionality present in n-MVs at pH 5 includes translational machinery, chaperonins, transporters, and proteins involved in organic compound catabolism. Furthermore, since the majority of the proteins unique to pH 5 are predicted to be localized in the cytoplasm (Figure 5.9) it may indicate different protein sorting, or perhaps a different mechanism of formation.

At pH 5, the most striking observation is the presence of three toluene ortho-monooxygenase (Tom) proteins (A1, A3, and A5) as well as BtxE and catechol 2,3-dioxygenase, all of which are involved in organic compound catabolism (Shields et al., 1995; Lee and Lee, 2001). These proteins are found on the same 107-kb contig in the annotated genome, which when inserted into *E. coli* conferred the ability to oxidize trichloroethylene, toluene, *m*-cresol, *o*-cresol, phenol, and catechol (Shields et al., 1995). Since PR1 is a constitutive TCE degrader and its parent strain, G4, was isolated from an organochlorine-contaminated holding pond, PR1 may use MVs to degrade organic molecules which may confer cell-dependent and cell-independent organic catabolism. Furthermore, MVs produced at pH 5 may accumulate organic compounds extracellularly, similar to how MVs from toluene-tolerant strain of *Pseudomonas putida* were able to accumulate toluene (Kobayashi et al., 2000). Together, this indicates a novel mechanism of organic compound tolerance that would involve accumulation and catabolism of organic compounds in MVs. Previous research has demonstrated that there was no difference in TCE utilization by PR1 over 24 h at pH 5 and 7 (Van Nostrand et al., 2007), therefore studies of the specific functional activity of n-MVs produced at pH 5 are necessary to confirm their possible involvement in organic compound degradation.

Overall, while proteomic changes at pH 5 and 7 are probably reflective of changes in the proteomic composition of the cell, the additional metabolic and translational proteins present at pH 5 indicate different protein sorting, or perhaps a different mechanism of formation. Also, n-MVs produced at pH 5 contain more proteins predicted to be localized to the cytoplasm (Figure 5.9), though TEM data demonstrated that only one bilayer is present indicating the inner membrane is absent in n-MVs (Figure 5.7),

therefore it seems unlikely that n-MV formation at pH 5 includes the cytoplasm. Taken together with nucleic acid content, Fe content, and protein composition, n-MVs produced at pH 5 and 7 have different functional capacities and probably have different roles at each pH. Additionally, pH could also affect the activity of proteins that are shared between pH, similar to the 26-kDa murein hydrolase that is present in n-MVs of *P. aeruginosa* PA01 (Li et al., 1996), which has a pH optima of 6.0 (Watt and Clarke, 1994). Although there may be a large number of shared proteins between n-MVs from pH 5 and 7, their activities at each pH could be different leading to further functional differences.

   (iv) Proteins involved in MV formation. Recently, Mashburn-Warren and Whitely (2006) proposed three mechanisms of MV formation (Figure 1.7): 1) detachment of lipoproteins as the outer membrane grows faster than the underlying peptidoglycan, 2) peptidoglycan build up in the periplasm, and 3) disruption of LPS salt bridges by quinolones leading to outer membrane destabilization. At both pH we detected LysM and a murein transglycosylase domain protein which are involved in cell wall and peptidoglycan degradation, respectively, which may support the first two mechanisms of formation (Table C.1). Additionally, because we observe the greatest n-MV concentrations when cell density is high, it is possible that a mechanism similar to that observed in *P. aeruginosa* where quinolone destabilizes outer membranes may also be occurring (Mashburn-Warren et al., 2009), although PR1 does not produce this class of signaling compound. It is interesting to note that all three mechanisms rely on membrane destabilization and don't seem to allow for specific protein sorting into MVs which has been observed (McBroom and Kuehn, 2007; Sidhu et al., 2008). A fourth mechanism

which allows for specific protein sorting has been demonstrated in by Deatherage et al. (2009), which indicates that MV formation is modulated by envelope interconnections and that MV formation can either occur during membrane remodeling or during cell division. In the case of the latter, it was proposed that this would allow for a mechanism to sort specific proteins into MVs. Although our proteomics data can neither support nor disprove this theory, the increased membrane fluidity predicted by the observed PLFA content of MVs as well as maximum production rates occurring when cells are dividing supports this theory.

Broader implications. Based on our results, n-MVs produced by PR1 have different functional capacities at pH 5 and 7. We detected virulence factors associated with n-MVs under both conditions, even though PR1 is not a clinical strain of *B. vietnamiensis*. A previous study of n-MVs produced by a clinical strain of *B. vietnamiensis* found that over 90% of its phospholipase C activity was due to MVs and similarly we identified numerous proteases, emphasizing the potentially crucial role MVs have in CF infection. Furthermore, since CF patients have acidified epithelial lining fluid, pH 5.3 versus pH 6.2 in control patients (Tate et al., 2002), changes in n-MV composition like we observed in this study may also occur during infection, highlighting the need to understand how environmental factors affect MV composition. Additionally, although we did not demonstrate that n-MV production correlated with biofilm formation, given the changes observed in the content of n-MVs at each pH as well as the presence of Fe and DNA at both pH, n-MVs may still play a crucial role in biofilm formation in PR1 and more broadly *Burkholderia* spp. This is important since Bcc biofilms are resistant to antibiotics (Caraher et al., 2007) and are key factors of infection.

Irrespective of the pathogenic nature of PR1, we can assume that many similar MV characteristics are shared by *B. vietnamiensis* strains and our results can be used to better understand MVs in CF infections. In addition to their potential roles in human pathogenesis, our data indicates other roles n-MVs produced by PR1 may play in the environment. Due to their high surface area to volume ratio, MVs could alter the way toxicants, including metal ions, are able to interact with the cell. Additionally, since the parent strain of PR1 was isolated from an environment containing organic contaminants, it is interesting that our results imply that PR1 may employ MVs as a way to extracellularly bind and degrade contaminants and thus limit exposure to the cell. In conclusion, although MVs are typically regarded as an efficient method for bacteria to disseminate virulence factors into their environment, it is evident that non-clinical strains of bacteria also possess diverse functions which we are just beginning to appreciate.

CHAPTER 6

DISCUSSION

This dissertation focused on the effect of pH on Zn toxicity to *Burkholderia vietnamiensis* PR1$_{301}$ (PR1) and how microbial processes may modulate Zn-toxicity. We found that pH affects Zn and ZnO nanoparticle (ZnO-NP) toxicity to PR1, resulting in greater toxicity at pH 7 versus pH 5 and 6. This same trend has been observed in Ni-toxicity to PR1 (Van Nostrand et al., 2005). In addition to evaluating changes in toxicity with pH, we also found that membrane vesicle (MV) production by PR1 is influenced pH and Zn. Since this implies that MVs may be involved in modulating pH-dependent Zn toxicity we focused on exploring this potential. We found that MVs do not alter Zn-bioavailability to PR1, though MVs produced by PR1 appear to have the capacity to function in numerous interactions beyond metal-toxicity. These results highlight the complexity of investigating the interface between dynamic biotic and abiotic factors in metal-microbe interactions.

6.1 pH-dependent Zn toxicity

Nanotoxicity to bacteria is a burgeoning field of research due to commercial applications of nanomaterials (e.g., antimicrobials) and potential environmental impacts of released nanomaterials. Specially, ZnO-NP is used in diverse applications and has also been found to be toxic to bacteria. We evaluated the toxicity of ZnO-NP to PR1 using Zn^{2+} (as $ZnCl_2$) as a reference toxicant. Toxicity of ZnO-NP to growing cells and resting cells was similar to Zn^{2+}, and toxicity to growing cells was 3-fold greater at pH 7 than pH 6. To our knowledge this is the first study to evaluate the effect of pH on NP toxicity, and is one of few ZnO-NP toxicity to bacteria studies to date which use a Zn^{2+} reference toxicant (Gajjar et al., 2009; Applerot et al., 2009; Jiang et al., 2009; Heinlaan

et al., 2008; Mortimer et al., 2008). Of these studies, only one has shown that ZnO-NP is

more toxic to bacteria than a bulk (ZnO) or ionic (Zn^{2+}) reference toxicant (Applerot et

al., 2009), while the remaining studies have demonstrated that ZnO-NP has similar

toxicity as bulk ZnO (Jiang et al., 2009) and Zn^{2+} (Mortimer et al., 2008), or that ZnO-NP

is less toxic than Zn^{2+} (Gaijjar et al., 2009; Heinlaan et al., 2008). Similar to the majority

of these studies, we found that ZnO-NP and $ZnCl_2$ had similar toxicities. Overall, the

discrepancy in ZnO-NP toxicity data reflects the complexity of comparing different ZnO-

NP formulations and test bacteria, highlighting the need to understand what biotic and

abiotic factors contribute to NP toxicity.

Since the ZnO-NP formulation we used contained acetate as a counter-ion, we

investigated whether bacterial growth affected ZnO-NP structure and toxicity through

counter-ion utilization, using Zn amended with acetate as a control. Acetate can be

utilized by bacteria and it can also be cytotoxic at low pH, while removal of acetate by

calcination resulted in larger ZnO-NP (Figure 2.1); therefore it was necessary to account

for these potential affects. These studies resulted in three important findings. First, we

found that 10.7 mM acetate was toxic to PR1 at pH 5 and increased growth of PR1 at pH

6 and 7 (Figure 2.3). This clearly demonstrates the need to quantify counter-ion

dependent effects when studying nanotoxicity. Second, we found that at pH 6 PR1 was

able to utilize ZnO-NP associated acetate (Figure 2.5), but this did not affect ZnO-NP

toxicity relative to $ZnCl_2$ nor did it result in formation of larger ZnO-NP. Lastly, we were

not able to confirm the presence of ZnO-NPs associated with cells by electron

microscopy and EDX, although we did identify 10 nm electron dense regions which

contained P but not Zn (Figure 2.5). These results stress that it is essential to confirm the

elemental composition of electron dense regions when studying nanoparticle toxicity since not doing so can easily lead to mis-identification of NPs. Overall, the results suggest that the observed ZnO-NP toxicity is due to Zn^{2+} from ZnO-NP dissolution which occurred intracellularly or extracellularly due to biotic or abiotic processes. These results suggest that the affects of acetate stabilized ZnO-NP entering the environment would be similar to Zn^{2+}, while in general the fate and toxicity of ZnO-NP in the environment may be dependent on ZnO-NP formulation and, perhaps, different from Zn^{2+}.

Previous research on metal-toxicity to PR1 focused mainly on pH-dependent Ni toxicity; therefore we were interested in also evaluating pH-dependent Zn toxicity to PR1. We found that Zn was 16-fold more toxic to PR1 at pH 7 than pH 5 (Chapter 3), similar to previous studies of pH-dependent Ni toxicity to PR1 (Van Nostrand et al., 2005) as well as Cd toxicity to a *Burkholderia* sp. (Sandrin and Maier, 2002) and *Escherichia coli* (Worden et al., 2009). Using thermodynamic modeling to predict Zn-speciation under experimental conditions, we demonstrated that $ZnOH^+$ and $ZnNH_3^+$ better correlated to pH-dependent Zn toxicity to PR1 than did total dissolved Zn or Zn^{2+} concentrations. Although it has been suggested that metal-hyroxo species are responsible for toxicity to bacteria (Ivanov et al., 1997; Worden et al., 2009), these two Zn-species may be best viewed as indicators of pH-dependent Zn toxicity, i.e., not necessarily the most toxic Zn-species.

Experiments performed in 4M demonstrated that Zn precipitated in a pH-dependent manner (e.g., at decreasing total Zn concentrations with increasing pH) in the absence of growing cells. The resulting precipitate was a spherical nano-phase which we

hypothesize may be a Zn-pyrophosphate phase (Chapter 4). This conclusion is based on

SEM- and STEM-EDX data demonstrating the presence of Zn, Fe, P, S, and O, the size

of precipitates and thermodynamic speciation modeling which predicts the formation of

$Zn_2(PO_4)_2$:$4H_2O$ (Appendix A). Additionally, these observations are similar to analysis

and observations of Zn-pyrophosphate granules formed under neutral pH with Zn and

pyrophosphate (Masala et al., 2003). Although 4M was developed to minimize metal

phosphate complexation or precipitation by using 2 mM β-glycerophosphate as the only

source of phosphate, it was previously found to have 0.2 mM dissolved phosphate

following autoclaving (Van Nostrand et al., 2005). The distribution between phosphate

species, i.e., ortho- or pyrophosphate is not known, but both these species can be in

equilibrium (Goldberg and Tewari, 2002). It seems unlikely that formation of Zn-

pyrophosphate precipitate is responsible for pH-dependent toxicity since formation of this

phase would result in lower aqueous Zn concentrations. On the other hand, formation of

a metal-pyrophosphate precipitate could confound sorption experiments depending on

how they are performed. For this reason, when performing sorption studies we used non-

phosphate containing MES or HEPES instead of 4M. These results demonstrate the need

for appropriate abiotic controls when studying metal-microbe interactions, and suggest

that future experiments should not use autoclaved 4M.

In addition to evaluating how changes in Zn-speciation correlate to pH-dependent

toxicity, we also evaluated pH-dependent changes in PR1 (i.e., membrane composition,

protein composition of MVs, and membrane chemistry). The fatty acid composition of

PR1 has been shown to be affected by pH (Van Nostrand et al., 2008) and likewise we

found the cellular polar lipid fatty acid (PLFA) profile of PR1 at pH 5 had relatively

decreased levels of C16:0, C18:1ω9t/ C18:1ω7c, and increased levels of C18:0 in comparison to pH 7 (Figure 5.5). At lower pH, increased membrane rigidity from increased long chain fatty acids (i.e., C18:O) has been linked to acid tolerance (Fozo and Quivey, 2004), though the observed decrease in cyclopropane fatty acid (CFA; i.e. C18:1ω9t/ C18:1ω7c) is counter to this hypothesis since CFA increases rigidity and is associated with acid-tolerance (Brown et al., 1997; Yuk and Marshall, 2004; Hartig et al., 2005). Additionally, Van Nostrand et al. (2007) found 17 proteins were differentially expressed by PR1 at pH 5 and 7 (Van Nostrand et al., 2007). Similarly, we found 78 and 14 proteins unique to MVs produced by PR1 at pH 5 and 7 (Figure 5.8), highlighting the fact that PR1 responds to changes in pH by altering cellular processes, which may in turn affect Zn resistance.

Using cells grown at pH 5 and 7, we evaluated the influence of pH on the surface chemistry of PR1 by measuring changes in surface charge and Zn-sorption in pH 5 and 7 buffer. We found that cells grown at pH 5 were less negative than cells grown at pH 7 at any pH. Predictably, cells grown at both pHs were more negative in pH 7 buffer than pH 5 (Figure 4.1). We predicted that more Zn would sorb to cells in pH 7 versus pH 5 buffer. We found this to be true for cells grown at pH 7, but cells grown at pH 5 sorbed similar amounts of Zn at both pH 5 and 7 (Figure 4.3). Although we did not discriminate between weakly bound surface Zn or internal Zn, this suggests that Zn is being internalized by pH 5 grown cells at pH 5, while Zn-sorption by pH 5 grown cells at pH 7 is driven solely by surface chemistry.

Increased Zn influx into cells grown at pH 5 initially seems counter-intuitive since PR1 is more resistant to Zn at pH 5 and would predictably either limit Zn entering the

cell or increase Zn efflux from the cell. Recently, the paradigm of metal efflux in Gram-

negative bacteria has shifted to identifying interactions in the periplasm as being key

steps in modulating metal efflux (Nies, 2007). For example, sigma factor RpoE, which

modulates extra-cytoplasmic stress via σ^E, is necessary for Zn-resistance in *E. coli* (Egler

et al., 2005) and Cd and Zn resistance in *Cupriavidus metallidurans* CH34 (CH34; Grobe

et al., 2007). Additionally, RND pumps which span the inner and outer membrane are

now understood to serve a vital role in exporting metal ions from the periplasm (Nies,

2007). Metal ions in the periplasm can induce expression of proteins involved in efflux

from the periplasm (Grobe et al., 2007). This framework of periplasmic dependent

metal-efflux would predict that observed increases in Zn sorption at pH 5 occurs so that

Zn-efflux transporters are induced. Therefore increased Zn influx by pH 5 grown cells

could indicate that pH 5 grown cells are more adept at responding to increased Zn

concentrations than cells grown at pH 7.

A more complete model of how Zn-efflux at pH 5 might occur can be generated

by using the proteomic study of MVs produced by PR1 at pH 5 and 7, which may be

viewed as a proxy for the protein composition of the membrane of PR1, as well as the

genome of the parent strain of PR1, *B. vietnamiensis* G4. We found that the outer

membrane proteins (i.e., porins) present in the genome are present in MVs, OmpC and

OmpW (Table C.1). OmpW is not well characterized, but seems to be involved in

osmotic regulation (Wu et al., 2006; Lin et al., 2008). In *E. coli* OmpC is necessary for

Cu resistance, leading to the conclusion that Cu diffusion into the periplasm is coupled to

export via an RND pump (Egler et al., 2005). It is now understood that metal ion

concentrations in the periplasm are maintained via "kinetic flow equilibrium" with porins

internalizing metals and RND pumps moving metals out (Nies, 2007). Another protein

identified in MVs grown at pH 5 was CzcD, which is involved in periplasmic metal

sensing in CH34 (Mergeay et al., 1985; Grobe et al., 2004) and could be serving a similar

role in PR1 grown at pH 5. Furthermore, RND pumps were detected in MVs grown at

both pHs (Table C.1). Taken together, our results suggest that PR1 may be more adept at

sensing Zn^{2+} at pH 5 than pH 7, which in turn could lead to a response involving RND

mediated Zn^{2+} efflux from the periplasm. To experimentally address this hypothesis,

Zn-efflux rates of PR1 cells grown at both pH 5 and 7 could be determined. Additional

studies using quantitative proteomics should facilitate the confirmation of the effects of

pH and Zn on protein expression in the periplasm and associated with membranes.

6.2 <u>Membrane vesicles in metal-microbe interactions</u>

During studies examining ZnO-NP toxicity to PR1, MV production in cell

cultures was evident. Every Gram-negative bacteria that have been examined for MV

production have demonstrated positive responses (Table 1.3), implying that it is a

conserved phenotype. Additionally, other *Burkholderia* spp. are known to produce MVs,

including *B. vietnamiensis* (Allan et al., 2003). With increased research in the field of

nanotoxicity, we expect MVs to be reported more frequently, similar to observations of

Li et al. (2009) when studying Ag-NP toxicity to *E. coli*. Additionally, MVs can be mis-

identified as virus particles (Soler et al., 2008), suggesting careful evaluation of cultures

is warranted.

Since bacteria are known to produce extracellular compounds such as proteins

(Kurek et al., 1991) and exopolymers (e.g., EPS; Kamashwaran and Crawford, 2003;

Jackson et al., 2005) which can decrease metal toxicity by extracellular sequestration, the question of whether MVs may serve to decrease Zn-toxicity to PR1 arose. If MVs were involved in metal toxicity abatement they might be functioning as a vector for exporting Zn from the cell or as an extracellular sink for Zn-sequestration. They might also increase Zn-toxicity by serving as an initial sink for Zn sorption followed by uptake of the Zn containing MVs, resulting in increased Zn-bioavailability. Our results demonstrate that MV production in the absence of Zn is two-fold lower at pH 5 and increasing sub-lethal Zn concentrations negatively affect MV production at both pHs (Figures 3.5 and 3.6). These results indicate that MVs are not functioning in Zn-resistance via MV mediated Zn export. MV production at sub-lethal Zn concentrations was different at pH 5 and 7, which supports the hypothesis that PR1 responds better to increasing Zn concentrations at pH 5 than pH 7 (relative to toxicity).

MVs have been shown to sorb DNA (Schooling et al., 2009) and sorb metals on their surface (Gorby et al., 2008). Therefore the question of whether MVs were also capable of sorbing Zn was explored (Chapter 4). It was discovered that MVs are capable of sorbing Zn, albeit 1.5-fold less sorption was observed compared to Zn-sorbed by cells (Figure 4.3). Also, MVs from pH 5 grown cells sorbed similar amounts of Zn at pH 5 and 7, while MVs from pH 7 grown cells sorbed more Zn at pH 7 compared to pH 5. Since this same trend was observed with cells grown at pH 5 and 7 and because MVs are believed to maintain similar properties to the cell membrane we believe this further supports the idea that cells grown at pH 5 have a porin which mediates Zn influx at pH 5.

In addition to characterizing MV chemistry, we also developed a method to accurately quantify MV size and number. By utilizing AF^4-MALS we were able to

measure the *in situ* geometric radius of MVs, and found that the size distribution of MVs

produced at pH 5 and 7 was different, with mean radii of 96.5 and 112.8 nm respectively

(Figure 4.4). Using absolute numbers of MV, we extrapolated that at late stationary

phase growth, there would be twice as many MVs than cells, but due to the greater

surface area of MVs, this translates into MVs accounting for 15% of total surface area.

This type of conclusion cannot be reached using other techniques such as EM

(Deatherage et al., 2009) or antibodies (McBroom et al., 2006), highlighting the value of

integrating AF[4]-MALS analysis into MV studies. Furthermore, this technique should

prove beneficial to quantifying MV production from different species which can easily be

compared between laboratories.

Given that MVs did not sorb significant amounts of Zn, an increase or decrease in

Zn toxicity to PR1 through extracellular sorption of Zn was not predicted. This was

confirmed by adding MVs and Zn at sub-lethal and toxic concentrations to growing

cultures of PR1. Although these results suggest that MVs do not modulate Zn-toxicity,

this mechanism may still occur in other microorganisms. For instance, *P. aeruginosa*

produces similar concentrations of MVs as PR1 (Bauman and Kuehn, 2006), but in

contrast to PR1, these MVs are enriched in negative LPS (Sabra et al., 2003). Also, since

MVs have similar properties as the cell outer membrane, MVs produced by bacteria that

sorb high levels of metal may be capable of binding more metal ions than we observed.

Although our results suggest that MVs are not involved in Zn-efflux, this type of

mechanism might occur in a bacterium such as *Pseudomonas putida* which sequesters Zn

and Ni in the periplasm (Choudhury and Srivastava, 2001; Tripathi and Srivastava,

191

2006). The results highlight that MVs, due to their size and number, must be accounted for when studying metal-microbe interactions.

6.3 MV function and formation

In addition to evaluating changes in the chemistry of cells, MVs and Zn with pH, additional physical and molecular changes in MVs with pH were evaluated (Chapter 5). One other study to date has examined MVs produced under different conditions (i.e., different media) and found that only 30% of proteins were shared between the different conditions. We found the protein composition of MVs produced by PR1 at pH 5 and 7 were 60% similar, and MVs produced at pH 5 contained the majority of unique proteins between the two conditions. The unique MV proteins expressed during growth at pH 5 include translational machinery, chaperonins, transporters, and proteins involved in organic compound catabolism, suggesting a different function than MVs produced at pH 7. This result can be extrapolated to MV function in other microorganisms. For example, MVs from clinical strains of bacteria often contain virulence factors (Scorza et al. 2008) and a study of environmental and clinical strains of *Pseudomonas aeruginosa* found that the environmental strains were not as immunogenic (Bauman and Kuehn, 2006). The authors of these studies conclude that their findings represent the MV functions of that specific microorganism. Conversely, our results suggest that MVs do not have one specific suite of functions. Rather, it is proposed that MVs possess a combination of core functions and dynamic functions which can reflect broader changes in cellular processes. Given that bacterial function is affected by numerous external stimuli (e.g., pH, ionic strength, temperature), it would be predicted that MV function

could change accordingly. Therefore, MVs from a single species should possess dynamic functions dependent on external stimuli. For example, our results demonstrate that MVs produced by PR1 have a shared composition between pH, but there are also distinct differences in protein composition between pH. If applied to pathogenic bacteria, this hypothesis could address how conditions during bacterial pathogenesis affect MV production, virulence factor composition, and the ability of MVs to illicit immunological responses.

The core functionality of MVs produced by PR1 can be predicted based on the proteomics results and analysis that found that MVs contained Fe, Zn, DNA, and RNA. These components along with identified proteins involved in secondary metabolite transport, siderophore uptake, and carbon storage, suggests MVs would be beneficial in bacteria-bacteria interactions. In the environment or in the human body MVs could aid in colonization. Additionally, although PR1 is not an environmental isolate, we identified virulence factors, antigens and proteases, all of which could affect host-cell interactions. Overall, this diversity of within core MV function confirms other studies describing the multifarious nature of MVs (reviewed by Lee et al., 2008).

Presently MV formation is not well understood, but the results of our characterization studies seem to suggest a model of formation. Since we found that MV production is greatest when cells are rapidly dividing (Figures 3.4 and 5.1), MV formation appears to be related to cell division, which has been recently proposed (Deatherage et al., 2009). This model does not explain why MV levels would remain constant during stationary phase growth unless MVs are either remaining in solution, or are continuing to be produced as well as taken up by cells. Assuming that the latter is

true, we propose the following model for MV formation based on studies with PR1 (Figure 6.1). First, regions on the outer membrane begin to form which are less rigid due to lower amounts of LPS and cyclopropane fatty acids. Previous studies of MVs produced by *Burkholderia cepacia* and *P. aeruginosa* demonstrate that MVs contain LPS compositions which are different than the cell (Kadurugamuwa and Beveridge, 1995; Sabra et al., 2003; Allan et al., 2003), though in the case of *Burkholderia* the change in LPS was qualitatively determined but not identified (Allan et al., 2003). We predict that MVs produced by PR1 have less LPS than the parent cell based on the observation that MVs are not as negatively charged as cells (Figure 4.1). Since LPS in *Burkholderia* spp. contains less net negative charge than LPS from *Pseudomonas* spp. (Shimomura et al., 2003), the most appropriate explanation of our results is a decrease in LPS, not merely a shift to a less charged LPS. In conjunction with a decrease in LPS content, there is also a decrease in cyclopropane fatty acids as we observed in our PLFA analysis (Figure 5.5), which should also increases the fluidity of the membrane.

The second stage of MV formation occurs as the outer membrane forms an outward curve, which is facilitated by a detachment of lipoproteins and structural components that connect the outer membrane to the underlying periplasm. This assumption is based on observations that mutations of proteins which anchor the outer membrane to the peptidoglycan layer results in greater MV formation (Deatherage et al., 2009). Once the membrane begins to curve outward, this structure allows for preservation of the less rigid membrane by decreasing the flow of phospholipids into the surrounding membrane (Ursell et al., 2009); therefore, once this outward curve is formed, the LPS and phospholipid composition should be maintained.
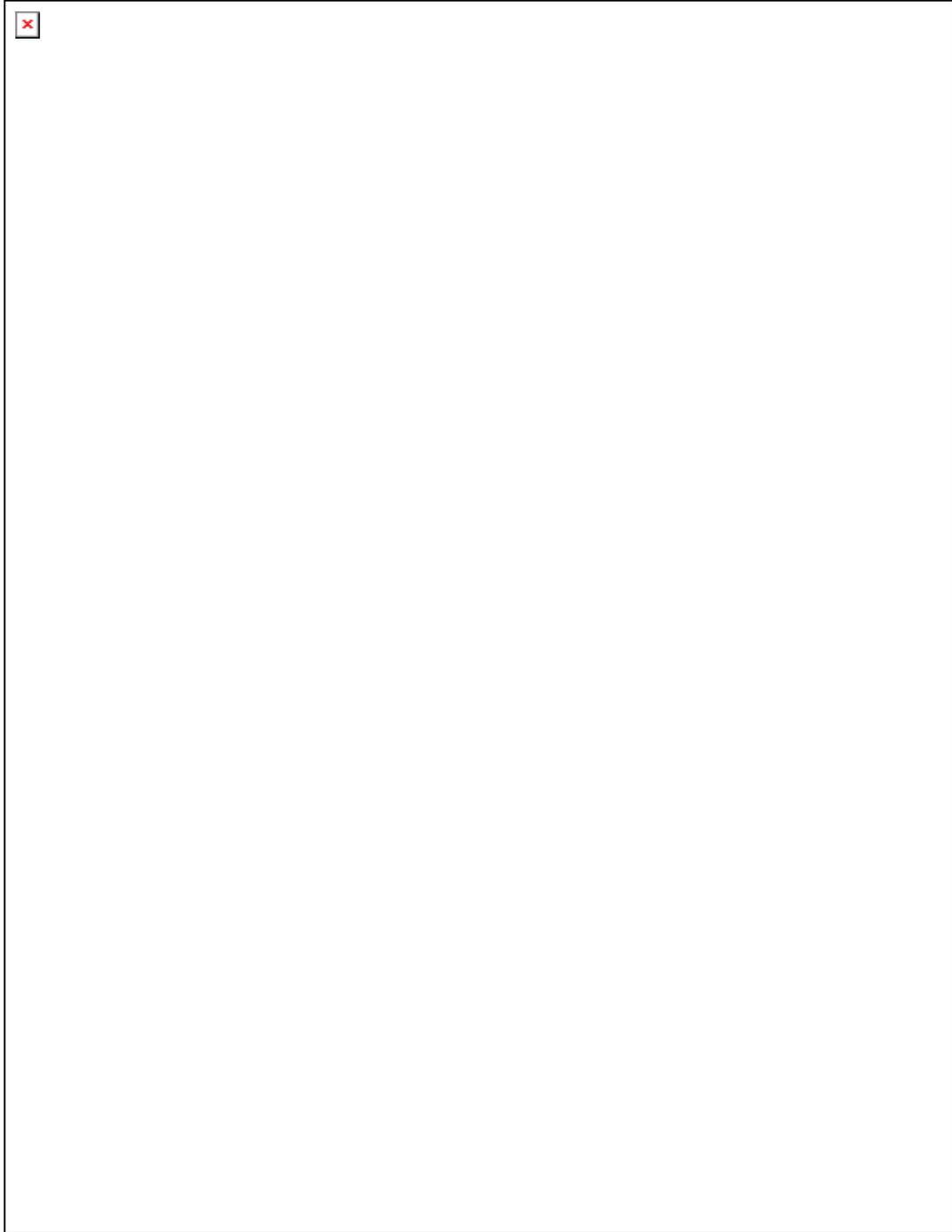
Figure 6.1. Proposed model of MV formation. (A,B) Scanning electron micrographs of PR1 demonstrating formation of curved membrane (A) and blebbing (B), as indicated by box. Scale bars are 500 nm. **(C)** Model of MV formation. Numbers inside squares are the four stages of MV formation discussed in the text. OM, outer membrane; P, periplasm; IM, inner membrane.

The third stage of MV formation would involve recruitment of proteins to the outwardly curved membrane through an unknown mechanism. In *Bacillus subtilis*, proteins are recruited to curved regions of membrane during sporulation via a geometric cue dependent on positive curvature of the membrane (Ramamurthi et al., 2009). Finally, the fourth stage of MV formation would occur as outward pressure forces the already fluid outer membrane to detach, carrying with it the underlying periplasmic components.

This model allows for protein sorting observed in other studies (McBroom and Kuehn, 2007; Sidhu et al., 2008), and may also explain why extra-cytoplasmic stress factors are linked to MV formation (McBroom and Kuehn, 2007). In addition to the stages of this model that can be pieced together based on our experimental results, our results also indicate that there may be an initiator protein involved in MV formation. During proteomic analysis of MVs, we observed an abundant 42.5 kDa protein [as determined by LDS-PAGE (Figures 5.4 and 5.7), as well as MS/MS when between 500 and 900 peptides were matched to it across all conditions], which contains little homology to known proteins. Extensive bioinformatic searching did not yield any conserved domains, and the closest homology was an upshift protein involved with nonsense mediated decay of mRNA. Due to the high abundance of this 42.5 kDa protein, as well as its possible presence in the only other study of n-MVs from *B. vietnamiensis* (Allan et al., 2003), it may have a key function in n-MVs produced by *Burkholderia* spp. As more proteomics studies are performed on MVs from different species, there is the chance that a specific protein involved in MV formation will be identified.

This proposed model of MV formation as well as the MV characterization work presented herein emphasizes the remaining unanswered questions involving protein, lipid

and LPS sorting into budding MVs. A novel approach to answer these questions would be to utilize FFF-MALS to determine the total surface area of samples which could be analyzed by quantitative proteomics, lipidomics and glycomics. This would allow for absolute identification of protein, lipid and LPS composition of MVs compared to cells. Furthermore, additional purification methods could be developed to characterize different populations of MVs based on size, since our results indicate that a smaller (<10nm) MV population may be present in addition to the one visible by EM and detected by MALS. These studies would undoubtedly further our understanding of the complex processes involved in how bacteria can interact with their environment beyond the cell wall.

APPENDIX A

Table A.1. Input concentrations used for thermodynamic modeling with MINTEQA2. Concentrations are given as millimolar (mM) and are based on the components in modified minimal mineral media (4M). For each reaction, oversaturated solids were allowed to precipitate, pH was fixed, ionic strength was allowed to vary, temperature was 30°C, and atmospheric CO_2 partial pressure was fixed at 0.00038 atm. For the pH-sweep experiment, a 0.1 pH unit change from pH 4 and 8 was used.

Component	pH 5 Normalized [Na]	[a] pH 7	pH 5 Low [Na]	pH 6	pH 6 + Acetate	pH 7 + acetate
SO_4^{2-}	10.04	10.04	10.04	10.04	10.04	10.04
MES^-	100	100	100	100	100	100
PO_4^{3-}	0.20	0.20	0.20	0.20	0.20	0.20
NH_4^+	15.14	15.14	15.14	15.14	15.14	15.14
$Lactate^-$	20.00	20.00	20.00	20.00	20.00	20.00
NTA^{2-}	0.85	0.85	0.85	0.85	0.85	0.85
Mg^{2+}	2.4	2.4	2.4	2.4	2.4	2.4
Ca^{2+}	0.45	0.45	0.45	0.45	0.45	0.45
Cl^-	100.63	0.91	0.91	0.91	0.91	0.91
Fe^{2+}	0.03	0.03	0.03	0.03	0.03	0.03
K^+	2.6	2.6	2.6	2.6	2.6	2.6
$EDTA^{4-}$	0.01	0.01	0.01	0.01	0.01	0.01
Zn^{2+}	0.04	0.04	0.04	0.04	0.04	0.04
Mn^{2+}	0.01	0.01	0.01	0.01	0.01	0.01
Na^+	99.72	99.72	5.72	41.72	51.78	110.1
$Acetate^-$	-	-	-	-	10.7	10.7

[a] inputs used for pH-sweep experiment with 1.53 mM Zn

Table A.2. Zn concentrations used for modeling with respective ionic strengths. MINTEQA2 was used to predict Zn-speciation at a fixed pH using a Davies b parameter of 0.3 which is appropriate for the predicted ionic strengths for each reaction. Acetate is abbreviated as AcOH.

Condition	[Zn] (mM) / *Ionic strength (M)*								Zn EC$_{50}$
pH 5 normal Na	0.04	1.53	3.82	7.65	15.29	22.94	30.59	45.88	23.40
Ionic strength	*0.141*	*0.1402*	*0.1416*	*0.1443*	*0.151*	*0.1592*	*0.1687*	*0.1901*	*0.1598*
pH 7 normal	0.04	0.38	0.76	1.53	2.29	3.06	3.82		1.47
Ionic strength	*0.1337*	*0.1337*	*0.1337*	*0.134*	*0.1344*	*0.1349*	*0.1353*		*0.134*
pH 5 low Na	0.04	15.29	38.23	53.53	76.46				43.63
Ionic strength	*0.0475*	*0.0546*	*0.0839*	*0.109*	*0.1498*				*0.0924*
pH 6 no AcOH	0.04	1.53	3.82	7.65	15.30				9.49
Ionic strength	*0.1107*	*0.1102*	*0.1112*	*0.1138*	*0.1208*				*0.0874*
pH 6 + AcOH	0.04	0.76	1.15	1.53	2.29	3.06	3.82		3.20
Ionic strength	*0.0934*	*0.0927*	*0.0927*	*0.0928*	*0.093*	*0.0933*	*0.0937*		*0.0934*
pH 7 + AcOH	0.04	0.38	0.76	1.15	1.53	3.82			1.03
Ionic strength	*0.1436*	*0.1435*	*0.1435*	*0.1437*	*1.1438*	*0.1451*			*0.1436*
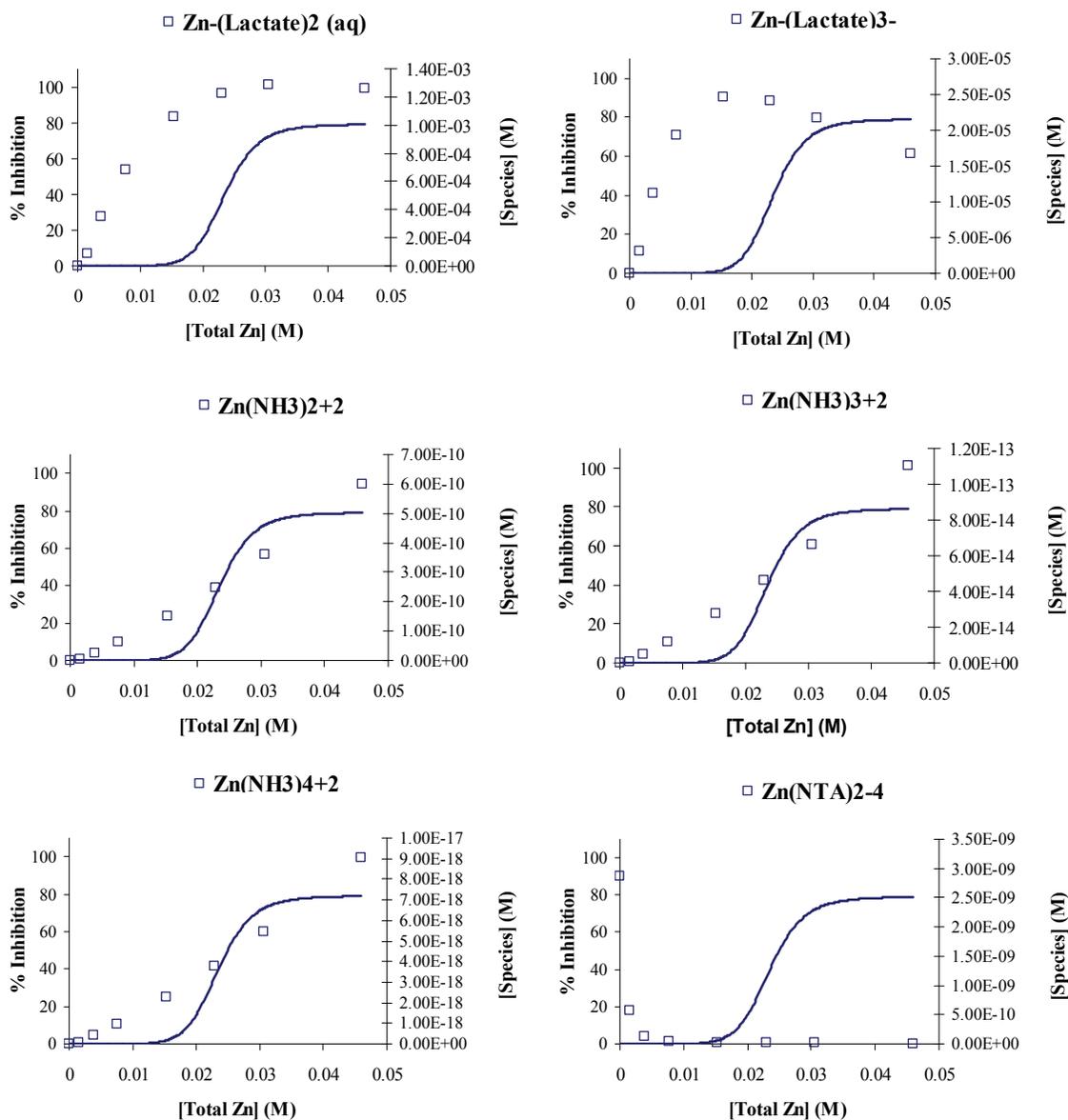
Figure A.1. Plots of Zn-species at different total Zn concentrations in pH 5 media with normalized Na concentrations. Changes in Zn-species concentrations are plotted along with EC_{50} curves. All concentrations are molar (M).

Figure A.1. – continued

202

Figure A.1. – continued

203
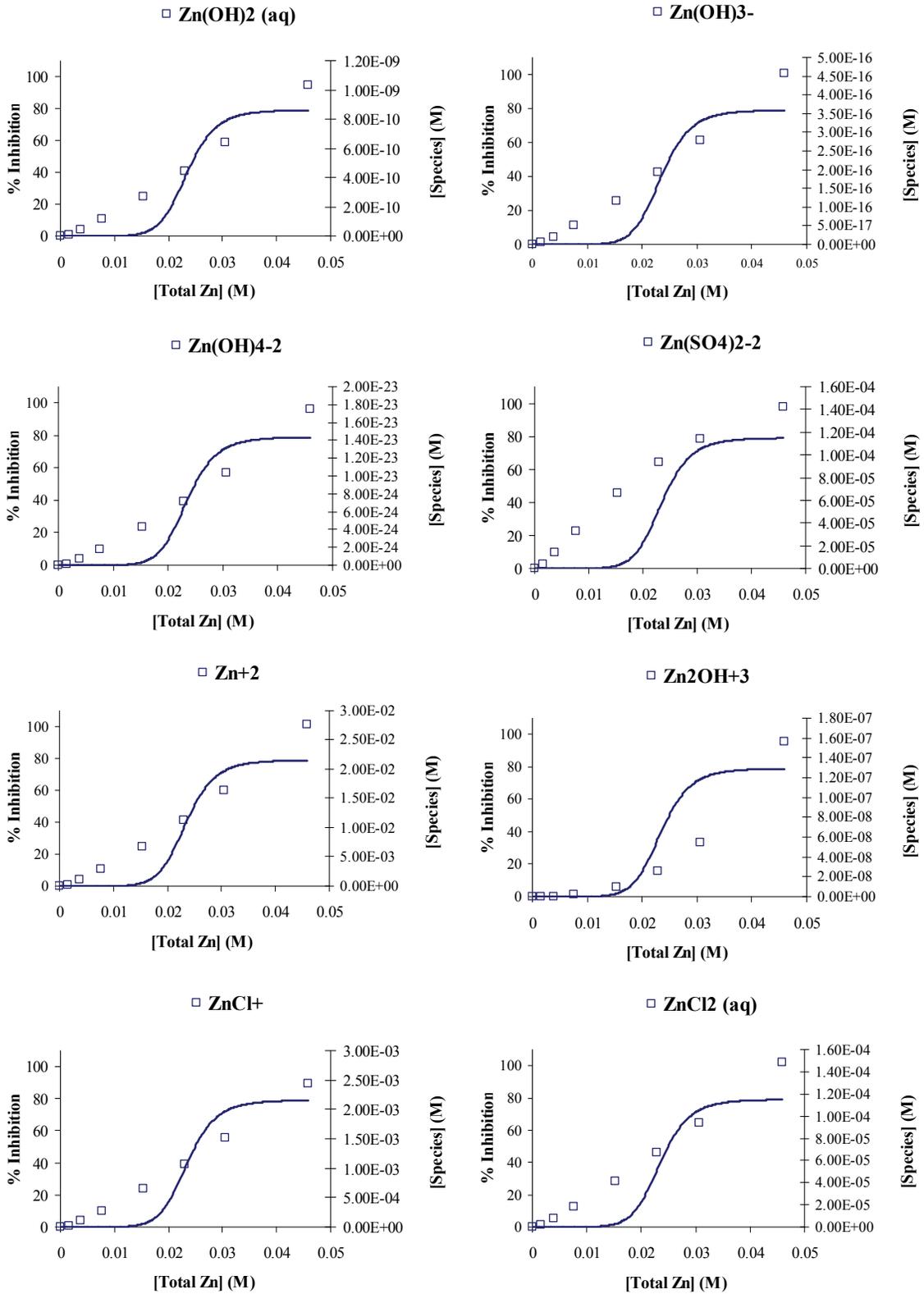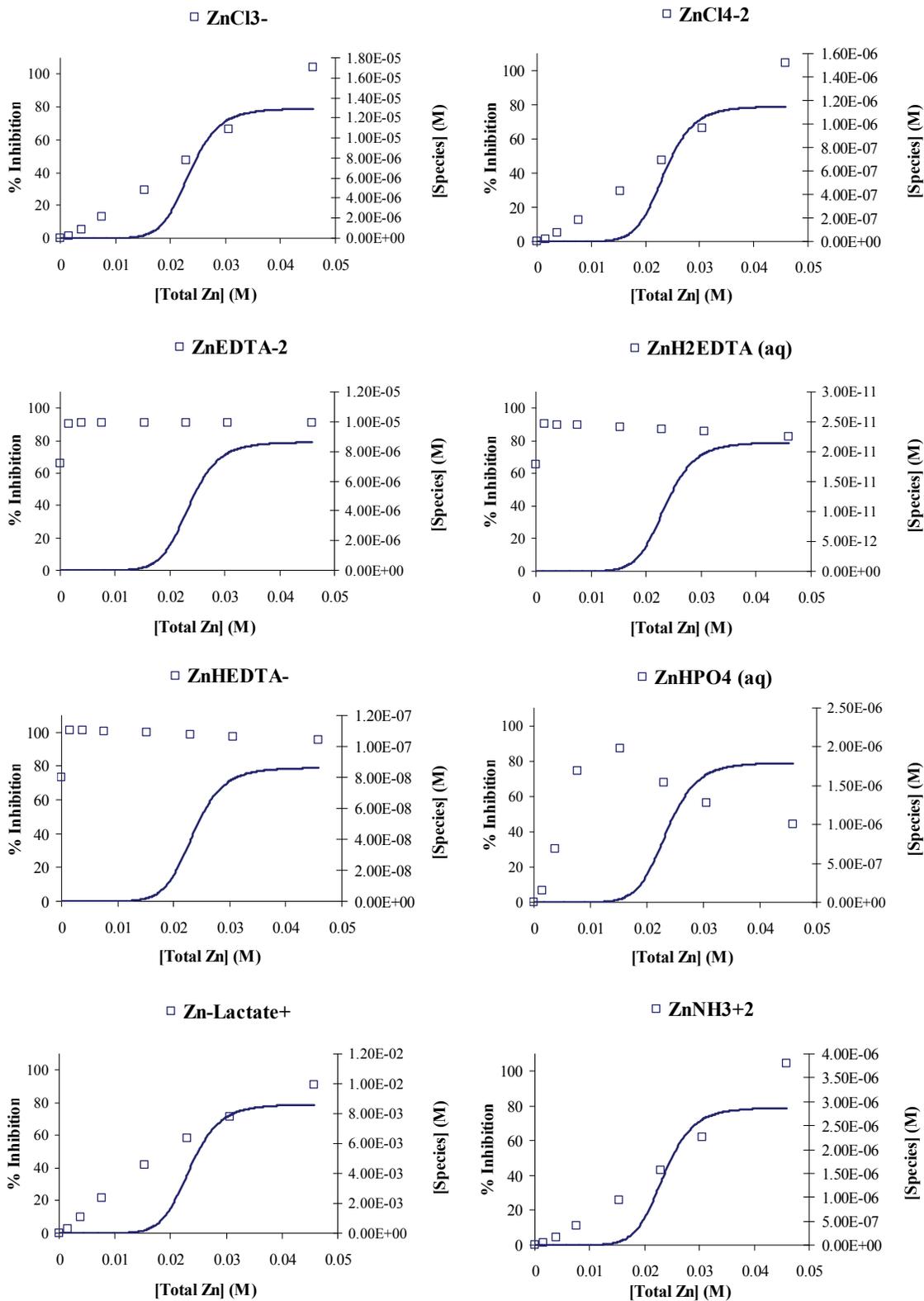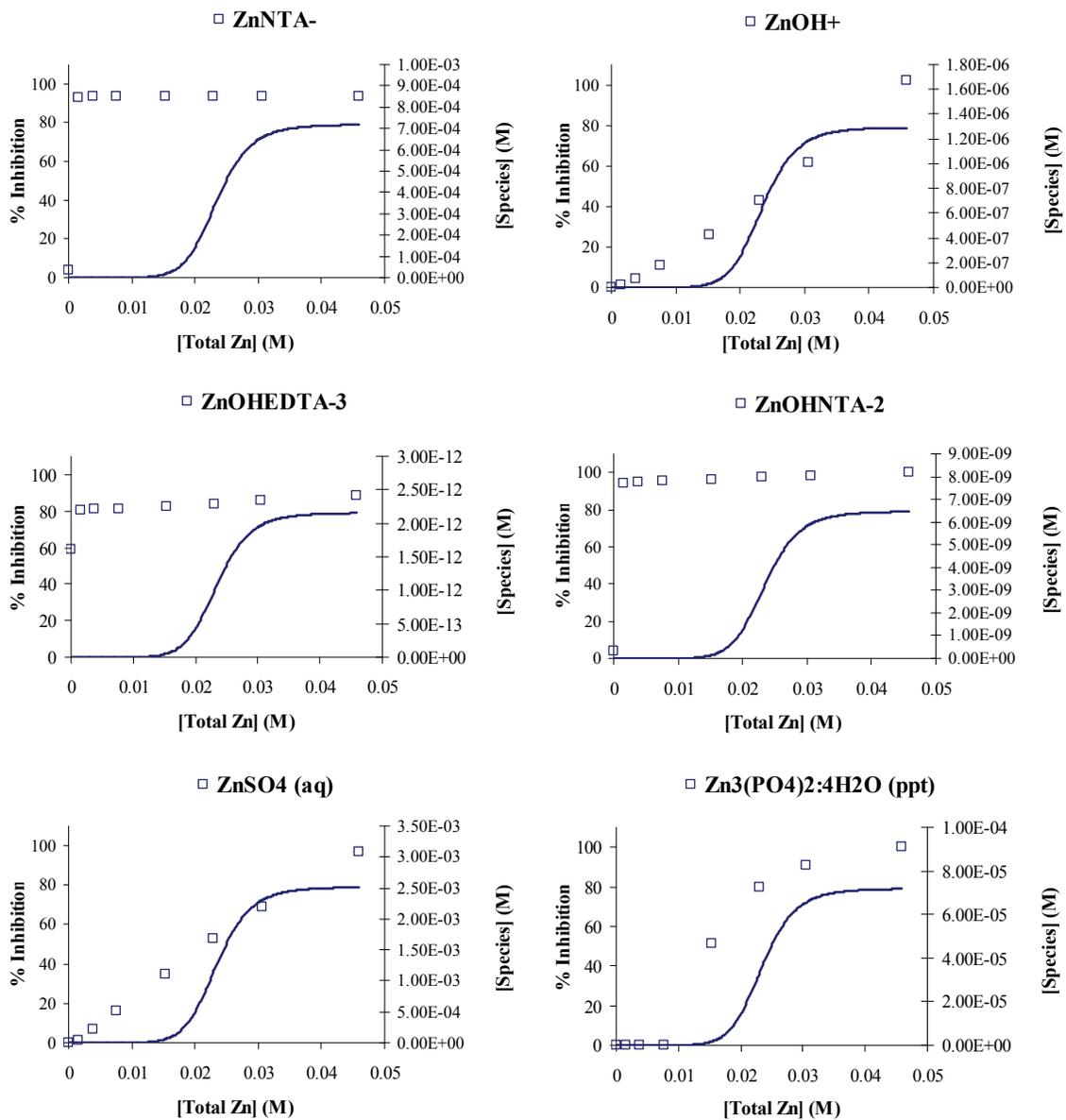
Figure A.1. – continued
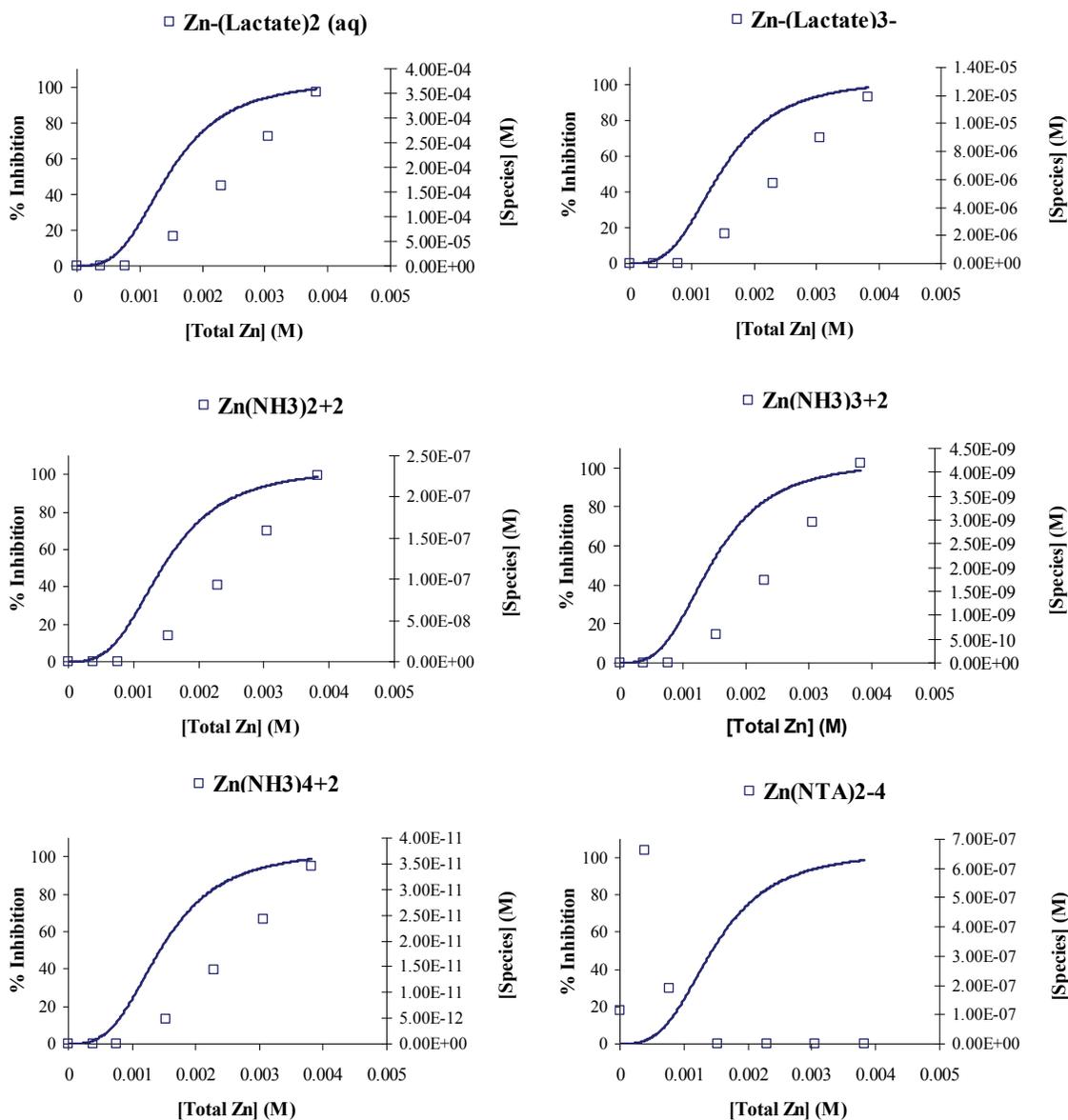
Figure A.2. Plots of Zn-species at different total Zn concentrations in pH 7 media. Changes in Zn-species concentrations are plotted along with EC_{50} curves. All concentrations are molar (M).
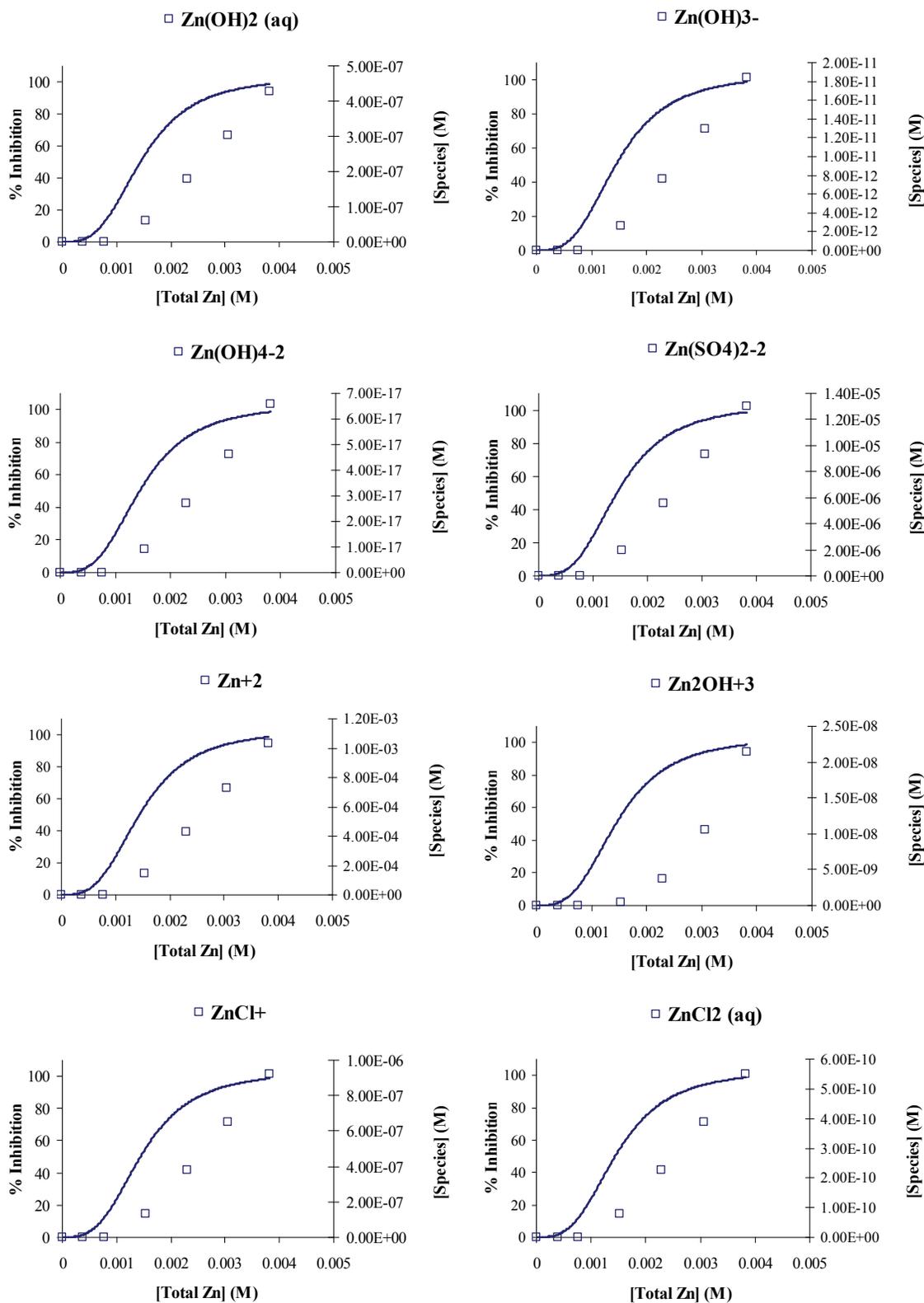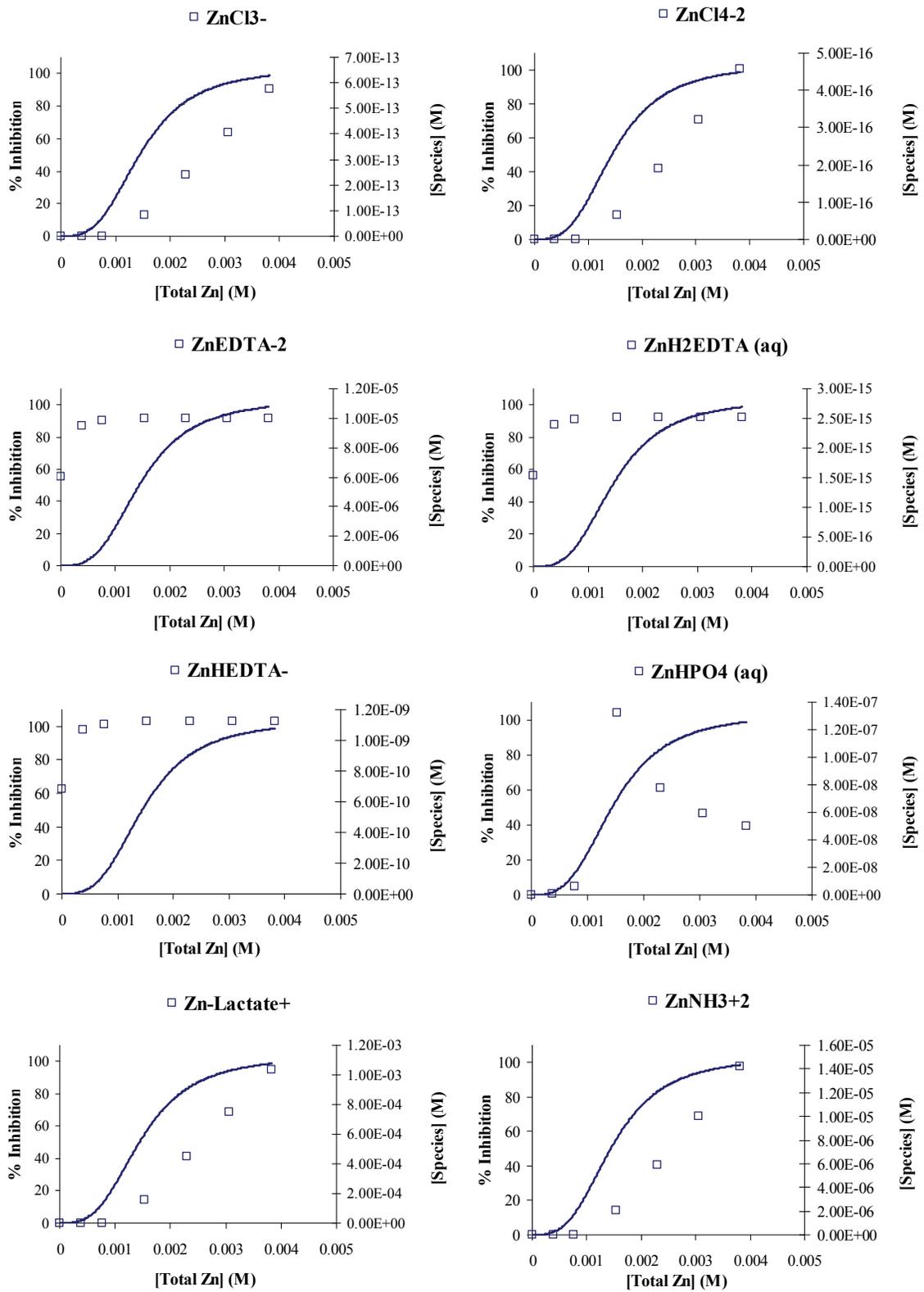
Figure A.2. – continued

Figure A.2. – continued

ZnNTA-

ZnOH+

ZnOHEDTA-3

ZnOHNTA-2

ZnSO4 (aq)

Zn3(PO4)2:4H2O (ppt)

Figure A.2. – continued

208
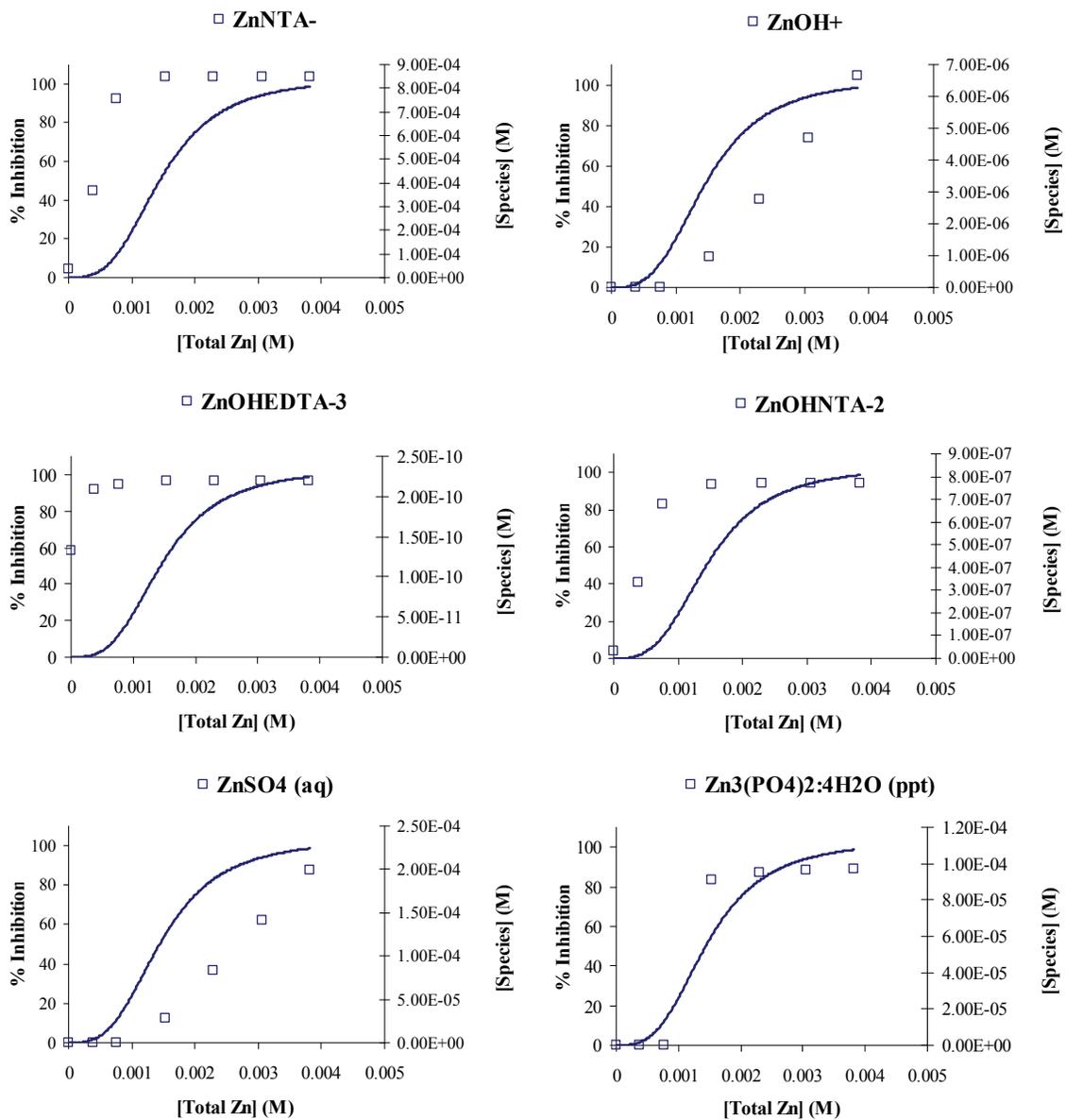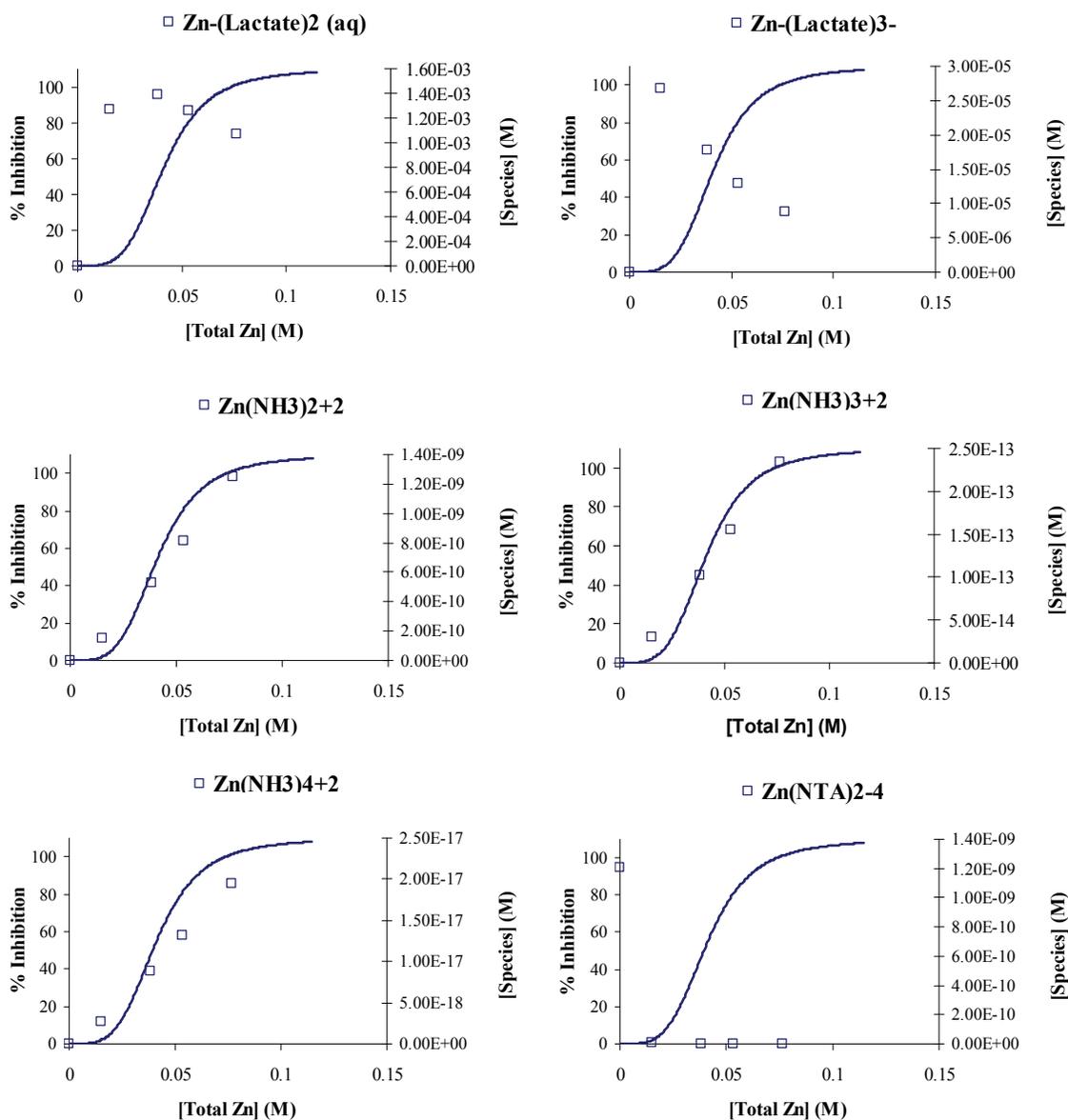
Figure A.3. Plots of Zn-species at different total Zn concentrations in pH 5 media with 5.72 mM Na. Changes in Zn-species concentrations are plotted along with EC_{50} curves. All concentrations are molar (M).
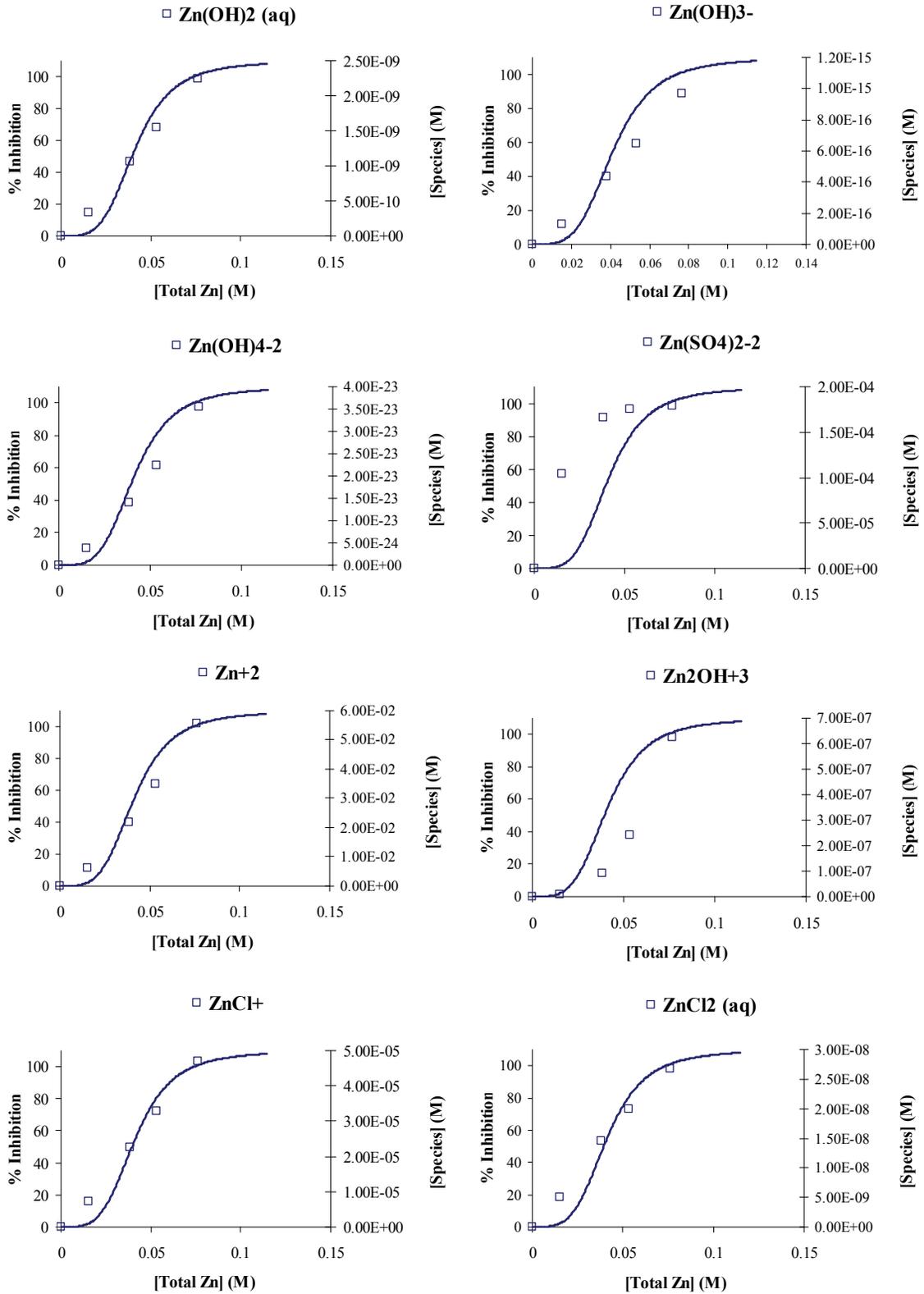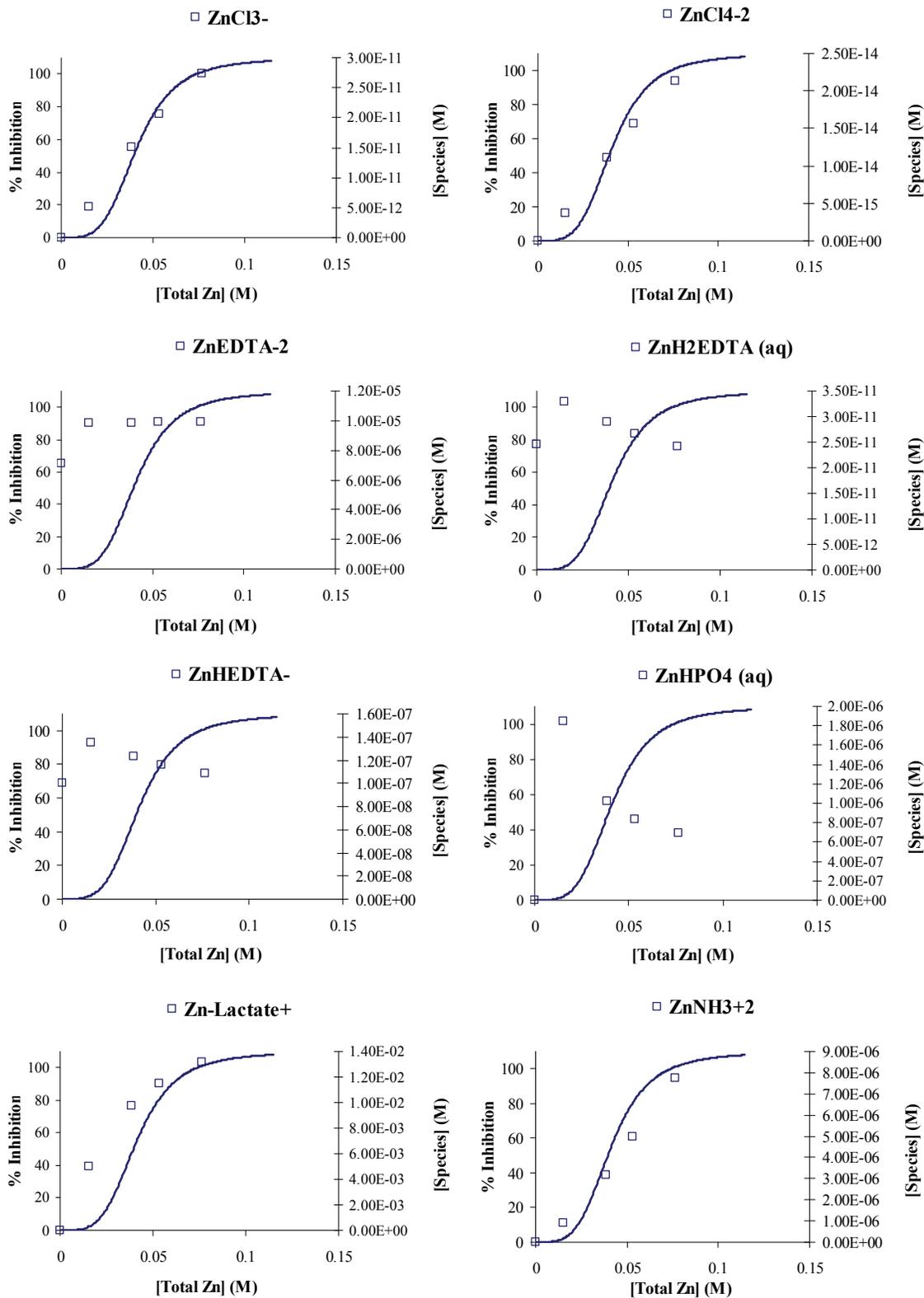
Figure A.3. – continued

Figure A.3. – continued

211
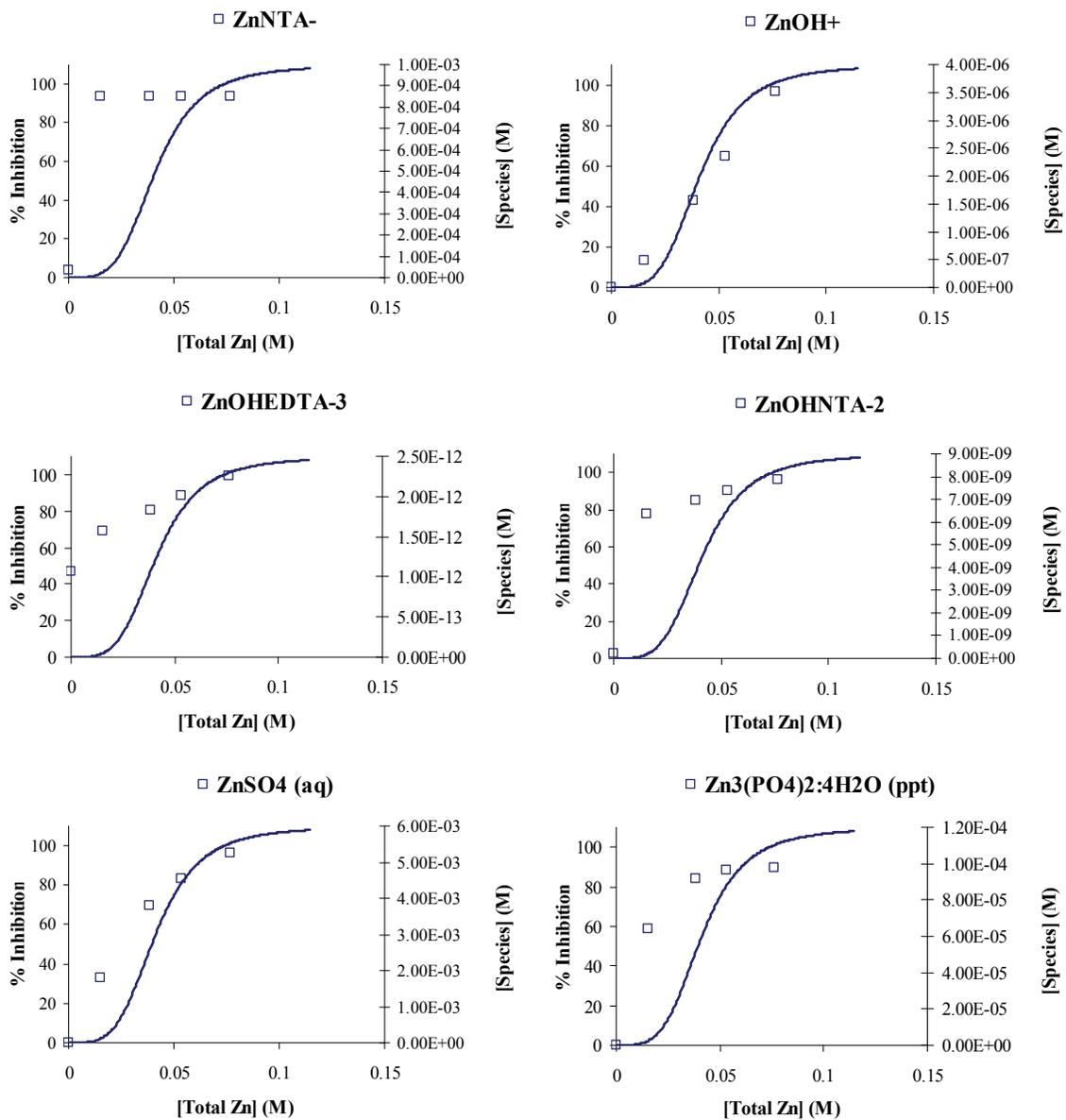
Figure A.3. – continued
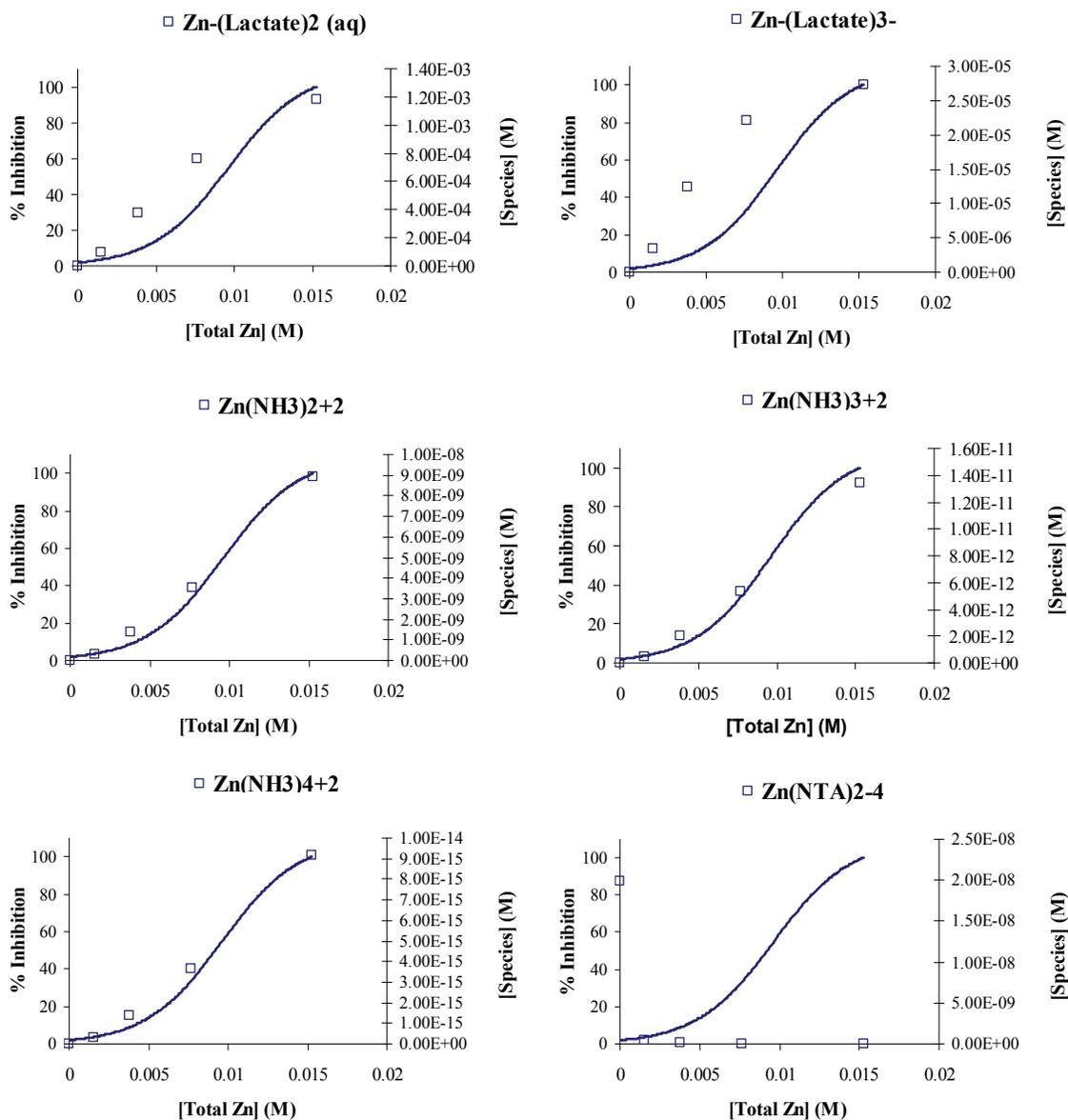
Figure A.4. Plots of Zn-species at different total Zn concentrations in pH 6 media.
Changes in Zn-species concentrations are plotted along with EC_{50} curves. All concentrations are molar (M).

Figure A.4. – continued

Figure A.4. – continued

Figure A.4. – continued

216
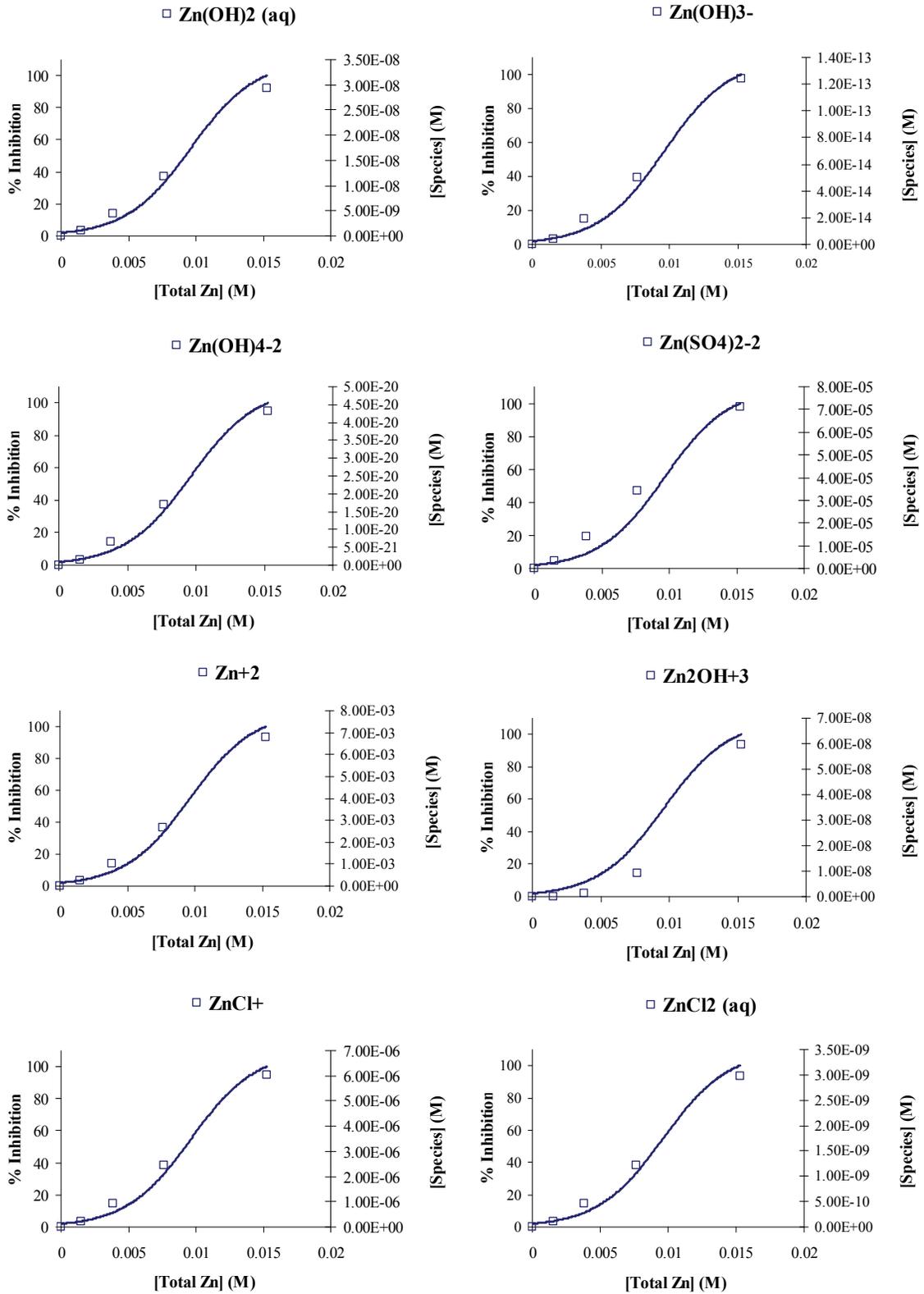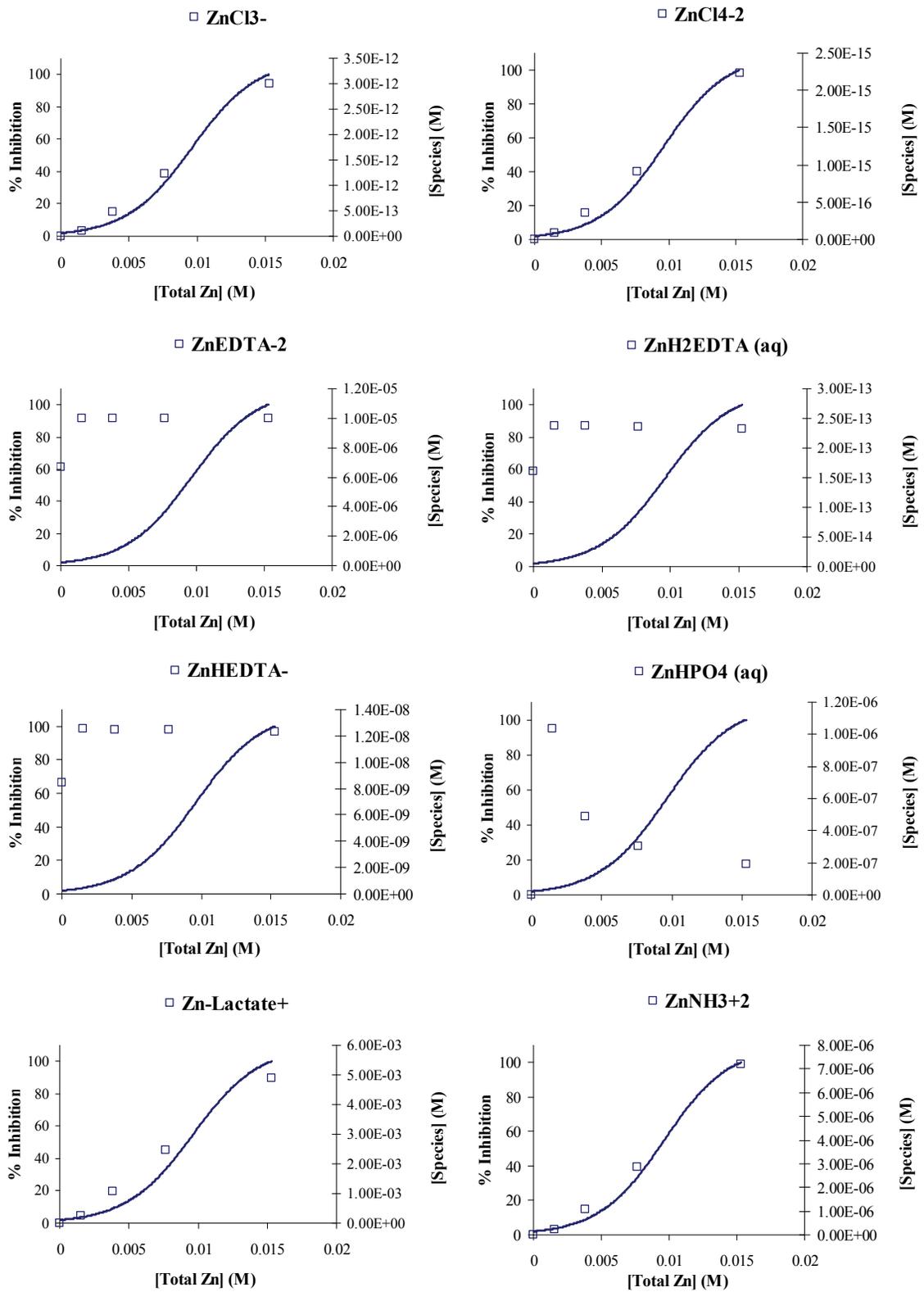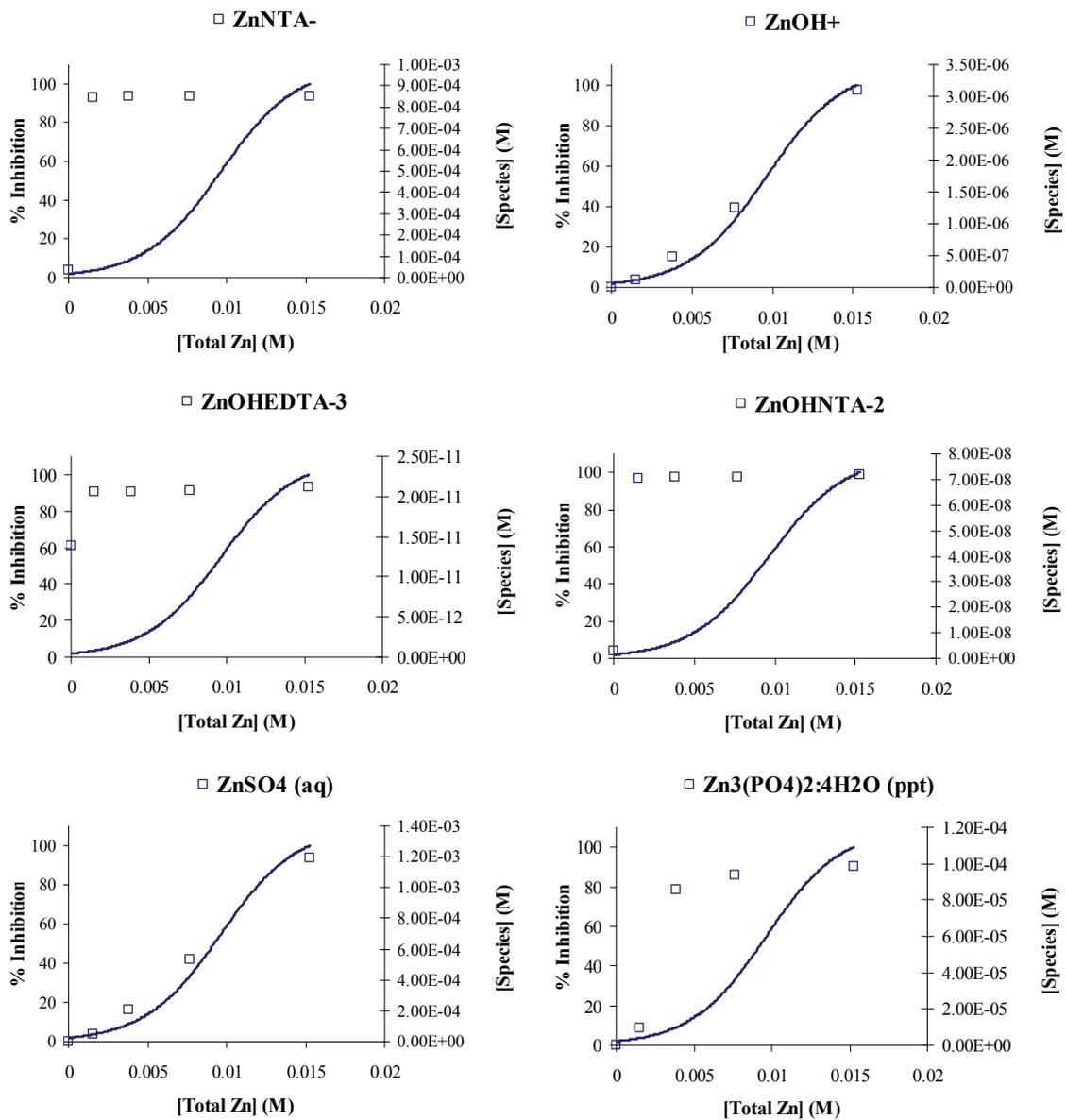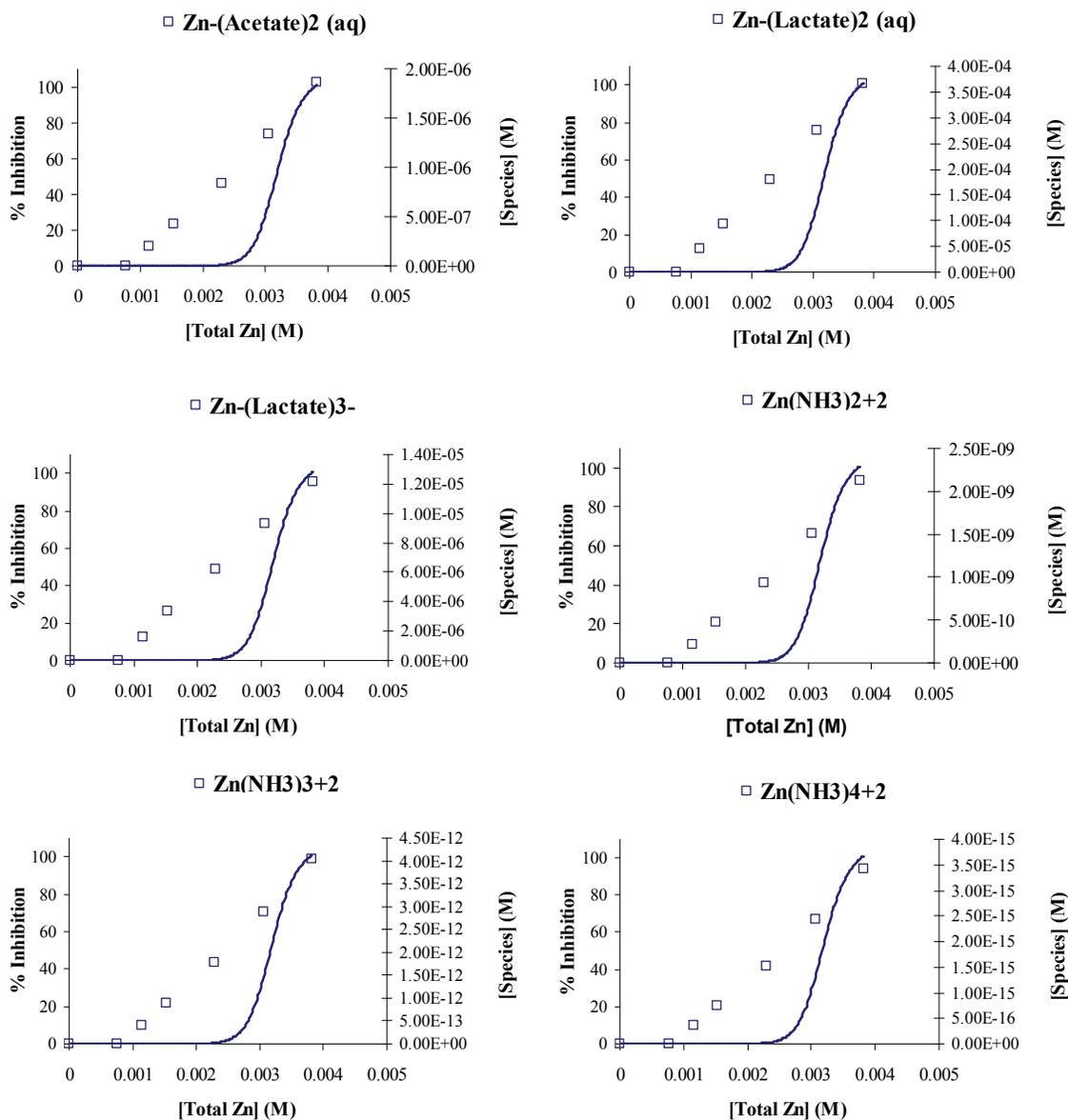
Figure A.5. Plots of Zn-species at different total Zn concentrations in pH 6 media with 10.7 mM acetate. Changes in Zn-species concentrations are plotted along with EC_{50} curves. All concentrations are molar (M).

Zn(NTA)2-4

Zn(OH)2 (aq)

Zn(OH)3-

Zn(OH)4-2

Zn(SO4)2-2

Zn+2

Zn2OH+3

Zn-Acetate+

Figure A.5. – continued

ZnCl+

ZnCl2 (aq)

ZnCl3-

ZnCl4-2

ZnEDTA-2

ZnH2EDTA (aq)

ZnHEDTA-

ZnHPO4 (aq)
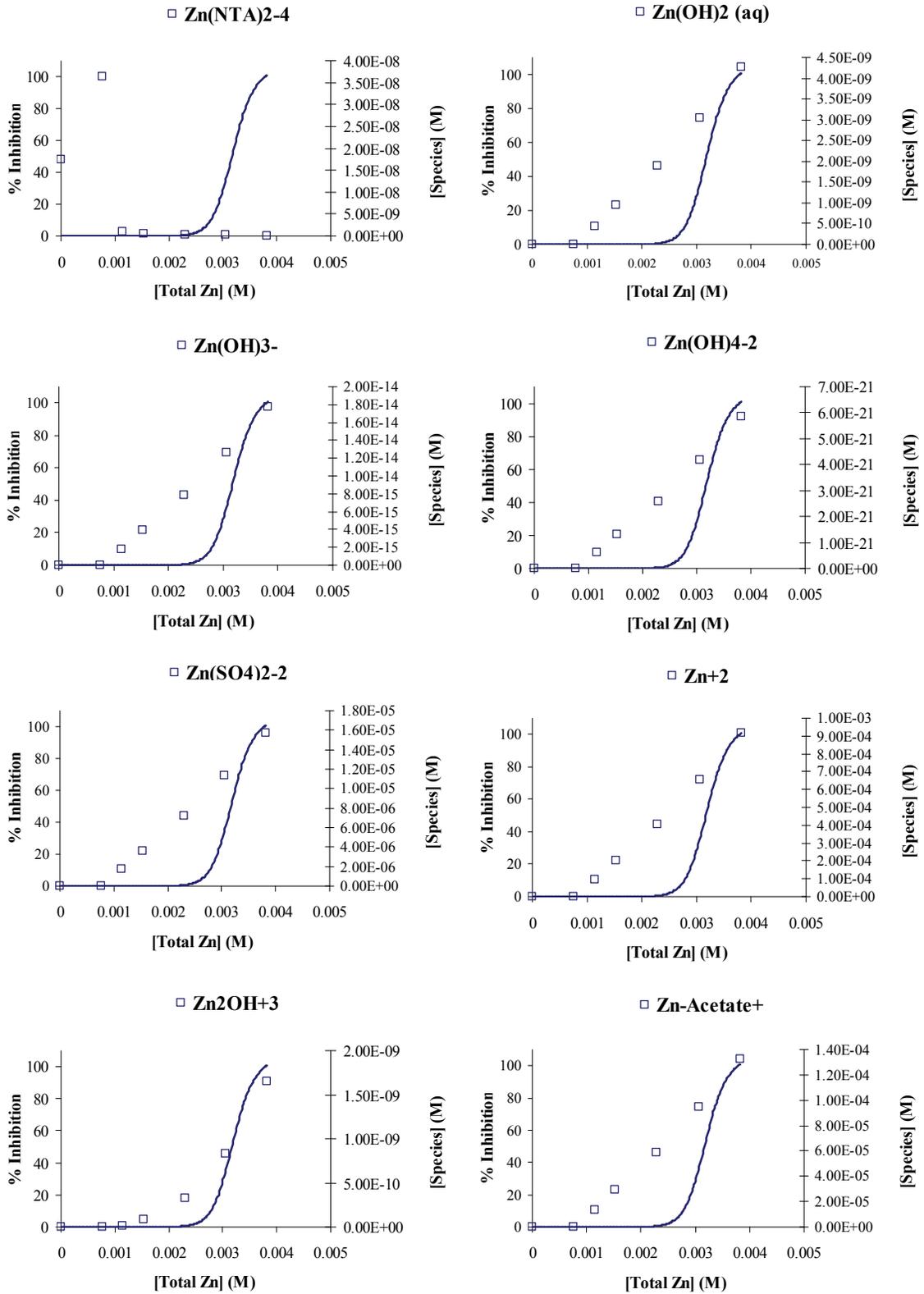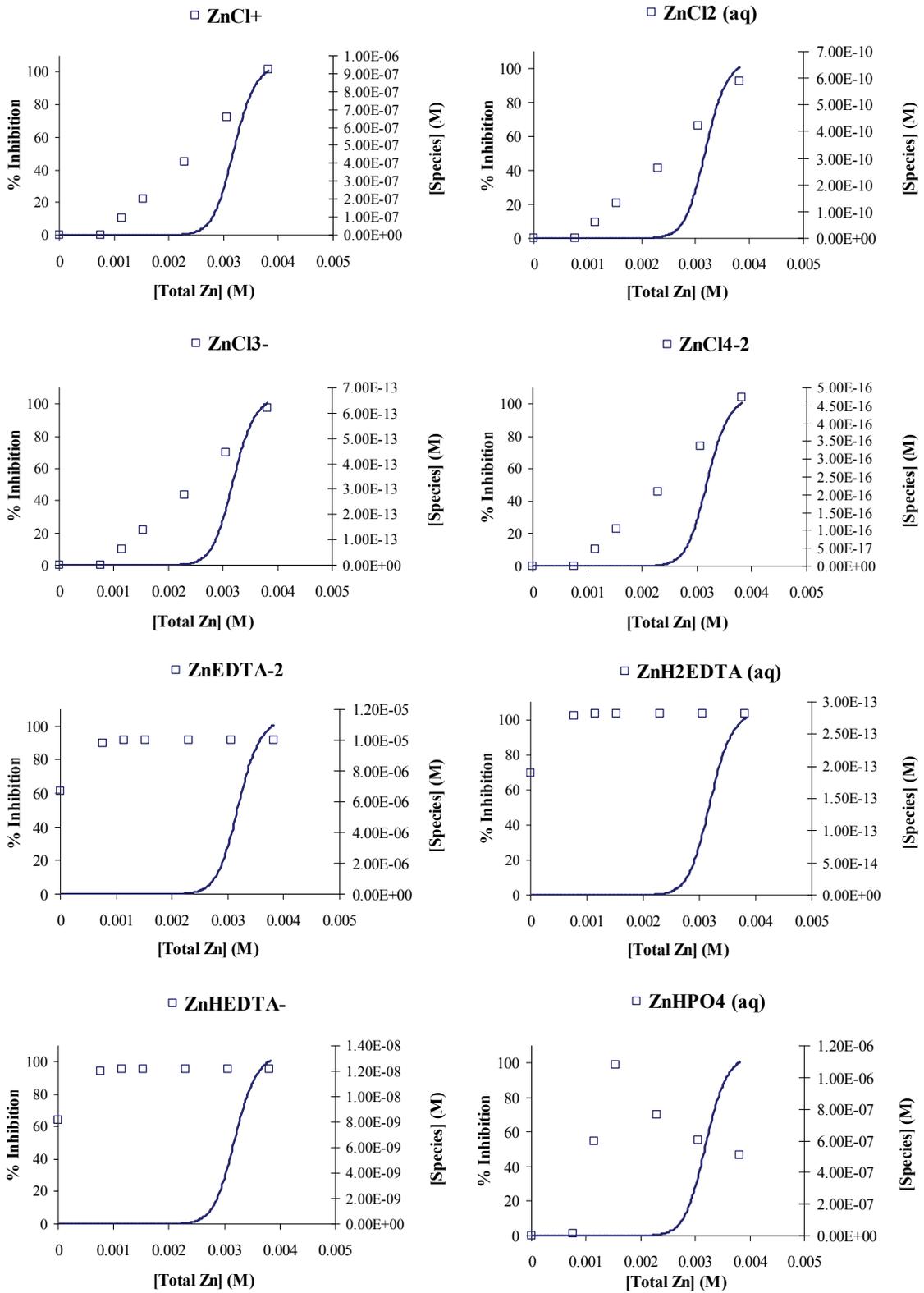
Figure A.5. – continued

Figure A.5. – continued

220
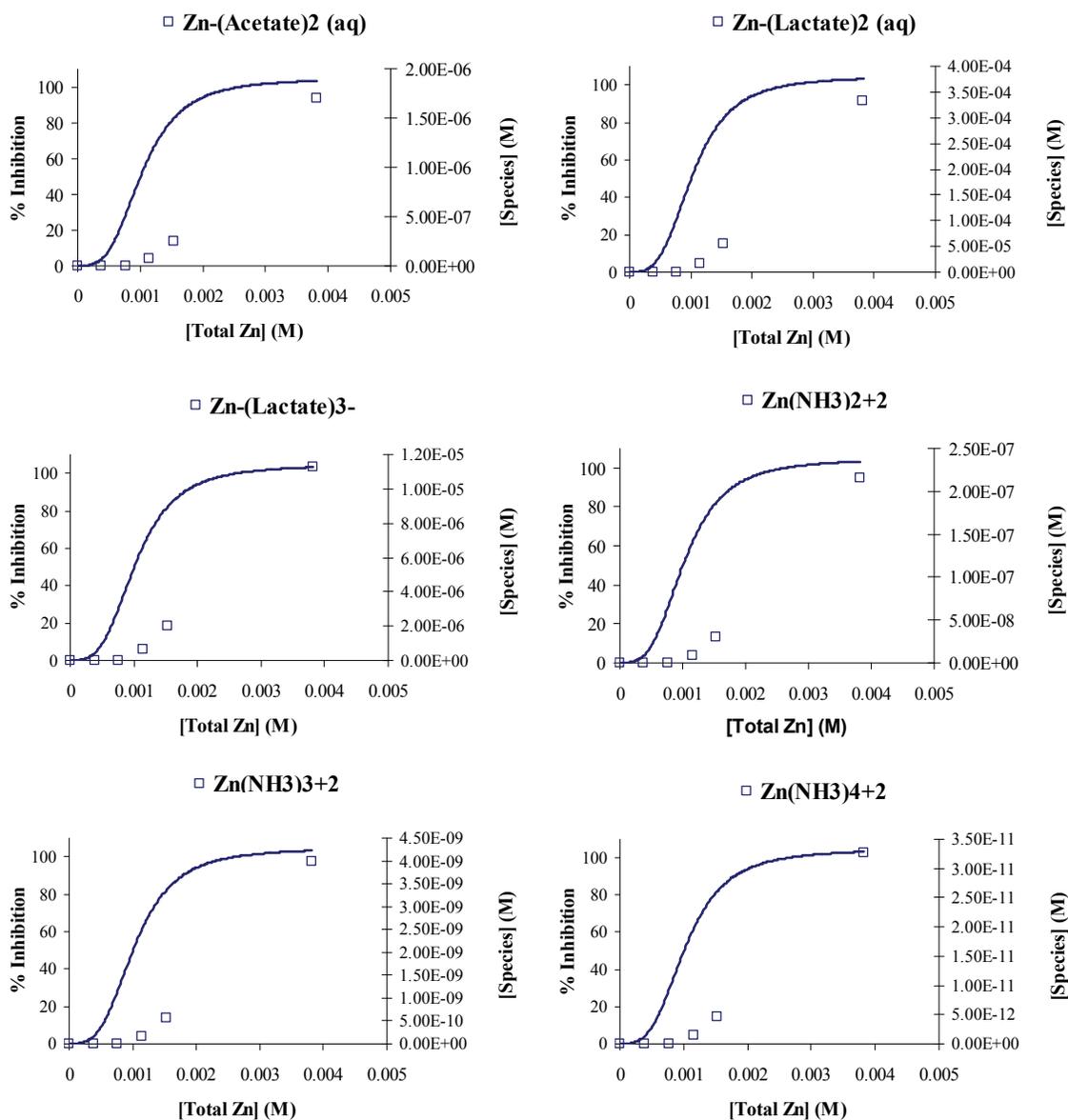
Figure A.6. Plots of Zn-species at different total Zn concentrations in pH 7 media with 10.7 mM acetate. Changes in Zn-species concentrations are plotted along with EC_{50} curves. All concentrations are molar (M).

Zn(NTA)2-4

Zn(OH)2 (aq)

Zn(OH)3-

Zn(OH)4-2

Zn(SO4)2-2

Zn+2

Zn2OH+3

Zn-Acetate+
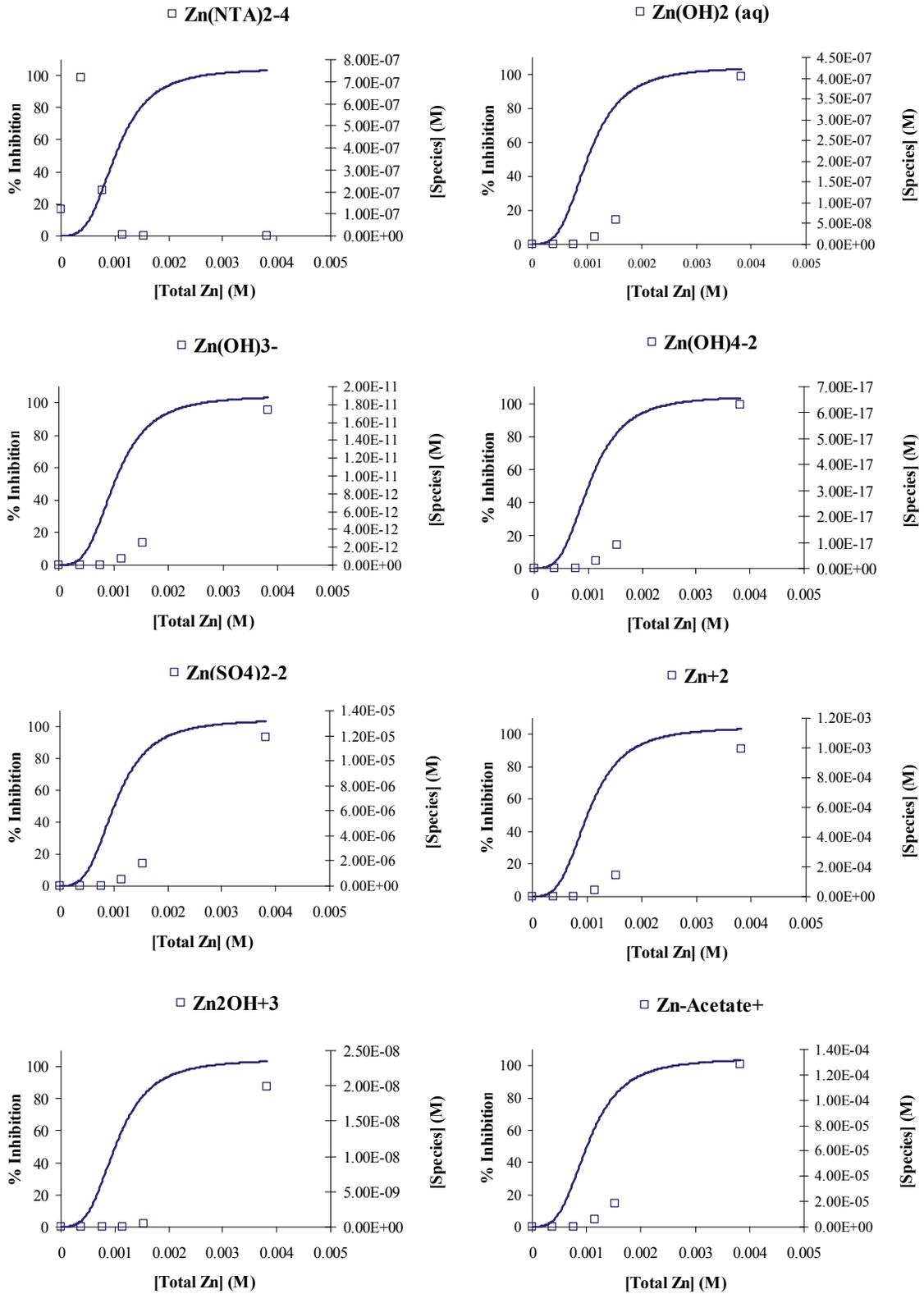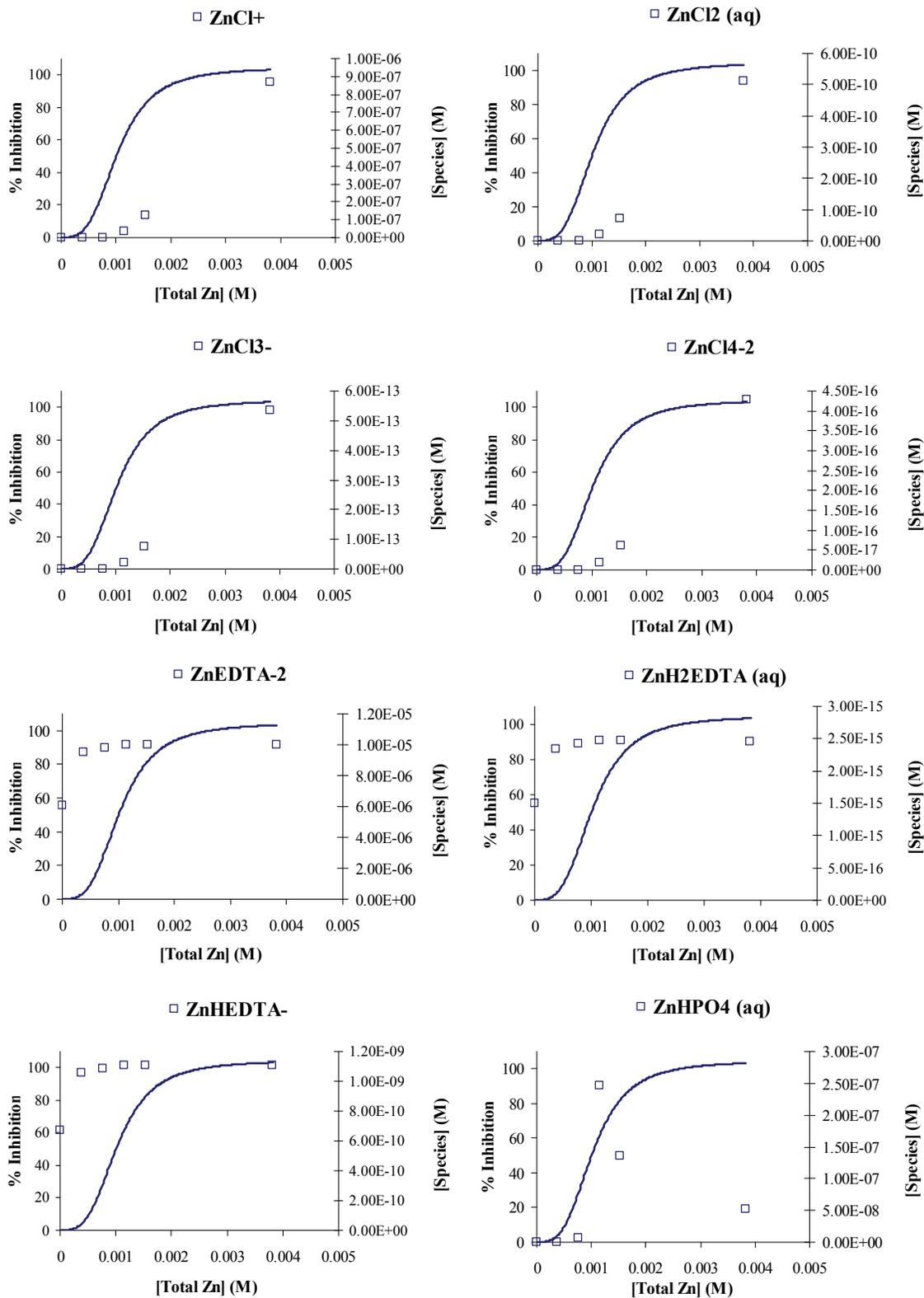
Figure A.6. – continued

Figure A.6. – continued

223

Figure A.6. – continued

224
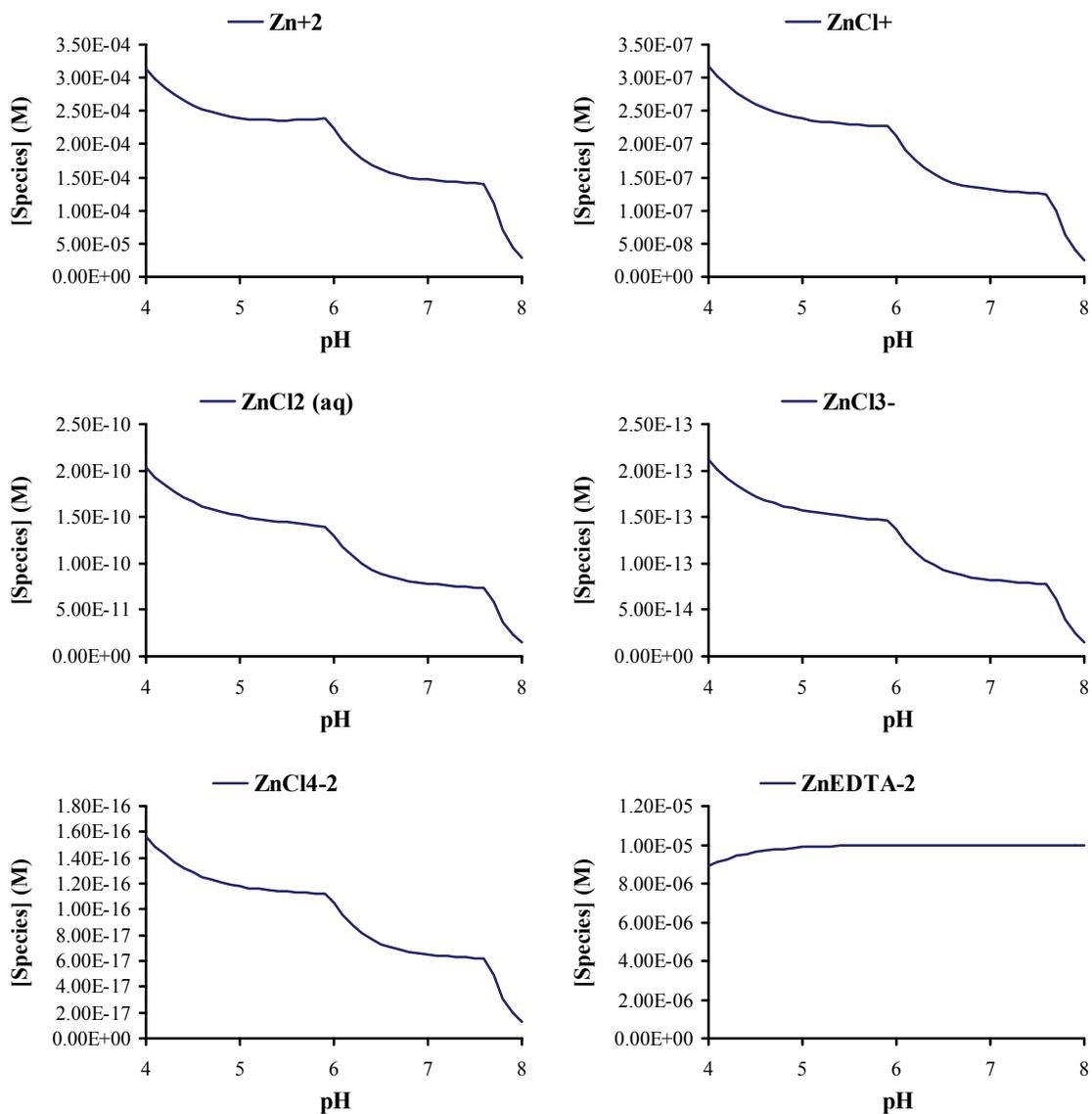
Figure A.7. Changes in Zn species concentration in relation to pH. Graphs were plotted using data generated by modeling a pH sweep in modified 4M with 1.53 mM Zn. Zincite is a mineral phase of ZnO. Vivianite formation is also shown, though it is a mineral phase of $Fe_3(PO_4)_2$.

Figure A.7. – continued

Figure A.7. – continued

Figure A.7. – continued

228
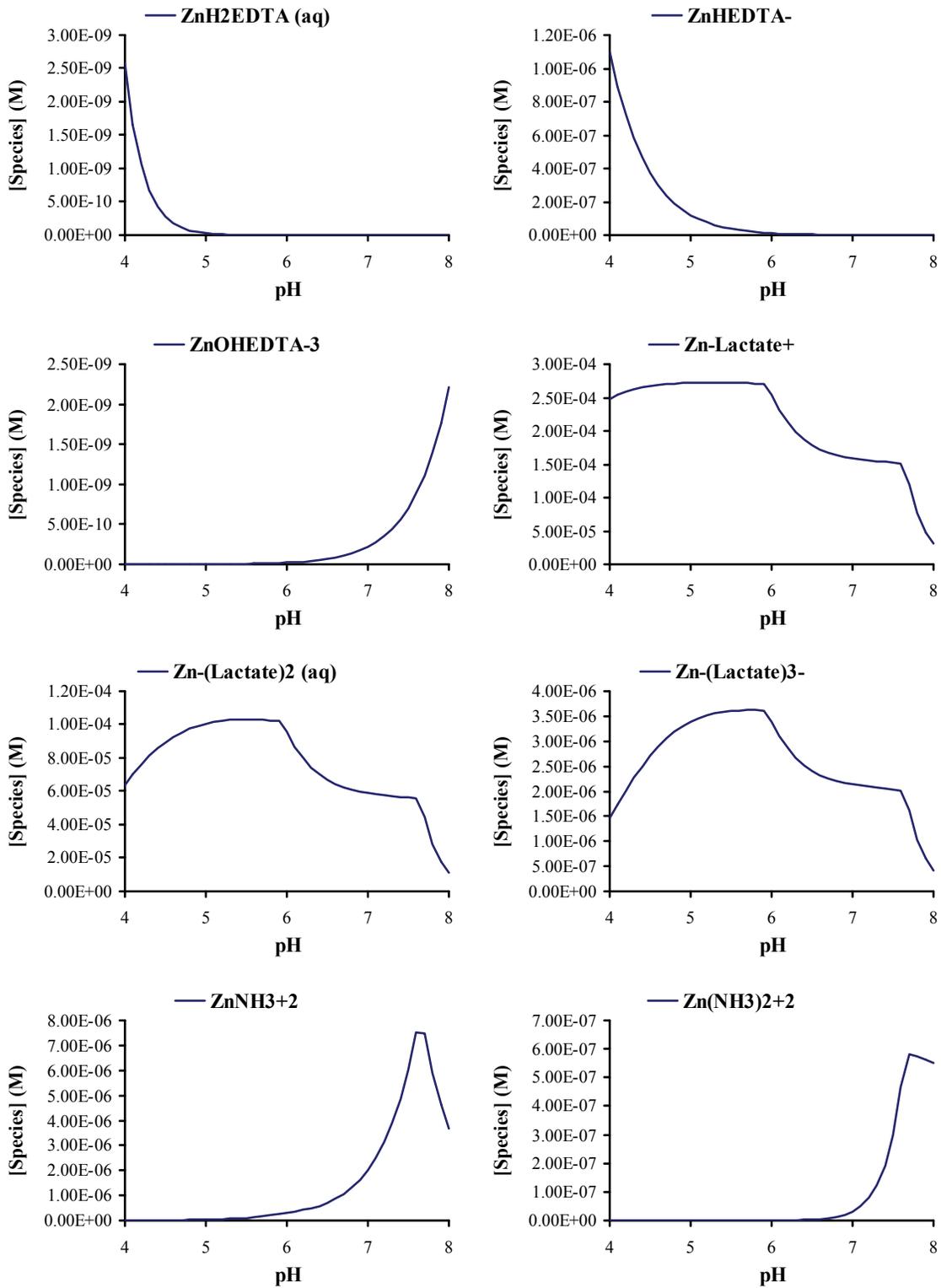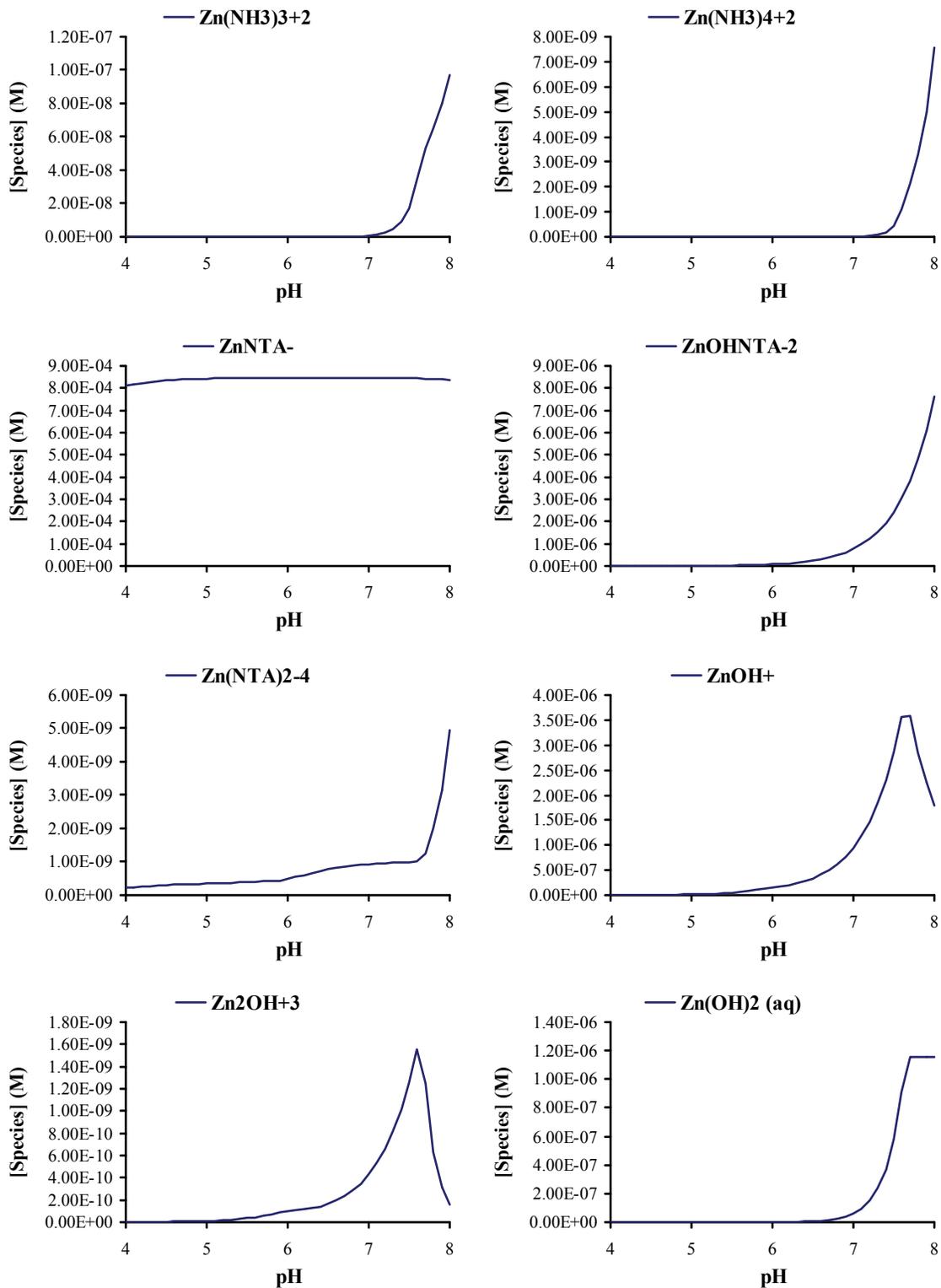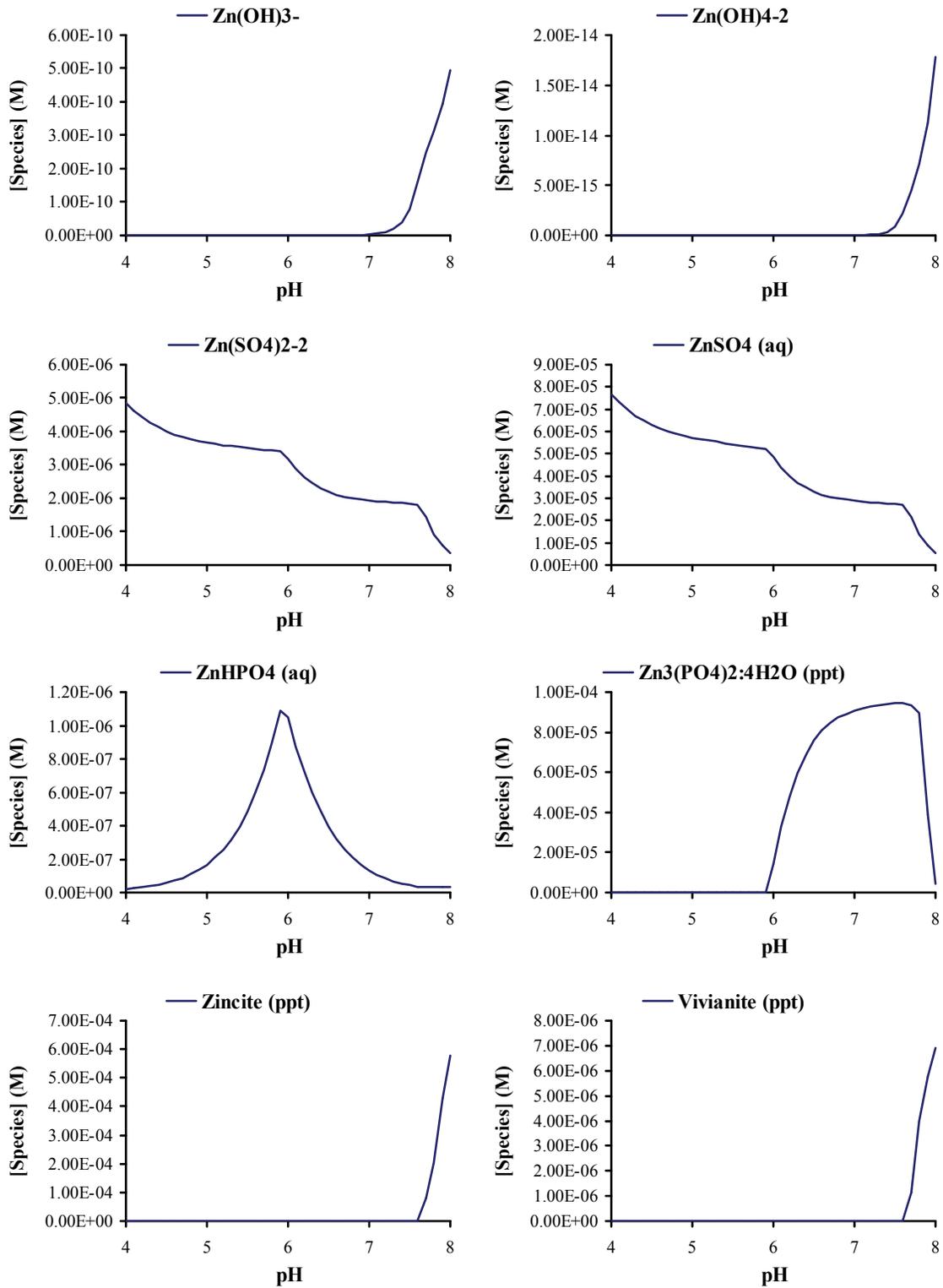
APPENDIX B

Table B.1. Zn concentrations used for predicting Zn-speciation relative to MV production. Percent MV production inhibition and ionic strength is given for each condition. MINTEQA2 was used to predict Zn-speciation at a fixed pH using a Davies b parameter of 0.3 which is appropriate for the predicted ionic strengths for each reaction.

Condition	[Zn] (mM)			
pH 5	0.04	0.77	3.82	7.65
% MV production inhibition	0	0	96.5	100
Ionic strength (M)	0.1410	0.1400	0.1416	0.1443
pH 7	0.04	0.153	0.38	0.765
% MV production inhibition	0	23.4	40.3	83.8
Ionic strength (M)	0.1337	0.1337	0.1337	0.1337
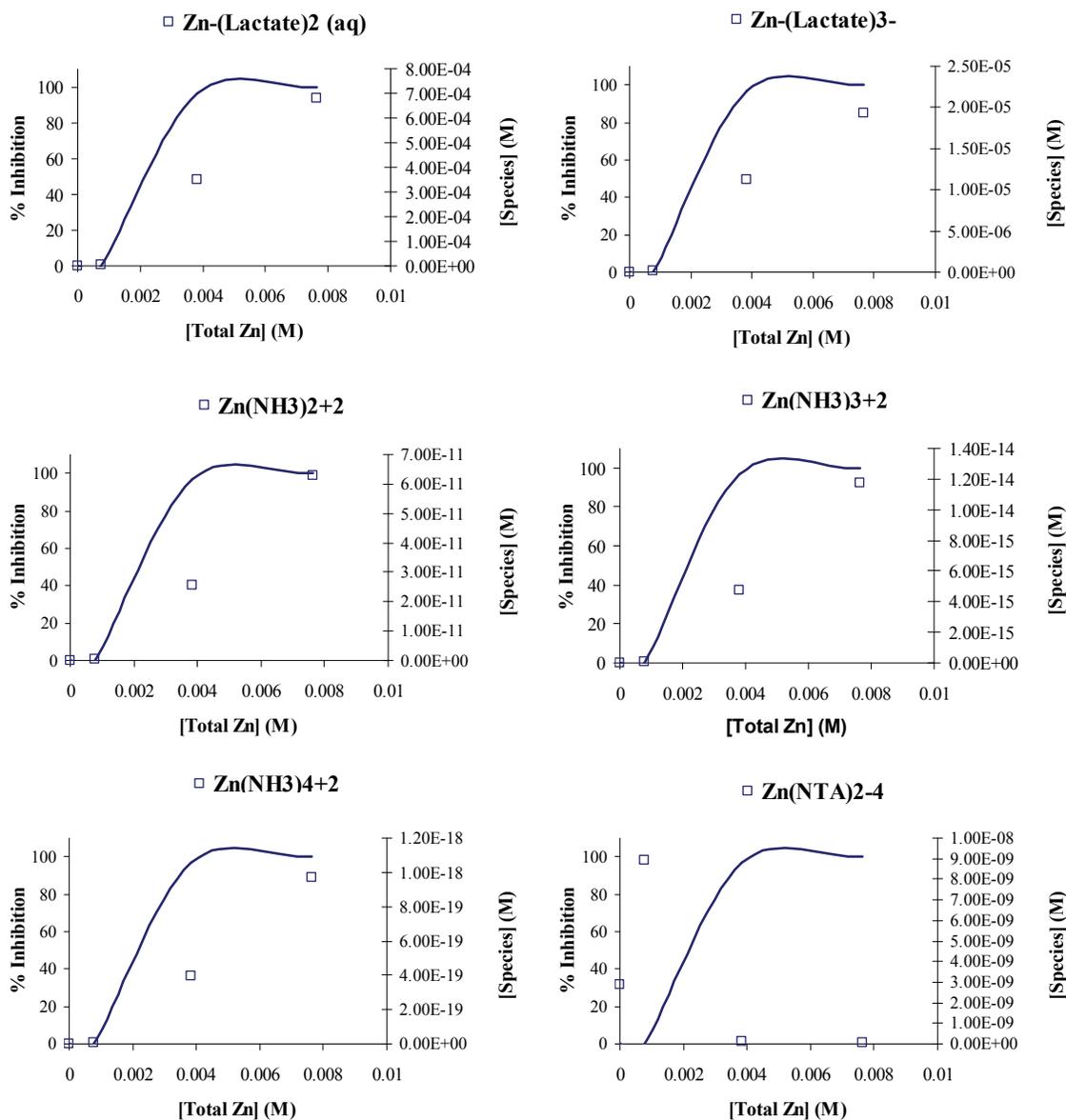
Figure B.1. Plots of Zn-species at different total Zn concentrations in pH 5 media with normalized Na concentrations. Changes in Zn-speciation at pH 5 plotted against % MV production inhibition curves. All concentrations are molar (M). Curves are only four points connected.

Zn(OH)2 (aq)

Zn(OH)3-

Zn(OH)4-2

Zn(SO4)2-2

Zn+2

Zn2OH+3

ZnCl+

ZnCl2 (aq)

Figure B.1. – continued

232

Figure B.1. – continued

233

ZnNTA-

ZnOH+

ZnOHEDTA-3

ZnOHNTA-2

ZnSO4 (aq)

Zn3(PO4)2:4H2O (ppt)
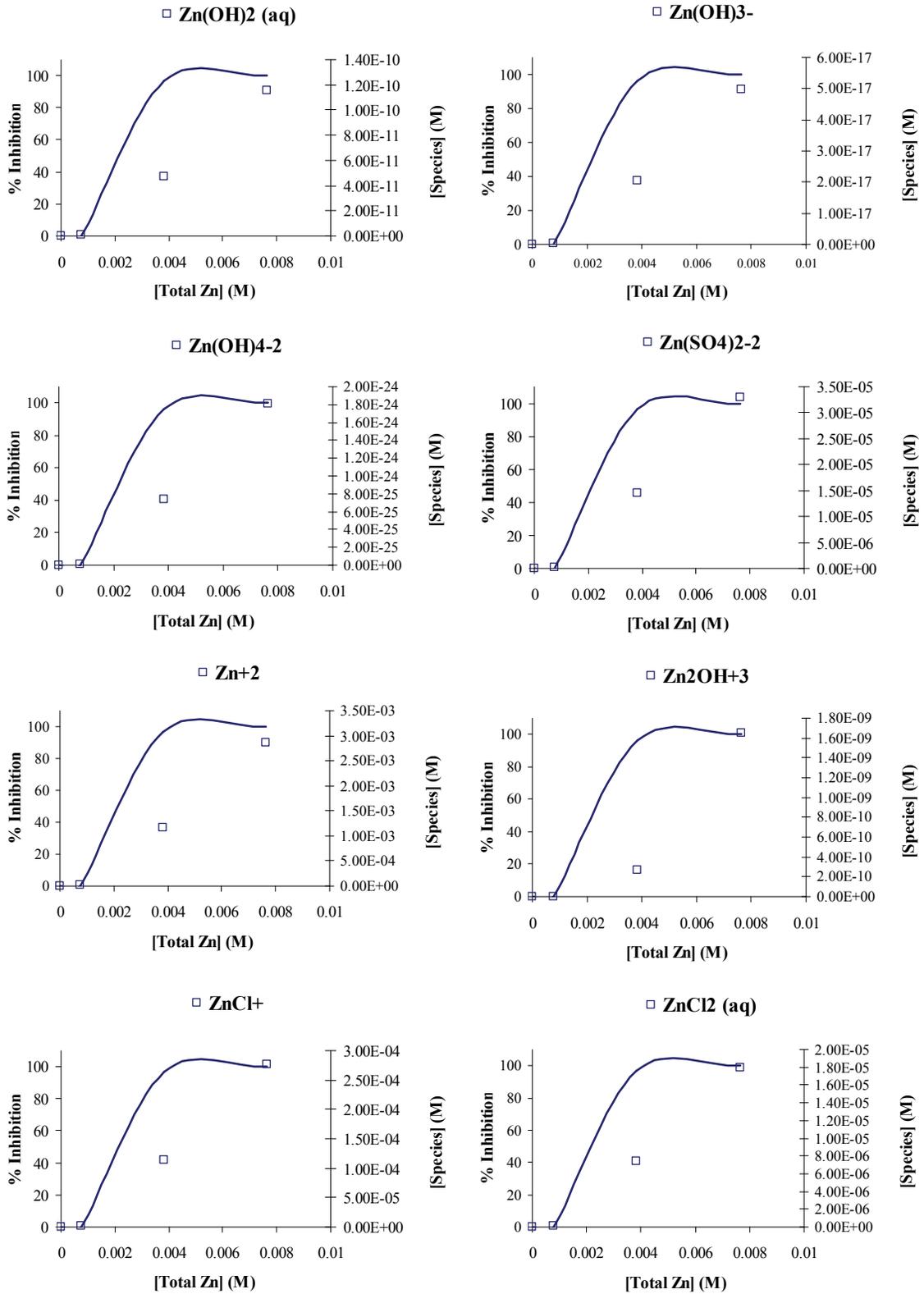
Figure B.1. – continued
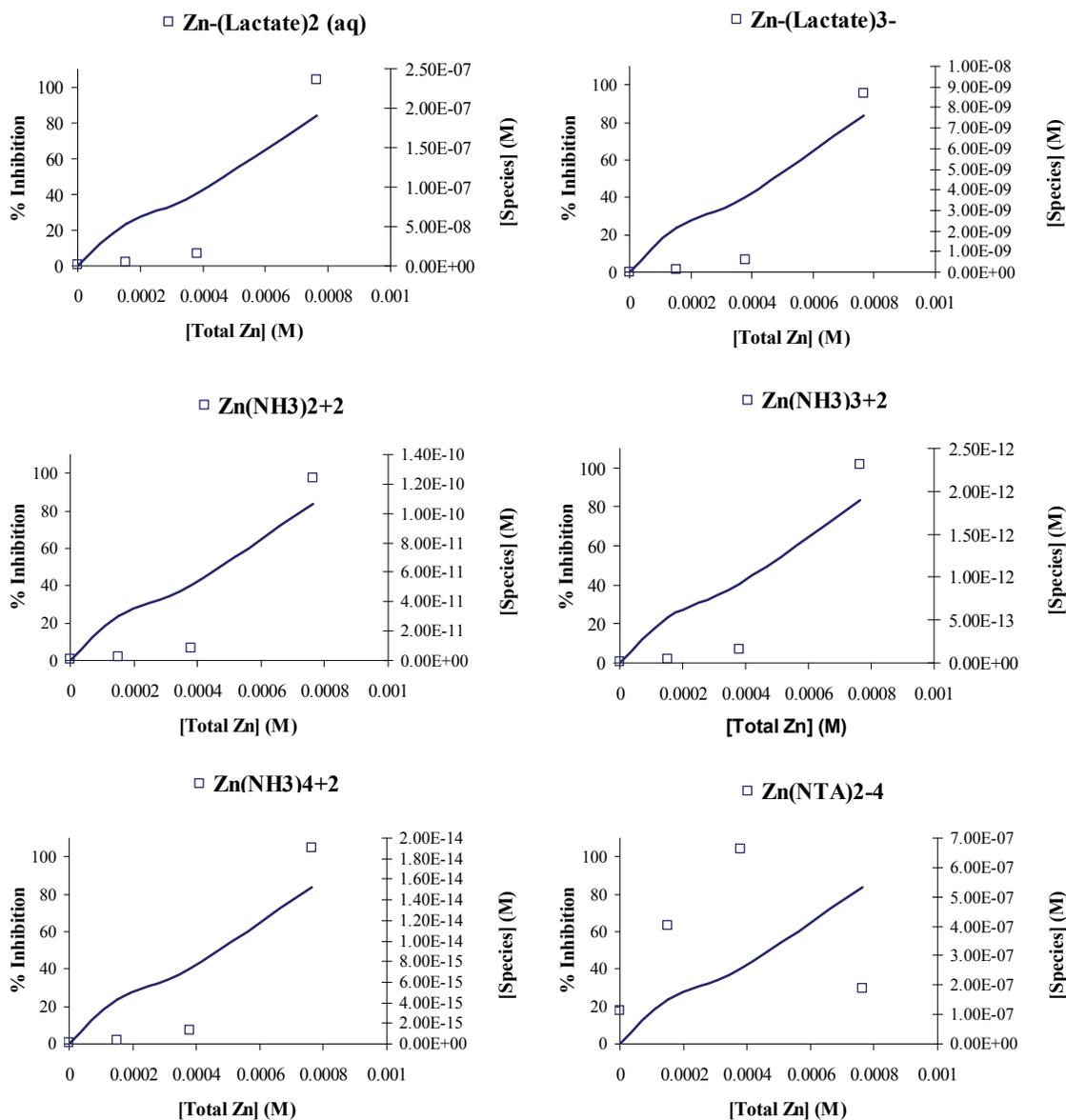
Figure B.2. Plots of Zn-species at different total Zn concentrations in pH 7 media.
Changes in Zn-speciation at 7 plotted against % MV production inhibition curves. All
concentrations are molar (M). Curves are only four points connected.

Figure B.2. – continued

236
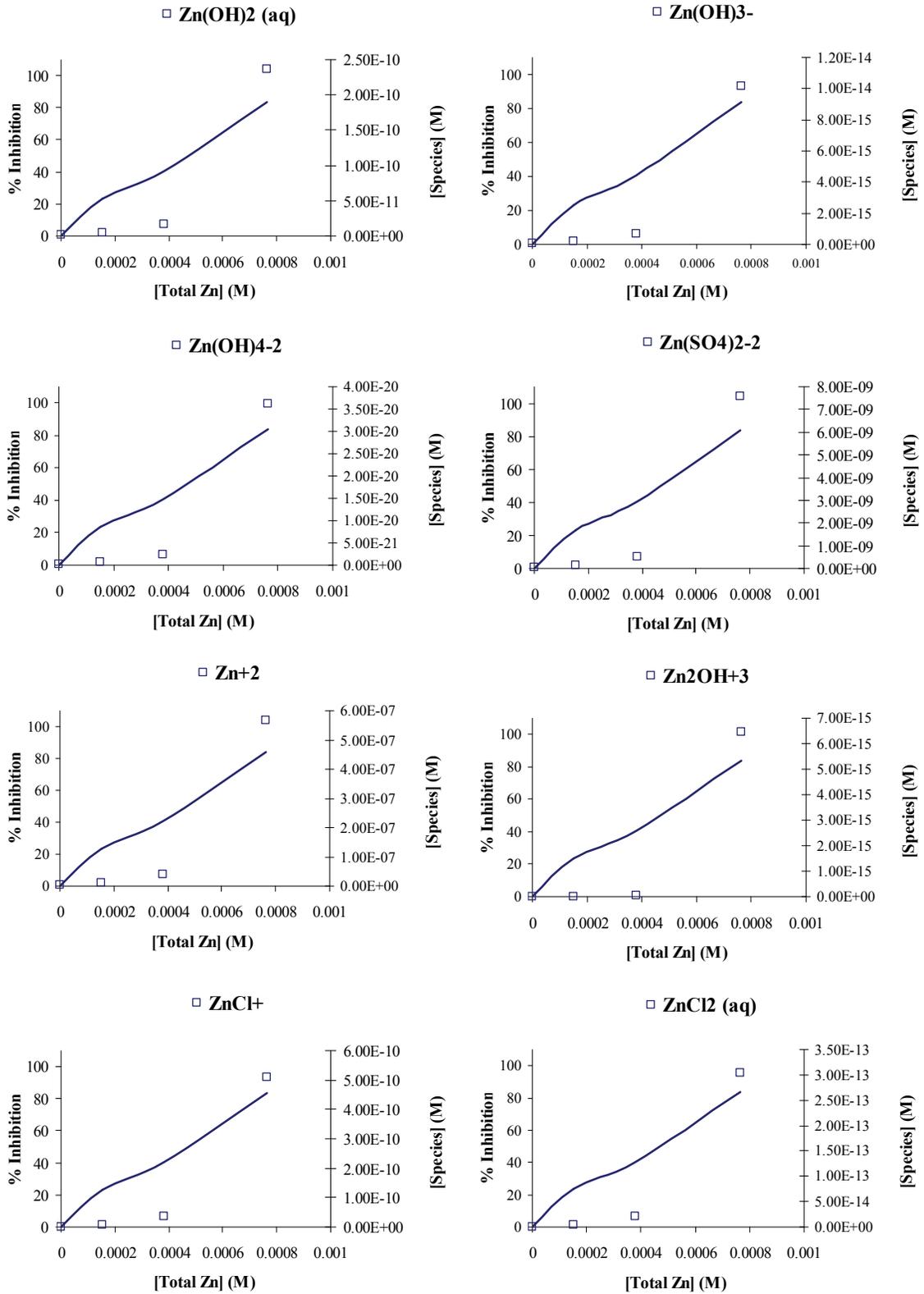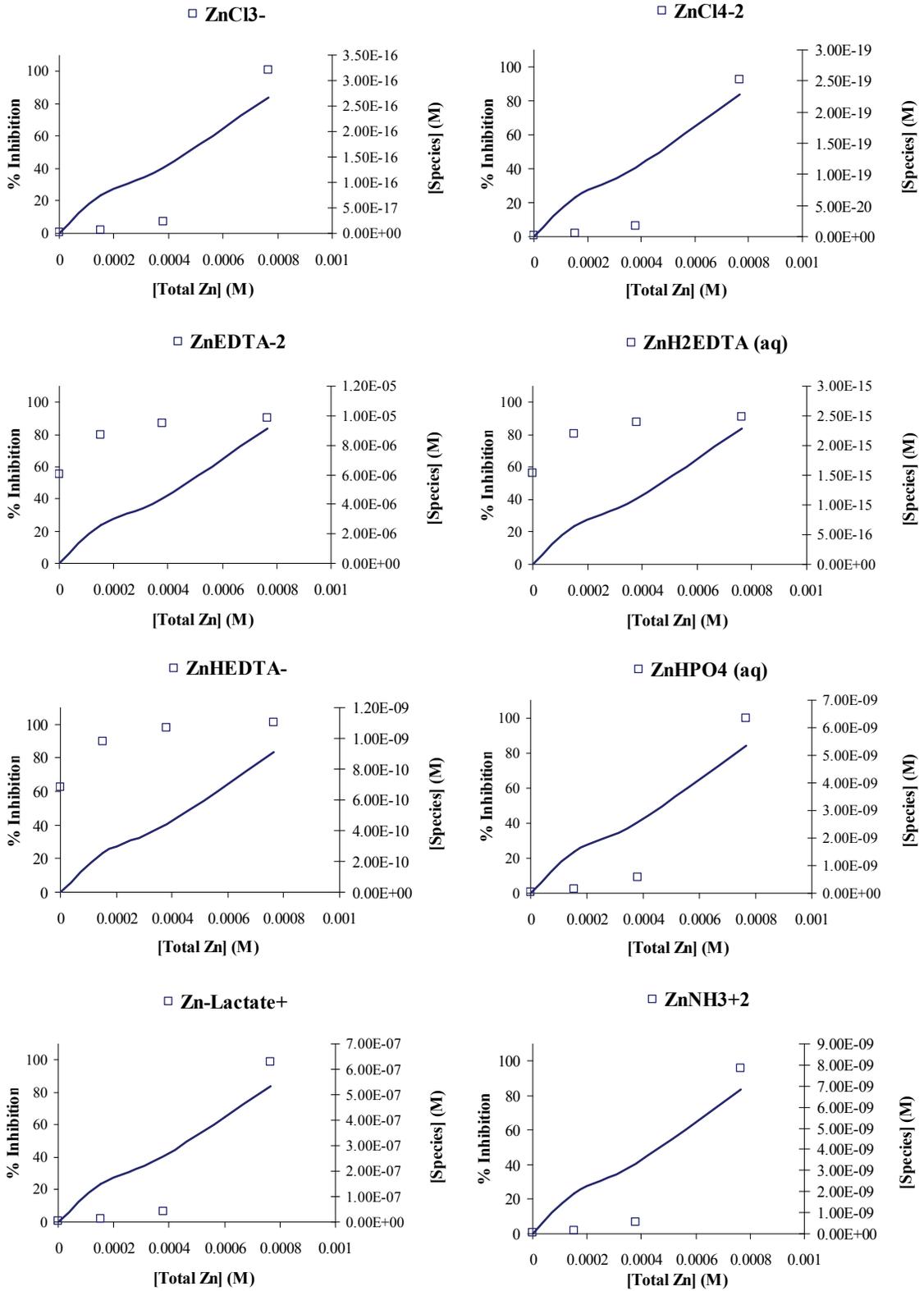
Figure B.2. – continued
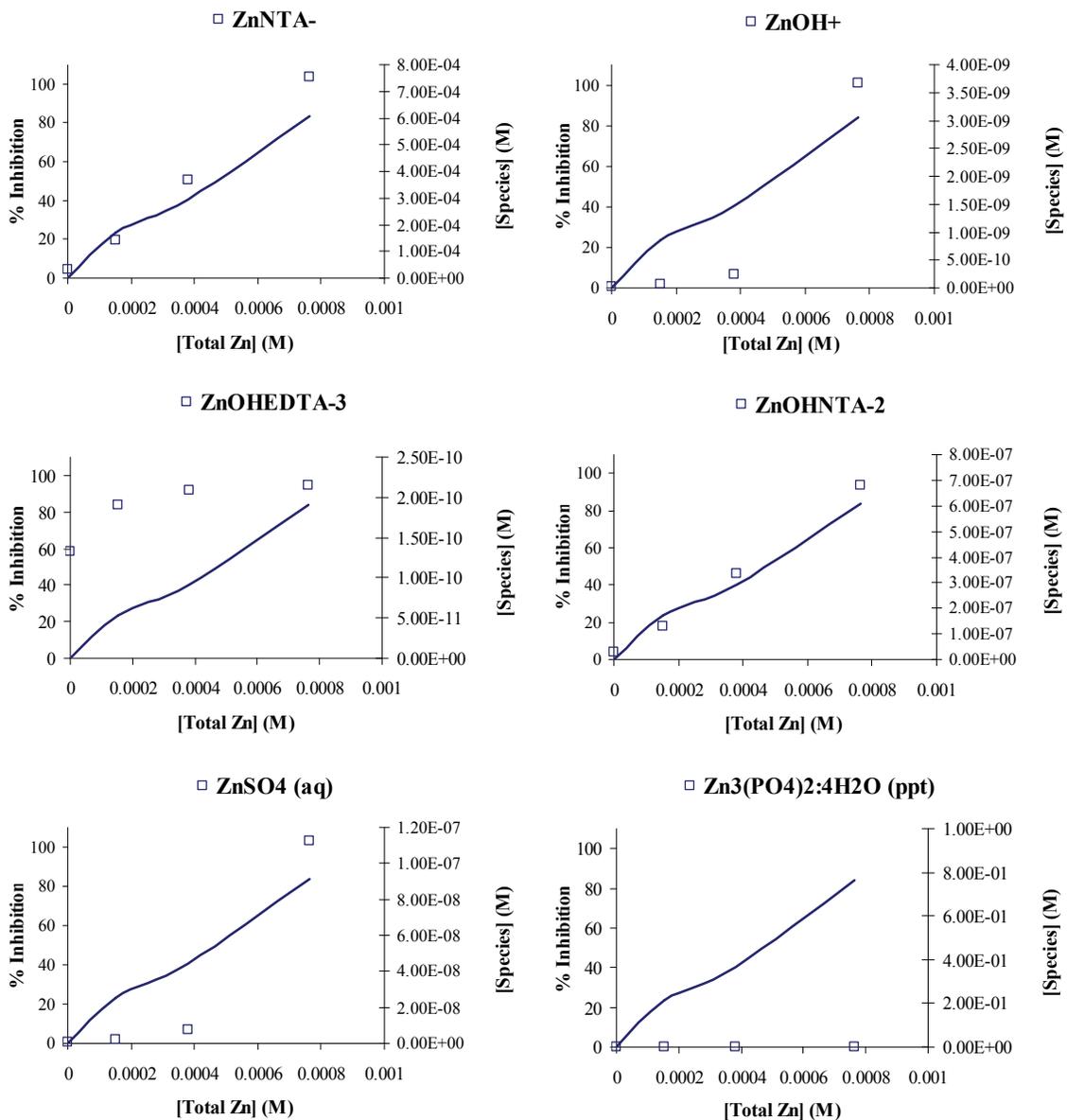
Figure B.2. – continued

APPENDIX C

Table C.1. Unique proteins identified in n-MVs produced by *Burkholderia vietnamiensis* PR1$_{301}$ (PR1) at pH 5 and 7.
Information about proteins identified was determined using the annotated genome of *Burkholderia vietnamiensis* G4 (ORNL, 2007), the parent strain of PR1. The GI number is based on the uploaded annotated sequence available in GenBank, while the gene annotation number refers to the genes identifier in the annotated genome data set. The gene identifier (i.e., 'Gene') is based on the closest COGS hit, available in the annotated genome. Functions are based on clusters of orthologous groups (COGs) functional categories and broader groups in bold were those used by Oak Ridge National Laboratory (ORNL, 2007). Also, proteins which were considered unique to a pH by comparison of the presence in two of three replicates but is present in at least one replicate of another condition are indicated by an (*****) on the gene annotation.

GI Number	Gene Annotation Number	Gene	Gene Annotation	Function	Previously Described [a]
pH 5 only					
				Cellular Processes	
67546796	Bcen18080974	WcaG	NAD-dependent epimerase/dehydratase	Cell envelope biogenesis	
67545288	Bcen18083218	RfbB	dTDP-glucose 4,6-dehydratase	Cell envelope biogenesis	
67544492	Bcen18083909	MscS	* MscS Mechanosensitive ion channel	Cell envelope biogenesis	
67548722	Bcen18080364	CcmC	* Cytochrome c assembly protein	PTM, protein turnover, chaperones	
77965764	Bcen18080423	Gst	Glutathione S-transferase	PTM, protein turnover, chaperones	
67547616	Bcen18080712	DnaK	* Heat shock protein Hsp70	PTM, protein turnover, chaperones	G, F
67549650	Bcen18081853	Lon	Peptidase S16, ATP-dependent protease	PTM, protein turnover, chaperones	

Table C.1. - continued

GI Number	Gene Annotation Number	Gene	Gene Annotation	Function	Previously Described [a]
67549652	Bcen18081855	ClpP	Peptidase S14, ClpP	PTM, protein turnover, chaperones	
67549653	Bcen18081856	Tig	* Trigger factor	PTM, protein turnover, chaperones	F
67545093	Bcen18081983	PpiB	Peptidyl-prolyl cis-trans isomerase, cyclophilin type	PTM, protein turnover, chaperones	
67547166	Bcen18082815	ATM1	* ABC transporter, transmembrane region	PTM, protein turnover, chaperones	
67549687	Bcen18081473	TypA	Small GTP-binding protein domain	Signal transduction mechanisms	
67543782	Bcen18081792	PhoH	PhoH-like protein	Signal transduction mechanisms	
67544078	Bcen18083177	BaeS	ATP-binding region, ATPase-like Histidine kinase A, N-terminal	Signal transduction mechanisms	
67547646	Bcen18080680	SecF	SecD/SecF/SecDF export membrane protein SecF protein	Intracellular trafficking and secretion	
67547298	Bcen18083999	TadD	* Hypothetical protein	Intracellular trafficking and secretion	

Table C.1. - continued

GI Number	Gene Annotation Number	Gene	Gene Annotation	Function	Previously Described [a]
				Information storage and processing	
72606951	Bcen18080318	RplK	Ribosomal protein L11	Translation	
67549783	Bcen18080319	RplA	* Ribosomal protein L1	Translation	L
72606953	Bcen18080320	RplJ	* Ribosomal protein L10	Translation	L
72606917	Bcen18080330	RplC	Ribosomal protein L3	Translation,	
67550033	Bcen18080333	RplB	* Ribosomal protein L2	Translation	L
52211230	Bcen18080335	RplV	* 50S ribosomal protein L22	Translation	L
77965676	Bcen18080337	RplP	* Ribosomal protein L16	Translation	L
67548701	Bcen18080342	RplE	Ribosomal protein L5	Translation	L
72607806	Bcen18080353	RpsM	* Ribosomal protein S13	Translation	L
67546199	Bcen18080645	RplM	Ribosomal protein L13	Translation	L
72611249	Bcen18081030	CafA	* Ribonuclease E and G	Translation	

Table C.1. - continued

GI Number	Gene Annotation Number	Gene	Gene Annotation	Function	Previously Described [a]
67546958	Bcen18081466	InfB	Initiation factor 2 Small GTP-binding protein domain	Translation	
67543787	Bcen18081797	RplI	* Ribosomal protein L9	Translation	L
72608111	Bcen18081800	RpsF	* Ribosomal protein S6	Translation	
77967796	Bcen18082339	RpsO	* Ribosomal protein S15	Translation	L
67547182	Bcen18082831	AspS	Aspartyl-tRNA synthetase	Translation	
67549786	Bcen18080322	RpoB	DNA-directed RNA polymerase, beta subunit	Transcription	L
67549787	Bcen18080323	RpoC	* DNA-directed RNA polymerase	Transcription	L
77965695	Bcen18080356	RpoA	DNA-directed RNA polymerase, alpha subunit	Transcription	
77967344	Bcen18081756	Rho	* Transcription termination factor Rho	Transcription	
67549405	Bcen18080003	GyrB	DNA gyrase, beta subunit	DNA replication	
67549566	Bcen18087726		Initiator RepB protein	DNA replication	

Table C.1. - continued

GI Number	Gene Annotation Number	Gene	Gene Annotation	Function	Previously Described [a]
				Metabolism	
67547738	Bcen18081090		* Radical SAM	Energy production and conversion	
67547989	Bcen18081542	Tas	Aldo/keto reductase	Energy production and conversion	
72609633	Bcen18082216 Bcen18085424	AceF	Dihydrolipoamide acetyltransferase	Energy production and conversion	
67549752	Bcen18082280	TtdA	Fe-S type hydro-lyases tartrate/fumarate alpha region Fe-S type hydro-lyases tartrate/fumarate beta region	Energy production and conversion	
67548296	Bcen18082327	NuoH	Respiratory-chain NADH dehydrogenase, subunit 1	Energy production and conversion	
67548297	Bcen18082328	NuoG	NADH-quinone oxidoreductase, chain G	Energy production and conversion	
67548298	Bcen18082329	NuoF	NADH-quinone oxidoreductase, F subunit	Energy production and conversion	
67548303	Bcen18082334	NuoA	NADH-ubiquinone/plastoquinone oxidoreductase, chain 3	Energy production and conversion	

Table C.1. - continued

GI Number	Gene Annotation Number	Gene	Gene Annotation	Function	Previously Described [a]
67547113	Bcen18082601	Icd	Isocitrate dehydrogenase NADP-dependent, monomeric type	Energy production and conversion	
67548608	Bcen18082760	SucC	Succinyl-CoA synthetase, beta subunit	Energy production and conversion	
67549021	Bcen18082790	GlpK	Glycerol kinase	Energy production and conversion	L
67546586	Bcen18082946	CyoB	Cytochrome-c oxidase	Energy production and conversion	
67548769	Bcen18084408	Mdh	Malate dehydrogenase, NAD or NADP	Energy production and conversion	G
67548762	Bcen18084415	GltA	Citrate synthase I	Energy production and conversion	
17979889	Bcen18087598	NqrF	TomA5	Energy production and conversion	
67549263	Bcen18087602	PutA	Betaine-aldehyde dehydrogenase	Energy production and conversion	
67548740	Bcen18080384	GltB	Glutamate synthase (ferredoxin)	Amino acid transport and metabolism	
67546152	Bcen18080589		Putative lipoprotein	Amino acid transport and metabolism	
67546216	Bcen18080662	GltB	Glutamate synthase (NADPH)	Amino acid transport and metabolism	

Table C.1. - continued

GI Number	Gene Annotation Number	Gene	Gene Annotation	Function	Previously Described [a]
67545550	Bcen18082228	GlnA	Glutamine synthetase type I	Amino acid transport and metabolism	L, G
72609561	Bcen18082296	TyrB	Aspartate transaminase	Amino acid transport and metabolism	
107023202	Bcen18082347	IlvC	Ketol-acid reductoisomerase	Amino acid transport and metabolism	
67548317	Bcen18082349	IlvB	Acetolactate synthase, large subunit	Amino acid transport and metabolism	
67544530	Bcen18083948	GlyA	Glycine hydroxymethyltransferase	Amino acid transport and metabolism	
67548178	Bcen18084112	ArgG	Argininosuccinate synthase	Amino acid transport and metabolism	
67549260	Bcen18087605	LeuA	HMG-CoA lyase-like Aminotransferase, class-II	Amino acid transport and metabolism	
67549470	Bcen18081897	GuaB	IMP dehydrogenase	Nucleotide transport and metabolism	
67542131	Bcen18083585	NUP	Purine nucleoside permease	Nucleotide transport and metabolism	
67546171	Bcen18080612	GapA	Glyceraldehyde-3-phosphate dehydrogenase, type I	Carbohydrate transport and metabolism	F
67542336	Bcen18081235	AraJ	General substrate MJS transporter	Carbohydrate transport and metabolism	

Table C.1. - continued

GI Number	Gene Annotation Number	Gene	Gene Annotation	Function	Previously Described [a]
67548627	Bcen18082741	Fba	Ketose-bisphosphate aldolase, class-II Fructose-bisphosphate aldolase, class II, Calvin cycle subtype	Carbohydrate transport and metabolism	S
67544839	Bcen18084687	PrpB	Phosphoenolpyruvate phosphomutase	Carbohydrate transport and metabolism	
67547621	Bcen18080707	HemH	* Ferrochelatase	Coenzyme metabolism	
67544067	Bcen18083166	MetK	* S-adenosylmethionine synthetase	Coenzyme metabolism	G
67546144	Bcen18080579	AccC	Acetyl-CoA carboxylase	Lipid metabolism	
67547694	Bcen18081044	FabB	β-ketoacyl synthase β-ketoacyl synthase	Lipid metabolism	
67542271	Bcen18080242	CzcD	Cation efflux protein	Inorganic ion transport and metabolism	
67547072	Bcen18082558	CysI	Nitrite/sulfite reductase, hemoprotein β-component, ferrodoxin-like Nitrite and sulphite reductase 4Fe-4S region	Inorganic ion transport and metabolism	
67548949	Bcen18082636	SodA	Superoxide dismutase	Inorganic ion transport and metabolism	

Table C.1. - continued

GI Number	Gene Annotation Number	Gene	Gene Annotation	Function	Previously Described [a]
67547223	Bcen18082876	FabG	Acetoacetyl-CoA reductase	Secondary metabolites	
				Poorly Characterized or Unknown	
67543804	Bcen18081814	Arp	Ankyrin	General function	
67543833	Bcen18084991	AdhP	Zinc-containing alcohol dehydrogenase	General function	F
67549264	Bcen18087600		* Catechol 2,3-dioxygenase	General function	
94310250	Bcen18087611	MhpC	alpha/beta hydrolase fold	General function	
67547603	Bcen18080730		Putative exported protein	Function unknown	
67547674	Bcen18081024		* Protein of unknown function DUF195	Function unknown	
12746250	Bcen18087596		TomA3	Function unknown	
67549575	Bcen18087716		Hypothetical protein	Function unknown	
67545271	Bcen18083236		Probable bacteriophage-related protein		
67542288	Bcen18080224		Gly/Ala/Ser-rich lipoprotein		

Table C.1. - continued

GI Number	Gene Annotation Number	Gene	Gene Annotation	Function	Previously Described [a]
67549102	Bcen18081932		Putative membrane protein		
67545017	Bcen18082392		Putative lipoprotein		
67546561	Bcen18082919		Putative exported protein		
67543335	Bcen18083474		Probable transmembrane protein		
67547906	Bcen18087571		Hypothetical protein		
17979885	Bcen18087594		TomA1		
110672107	Bcen18087597		BtxE		
67547925	Bcen18087630		Hypothetical protein		
67547882	Bcen18087654		Hypothetical protein		
67550111	Bcen18087672		Hypothetical protein		
67549588	Bcen18087698		Hypothetical protein		
67549576	Bcen18087712		Hypothetical protein		
67549571	Bcen18087720		Hypothetical protein		

Table C.1. - continued

GI Number	Gene Annotation Number	Gene	Gene Annotation	Function	Previously Described [a]
67549631	Bcen18087742		Hypothetical protein		
67549875	Bcen18087767		Hypothetical protein		

pH 7 only

Cellular Processes

67545791	Bcen18080891	FtsK	Cell division FtsK/SpoIIIE protein	Cell division	
67547600	Bcen18080733	TolA	* TonB, C-terminal	Cell envelope biogenesis	
67543751	Bcen18081761	ArnT	Putative membrane protein	Cell envelope biogenesis	
67549447	Bcen18081874	MrcA	* Glycosyl transferase, family 51 Penicillin-binding protein, transpeptidase	Cell envelope biogenesis	
67546775	Bcen18080997	HtpX	* Ste24 endopeptidase	PTM, protein turnover, chaperones	
67549747	Bcen18082286	ExbD	* Biopolymer transport protein ExbD/TolR	Intracellular trafficking and secretion	

Table C.1. - continued

GI Number	Gene Annotation Number	Gene	Gene Annotation	Function	Previously Described [a]
				Metabolism	
67545721	Bcen18080420	QcrA	Ubiquinol-cytochrome *c* reductase, iron-sulfur subunit	Energy production and conversion	
67549020	Bcen18082789	GlpA	* FAD dependent oxidoreductase	Energy production and conversion	
67542770	Bcen18085641	PntA	* NAD(P) transhydrogenase, α subunit	Energy production and conversion	
67545111	Bcen18086274	GlcD	* D-lactate dehydrogenase	Energy production and conversion	
67544082	Bcen18083183	MET2	Homoserine O-acetyltransferase	Amino acid transport and metabolism	
67548993	Bcen18084561	TesA	Lipolytic enzyme, G-D-S-L	Amino acid transport and metabolism	
67543785	Bcen18081795		Protein of unknown function DUF47	Inorganic ion transport and metabolism	
67542665	Bcen18085514	HcaE	Rieske [2Fe-2S] region	Inorganic ion transport and metabolism	
67545747	Bcen18080394	Ttg2B	* Protein of unknown function DUF140	Secondary metabolites	

Table C.1. - continued

GI Number	Gene Annotation Number	Gene	Gene Annotation	Function	Previously Described [a]
				Poorly Characterized or Unknown	
67548022	Bcen18081533	LprI	Putative lipoprotein	Function unknown	
67549796	Bcen18082522		Protein of unknown function DUF490	Function unknown	
67542289	Bcen18080223		Conserved hypothetical protein		
67546831	Bcen18080936		Putative lipoprotein		
67545319	Bcen18081302		* Hypothetical protein		
67542172	Bcen18083629		Putative membrane protein		
67549532	Bcen18087481		Hypothetical protein		
67549591	Bcen18087695		Hypothetical protein		

Table C.1. - continued

GI Number	Gene Annotation Number	Gene	Gene Annotation	Function	Previously Described [a]
pH 5 and 7					
				Cellular Processes	
67542304	Bcen18081280 Bcen18084386, Bcen18081748		Peptidoglycan-binding LysM Peptidase M23B	Cell division	
67546884	Bcen18080058 Bcen18081471 Bcen18081576 Bcen18081685 Bcen18082721 Bcen18083578 Bcen18085402 Bcen18085470 Bcen18086315	TolC	RND efflux system, outer membrane lipoprotein, NodT	Cell envelope biogenesis	N
67548726	Bcen18080369	MrcA	Peptidoglycan glycosyltransferase	Cell envelope biogenesis	
67545745	Bcen18080396 Bcen18083811	VacJ	VacJ-like lipoprotein	Cell envelope biogenesis	L, F

Table C.1. - continued

GI Number	Gene Annotation Number	Gene	Gene Annotation	Function	Previously Described [a]
67545645	Bcen18080515	MltA	MltA 3D	Cell envelope biogenesis	L
67548916	Bcen18080524 Bcen18083093 Bcen18084483 Bcen18084829 Bcen18085081 Bcen18085274	OmpC	Porin, Gram-negative type	Cell envelope biogenesis	N, P, F
67546140	Bcen18080574	SlyB	Rickettsia 17 kDa surface antigen	Cell envelope biogenesis	
67546232	Bcen18080623	RlpB	Putative lipoprotein	Cell envelope biogenesis	
67547602	Bcen18080731 Bcen18082520 Bcen18083483 Bcen18080960	OmpA	OmpA/MotB	Cell envelope biogenesis	L, S, Si
67546793	Bcen18080977	MltB	Murein transglycosylase domain protein	Cell envelope biogenesis	S, N, P
67542333	Bcen18081241	MltE	Peptidoglycan-binding LysM SLT	Cell envelope biogenesis	L, G, N, P, F
67546968	Bcen18081453	NlpB	Putative exported protein	Cell envelope biogenesis	

Table C.1. - continued

GI Number	Gene Annotation Number	Gene	Gene Annotation	Function	Previously Described [a]
67543686	Bcen18081696 Bcen18080382	OmpW	OmpW	Cell envelope biogenesis	
67543774	Bcen18081784	ArnT	Glycosyl transferase, family 39	Cell envelope biogenesis	
67543777	Bcen18081787 Bcen18083219	WcaA	Glycosyl transferase, family 2	Cell envelope biogenesis	
67549450	Bcen18081877	MscL	Large-conductance mechanosensitive channel	Cell envelope biogenesis	
67549222	Bcen18081917 Bcen18082523		Surface antigen (D15) Surface antigen variable number	Cell envelope biogenesis	
67549698	Bcen18082173	NlpB	Putative lipoprotein	Cell envelope biogenesis	
67544933	Bcen18082498	OmpC	Putative exported outer membrane porin protein	Cell envelope biogenesis	
67548612	Bcen18082756	RfaL	O-antigen polymerase	Cell envelope biogenesis	
67547163	Bcen18082812	Imp	Organic solvent tolerance protein	Cell envelope biogenesis	L, S, N
67546549	Bcen18082905	LolB	Outer membrane lipoprotein LolB	Cell envelope biogenesis	

Table C.1. - continued

GI Number	Gene Annotation Number	Gene	Gene Annotation	Function	Previously Described [a]
67546598	Bcen18082958	Prc	Peptidase S41A, C-terminal protease	Cell envelope biogenesis	
67546626	Bcen18082989	DacC	Serine-type D-Ala-D-Ala carboxypeptidase	Cell envelope biogenesis	
67543995	Bcen18083091	CsgG	Curli production assembly/transport component CsgG	Cell envelope biogenesis	
67544094	Bcen18083195	MreC	Rod shape-determining protein MreC	Cell envelope biogenesis	G
67545379	Bcen18083211	RgpF	Similar to Lipopolysaccharide biosynthesis protein	Cell envelope biogenesis	
67543830	Bcen18084995	PlcC	Phosphoesterase	Cell envelope biogenesis	
72608328	Bcen18085348	OprB	Carbohydrate-selective porin OprB	Cell envelope biogenesis	
67546012	Bcen18086173	TolC	Outer membrane efflux protein	Cell envelope biogenesis	
67549634	Bcen18087745 Bcen18083119		Soluble lytic transglycosylase	Cell envelope biogenesis	
67549973	Bcen18087755	TonB	Hypothetical protein	Cell envelope biogenesis	
67546892	Bcen18080066	PulG	General secretion pathway protein G	Cell motility and secretion	

Table C.1. - continued

GI Number	Gene Annotation Number	Gene	Gene Annotation	Function	Previously Described [a]
67548717	Bcen18080359		Protein-disulfide reductase	PTM, protein turnover, chaperones	
67548721	Bcen18080363	ResB	ResB-like	PTM, protein turnover, chaperones	
67545723	Bcen18080418 Bcen18081049 Bcen18082731	DegQ	Peptidase S1, chymotrypsin PDZ/DHR/GLGF	PTM, protein turnover, chaperones	L
67545656	Bcen18080503	DsbG	Thiol disulfide interchange protein	PTM, protein turnover, chaperones	
3916739	Bcen18080794	GroL	57 kDa heat shock protein GroEL	PTM, protein turnover, chaperones	L, S, F
67542324	Bcen18081250 Bcen18087277	HflB	Peptidase M41, FtsH	PTM, protein turnover, chaperones	
67543721	Bcen18081731 Bcen18081906	HflC	Band 7 protein	PTM, protein turnover, chaperones	
67543722	Bcen18081732	HflC	HflK	PTM, protein turnover, chaperones	
67549299	Bcen18081844 Bcen18081852 Bcen18082811	SurA	PpiC-type peptidyl-prolyl cis-trans isomerase	PTM, protein turnover, chaperones	
84362113	Bcen18081867	AhpC	Peroxiredoxin	PTM, protein turnover, chaperones	

Table C.1. - continued

GI Number	Gene Annotation Number	Gene	Gene Annotation	Function	Previously Described [a]
67545044	Bcen18082409	HslJ	Protein of unknown function DUF306	PTM, protein turnover, chaperones	
67547209	Bcen18082860 Bcen18083283	HtpX	Peptidase M48, Ste24p	PTM, protein turnover, chaperones	
67546609	Bcen18082970	TrxA	similar to Thiol-disulfide isomerase and thioredoxins	PTM, protein turnover, chaperones	
67547881	Bcen18087653	DsbG	Hypothetical protein	PTM, protein turnover, chaperones	
67542257	Bcen18083723	CstA	Carbon starvation protein CstA	Signal transduction mechanisms	
67548709	Bcen18080350	SecY	SecY protein	Intracellular trafficking and secretion	
72607861	Bcen18080415	TatA	Twin-arginine translocation protein	Intracellular trafficking and secretion	
67547645	Bcen18080681	SecD	SecD/SecF/SecDF export membrane protein	Intracellular trafficking and secretion	
67547644	Bcen18080682	YajC	YajC	Intracellular trafficking and secretion	
67547601	Bcen18080732	TolB	TolB, N-terminal TolB, N-terminal	Intracellular trafficking and secretion	L, S, G, P
67547598	Bcen18080735 Bcen18082285	TolQ	MotA/TolQ/ExbB proton channel	Intracellular trafficking and secretion	

Table C.1. - continued

GI Number	Gene Annotation Number	Gene	Gene Annotation	Function	Previously Described [a]
67547701	Bcen18081052	LepB	Signal peptidase I	Intracellular trafficking and secretion	
67549773	Bcen18083310	YidC	60 kDa inner membrane protein	Intracellular trafficking and secretion	
67548645	Bcen18082722 Bcen18083579	AcrB	Hydrophobe/amphiphile efflux-1 HAE1	Defense mechanisms	
67548524	Bcen18085469 Bcen18081113 Bcen18081408 Bcen18081470 Bcen18081574 Bcen18082723 Bcen18086316	EmrA	Secretion protein HlyD	Defense mechanisms	
67549969	Bcen18086170	EmrA	Membrane-fusion protein	Defense mechanisms	
67549642	Bcen18087753	HsdM	Hypothetical protein	Defense mechanisms	

Table C.1. - continued

GI Number	Gene Annotation Number	Gene	Gene Annotation	Function	Previously Described [a]
				Information Storage and Processing	
67550028	Bcen18080315	TufB	Translation elongation factor Tu Small GTP-binding protein domain	Translation	L, S, G, N, P
77965665	Bcen18080326	RpsG	Ribosomal protein S7	Translation	
67663348	Bcen18080327	FusA	Translation elongation factor G Small GTP-binding protein domain	Translation	L, F
107024302	Bcen18080331	RplD	Ribosomal protein L4/L1e	Translation	
77965675	Bcen18080336	RpsC	Ribosomal protein S3	Translation	L
67548699	Bcen18080340	RplN	Ribosomal protein L14	Translation	
67548702	Bcen18080343	RpsN	Ribosomal protein S14	Translation	
77965685	Bcen18080346	RplR	Ribosomal protein L18	Translation	
67548713	Bcen18080355	RpsD	Ribosomal protein S4	Translation	L
77965696	Bcen18080357	RplQ	Ribosomal protein L17	Translation	L
67546176	Bcen18080618	SmpA	SmpA/OmlA	Translation	

Table C.1. - continued

GI Number	Gene Annotation Number	Gene	Gene Annotation	Function	Previously Described [a]
67546200	Bcen18080646	RpsI	Ribosomal protein S9	Translation	L
67549214	Bcen18081925	RpsB	Ribosomal protein S2	Translation	L
			Metabolism		
67546931	Bcen18080109	AtpB	H^+ transporting two-sector ATPase, A subunit	Energy production and conversion	
67546933	Bcen18080111	AtpF	ATP synthase F0, subunit B	Energy production and conversion	
67546935	Bcen18080113	AtpA	ATP synthase F1, alpha subunit	Energy production and conversion	S, G
67546937	Bcen18080115	AtpD	ATP synthase F1, beta subunit	Energy production and conversion	
67548292	Bcen18082323	NuoL	NADH-plastoquinone oxidoreductase, chain 5	Energy production and conversion	
67548294	Bcen18082325	NuoJ	NADH-ubiquinone/plastoquinone oxidoreductase, chain 6	Energy production and conversion	
67548295	Bcen18082326	NuoI	NADH-quinone oxidoreductase, chain I	Energy production and conversion	

Table C.1. - continued

GI Number	Gene Annotation Number	Gene	Gene Annotation	Function	Previously Described [a]
67548300	Bcen18082331	NuoD	NADH dehydrogenase I, D subunit	Energy production and conversion	
67548301	Bcen18082332	NuoC	NADH (or F420H2) dehydrogenase, subunit C	Energy production and conversion	
67549012	Bcen18082780 Bcen18086158 Bcen18080156 Bcen18082780 Bcen18082781 Bcen18080362 Bcen18085083 Bcen18080156 Bcen18082780 Bcen18082781 Bcen18080362 Bcen18085083		Cytochrome c, class I	Energy production and conversion	
67547174	Bcen18082823 Bcen18081973 Bcen18082823	CyoA	Cytochrome o ubiquinol oxidase subunit II	Energy production and conversion	
107023670	Bcen18082841	GlpC	FAD linked oxidase-like	Energy production and conversion	
67547208	Bcen18082859	LldP	L-lactate permease	Energy production and conversion	

Table C.1. - continued

GI Number	Gene Annotation Number	Gene	Gene Annotation	Function	Previously Described [a]
67546564	Bcen18082922	CydA	Cytochrome bd ubiquinol oxidase, subunit I	Energy production and conversion	
67548767	Bcen18084410	SdhC	Succinate dehydrogenase, cytochrome b subunit	Energy production and conversion	
67548765	Bcen18084412	SdhA	Succinate dehydrogenase or fumarate reductase, flavoprotein subunit Succinate dehydrogenase, flavoprotein subunit	Energy production and conversion	S
67548764	Bcen18084413 Bcen18085821	FrdB	Succinate dehydrogenase/fumarate reductase iron-sulfur protein	Energy production and conversion	
67542772	Bcen18085643	FixC	Electron-transferring-flavoprotein dehydrogenase	Energy production and conversion	
67549934	Bcen18086156 Bcen18082947	CyoA	Cytochrome c oxidase, subunit II	Energy production and conversion	
67545670	Bcen18080486 Bcen18085439	PotE	Amino acid permease-associated region	Amino acid transport and metabolism	
67546193	Bcen18080636	HisM	Amino acid ABC transporter, permease protein, 3-TM region, His/Glu/Gln/Arg/opine	Amino acid transport and metabolism	N, P, F

Table C.1. - continued

GI Number	Gene Annotation Number	Gene	Gene Annotation	Function	Previously Described [a]
67543683	Bcen18081693 Bcen18083083	PotA	Spermidine/putrescine ABC transporter ATP-binding subunit	Amino acid transport and metabolism	F
67544620	Bcen18085084	BetA	Similar to Choline dehydrogenase and related flavoproteins	Amino acid transport and metabolism	
67545795	Bcen18080887	MalK	ABC transporter TOBE	Carbohydrate transport and metabolism	
67545303	Bcen18081284	LacA	Beta-galactosidase	Carbohydrate transport and metabolism	
67549711	Bcen18082186	Eno	Enolase	Carbohydrate transport and metabolism	F
67549035	Bcen18082791	GlpF	Major intrinsic protein	Carbohydrate transport and metabolism	
67547290	Bcen18084007	AraJ	Major facilitator superfamily	Carbohydrate transport and metabolism	
67549372	Bcen18080268		UBA/THIF-type NAD/FAD binding fold	Coenzyme metabolism	
67548915	Bcen18080525	CAT5	Conserved hypothetical protein	Coenzyme metabolism	
67544924	Bcen18082507	HemY	HemY, N-terminal HemY, N-terminal	Coenzyme metabolism	
67544923	Bcen18082508	HemX	Uroporphyrinogen III synthase HEM4 Protein of unknown function DUF513	Coenzyme metabolism	

Table C.1. - continued

GI Number	Gene Annotation Number	Gene	Gene Annotation	Function	Previously Described [a]
67549342	Bcen18084257	Dxs	Deoxyxylulose-5-phosphate synthase	Coenzyme metabolism	
67550109	Bcen18087674	UbiE	similar to Methylase involved in ubiquinone/menaquinone biosynthesis	Coenzyme metabolism	
67547224	Bcen18081717 Bcen18084015	PaaJ	Thiolase	Lipid metabolism	
67548314	Bcen18082346	Psd	Phosphatidylserine decarboxylase-related protein	Lipid metabolism	
67548632	Bcen18082736		conserved hypothetical protein	Lipid metabolism	
67544402	Bcen18083808	SqhC	Terpene synthase	Lipid metabolism	
67547295	Bcen18084002	FabB	Beta-ketoacyl synthase	Lipid metabolism	
67547293	Bcen18084004	DesA	Fatty acid desaturase	Lipid metabolism	
67547286	Bcen18084011	AcpP	Phosphopantetheine-binding	Lipid metabolism	
67546316	Bcen18081588 Bcen18083500 Bcen18084630	Fiu	TonB-dependent siderophore receptor	Inorganic ion transport and metabolism	L, S, Si, N, P, F

Table C.1. - continued

GI Number	Gene Annotation Number	Gene	Gene Annotation	Function	Previously Described [a]
67543716	Bcen18081726	Kup	K potassium transporter	Inorganic ion transport and metabolism	
67545035	Bcen18082371	KdpC	K transporting ATPase, KdpC subunit	Inorganic ion transport and metabolism	
67545034	Bcen18082372	KdpB	Haloacid dehalogenase-like hydrolase E1-E2 ATPase-associated region	Inorganic ion transport and metabolism	
67545033	Bcen18082373	KdpA	K transporting ATPase, A subunit	Inorganic ion transport and metabolism	
67546596	Bcen18082956	PspE	Rhodanese-like	Inorganic ion transport and metabolism	
67543504	Bcen18087270	ZntA	Copper-translocating P-type ATPase Heavy metal translocating P-type ATPase	Inorganic ion transport and metabolism	
67549531	Bcen18087480	ChrA	Chromate transporter	Inorganic ion transport and metabolism	
67545748	Bcen18080393	Ttg2A	ABC transporter	Secondary metabolites	
67545746	Bcen18080395	Ttg2C	Mce4/Rv3499c/MTV023.06c protein	Secondary metabolites	

Table C.1. - continued

GI Number	Gene Annotation Number	Gene	Gene Annotation	Function	Previously Described [a]
				Poorly Characterized or Unknown	
67542264	Bcen18080250	OsmY	Transport-associated	General function	
67548743	Bcen18080388		ABC transporter, N-terminal	General function	
67547654	Bcen18080672	PqiB	Paraquat-inducible protein	General function	
67545318	Bcen18081301		Conserved hypothetical protein	General function	
67549112	Bcen18081507		Inner-membrane translocator	General function	
67543711	Bcen18081721	ComL	Competence lipoprotein ComL	General function	
67543808	Bcen18081818		Protein of unknown function DUF175	General function	
107028763	Bcen18081963	RssA	Patatin	General function	
67547065	Bcen18082551 Bcen18082550		Permease YjgP/YjgQ	General function	
67546578	Bcen18082936		Electron transport protein SCO1/SenC	General function	

Table C.1. - continued

GI Number	Gene Annotation Number	Gene	Gene Annotation	Function	Previously Described [a]
67546630	Bcen18082993		Putative lipoprotein	General function	
67544073	Bcen18083172		Cobalamin synthesis protein/P47K	General function	
67544406	Bcen18083812		Putative membrane protein	General function	
67544621	Bcen18085086		Alpha-2-macroglobulin, N-terminal	General function	
67543513	Bcen18087282		Protein of unknown function DUF477	General function	
67549620	Bcen18087729		Putative chitinase	General function	
67547655	Bcen18080671		Protein of unknown function DUF330	Function unknown	
67543726	Bcen18081736		Quinoprotein	Function unknown	
67543727	Bcen18081737		Putative membrane protein	Function unknown	
67543730	Bcen18081740 Bcen18087702		Helix-turn-helix motif	Function unknown	
67543795	Bcen18081805	XkdP	Peptidoglycan-binding LysM Transport-associated	Function unknown	

Table C.1. - continued

GI Number	Gene Annotation Number	Gene	Gene Annotation	Function	Previously Described [a]
67543799	Bcen18081809 Bcen18084191		Putative lipoprotein	Function unknown	
67547183	Bcen18082832		Protein of unknown function DUF502	Function unknown	
67547186	Bcen18082837		Mitochondrial import inner membrane translocase, subunit Tim44	Function unknown	
67549502	Bcen18082893		Protein of unknown function DUF1239	Function unknown	
67549501	Bcen18082894		OstA-like protein	Function unknown	
67542205	Bcen18083664		Protein of unknown function DUF1214	Function unknown	
67547382	Bcen18084444		similar to uncharacterized protein conserved in bacteria	Function unknown	
67547357	Bcen18084467 Bcen18083015	DedD	Sporulation related	Function unknown	
67545966	Bcen18085374		Protein of unknown function DUF1311	Function unknown	
67546391	Bcen18086998		Autotransporter beta-domain	Function unknown	

Table C.1. - continued

GI Number	Gene Annotation Number	Gene	Gene Annotation	Function	Previously Described [a]
67543514	Bcen18087283 Bcen18083892	LemA	LemA	Function unknown	
67545696	Bcen18080459 Bcen18080971 Bcen18081981 Bcen18082904		TPR repeat		G
67546129	Bcen18080561		Putative lipoprotein		
67546808	Bcen18080962		Putative exported protein		
67545360	Bcen18081349		Cellulose synthase, subunit B		
67547014	Bcen18081401		Putative lipoprotein		
67549449	Bcen18081876		Putative membrane protein		
67549469	Bcen18081896		Conserved hypothetical protein		
67549709	Bcen18082184		Putative lipoprotein		
67545536	Bcen18082214 Bcen18082878		Phasin		

Table C.1. - continued

GI Number	Gene Annotation Number	Gene	Gene Annotation	Function	Previously Described [a]
67549019	Bcen18082788		Putative exported protein		
67543990	Bcen18083086		Putative exported protein		
67662920	Bcen18084044		Hypothetical protein		
67549354	Bcen18084244		Putative exported protein		
67548771	Bcen18084406		Putative exported protein		
67542941	Bcen18085969		Conserved hypothetical signal peptide protein		
67545390	Bcen18086839		Hypothetical protein		
67543556	Bcen18087071		Hypothetical protein		
67547898	Bcen18087562		Hypothetical protein		
67547902	Bcen18087567		Hypothetical protein		
67547908	Bcen18087573		Hypothetical protein		
67547909	Bcen18087574		Hypothetical protein		
67547910	Bcen18087575		Hypothetical protein		

Table C.1. - continued

GI Number	Gene Annotation Number	Gene	Gene Annotation	Function	Previously Described [a]
67547911	Bcen18087576		Hypothetical protein		
67547923	Bcen18087627		Hypothetical protein		
67547930	Bcen18087635		Hypothetical protein		
67547931	Bcen18087636		Hypothetical protein		
67547886	Bcen18087658		Hypothetical protein		
91769445	Bcen18087665		Hypothetical protein		
67550005	Bcen18087687		Hypothetical protein		
67549590	Bcen18087696		Hypothetical protein		
67549621	Bcen18087730		Hypothetical protein		
67549622	Bcen18087732		Hypothetical protein		
67549625	Bcen18087735		Hypothetical protein		
67549627	Bcen18087737		Hypothetical protein		
67549628	Bcen18087738		Hypothetical protein		

Table C.1. - continued

GI Number	Gene Annotation Number	Gene	Gene Annotation	Function	Previously Described [a]
67549632	Bcen18087743		Hypothetical protein		
67549633	Bcen18087744		Hypothetical protein		
67549636	Bcen18087747		Hypothetical protein		
67549974	Bcen18087754		Hypothetical protein		
67549883	Bcen18087768 Bcen18087769		Hypothetical protein		
67549873	Bcen18087771		Hypothetical protein		
67549871	Bcen18087773		Hypothetical protein		
67549870	Bcen18087774		Hypothetical protein		
67549869	Bcen18087775		Hypothetical protein		

[a] Abbreviations in 'Previously Described' column refer to: F = (Ferrari et al., 2006), G = (Galka et al., 2008), L = (Lee et al., 2007), N = (Nevot et al., 2006), P = (Post et al., 2005), S = (Scorza et al., 2008), and Si = (Sidhu et al., 2008)

REFERENCES

Adams, L. K., D. Y. Lyon, and P. J. J. Alvarez. 2006. Comparative eco-toxicity of nanoscale TiO2, SiO2, and ZnO water suspensions. Water Research 40:3527-3532.

Allan, N. D., C. Kooi, P. A. Sokol, and T. J. Beveridge. 2003. Putative virulence factors are released in association with membrane vesicles from *Burkholderia cepacia*. Can J Microbiol 49:613-24.

Anton, A., A. Weltrowski, C. J. Haney, S. Franke, G. Grass, C. Rensing, and D. H. Nies. 2004. Characteristics of zinc transport by two bacterial cation diffusion facilitators from *Ralstonia metallidurans* CH34 and *Escherichia coli*. J Bacteriol 186:7499-507.

Applerot, G., A. Lipovsky, R. Dror, N. Perkas, Y. Nitzan, R. Lubart, and A. Gedanken. 2009. Enhanced antibacterial activity of nanocrystalline ZnO due to increased ROS-mediated cell injury. Advanced Functional Materials 19:842-852.

Baalousha, M., A. Manciulea, S. Cumberland, K. Kendall, and J. Lead. 2008. Aggregation and surface properties of iron oxide nanoparticles: Influence of pH and natural organic matter. Environ Toxicol Chem 27:1875–1882.

Baker-Austin, C., M. S. Wright, R. Stepanauskas, and J. V. McArthur. 2006. Co-selection of antibiotic and metal resistance. Trends Microbiol 14:176-82.

Bauman, S. J., and M. J. Kuehn. 2006. Purification of outer membrane vesicles from *Pseudomonas aeruginosa* and their activation of an IL-8 response. Microbes Infect 8:2400-8.

Bayer, M. E., and J. L. Sloyer, Jr. 1990. The electrophoretic mobility of gram-negative and gram-positive bacteria: an electrokinetic analysis. J Gen Microbiol 136:867-74.

Beard, S. J., R. Hashim, J. Membrillo-Hernandez, M. N. Hughes, and R. K. Poole. 1997. Zinc(II) tolerance in *Escherichia coli* K-12: evidence that the zntA gene (o732) encodes a cation transport ATPase. Mol Microbiol 25:883-91.

Beard, S. J., R. Hashim, G. Wu, M. R. Binet, M. N. Hughes, and R. K. Poole. 2000. Evidence for the transport of zinc(II) ions via the pit inorganic phosphate transport system in *Escherichia coli*. FEMS Microbiol Lett 184:231-5.

Beard, S. J., M. N. Hughes, and R. K. Poole. 1995. Inhibition of the cytochrome bd-terminated NADH oxidase system in *Escherichia coli* K-12 by divalent metal cations. FEMS Microbiol Lett 131:205-10.

Bell, A. W., M. A. Ward, W. P. Blackstock, H. N. M. Freeman, J. S. Choudhary, A. P. Lewis, D. Chotai, A. Fazel, J. N. Gushue, J. Paiement, S. Palcy, E. Chevet, M. Lafreniere-Roula, R. Solari, D. Y. Thomas, A. Rowley, and J. J. M. Bergeron. 2001. Proteomics characterization of abundant golgi membrane proteins. J Biol Chem 276:5152-5165.

Belzer, C., J. Stoof, and A. van Vliet. 2007. Metal-responsive gene regulation and metal transport in *Helicobacter* species. Biometals 20:417-429.

Beveridge, T. J. 1999. Structures of gram-negative cell walls and their derived membrane vesicles. J Bacteriol 181:4725-33.

Beveridge, T. J., and S. Schultze-Liam. 1995. Detection of anionic sites on bacterial walls, their ability to bind toxic heavy metals and form sedimental flocs and their contribution to mineralization, p. 183-205. *In* H. E. Allen, C. P. Huang, and G. W. Bailey (ed.), Metal speciation and contamination of soil. CRC Press, Boca Raton, FL.

Blencowe, D. K., and A. P. Morby. 2003. Zn(II) metabolism in prokaryotes. FEMS Microbiol Rev 27:291-311.

Bomberger, J. M., D. P. MacEachran, B. A. Coutermarsh, S. Ye, G. A. O'Toole, and B. A. Stanton. 2009. Long-distance delivery of bacterial virulence factors by *Pseudomonas aeruginosa* outer membrane vesicles. PLoS Pathog 5:e1000382.

Bradford, A., R. D. Handy, J. W. Readman, A. Atfield, and M. Muhling. 2009. Impact of silver nanoparticle contamination on the genetic diversity of natural bacterial assemblages in estuarine sediments. Environ Sci Technol 43:4530-6.

Bradford, M. M. 1976. A rapid and sensitive method for the quantitation of microgram quantities of protein utilizing the principle of protein-dye binding. Anal Biochem 72:248-54.

Bradley, J. 2008. Nanomaterials state of the market Q3 2008: Stealth success, broad impact. Lux Research Inc., New York, NY.

Brayner, R., R. Ferrari-Iliou, N. Brivois, S. Djediat, M. F. Benedetti, and F. Fievet. 2006. Toxicological impact studies based on *Escherichia coli* bacteria in ultrafine ZnO nanoparticles colloidal medium. Nano Lett 6:866-70.

Brocklehurst, K. R., J. L. Hobman, B. Lawley, L. Blank, S. J. Marshall, N. L. Brown, and A. P. Morby. 1999. ZntR is a Zn(II)-responsive MerR-like transcriptional regulator of zntA in *Escherichia coli*. Mol Microbiol 31:893-902.

Brown, J. L., T. Ross, T. A. McMeekin, and P. D. Nichols. 1997. Acid habituation of *Escherichia coli* and the potential role of cyclopropane fatty acids in low pH tolerance. Int J Food Microbiol 37:163-73.

BSD. 2007. Biodegradative Strain Database. Center for Microbial Ecology, Michigan State University, http://bsd.cme.msu.edu/, (accessed February 2007).

Burton, E., N. Yakandawala, K. LoVetri, and M. S. Madhyastha. 2007. A microplate spectrofluorometric assay for bacterial biofilms. J Ind Microbiol Biotechnol 34:1-4.

Button, J. E., T. J. Silhavy, and N. Ruiz. 2007. A suppressor of cell death caused by the loss of σ^E downregulates extracytoplasmic stress responses and outer membrane vesicle production in *Escherichia coli*. J. Bacteriol. 189:1523-1530.

Camargo, F., B. Okeke, F. Bento, and W. Frankenberger. 2004. Hexavalent chromium reduction by immobilized cells and the cell-free extract of *Bacillus* sp. ES 29. Bioremediation J 8:23-30.

Campbell, P. G. C. 1995. Interactions between trace metals and aquatic organisms: a critique of the free-ion activity model. *In* A. Tessier and D. R. Turner (ed.), Metal speciation and bioavailability in aquatic systems. John Wiley and Sons, New York.

Caraher, E., G. Reynolds, P. Murphy, S. McClean, and M. Callaghan. 2007. Comparison of antibiotic susceptibility of *Burkholderia cepacia* complex organisms when grown planktonically or as biofilm in vitro. Eur J Clin Microbiol Infect Dis 26:213-6.

Carpenter, B. M., J. M. Whitmire, and D. S. Merrell. 2009. This is not your mother's repressor: the complex role of Fur in pathogenesis. Infect. Immun. 77:2590-2601.

CERCLIS. 2009. Comprehensive Environmental Response, Compensation and Liability Information System Database. U.S. Environmental Protection Agency, http://cfpub.epa.gov/supercpad/cursites/srchsites.cfm, (accessed July 28, 2009).

Chatterjee, S. N., and J. Das. 1967. Electron microscopic observations on the excretion of cell-wall material by *Vibrio cholerae*. J Gen Microbiol 49:1-11.

Chitcholtan, K., M. B. Hampton, and J. I. Keenan. 2008. Outer membrane vesicles enhance the carcinogenic potential of *Helicobacter pylori*. Carcinogenesis 29:2400-2405.

Cho, K. H., J. E. Park, T. Osaka, and S. G. Park. 2005. The study of antimicrobial activity and preservative effects of nanosilver ingredient. Electrochimica Acta 51:956-960.

Choudhury, R., and S. Srivastava. 2001. Zinc resistance mechanisms in bacteria. Current Science 81:768-775.

Christian, P., F. Von der Kammer, M. Baalousha, and T. Hofmann. 2008. Nanoparticles: structure, properties, preparation and behaviour in environmental media. Ecotoxicology 17:326-343.

Chubar, N., T. Behrends, and P. Van Cappellen. 2008. Biosorption of metals (Cu2+, Zn2+) and anions (F-, H2PO4-) by viable and autoclaved cells of the Gram-negative bacterium *Shewanella putrefaciens*. Colloids Surf B 65:126-133.

Ciofu, O., T. J. Beveridge, J. Kadurugamuwa, J. Walther-Rasmussen, and N. Hoiby. 2000. Chromosomal beta-lactamase is packaged into membrane vesicles and secreted from *Pseudomonas aeruginosa*. J Antimicrob Chemother 45:9-13.

Claassen, I., J. Meylis, P. van der Ley, C. Peeters, H. Brons, J. Robert, D. Borsboom, A. van der Ark, I. van Straaten, P. Roholl, B. Kuipers, and J. Poolman. 1996. Production, characterization and control of a *Neisseria meningitidis* hexavalent class 1 outer membrane protein containing vesicle vaccine. Vaccine 14:1001-8.

Coenye, T., and P. Vandamme. 2003. Diversity and significance of *Burkholderia* species occupying diverse ecological niches. Environ Microbiol 5:719-29.

Conway, B.-A., and E. P. Greenberg. 2002. Quorum-sensing signals and quorum-sensing genes in *Burkholderia vietnamiensis*. J. Bacteriol. 184:1187-1191.

Correa Junior, J. D., S. Allodi, G. M. Amado-Filho, and M. Farina. 2000. Zinc accumulation in phosphate granules of *Ucides cordatus* hepatopancreas. Braz J Med Biol Res 33:217-21.

Deatherage, B. L., J. C. Lara, T. Bergsbaken, S. L. R. Barrett, S. Lara, and B. T. Cookson. 2009. Biogenesis of bacterial membrane vesicles. Molecular Microbiology 72:1395-1407.

DebRoy, S., J. Dao, M. Soderberg, O. Rossier, and N. P. Cianciotto. 2006. *Legionella pneumophila* type II secretome reveals unique exoproteins and a chitinase that promotes bacterial persistence in the lung. Proc Natl Acad Sci U S A 103:19146-51.

Deheyn, D. D., R. Bencheikh-Latmani, and M. I. Latz. 2004. Chemical speciation and toxicity of metals assessed by three bioluminescence-based assays using marine organisms. Environ Toxicol 19:161-78.

Di Toro, D. M., H. E. Allen, H. L. Bergman, J. S. Meyer, P. R. Paquin, and R. C. Santore. 2001. Biotic ligand model of the acute toxicity of metals. 1. Technical basis. Environ Toxicol Chem 20:2383-96.

Diez-Gonzalez, F., and J. B. Russell. 1997. The ability of *Escherichia coli* O157:H7 to decrease its intracellular pH and resist the toxicity of acetic acid. Microbiology 143:1175-1180.

Dorward, D. W., and C. F. Garon. 1990. DNA is packaged within membrane-derived vesicles of Gram-negative but not Gram-positive bacteria. Appl Environ Microbiol 56:1960-1962.

Dorward, D. W., C. F. Garon, and R. C. Judd. 1989. Export and intercellular transfer of DNA via membrane blebs of *Neisseria gonorrhoeae*. J Bacteriol 171:2499-505.

Drechsel, H., and G. Jung. 1998. Peptide siderophores. J Pept Sci 4:147-81.

Egler, M., C. Grosse, G. Grass, and D. H. Nies. 2005. Role of the extracytoplasmic function protein family sigma factor RpoE in metal resistance of *Escherichia coli*. J. Bacteriol. 187:2297-2307.

Ellen, A. F., S. V. Albers, W. Huibers, A. Pitcher, C. F. Hobel, H. Schwarz, M. Folea, S. Schouten, E. J. Boekema, B. Poolman, and A. J. Driessen. 2009. Proteomic analysis of secreted membrane vesicles of archaeal *Sulfolobus* species reveals the presence of endosome sorting complex components. Extremophiles 13:67-79.

Fahey, R. C. 2001. Novel thiols of prokaryotes. Annu Rev Microbiol 55:333-56.

Fein, J. B., J. Boily, N. Yee, D. Gorman-Lewis, and B. F. Turner. 2005. Potentiometric titrations of *Bacillus subtilis* cells to low pH and a comparison of modeling approaches. Geochimica et Cosmochimica Acta 69:1123-1132.

Fein, J. B., C. J. Daughney, N. Yee, and T. A. Davis. 1997. A chemical equilibrium model for metal adsorption onto bacterial surfaces. Geochimica et Cosmochimica Acta 61:3319-3328.

Fernandez-Moreira, E., J. H. Helbig, and M. S. Swanson. 2006. Membrane vesicles shed by *Legionella pneumophila* inhibit fusion of phagosomes with lysosomes. Infect Immun 74:3285-95.

Ferrari, G., I. Garaguso, J. Adu-Bobie, F. Doro, A. R. Taddei, A. Biolchi, B. Brunelli, M. M. Giuliani, M. Pizza, N. Norais, and G. Grandi. 2006. Outer membrane vesicles from group B *Neisseria meningitidis* Δgna33 mutant: proteomic and immunological comparison with detergent-derived outer membrane vesicles. Proteomics 6:1856-66.

Ferry, J. L., P. Craig, C. Hexel, P. Sisco, R. Frey, P. L. Pennington, M. H. Fulton, I. G. Scott, A. W. Decho, S. Kashiwada, C. J. Murphy, and T. J. Shaw. 2009. Transfer of gold nanoparticles from the water column to the estuarine food web. Nat Nanotechnol 4:441-4.

Forsberg, C. W., T. J. Beveridge, and A. Hellstrom. 1981. Cellulase and xylanase release from *Bacteroides succinogenes* and its importance in the rumen environment. Appl Environ Microbiol 42:886-896.

Fozo, E. M., and R. G. Quivey, Jr. 2004. Shifts in the membrane fatty acid profile of *Streptococcus mutans* enhance survival in acidic environments. Appl Environ Microbiol 70:929-36.

Francois, L., C. Fortin, and P. G. C. Campbell. 2007. pH modulates transport rates of manganese and cadmium in the green alga *Chlamydomonas reinhardtii* through non-competitive interactions: Implications for an algal BLM. Aquatic Toxicology 84:123-132.

Franklin, N. M., N. J. Rogers, S. C. Apte, G. E. Batley, G. E. Gadd, and P. S. Casey. 2007. Comparative toxicity of nanoparticulate ZnO, bulk ZnO, and ZnCl2 to a freshwater microalga (*Pseudokirchneriella subcapitata*): The importance of particle solubility. Environ Sci Technol 41:8484-8490.

Fries, M. R., L. J. Forney, and J. M. Tiedje. 1997. Phenol- and toluene-degrading microbial populations from an aquifer in which successful trichloroethene cometabolism occurred. Appl Environ Microbiol 63:1523-1530.

Gadd, G. M. 2004. Microbial influence on metal mobility and application for bioremediation. Geoderma 122:109-119.

Gajjar, P., B. Pettee, D. W. Britt, W. Huang, W. P. Johnson, and A. J. Anderson. 2009. Antimicrobial activities of commercial nanoparticles against an environmental soil microbe, *Pseudomonas putida* KT2440. J Biol Eng 3:9.

Galka, F., S. N. Wai, H. Kusch, S. Engelmann, M. Hecker, B. Schmeck, S. Hippenstiel, B. E. Uhlin, and M. Steinert. 2008. Proteomic characterization of the whole secretome of *Legionella pneumophila* and functional analysis of outer membrane vesicles. Infect Immun 76:1825-36.

Gamazo, C., and I. Moriyon. 1987. Release of outer membrane fragments by exponentially growing *Brucella melitensis* cells. Infect Immun 55:609-15.

Garduno, R. A., E. Garduno, and P. S. Hoffman. 1998. Surface-associated hsp60 chaperonin of *Legionella pneumophila* mediates invasion in a HeLa cell model. Infect Immun 66:4602-10.

Geisenberger, O., M. Givskov, K. Riedel, N. Hoiby, B. Tummler, and L. Eberl. 2000. Production of N-acyl-L-homoserine lactones by *P. aeruginosa* isolates from chronic lung infections associated with cystic fibrosis. FEMS Microbiol Lett 184:273-8.

Giddings, J. C. 1995. Measuring colloidal and macromolecular properties by FFF. Anal Chem 67:592A-598A.

Gillis, M., T. Van Van, R. Bardin, M. Goor, P. Hebbar, A. Willems, P. Segers, K. Kersters, T. Heulin, and M. P. Fernandez. 1995. Polyphasic taxonomy in the genus *Burkholderia* leading to an emended description of the genus and proposition of *Burkholderia vietnamiensis* sp. nov. for N2-fixing isolates from rice in Vietnam. Int J Syst Bacteriol 45:274-289.

Goldberg, R. N., and Y. B. Tewari. 2002. Thermochemistry of the biochemical reaction: { pyrophosphate(aq) + H2O(l) = 2 phosphate(aq)}. J Chem Thermodynamics 34:821-839.

Goodwin, F. E. 1998. Zinc compounds, p. 840-853. *In* J. Kroschwitz and M. Howe-Grant (ed.), Kirk-Othmer encyclopedia of chemical technology. John Wiley & Sons, Inc., New York, NY.

Gorby, Y., J. McLean, A. Korenevsky, K. Rosso, M. Y. El-Naggar, and T. J. Beveridge. 2008. Redox-reactive membrane vesicles produced by *Shewanella*. Geobiology 6:232-41.

Grage, K., A. C. Jahns, N. Parlane, R. Palanisamy, I. A. Rasiah, J. A. Atwood, and B. H. Rehm. 2009. Bacterial polyhydroxyalkanoate granules: biogenesis, structure, and potential use as nano-/micro-beads in biotechnological and biomedical applications. Biomacromolecules 10:660-9.

Green-Ruiz, C., V. Rodriguez-Tirado, and B. Gomez-Gil. 2008. Cadmium and zinc removal from aqueous solutions by *Bacillus jeotgali*: pH, salinity and temperature effects. Bioresource Technol 99:3864-3870.

Grobe, C., A. Anton, T. Hoffmann, S. Franke, G. Schleuder, and D. Nies. 2004. Identification of a regulatory pathway that controls the heavy-metal resistance system Czc via promoter czcNp in *Ralstonia metallidurans*. Archives of Microbiology 182:109-118.

Grobe, C., S. Friedrich, and D. H. Nies. 2007. Contribution of extracytoplasmic function sigma factors to transition metal homeostasis in *Cupriavidus metallidurans* strain CH34. J Mol Microbiol Biotechnol 12:227-240.

Grogan, D. W., and J. E. Cronan, Jr. 1997. Cyclopropane ring formation in membrane lipids of bacteria. Microbiol Mol Biol Rev 61:429-41.

Guine, V., L. Spadini, G. Sarret, M. Muris, C. Delolme, J. P. Gaudet, and J. M. Martins. 2006. Zinc sorption to three gram-negative bacteria: combined titration, modeling, and EXAFS study. Environ Sci Technol 40:1806-13.

Gustafsson, J. P. 2009. Visual MINTEQ, v. 2.61, KTH Royal Institute of Technology.

Hantke, K. 2001. Bacterial zinc transporters and regulators. Biometals 14:239-49.

Harrison, J. J., H. Ceri, and R. J. Turner. 2007. Multimetal resistance and tolerance in microbial biofilms. Nat Rev Microbiol 5:928-38.

Hassler, C. S., V. I. Slaveykova, and K. J. Wilkinson. 2004. Some fundamental (and often overlooked) considerations underlying the free ion activity and biotic ligand models. Environ Toxicol Chem 23:283-91.

Hassler, C. S., and K. J. Wilkinson. 2003. Failure of the biotic ligand and free-ion activity models to explain zinc bioaccumulation by *Chlorella kesslerii*. Environ Toxicol Chem 22:620-6.

Hartig, C., N. Loffhagen, and H. Harms. 2005. Formation of trans fatty acids is not involved in growth-linked membrane adaptation of *Pseudomonas putida*. Appl Environ Microbiol 71:1915-22.

Hausinger, R. P. 1993. Biochemistry of Nickel, 2nd ed. Plenum Press, New York, NY.

Hayashi, J., N. Hamada, and H. K. Kuramitsu. 2002. The autolysin of *Porphyromonas gingivalis* is involved in outer membrane vesicle release. FEMS Microbiol Lett 216:217-22.

HazDat. 2006. HazDat Database: ATSDR's Hazardous Substance Release and Health Effects Database. Agency for Toxic Substances and Disease Registry, http://www.atsdr.cdc.gov/ (accessed February 12, 2007).

Heijerick, D. G., K. A. De Schamphelaere, and C. R. Janssen. 2002. Biotic ligand model development predicting Zn toxicity to the alga *Pseudokirchneriella subcapitata*: possibilities and limitations. Comp Biochem Physiol C Toxicol Pharmacol 133:207-18.

Heinlaan, M., A. Ivask, I. Blinova, H. C. Dubourguier, and A. Kahru. 2008. Toxicity of nanosized and bulk ZnO, CuO and TiO2 to bacteria *Vibrio fischeri* and crustaceans *Daphnia magna* and *Thamnocephalus platyurus*. Chemosphere 71:1308-1316.

Hirschey, M. D., Y. J. Han, G. D. Stucky, and A. Butler. 2006. Imaging *Escherichia coli* using functionalized core/shell CdSe/CdS quantum dots. J Biol Inorg Chem 11:663-9.

Hong, G. E., D. G. Kim, E. M. Park, B. H. Nam, Y. O. Kim, and I. S. Kong. 2009. Identification of *Vibrio anguillarum* outer membrane vesicles related to immunostimulation in the Japanese flounder, *Paralichthys olivaceus*. Biosci Biotechnol Biochem 73:437-9.

Horstman, A. L., and M. J. Kuehn. 2000. Enterotoxigenic *Escherichia coli* secretes active heat-labile enterotoxin via outer membrane vesicles. J Biol Chem 275:12489-96.

Hoyle, B., and T. J. Beveridge. 1983. Binding of metallic ions to the outer membrane of *Escherichia coli*. Appl Environ Microbiol 46:749-752.

Hu, L., M. Ye, X. Jiang, S. Feng, and H. Zou. 2007. Advances in hyphenated analytical techniques for shotgun proteome and peptidome analysis--a review. Anal Chim Acta 598:193-204.

Hu, X., S. Cook, P. Wang, and H. M. Hwang. 2009. In vitro evaluation of cytotoxicity of engineered metal oxide nanoparticles. Sci Total Environ 407:3070-2.

Huang, Z., X. Zheng, D. Yan, G. Yin, X. Liao, Y. Kang, Y. Yao, D. Huang, and B. Hao. 2008. Toxicological effect of ZnO nanoparticles based on bacteria. Langmuir 24:4140-4.

Ismail, S., M. B. Hampton, and J. I. Keenan. 2003. *Helicobacter pylori* outer membrane vesicles modulate proliferation and interleukin-8 production by gastric epithelial cells. Infect Immun 71:5670-5.

Ivanov, A., V. M. Fomchenkov, L. A. Khasanova, and A. V. Gavriushkin. 1997. Toxic effect of hydroxylated ions of heavy metals on the cytoplasmic membrane of bacterial cells. Mikrobiologiia 66:588-94.

Jackson, B. P., J. F. Ranville, and A. L. Neal. 2005. Application of flow field flow fractionation-ICPMS for the study of uranium binding in bacterial cell suspensions. Anal Chem 77:1393-7.

Jiang, W., H. Mashayekhi, and B. Xing. 2009. Bacterial toxicity comparison between nano- and micro-scaled oxide particles. Environ Pollut 157:1619-25.

Jiang, W., A. Saxena, B. Song, B. B. Ward, T. J. Beveridge, and S. C. Myneni. 2004. Elucidation of functional groups on gram-positive and gram-negative bacterial surfaces using infrared spectroscopy. Langmuir 20:11433-42.

Jones, N., B. Ray, K. T. Ranjit, and A. C. Manna. 2008. Antibacterial activity of ZnO nanoparticle suspensions on a broad spectrum of microorganisms. FEMS Microbiology Letters 279:71-76.

Joshi-Tope, G., and A. J. Francis. 1995. Mechanisms of biodegradation of metal-citrate complexes by *Pseudomonas fluorescens*. J Bacteriol 177:1989-93.

Kachur, A. V., C. J. Koch, and J. E. Biaglow. 1998. Mechanism of copper-catalyzed oxidation of glutathione. Free Radic Res 28:259-69.

Kadurugamuwa, J. L., and T. J. Beveridge. 1996. Bacteriolytic effect of membrane vesicles from *Pseudomonas aeruginosa* on other bacteria including pathogens: conceptually new antibiotics. J Bacteriol 178:2767-74.

Kadurugamuwa, J. L., and T. J. Beveridge. 1999. Membrane vesicles derived from *Pseudomonas aeruginosa* and *Shigella flexneri* can be integrated into the surfaces of other gram-negative bacteria. Microbiology 145:2051-60.

Kadurugamuwa, J. L., and T. J. Beveridge. 1997. Natural release of virulence factors in membrane vesicles by *Pseudomonas aeruginosa* and the effect of aminoglycoside antibiotics on their release. J Antimicrob Chemother 40:615-21.

Kadurugamuwa, J. L., and T. J. Beveridge. 1995. Virulence factors are released from *Pseudomonas aeruginosa* in association with membrane vesicles during normal growth and exposure to gentamicin: a novel mechanism of enzyme secretion. J Bacteriol 177:3998-4008.

Kahn, M. E., F. Barany, and H. O. Smith. 1983. Transformasomes: specialized membranous structures that protect DNA during *Haemophilus* transformation. Proc Natl Acad Sci U S A 80:6927-31.

Kamashwaran, S. R., and D. L. Crawford. 2003. Mechanisms of cadmium resistance in anaerobic bacterial enrichments degrading pentachlorophenol. Can J Microbiol 49:418-424.

Karched, M., R. Ihalin, K. Eneslatt, D. Zhong, J. Oscarsson, S. N. Wai, C. Chen, and S. E. Asikainen. 2008. Vesicle-independent extracellular release of a proinflammatory outer membrane lipoprotein in free-soluble form. BMC Microbiol 8:18.

Keenan, J. I., and R. A. Allardyce. 2000. Iron influences the expression of *Helicobacter pylori* outer membrane vesicle-associated virulence factors. Eur J Gastroenterol Hepatol 12:1267-73.

Kesty, N. C., and M. J. Kuehn. 2004. Incorporation of heterologous outer membrane and periplasmic proteins into *Escherichia coli* outer membrane vesicles. J Biol Chem 279:2069-76.

Khandelwal, P., and N. Banerjee-Bhatnagar. 2003. Insecticidal activity associated with the outer membrane vesicles of *Xenorhabdus nematophilus*. Appl Environ Microbiol 69:2032-7.

Klaine, S. J., P. J. Alvarez, G. E. Batley, T. F. Fernandes, R. D. Handy, D. Y. Lyon, S. Mahendra, M. J. McLaughlin, and J. R. Lead. 2008. Nanomaterials in the environment: Behavior, fate, bioavailability, and effects. Environ Toxicol Chem 27:1825-1851.

Kloepfer, J. A., R. E. Mielke, and J. L. Nadeau. 2005. Uptake of CdSe and CdSe/ZnS quantum dots into bacteria via purine-dependent mechanisms. Appl Environ Microbiol 71:2548-57.

Knox, K. W., M. Vesk, and E. Work. 1966. Relation between excreted lipopolysaccharide complexes and surface structures of a lysine-limited culture of *Escherichia coli*. J. Bacteriol. 92:1206-1217.

Kobayashi, H., K. Uematsu, H. Hirayama, and K. Horikoshi. 2000. Novel toluene elimination system in a toluene-tolerant microorganism. J Bacteriol 182:6451-5.

Kolling, G. L., and K. R. Matthews. 1999. Export of virulence genes and Shiga toxin by membrane vesicles of *Escherichia coli* O157:H7. Appl Environ Microbiol 65:1843-8.

Kondo, K., A. Takade, and K. Amako. 1993. Release of the outer membrane vesicles from *Vibrio cholerae* and *Vibrio parahaemolyticus*. Microbiol Immunol 37:149-52.

Koukal, B., P. Rossé, A. Reinhardt, B. Ferrari, K. J. Wilkinson, J.-L. Loizeau, and J. Dominik. 2007. Effect of *Pseudokirchneriella subcapitata* (*Chlorophyceae*) exudates on metal toxicity and colloid aggregation. Water Research 41:63-70.

Kouokam, J. C., S. N. Wai, M. Fallman, U. Dobrindt, J. Hacker, and B. E. Uhlin. 2006. Active cytotoxic necrotizing factor 1 associated with outer membrane vesicles from uropathogenic *Escherichia coli*. Infect Immun 74:2022-30.

Kuehn, M. J., and N. C. Kesty. 2005. Bacterial outer membrane vesicles and the host-pathogen interaction. Genes Dev 19:2645-55.

Kurek, E., A. J. Francis, and J. M. Bollag. 1991. Immobilization of cadmium by microbial extracellular products. Archives of Environmental Contamination and Toxicology 21:106-111.

Langley, S. 2006. Metal Inclusions in Bacteria, p. 311-319, Inclusions in Prokaryotes.

Lee, E. Y., J. Y. Bang, G. W. Park, D. S. Choi, J. S. Kang, H. J. Kim, K. S. Park, J. O. Lee, Y. K. Kim, K. H. Kwon, K. P. Kim, and Y. S. Gho. 2007. Global proteomic profiling of native outer membrane vesicles derived from *Escherichia coli*. Proteomics 7:3143-53.

Lee, E. Y., D. S. Choi, K. P. Kim, and Y. S. Gho. 2008. Proteomics in gram-negative bacterial outer membrane vesicles. Mass Spectrom Rev 27:535-55.

Lee, S. K., and S. B. Lee. 2001. Isolation and characterization of a thermotolerant bacterium *Ralstonia* sp. strain PHS1 that degrades benzene, toluene, ethylbenzene, and o-xylene. Appl Microbiol Biotechnol 56:270-5.

Legatzki, A., G. Grass, A. Anton, C. Rensing, and D. H. Nies. 2003. Interplay of the Czc system and two P-type ATPases in conferring metal resistance to *Ralstonia metallidurans*. J Bacteriol 185:4354-61.

Li, W. R., X. B. Xie, Q. S. Shi, H. Y. Zeng, Y. S. Ou-Yang, and Y. B. Chen. 2009. Antibacterial activity and mechanism of silver nanoparticles on *Escherichia coli*. Appl Microbiol Biotechnol.

Li, Z., A. J. Clarke, and T. J. Beveridge. 1998. Gram-negative bacteria produce membrane vesicles which are capable of killing other bacteria. J Bacteriol 180:5478-83.

Li, Z., A. J. Clarke, and T. J. Beveridge. 1996. A major autolysin of *Pseudomonas aeruginosa*: subcellular distribution, potential role in cell growth and division and secretion in surface membrane vesicles. J Bacteriol 178:2479-88.

Limbach, L. K., R. Bereiter, E. Muller, R. Krebs, R. Galli, and W. J. Stark. 2008. Removal of oxide nanoparticles in a model wastewater treatment plant: influence of agglomeration and surfactants on clearing efficiency. Environ Sci Technol 42:5828-33.

Lin, X. M., L. N. Wu, H. Li, S. Y. Wang, and X. X. Peng. 2008. Downregulation of Tsx and OmpW and upregulation of OmpX are required for iron homeostasis in *Escherichia coli*. J Proteome Res 7:1235-43.

Lindsay, W. L. 1979. Chemical equilibria in soils, p. 210-220. John Wiley & Sons, New York, NY.

LiPuma, J. J., T. Spilker, L. H. Gill, P. W. Campbell, 3rd, L. Liu, and E. Mahenthiralingam. 2001. Disproportionate distribution of *Burkholderia cepacia* complex species and transmissibility markers in cystic fibrosis. Am J Respir Crit Care Med 164:92-6.

Logan, S. M., and T. J. Trust. 1982. Outer membrane characteristics of *Campylobacter jejuni*. Infect Immun 38:898-906.

Lovley, D. R., and E. J. Phillips. 1994. Reduction of chromate by *Desulfovibrio vulgari*s and its c(3) cytochrome. Appl Environ Microbiol 60:726-728.

Lyon, D. Y., J. D. Fortner, C. M. Sayes, V. L. Colvin, and J. B. Hughe. 2005. Bacterial cell association and antimicrobial activity of a C60 water suspension. Environ Toxicol Chem 24:2757-62.

Lytle, D., C. Frietch, and T. Covert. 2004. Electrophoretic mobility of *Mycobacterium avium* complex organisms. Appl Environ Microbiol 70:5667-71.

Mahendra, S., H. Zhu, V. L. Colvin, and P. J. Alvarez. 2008. Quantum dot weathering results in microbial toxicity. Environ Sci Technol 42:9424-30.

Mahenthiralingam, E., T. A. Urban, and J. B. Goldberg. 2005. The multifarious, multireplicon *Burkholderia cepacia* complex. Nat Rev Micro 3:144-156.

Masala, O., P. O'Brien, and G. Rafeletos. 2003. Formation of spherical granules of calcium pyrophosphate. Crystal Growth Design 3:431-434.

Masala, O., P. O'Brien, and P. S. Rainbow. 2004. Analysis of metal-containing granules in the barnacle *Tetraclita squamosa*. J Inorg Biochem 98:1095-102.

Mashburn-Warren, L., J. Howe, K. Brandenburg, and M. Whiteley. 2009. Structural requirements of the Pseudomonas Quinolone Signal for membrane vesicle stimulation. J. Bacteriol. 191:3411-3414.

Mashburn-Warren, L., J. Howe, P. Garidel, W. Richter, F. Steiniger, M. Roessle, K. Brandenburg, and M. Whiteley. 2008. Interaction of quorum signals with outer membrane lipids: insights into prokaryotic membrane vesicle formation. Mol Microbiol 69:491-502.

Mashburn-Warren, L. M., and M. Whiteley. 2006. Special delivery: vesicle trafficking in prokaryotes. Mol Microbiol 61:839-46.

Mashburn, L. M., and M. Whiteley. 2005. Membrane vesicles traffic signals and facilitate group activities in a prokaryote. Nature 437:422-5.

Mathew, A., and R. I. Morimoto. 1998. Role of the heat-shock response in the life and death of proteins. Ann N Y Acad Sci 851:99-111.

Maurer, L. M., E. Yohannes, S. S. Bondurant, M. Radmacher, and J. L. Slonczewski. 2005. pH regulates genes for flagellar motility, catabolism, and oxidative stress in *Escherichia coli* K-12. J. Bacteriol. 187:304-319.

Mayer, F., and G. Gottschalk. 2003. The bacterial cytoskeleton and its putative role in membrane vesicle formation observed in a Gram-positive bacterium producing starch-degrading enzymes. J Mol Microbiol Biotechnol 6:127-32.

Maynard, A., and E. Michelson. 2008. A Nanotechnology Consumer Products Inventory. Woodrow Wilson Center Project on Emerging Nanotechnologies, http://www.nanotechproject.org/inventories/consumer/, (accessed September 15, 2008).

Mayrand, D., and S. C. Holt. 1988. Biology of asaccharolytic black-pigmented *Bacteroides* species. Microbiol Rev 52:134-52.

Mazzola, L. 2003. Commercializing nanotechnology. Nature Biotechnology 21:1137-1143.

McBroom, A. J., A. P. Johnson, S. Vemulapalli, and M. J. Kuehn. 2006. Outer membrane vesicle production by *Escherichia coli* is independent of membrane instability. J Bacteriol 188:5385-92.

McBroom, A. J., and M. J. Kuehn. 2007. Release of outer membrane vesicles by Gram-negative bacteria is a novel envelope stress response. Mol Microbiol 63:545-58.

McCance, R. A., and E. M. Widdowson. 1942. The absorption and excretion of zinc. Biochem J 36:692-6.

Mergeay, M., D. Nies, H. G. Schlegel, J. Gerits, P. Charles, and F. Van Gijsegem. 1985. *Alcaligenes eutrophus* CH34 is a facultative chemolithotroph with plasmid-bound resistance to heavy metals. J Bacteriol 162:328-34.

Meyer, D. H., and P. M. Fives-Taylor. 1994. Characteristics of adherence of *Actinobacillus actinomycetemcomitans* to epithelial cells. Infect Immun 62:928-35.

Mirimanoff, N., and K. J. Wilkinson. 2000. Regulation of Zn accumulation by a freshwater Gram-positive bacterium (*Rhodococcus opacus*). Environ Sci Technol 34:616-622.

Mortimer, M., K. Kasemets, M. Heinlaan, I. Kurvet, and A. Kahru. 2008. High throughput kinetic *Vibrio fischeri* bioluminescence inhibition assay for study of toxic effects of nanoparticles. Toxicol In Vitro 22:1412-1417.

Motulsky, H., and A. Christopoulos. 2003. Fitting Biological Models to Biological Data using Linear and Nonlinear Regression. GraphPad Software, Inc., San Diego, CA.

Munakata-Marr, J., P. L. McCarty, M. S. Shields, M. Reagin, and S. C. Francesconi. 1996. Enhancement of trichloroethylene degradation in aquifer microcosms bioaugmented with wild type and genetically altered *Burkholderia* (*Pseudomonas*) *cepacia* G4 and PR1. Environ Sci Technol 30:2045-2052.

Munoz-Rojas, J., P. Bernal, E. Duque, P. Godoy, A. Segura, and J. L. Ramos. 2006. Involvement of cyclopropane fatty acids in the response of *Pseudomonas putida* KT2440 to freeze-drying. Appl Environ Microbiol 72:472-7.

Nair, S., A. Sasidharan, V. V. Divya Rani, D. Menon, S. Nair, K. Manzoor, and S. Raina. 2008. Role of size scale of ZnO nanoparticles and microparticles on toxicity toward bacteria and osteoblast cancer cells. J Mater Sci Mater Med:[Epub ahead of print].

Nandi, B., R. K. Nandy, A. Sarkar, and A. C. Ghose. 2005. Structural features, properties and regulation of the outer-membrane protein W (OmpW) of *Vibrio cholerae*. Microbiology 151:2975-2986.

Nather, D. J., and R. Rachel. 2004. The outer membrane of the hyperthermophilic archaeon *Ignicoccus*: dynamics, ultrastructure and composition. Biochem Soc Trans 32:199-203.

Navarro, E., F. Piccapietra, B. Wagner, F. Marconi, R. Kaegi, N. Odzak, L. Sigg, and R. Behra. 2008. Toxicity of silver nanoparticles to *Chlamydomonas reinhardtii*. Environ Sci Technol 42:8959-64.

Neal, A. L. 2008. What can be inferred from bacterium-nanoparticle interactions about the potential consequences of environmental exposure to nanoparticles? Ecotoxicology 17:362-71.

Neal, A. L., S. N. Dublin, J. Taylor, D. J. Bates, J. L. Burns, R. Apkarian, and T. J. DiChristina. 2007. Terminal electron acceptors influence the quantity and chemical composition of capsular exopolymers produced by anaerobically growing *Shewanella* spp. Biomacromolecules 8:166-74.

Negrete-Abascal, E., R. M. Garcia, M. E. Reyes, D. Godinez, and M. de la Garza. 2000. Membrane vesicles released by *Actinobacillus pleuropneumoniae* contain proteases and Apx toxins. FEMS Microbiol Lett 191:109-13.

Nelson, M. J., S. O. Montgomery, J. O'Neill E, and P. H. Pritchard. 1986. Aerobic metabolism of trichloroethylene by a bacterial isolate. Appl Environ Microbiol 52:383-384.

Nesatyy, V. J., and M. J. Suter. 2008. Analysis of environmental stress response on the proteome level. Mass Spectrom Rev 27:556-74.

Nevot, M., V. Deroncele, P. Messner, J. Guinea, and E. Mercade. 2006. Characterization of outer membrane vesicles released by the psychrotolerant bacterium *Pseudoalteromonas antarctica* NF3. Environ Microbiol 8:1523-33.

Nies, D. 2007. Bacterial Transition Metal Homeostasis, p. 117-142, Molecular Microbiology of Heavy Metals.

Nies, D. H. 2003. Efflux-mediated heavy metal resistance in prokaryotes. FEMS Microbiol Rev 27:313-39.

Nies, D. H. 1999. Microbial heavy-metal resistance. Appl Microbiol Biotechnol 51:730-50.

O'Sullivan, L. A., and E. Mahenthiralingam. 2005. Biotechnological potential within the genus *Burkholderia*. Lett Appl Microbiol 41:8-11.

ORNL. 2007. *Burkholderia vietnamiensis* strain G4 (R1808) analysis files. Oak Ridge National Laboratory, http://genome.ornl.gov/microbial/bcep_1808/, (accessed 5 January 2007).

Outten, C. E., and T. V. O'Halloran. 2001. Femtomolar sensitivity of metalloregulatory proteins controlling zinc homeostasis. Science 292:2488-2492.

Pagenkopf, G. K. 2002. Gill surface interaction model for trace-metal toxicity to fishes: role of complexation, pH, and water hardness. Environ Sci Technol 17:342-347.

Palsdottir, H., J. P. Remis, C. Schaudinn, E. O'Toole, R. Lux, W. Shi, K. L. McDonald, J. W. Costerton, and M. Auer. 2009. Three-dimensional macromolecular organization of cryofixed *Myxococcus xanthus* biofilms as revealed by electron microscopic tomography. J Bacteriol 191:2077-82.

Panina, E. M., A. A. Mironov, and M. S. Gelfand. 2003. Comparative genomics of bacterial zinc regulons: enhanced ion transport, pathogenesis, and rearrangement of ribosomal proteins. Proc Natl Acad Sci U S A 100:9912-7.

Patrick, S., J. P. McKenna, S. O'Hagan, and E. Dermott. 1996. A comparison of the haemagglutinating and enzymic activities of *Bacteroides fragilis* whole cells and outer membrane vesicles. Microb Pathog 20:191-202.

Patzer, S. I., and K. Hantke. 1998. The ZnuABC high-affinity zinc uptake system and its regulator Zur in *Escherichia coli*. Mol Microbiol 28:1199-210.

Perry, J. J., and J. T. Staley. 1997. Microbiology: dynamics and diversity. Harcourt Brace College Publishers, Orlando, FL.

Poole, K. 2001. Multidrug efflux pumps and antimicrobial resistance in *Pseudomonas aeruginosa* and related organisms. J Mol Microbiol Biotechnol 3:255-64.

Post, D. M., D. Zhang, J. S. Eastvold, A. Teghanemt, B. W. Gibson, and J. P. Weiss. 2005. Biochemical and functional characterization of membrane blebs purified from *Neisseria meningitidis* serogroup B. J Biol Chem 280:38383-94.

Poulson, S. R., and J. I. Drever. 1996. Aqueous complexing of nickel and zinc with 3-(N-morpholino)propanesulfonic acid and the solubility products of nickel and zinc hydroxides. Talanta 43:1975-81.

Prangishvili, D., I. Holz, E. Stieger, S. Nickell, J. K. Kristjansson, and W. Zillig. 2000. Sulfolobicins, specific proteinaceous toxins produced by strains of the extremely thermophilic archaeal genus *Sulfolobus*. J Bacteriol 182:2985-8.

Priester, J. H., P. K. Stoimenov, R. E. Mielke, S. M. Webb, C. Ehrhardt, J. P. Zhang, G. D. Stucky, and P. A. Holden. 2009. Effects of soluble cadmium salts versus CdSe quantum dots on the growth of planktonic *Pseudomonas aeruginosa*. Environ Sci Technol 43:2589-94.

Radtke, A. L., and M. X. O'Riordan. 2006. Intracellular innate resistance to bacterial pathogens. Cell Microbiol 8:1720-9.

Ramamurthi, K. S., S. Lecuyer, H. A. Stone, and R. Losick. 2009. Geometric cue for protein localization in a bacterium. Science 323:1354-7.

Reddy, K. M., K. Feris, J. Bell, D. G. Wingett, C. Hanley, and A. Punnoose. 2007. Selective toxicity of zinc oxide nanoparticles to prokaryotic and eukaryotic systems. Appl Phys Lett 90:2139021-2139023.

Renelli, M., V. Matias, R. Y. Lo, and T. J. Beveridge. 2004. DNA-containing membrane vesicles of *Pseudomonas aeruginosa* PAO1 and their genetic transformation potential. Microbiology 150:2161-9.

Rosen, G., R. Naor, E. Rahamim, R. Yishai, and M. N. Sela. 1995. Proteases of *Treponema denticola* outer sheath and extracellular vesicles. Infect Immun 63:3973-9.

Sabra, W., H. Lunsdorf, and A. P. Zeng. 2003. Alterations in the formation of lipopolysaccharide and membrane vesicles on the surface of *Pseudomonas aeruginosa* PAO1 under oxygen stress conditions. Microbiology 149:2789-2795.

Said, W. A., and D. L. Lewis. 1991. Quantitative assessment of the effects of metals on microbial degradation of organic chemicals. Appl Environ Microbiol 57:1498-503.

Saier, M. H., Jr., R. Tam, A. Reizer, and J. Reizer. 1994. Two novel families of bacterial membrane proteins concerned with nodulation, cell division and transport. Mol Microbiol 11:841-7.

Salit, M. L., and G. C. Turk. 1998. A drift correction procedure. Analytical Chemistry 70:3184-3190.

Sandrin, T. R. 2000. Naphthalene biodegradation in a cadmium contaminated system: effects of rhamnolipid, pH, and divalent cations. University of Arizona, Tucson, AZ.

Sandrin, T. R., and R. M. Maier. 2002. Effect of pH on cadmium toxicity, speciation, and accumulation during naphthalene biodegradation. Environ Toxicol Chem 21:2075-9.

Sandrin, T. R., and R. M. Maier. 2003. Impact of metals on the biodegradation of organic pollutants. Environ Health Perspect 111:1093-101.

Santore, R. C., R. Mathew, P. R. Paquin, and D. DiToro. 2002. Application of the biotic ligand model to predicting zinc toxicity to rainbow trout, fathead minnow, and *Daphnia magna*. Comp Biochem Physiol C Toxicol Pharmacol 133:271-85.

Sayes, C. M., R. Wahi, P. A. Kurian, Y. P. Liu, J. L. West, K. D. Ausman, D. B. Warheit, and V. L. Colvin. 2006. Correlating nanoscale titania structure with toxicity: A cytotoxicity and inflammatory response study with human dermal fibroblasts and human lung epithelial cells. Toxicol Sci 92:174-185.

Schooling, S. R., and T. J. Beveridge. 2006. Membrane vesicles: an overlooked component of the matrices of biofilms. J Bacteriol 188:5945-57.

Schooling, S. R., A. Hubley, and T. J. Beveridge. 2009. Interactions of DNA with biofilm-derived membrane vesicles. J. Bacteriol. 191:4097-4102.

Schwyn, B., and J. B. Neilands. 1987. Universal chemical assay for the detection and determination of siderophores. Anal Biochem 160:47-56.

Scorza, F. B., F. Doro, M. J. Rodriguez-Ortega, M. Stella, S. Liberatori, A. R. Taddei, L. Serino, D. Gomes Moriel, B. Nesta, M. R. Fontana, A. Spagnuolo, M. Pizza, N. Norais, and G. Grandi. 2008. Proteomics characterization of outer membrane vesicles from the extraintestinal pathogenic *Escherichia coli* ΔtolR IHE3034 mutant. Mol Cell Proteomics 7:473-485.

Sharma, R., C. Rensing, B. P. Rosen, and B. Mitra. 2000. The ATP hydrolytic activity of purified ZntA, a Pb(II)/Cd(II)/Zn(II)-translocating ATPase from *Escherichia coli*. J Biol Chem 275:3873-8.

Shields, M. S., M. J. Reagin, R. R. Gerger, R. Campbell, and C. Somerville. 1995. TOM, a new aromatic degradative plasmid from *Burkholderia* (*Pseudomonas*) *cepacia* G4. Appl Environ Microbiol 61:1352-6.

Shimomura, H., M. Matsuura, S. Saito, Y. Hirai, Y. Isshiki, and K. Kawahara. 2003. Unusual interaction of a lipopolysaccharide isolated from *Burkholderia cepacia* with Polymyxin B. Infect Immun 71:5225-5230.

Sidhu, V. K., F. J. Vorholter, K. Niehaus, and S. A. Watt. 2008. Analysis of outer membrane vesicle associated proteins isolated from the plant pathogenic bacterium *Xanthomonas campestris pv. campestris*. BMC Microbiol 8:87.

Smirnova, I. A., D. Zaslavsky, J. A. Fee, R. B. Gennis, and P. Brzezinski. 2008. Electron and proton transfer in the ba(3) oxidase from *Thermus thermophilus*. J Bioenerg Biomembr 40:281-7.

Smith, R. L., L. J. Thompson, and M. E. Maguire. 1995. Cloning and characterization of MgtE, a putative new class of Mg2+ transporter from *Bacillus firmus* OF4. J Bacteriol 177:1233-8.

Snavely, M. D., J. B. Florer, C. G. Miller, and M. E. Maguire. 1989. Magnesium transport in *Salmonella typhimurium*: expression of cloned genes for three distinct Mg2+ transport systems. J Bacteriol 171:4752-60.

Soares, H. M. V. M., S. C. Pinho, and M. G. R. T. M. Barros. 1999. Influence of *N*-substituted aminosulfonic acids with a morpholinic ring pH buffers on the redox processes of copper or zinc Ions: a contribution to speciation studies. Electroanalysis 11:1312-1317.

Soler, N., E. Marguet, J. M. Verbavatz, and P. Forterre. 2008. Virus-like vesicles and extracellular DNA produced by hyperthermophilic archaea of the order *Thermococcales*. Res Microbiol 159:390-9.

Sondi, I., and B. Salopek-Sondi. 2004. Silver nanoparticles as antimicrobial agent: a case study on *E. coli* as a model for Gram-negative bacteria. J Colloid Interface Sci 275:177-82.

Sowder, A. G., P. M. Bertsch, and P. J. Morris. 2003. Partitioning and availability of uranium and nickel in contaminated riparian sediments. J Environ Qual 32:885-98.

Stepanovic, S., D. Vukovic, I. Dakic, B. Savic, and M. Svabic-Vlahovic. 2000. A modified microtiter-plate test for quantification of staphylococcal biofilm formation. J Microbiol Methods 40:175-9.

Stoimenov, P. K., R. L. Klinger, G. L. Marchin, and K. J. Klabunde. 2002. Metal oxide nanoparticles as bactericidal agents. Langmuir 18:6679-6686.

Suzuki, Y., and J. F. Banfield. 2004. Resistance to, and accumulation of, uranium by bacteria from a uranium-contaminated site. Geomicrobiology Journal 21:113-121.

Tablan, O. C., W. J. Martone, C. F. Doershuk, R. C. Stern, M. J. Thomassen, J. D. Klinger, J. W. White, L. A. Carson, and W. R. Jarvis. 1987. Colonization of the respiratory tract with *Pseudomonas cepacia* in cystic fibrosis. Risk factors and outcomes. Chest 91:527-532.

Tate, S., G. MacGregor, M. Davis, J. A. Innes, and A. P. Greening. 2002. Airways in cystic fibrosis are acidified: detection by exhaled breath condensate. Thorax 57:926-9.

Teitzel, G. M., and M. R. Parsek. 2003. Heavy metal resistance of biofilm and planktonic *Pseudomonas aeruginosa*. Appl Environ Microbiol 69:2313-2320.

Thill, A., O. Zeyons, O. Spalla, F. Chauvat, J. Rose, M. Auffan, and A. M. Flank. 2006. Cytotoxicity of CeO2 nanoparticles for *Escherichia coli*: Physico-chemical insight of the cytotoxicity mechanism. Environ Sci Technol 40:6151-6.

Tiedje, J. M., K. Konstantinidis, and V. Denef. 2005. "Diverse *Burkholderia* species and their diverse physiological capabilities", 105th National Meeting, American Society for Microbiology, Symposium 225.

Tong, Z. H., M. Bischoff, L. Nies, B. Applegate, and R. F. Turco. 2007. Impact of fullerene (C-60) on a soil microbial community. Environ Sci Technol 41:2985-2991.

Tripathi, V. N., and S. Srivastava. 2006. Extracytoplasmic storage as the nickel resistance mechanism in a natural isolate of *Pseudomonas putida* S4. Canadian J Microbiol 52:287-292.

Urbance, J. W., J. Cole, P. Saxman, and J. M. Tiedje. 2003. BSD: the biodegradative strain database. Nucleic Acids Res 31:152-5.

Ursell, T. S., W. S. Klug, and R. Phillips. 2009. Morphology and interaction between lipid domains. Proc Natl Acad Sci U S A 106:13301-13306.

USEPA. 2003. The Biotic Ligand Model: Technical Support Document for Its Application to the Evaluation of Water Quality Criteria for Copper. U.S. Environmental Protection Agency,

USEPA. 1999. MINTEQA2 v. 4.0, U.S. Environmental Protection Agency.

Vallee, B. L., and D. S. Auld. 1990. Zinc coordination, function, and structure of zinc enzymes and other proteins. Biochemistry 29:5647-59.

van der Lelie, D., T. Schwuchow, U. Schwidetzky, S. Wuertz, W. Baeyens, M. Mergeay, and D. H. Nies. 1997. Two-component regulatory system involved in transcriptional control of heavy-metal homoeostasis in *Alcaligenes eutrophus*. Mol Microbiol 23:493-503.

Van Nostrand, J. D. 2006. pH-Dependent Ni tolerance in *Burkholderia Vietnamiensis* PR1$_{301}$. Medical University of South Carolina, Charleston, SC.

Van Nostrand, J. D., J. M. Arthur, L. E. Kilpatrick, B. A. Neely, P. M. Bertsch, and P. J. Morris. 2008. Changes in protein expression in *Burkholderia vietnamiensis* PR1$_{301}$ at pH 5 and 7 with and without nickel. Microbiology 154:3813-24.

Van Nostrand, J. D., T. J. Khijniak, B. Neely, M. A. Sattar, A. G. Sowder, G. Mills, P. M. Bertsch, and P. J. Morris. 2007. Reduction of nickel and uranium toxicity and enhanced trichloroethylene degradation to *Burkholderia vietnamiensis* PR1$_{301}$ with hydroxyapatite amendment. Environ Sci Technol 41:1877-1882.

Van Nostrand, J. D., A. G. Sowder, P. M. Bertsch, and P. J. Morris. 2005. Effect of pH on the toxicity of nickel and other divalent metals to *Burkholderia cepacia* PR1$_{301}$. Environ Toxicol Chem 24:2742-2750.

Vial, L., F. Lepine, S. Milot, M. C. Groleau, V. Dekimpe, D. E. Woods, and E. Deziel. 2008. *Burkholderia pseudomallei*, *B. thailandensis*, and *B. ambifaria* produce 4-hydroxy-2-alkylquinoline analogues with a methyl group at the 3 position that is required for quorum-sensing regulation. J Bacteriol 190:5339-52.

Wai, S. N., B. Lindmark, T. Soderblom, A. Takade, M. Westermark, J. Oscarsson, J. Jass, A. Richter-Dahlfors, Y. Mizunoe, and B. E. Uhlin. 2003. Vesicle-mediated export and assembly of pore-forming oligomers of the enterobacterial ClyA cytotoxin. Cell 115:25-35.

Walker, G., P. S. Rainbow, P. Foster, and D. L. Holland. 1975. Zinc phosphate granules in tissue surrounding the midgut of the barnacle *Balanus balanoides*. Marine Biology 33:161-166.

Wang, Z. L. 2004a. Nanostructures of zinc oxide. Mater Today 7:26-33.

Wang, Z. L. 2004b. Zinc oxide nanostructures: growth, properties and applications. J Phys Condens Matter 16:R829-R858.

Watt, S. R., and A. J. Clarke. 1994. Initial characterization of two extracellular autolysins from *Pseudomonas aeruginosa* PAO1. J Bacteriol 176:4784-9.

Weiser, J. N., and E. C. Gotschlich. 1991. Outer membrane protein A (OmpA) contributes to serum resistance and pathogenicity of *Escherichia coli* K-1. Infect. Immun. 59:2252-2258.

Westermeier, R. 2006. Sensitive, quantitative, and fast modifications for Coomassie Blue staining of polyacrylamide gels. Proteomics 6 Suppl 2:61-4.

Whitby, P. W., T. M. Vanwagoner, J. M. Springer, D. J. Morton, T. W. Seale, and T. L. Stull. 2006. *Burkholderia cenocepacia* utilizes ferritin as an iron source. J Med Microbiol 55:661-8.

Whitchurch, C. B., T. Tolker-Nielsen, P. C. Ragas, and J. S. Mattick. 2002. Extracellular DNA required for bacterial biofilm formation. Science 295:1487.

White, D. 2000. The physiology and biochemistry of prokaryotes. Oxford University Press, New York, NY.

Whitmire, W. M., and C. F. Garon. 1993. Specific and nonspecific responses of murine B cells to membrane blebs of *Borrelia burgdorferi*. Infect. Immun. 61:1460-1467.

Williams, G. D., and S. C. Holt. 1985. Characteristics of the outer membrane of selected oral *Bacteroides* species. Can J Microbiol 31:238-50.

Williams, J. N., P. J. Skipp, H. E. Humphries, M. Christodoulides, C. D. O'Connor, and J. E. Heckels. 2007. Proteomic analysis of outer membranes and vesicles from wild-type serogroup B *Neisseria meningitidis* and a lipopolysaccharide-deficient mutant. Infect. Immun. 75:1364-1372.

Williams, R. J. P. 1987. The biochemistry of zinc. Polyhedron 6:61-69.

Worden, C. R., W. K. Kovac, L. A. Dorn, and T. R. Sandrin. 2009. Environmental pH affects transcriptional responses to cadmium toxicity in *Escherichia coli* K-12 (MG1655). FEMS Microbiol Lett 293:58-64.

Worms, I., D. F. Simon, C. S. Hassler, and K. J. Wilkinson. 2006. Bioavailability of trace metals to aquatic microorganisms: importance of chemical, biological and physical processes on biouptake. Biochimie 88:1721-1731.

Wu, L., X. Lin, F. Wang, D. Ye, X. Xiao, S. Wang, and X. Peng. 2006. OmpW and OmpV are required for NaCl regulation in *Photobacterium damsela*. J Proteome Res 5:2250-7.

Xu, X. H. N., W. J. Brownlow, S. V. Kyriacou, Q. Wan, and J. J. Viola. 2004. Real-time probing of membrane transport in living microbial cells using single nanoparticle optics and living cell imaging. Biochemistry 43:10400-10413.

Yamamoto, K., and A. Ishihama. 2005. Transcriptional response of *Escherichia coli* to external zinc. J Bacteriol 187:6333-40.

Yamamoto, O. 2001. Influence of particle size on the antibacterial activity of zinc oxide. International Journal of Inorganic Materials 3:643-646.

Yang, Z., and C. Xie. 2006. Zn2+ release from zinc and zinc oxide particles in simulated uterine solution. Colloids Surf B Biointerfaces 47:140-5.

Yaron, S., G. L. Kolling, L. Simon, and K. R. Matthews. 2000. Vesicle-mediated transfer of virulence genes from *Escherichia coli* O157:H7 to other enteric bacteria. Appl Environ Microbiol 66:4414-20.

Ybarra, G. R., and R. Webb. 1998. "Differential responses of GroEL and metallothionein genes to divalent metal cations and the oxyanions of arsenic in the cyanobacterium *Synechococcus* sp. strain PCC7942." Presented at the Conference on Hazardous Waste Research.

Yeager, C. M., K. M. Arthur, P. J. Bottomley, and D. J. Arp. 2004. Trichloroethylene degradation by toluene-oxidizing bacteria grown on non-aromatic substrates. Biodegradation 15:19-28.

Yee, N., and J. B. Fein. 2003. Quantifying metal adsorption onto bacteria mixtures: A test and application of the surface complexation model. Geomicrobiology Journal 20:43-60.

Yokoyama, K., T. Horii, T. Yamashino, S. Hashikawa, S. Barua, T. Hasegawa, H. Watanabe, and M. Ohta. 2000. Production of shiga toxin by *Escherichia coli* measured with reference to the membrane vesicle-associated toxins. FEMS Microbiol Lett 192:139-44.

Yuk, H. G., and D. L. Marshall. 2004. Adaptation of *Escherichia coli* O157:H7 to pH alters membrane lipid composition, verotoxin secretion, and resistance to simulated gastric fluid acid. Appl Environ Microbiol 70:3500-5.

Zeng, J., L. Yang, and W.-X. Wang. 2009. Cadmium and zinc uptake and toxicity in two strains of *Microcystis aeruginosa* predicted by metal free ion activity and intracellular concentration. Aquatic Toxicology 91:212-220.

Zhang, H., S. Hanada, T. Shigematsu, K. Shibuya, Y. Kamagata, T. Kanagawa, and R. Kurane. 2000. *Burkholderia kururiensis* sp nov., a trichloroethylene (TCE)-degrading bacterium isolated from an aquifer polluted with TCE. International Journal of Systematic and Evolutionary Microbiology 50:743-749.

Zhang, L. L., Y. H. Jiang, Y. L. Ding, M. Povey, and D. York. 2007. Investigation into the antibacterial behaviour of suspensions of ZnO nanoparticles (ZnO nanofluids). Journal of Nanoparticle Research 9:479-489.

Zheng, W., B. Bergman, B. Chen, S. Zheng, X. Guan, and U. Rasmussen. 2009. Cellular responses in the cyanobacterial symbiont during its vertical transfer between plant generations in the *Azolla microphylla* symbiosis. New Phytol 181:53-61.